AD-A254 794

WHOI-92-24

(2)

Woods Hole Oceanographic Institution
Massachusetts Institute of Technology

Joint Program
in Oceanography/
Applied Ocean Science
and Engineering

DTIC
ELECTE
AUG 25 1992
S A D

DOCTORAL DISSERTATION

Applications of Fluorescence Spectroscopy to Environmental Chemistry

by

Sarah Anita Green

June 1992

This document has been approved
for public release and sale; its
distribution is unlimited.

92 8 24 014

38/000

92-23507

228p

WHOI-92-24

Applications of Fluorescence Spectroscopy to Environmental Chemistry

by

Sarah Anita Green

Woods Hole Oceanographic Institution
Woods Hole, Massachusetts 02543

and

The Massachusetts Institute of Technology
Cambridge, Massachusetts 02139

June 1992

DOCTORAL DISSERTATION

Funding was provided by the Office of Naval Research
under Contract No. N00014-89-J-1260.

Reproduction in whole or in part is permitted for any purpose of the United States Government.

This thesis should be cited as: Sarah Anita Green, 1992. Applications of Fluorescence Spectroscopy to Environmental Chemistry. Ph.D. Thesis. MIT/WHOI, WHOI-92-24.

Approved for publication; distribution unlimited.

Approved for Distribution:

Geoffrey Thompson, Chairman
Department of Chemistry and Marine Geochemistry

John W. Farrington
Dean of Graduate Studies

Accesion For
NTIS CRA&I ☒
DTIC TAB ☐
Unannounced ☐
Justification ....
By ....
Distribution /
Availability Codes
Dist | Avail and / or Special
A-1

DTIC QUALITY INSPECTED 5

APPLICATIONS OF FLUORESCENCE SPECTROSCOPY TO ENVIRONMENTAL CHEMISTRY

by

SARAH ANITA GREEN

B.A. Chemistry, University of Minnesota
(1983)

submitted in partial fulfillment of the requirements for the degree of

DOCTOR OF PHILOSOPHY

at the

MASSACHUSETTS INSTITUTE OF TECHNOLOGY

and the

WOODS HOLE OCEANOGRAPHIC INSTITUTION

February 1992

© Portions copyright Sarah A. Green 1992
© Portions copyright American Chemical Society 1990
All rights reserved

The author hereby grants MIT permission to reproduce and
to distribute copies of this thesis document in whole or in part

Signature of Author Sarah A. G
Joint Program in Oceanography,
Massachusetts Institute of Technology/
Woods Hole Oceanographic Institution

Certified by Neil V. Blough
Neil V. Blough

and François
François M.M. Morel
Thesis Co-supervisors

Accepted by Ellen RM Druffel
Ellen R.M. Druffel
Joint Committee for Chemical Oceanography
Massachusetts Institute of Technology/
Woods Hole Oceanographic Institution

APPLICATIONS OF FLUORESCENCE SPECTROSCOPY TO ENVIRONMENTAL CHEMISTRY

by

SARAH ANITA GREEN

Abstract

The work presented in this thesis consists of three parts. The first is a photophysical study of the mechanism of fluorescence quenching by stable nitroxyl radicals, which are becoming an important analytical tool for the study of reactive transients in surface waters (1, 2). In part two, quenching of dissolved organic matter (DOM) fluorescence by nitroxides is employed to investigate the electrostatic properties of DOM in aqueous solution, with the goal of elucidating the apparent ionic strength and pH dependence of metal-fulvic acid binding constants. In part three, the intrinsic optical properties (absorbance, fluorescence, and fluorescence efficiency) of DOM are examined in a coastal region to understand how these properties vary with source, age and sunlight exposure time.

Nitroxide-fluorophore adducts were employed to investigate the mechanism by which nitroxyl radicals quench fluorescence (3). Fluorescence quantum yields and lifetimes were measured for a series of adducts, and quenching rates were shown to be quite high ($k_q \approx 10^8 - 10^{10}$ s^{-1}), even at distances of ≈12 Å. Förster or Dexter energy transfer mechanisms are unable to account for the observed rates and lack of solvent dependence in quenching. An excellent correlation is observed between k_q and the non-radiative relaxation rate. These results confirm that nitroxyl radicals are very non-selective in their quenching abilities, and suggest that the best analytical probe adducts will include a fluorophore with an appreciable non-radiative relaxation rate.

Diffusional quenching by charged and neutral nitroxides was employed to explore the electrostatic properties of fulvic (FA) and humic (HA) acids. Cationic nitroxides were found to be up to 16 times more effective than neutral analogues in quenching the fluorescence of humic materials. This result is attributed to the enhanced coulombic attraction of cations to the anionic FA or HA surface, and is interpreted as an estimate of surface electrostatic potential. Reduction of molecular charge at low pH and shielding of charge at high ionic strength (I) produced diminished enhancements, consistent with this interpretation. The potential was found to be particularly

sensitive to ionic strength, suggesting that this electrostatic effect should be of particular importance in transition zones, such as estuaries, where I increases from <5 mM to 0.7 M as river water and seawater mix. High molecular weight fractions of HA have a higher apparent surface potential than lower molecular weight fractions, indicating that larger humic molecules may have an enhanced ability to bind metal ions.

Optical properties of colored DOM may vary with source and age of the material. Absorption spectra can be characterized by their log-linearized slopes (*S*) as well as by their absolute intensities. The slope, S, is found to be much greater (steeper decrease in absorbance with increasing wavelength) for blue-water samples than for riverine and coastal samples, indicating that the visible-light absorbing fraction of DOM may be preferentially removed from surface waters. Fluorescence quantum yields were very similar for a wide variety of samples, but do show some minor differences; changes in quantum yield with excitation wavelength within a single sample are an indication of the heterogeneity of the chromophore mixture present in these materials. To better compare fluorescence data, complete excitation/emission matrix spectra were collected. When normalized to their respective absorbance spectra, these provide a full 'map' of fluorescence quantum efficiency over the entire uv-visible range. This technique is showing promise as a way to identify important spectral regions in these complex chromophore mixtures. DOM isolated on C-18 columns had somewhat different optical charateristics than whole water samples, suggesting selective isolation of absorbing material.

References

(1) Kieber, D.J., Blough N.V. (1990) Determination of carbon-centered radicals in aqueous solution by liquid chromatography with fluorescence detection *Anal. Chem.*,**62**, 2275-2283.

(2) Kieber, D.J., Blough N.V. (1990) Fluorescence detection of carbon-centered radicals in aqueous solution *Free Radical Res. Comm.*,**10**, 109-117.

(3) Green, S.A., Simpson D.J., Zhou G., Ho P.S., Blough N.V. (1991) Intramolecular quenching of excited singlet states by stable nitroxyl radicals *J. Amer. Chem. Soc.*, **112**, 7337-7346.

To the memory of my grandmother, Marjorie Benson, who endowed me with curiousity and wonder about the natural world.

We have to learn what we can, but remain mindful that our knowledge not close the circle, closing out the void, so that we forget that what we do not know remains boundless, without limit or bottom, and that what we know may have to share the quality of being known with what denies it. What is seen with one eye has no depth.

Always coming home
Ursula K. LeGuin

The Road Not Taken

Two roads diverged in a yellow wood
And sorry I could not travel both
And be one traveler, long I stood
And looked down one as far as I could
To where it bent in the undergrowth;

Then took the other, as just as fair,
And having perhaps the better claim,
Because it was grassy and wanted wear;
Though as for that the passing there
Had worn them really about the same,

And both that morning equally lay
In leaves no step had trodden black.
Oh, I kept the first for another day!
Yet knowing how way leads on to way,
I doubted if I should ever come back.

I shall be telling this with a sigh
Somewhere ages and ages hence:
Two roads diverged in a wood, and I-
I took the one less traveled by,
And that has made all the difference.

Robert Frost

Acknowledgements

Many people have contributed to the development of this thesis and of its author. The folks in Fye and Parsons Labs made me feel like part of the family in both Woods Hole and Cambridge. Scott, Bonanza, and Yankee made my commute between the two places possible; infinitely tolerant housemates made my split lifestyle possible, and even fun. In the Joint Program Education Offices, Abbie, Ronnie, Jake and John made complex multi-institutional bureaucracy nearly invisible. Pat let me be an honorary civil engineer in Parsons Lab. Dave and Larry provided lab help and company. Debbie, Chris, Kathleen, John, Andy, Ed, Gary, Luanne, Becky, Paul and numerous other JP students helped keep the world in perspective throughout it all. The Morel research group (past and present) has never failed to broaden my horizons.

Samples for chapters 4, 5, and 6 were collected with the assistance of the Captain and Crew of the R/V Iselin. Funding was supplied by the Office of Naval Research, the Environmental Protection Agency, and the National Science Foundation.

I am extremely fortunate to have had the support of an ever-expanding network of scientific sisters throughout my tenure at MIT and WHOI. Nobody could wish for a finer collection of roomates, officemates, colleagues, and, above all, friends. deb, Liz, Janet, Leah, and Lynn have all been wonderful, and continue to inspire me as I follow in their footsteps. Carol, Suzie, Elise, and Kathleen conspired to keep me fed, caffinated and coherent during several critical months. Thanks to you all; may your generosity be repaid many times over.

My advisors, Neil and François, provided me with the perfect balance of support and freedom throughout this project. Neil's enthusiasm was contagious; I can only hope that some of his scientific insight was, too. François kept me thinking about the links between the test tube and the globe, and kept the whiches in their places.

My committee members, Ellen, Mark, and Nelson lent a hand or an ear whenever they were called upon.

My family near and far has always supported my endeavors. I especially thank my father for his wisdom in allowing me to find and to follow my own path.

Rachel has remained the best of friends and has kept me going more often than she knows.

Floyd, my friend and lover, has sustained me, body and soul, from the beginning.

Table of Contents

Abstract 3

Acknowledgements 7

Table of Contents..8

List of Figures 9

List of Tables..11

Chapter One: Introduction..13

Chapter Two: Intramolecular Quenching of Excited Singlet States by Stable Nitroxyl Radicals 17
  Abstract 17
  Introduction 17
  Results and Discussion..18
  Conclusions..24
  Experimental Section 24

Chapter Three: Investigation of the Electrostatic properties of Humic Substances by Fluorescence Quenching..27
  Abstract 27
  Introduction 27
  Experimental Rationale..28
  Experimental Section 30
  Results and Discussion..30
  Pseudostatic and Kinetic Model Fits..32
  Conclusions..33
  Literature Cited..34

Chapter Four: Absorbance of waters of coastal South Florida and the Gulf of Mexico..37
  Introduction 37
  Background..39
  Methods 45
  Results..49
  Discussion 70
  Case Study: Variations in Absorbance in Oyster Bay..78
  Conclusions..90
  References..91

Chapter Five: Fluorescence of waters of coastal South Florida and the Gulf of Mexico..95
  Introduction 95
  Background..97
  Methods 105
  Results..108
  Discussion 137
  Conclusions..151
  References..153

Chapter Six: COM isolates 157
  Introduction 157
  Methods 158
  Results and Discussion 159
  Conclusions 185
  References 185

Chapter Seven: Summary 187

Appendix A: Refractive Index Correction to Absorption Spectra 191

Appendix B. Characterization of dissolved organic matter in the Black Sea by fluorescence spectroscopy 193
  references 197

Appendix C: Computer Programs 199

List of Figures

Chapter Two

fig. 1 Naphthalene derivatives 18
fig. 2 Fluorescence spectra of compound IVD in hexane 18
fig. 3 Fluorescence decays of nitroxide derivatives 18
fig. 4 Absorption spectra of TEMPOL 21
fig. 5 Quenching constants vs. spectral overlap 21
fig. 6 Hematoporphyrin derivatives 23
fig. 7 Intramolecular quenching rates vs nonradiative relaxation rates 23
fig. 8 Fluorescence and phosphorescence emission spectra of IA, IB, and ID 23

Chapter Three

fig. 1 Nitroxide quenchers 28
fig. 3 Stern-Volmer plots of FA quenching by nitroxides 31
fig. 4 Fluorescence spectra of HA size fractions 31
fig. 5 l vs ionic strength for FA and PTC 32
fig. 6 lnl vs k' for FA and PTC 33
fig. 7 Time evolution of quencher distribution 33

Chapter Four

fig. 1. Absorption spectrum of sample I-12. 40
fig. 2. Map of sampling locations around South Florida and the Gulf of Mexico 46
fig. 3. Absorption coefficients (a(300)) vs longitude for spring samples. 54
fig. 4. Absorption coefficients (a(300)) vs longitude for fall samples. 56
fig. 5. Absorption coefficients (a(300)) vs longitude for spring and fall samples. 58
fig. 6. A series of absorbance spectra plotted as the natural log of the absorption coefficient. 62
fig. 7 Example of good and not so good linear fits to log-linearized absorbance spectra. 64
fig. 8 Correlation between a(300) values measured on field and stored samples. 66
fig. 9 Comparison of spectral slopes measured on shipboard and in the lab 68
fig. 10 Absorption coefficients (a(300)) vs S on a semi-log scale. 72

fig. 11. Map of South Florida showing Oyster Bay and the Shark River Slough. 76
fig. 12 Spring and fall log-linearized absorbance spectra for waters with salinities of 0‰ and 32‰. 80
fig. 13 Normalized spectra. 84
fig. 14 Dilution transect into Oyster Bay. 88

Chapter Five

fig. 1a 3D fluorescence spectrum of a dilute aqueous solution of rhodamine B. 98
fig. 1b. Contour view of figure 1a. 100
fig. 2 Fluorescence emission spectra of sample II-50 with excitation at 337, 355, 385 nm. 110
fig. 3 3D matrix spectrum of sample II-50. 112
fig. 4 Same spectrum as in previous figure, viewed in contour. 114
fig. 5 Comparison between blue and brown water matrix spectra. 118
fig. 6 Integrated spectra of quinine sulfate standard. 120
fig. 7 Integrated spectra of sample II-50. 122
fig. 8 Integrated spectra of several coastal samples. 130
fig. 9 Integrated fluorescence vs absorption coefficient at 337 nm. 132
fig. 10 Same as previous figure, on an expanded scale. 134
fig. 11 Fluorescence vs absorption coefficient for all available data on a linear scale. 138
fig 12 Fluorescence vs absorption coefficient for all available data on a log-log scale. 140
fig. 13 Normalized matrix spectrum of II-50. 142
fig. 14 Integrated, normalized spectra of II-50. 144
fig. 15 Integrated, normalized spectra of waters in and around Oyster Bay. 146
fig. 16 Integrated, normalized spectra of various water and extracted COM samples. 148

Chapter Six

fig. 1 Log-linearized absorption spectra of acidified seawater before and after passage through a C-18 Mega-Bond Elute column. 162
fig. 2 Log-linearized absorption spectra of acidified seawater before and after passage through a C-18 Mega-Bond Elute column. 164
fig. 3 Log-linearized absorption spectra of acidified seawater before and after passage through a C-18 Mega-Bond Elute column. 166
fig. 4 Fraction of original absorbance retained (R(l)) as a function of wavelength. 168
fig. 5 Fraction of original absorbance retained (R(l)) as a function of wavelength. 170
fig. 6 Integrated fluorescence of acidified water (sample II-50) before and after passage through a C-18 column 174
fig. 7 3D fluorescence spectrum of extract 4 reconstituted into oligotrophic seawater. 178
fig. 8 Absorbance normalized 3D fluorescence spectrum of extract 4 reconstituted into oligotrophic seawater. 180
fig. 9 Integrated, normalized excitation spectra of riboflavin compared with spectrum of extract 4. 182
fig. 10 Integrated, normalized emission spectra of riboflavin compared with spectrum of extract 4. 182

Appendix B.

fig. 1 Uncorrected EEM spectra for Black Sea concentrates 196
fig. 2 Corrected EEM spectra for Black Sea concentrates. 197
fig. 3 Contour plots of EEM spectra 197

List of Tables

Chapter Two

Table I. Absorption and fluorescence maxima of nitroxide derivatives 19
Table II. Fluorescence lifetimes and quantum yields of nitroxide derivatives 19
Table III. Quenching rate constants 20
Table IV. Nitroxide-fluorophore distances 20
Table V. Förster energy transfer rates 22
Table VI. Electron transfer driving forces 22

Chapter Three

Table I. Fluorescence maxima and quenching constants of FA and HA fractions 31

Chapter Four

Table I. Absorption coefficients, slopes and positions of surface samples collected in May 1991 50
Table II. Absorption coefficients, slopes, and positions of surface samples collected in August 1991 52
Table III. a(300) and S values for 0‰ and 32‰ salinity samples. 82

Chapter Five

Table I. Peak maxima in matrix spectra. 116
Table II Quantum Yields for samples collected in May 1991 124
Table III Quantum Yields for samples collected in August 1991 125
Table IV. Absorption coefficients, integrated fluorescence, and quantum yields for extracts reconstituted into oligotrophic seawater. 127
Table V. Quantum yields of Sargasso Sea isolates. 127

Chapter Six

Table I. Extraction efficiencies measured by a(280). 160
Table II. S values for extracts and unconcentrated seawater. 176

Appendix B

Table I. Fluorescence maxima for natural water samples 195

Chapter One: Introduction

Fluorescence techniques are widely applicable to the elucidation of chemical and environmental questions. On a scale of ångströms, precise measurement of fluorescence parameters can provide detailed information about molecular interactions, and on scales of many kilometers, fluorescence detected by remote sensors can provide clues about the global cycle of organic carbon. The work described herein consists of three parts which span much of this range. The first studies intramolecular perturbations to fluorescence emission at the molecular level. The second employs fluorescence to examine intermolecular processes and to consider the effects of solvent environment on bimolecular interactions. In part three, which consists of chapters four through six, the intrinsic optical properties (absorbance, fluorescence, and fluorescence efficiency) of dissolved organic matter are examined in a coastal region to understand how they may vary with source, age and sunlight exposure time.

Chapter two. Nitroxide-fluorophore adducts are becoming an important analytical tool for the trapping of carbon-centered radicals (*1, 2*). Their use promises to make possible the identification of photochemically-generated reactive transients in surface waters. In order to facilitate the futher development of such probes, and improve our ability to predict any possible limitations and interferences, their photophysical properties must be thoroughly understood. In chapter two of this thesis naphthalene-nitroxide adducts were employed to investigate the mechanism by which nitroxyl radicals quench fluorescence (*3*). Fluorescence quantum yields and lifetimes were measured for a series of adducts, and quenching rates were shown to be extremely high ($k_q \approx 10^8$–10^{10} s^{-1}), even at distances of ≈12 Å. Förster or Dexter energy transfer mechanisms are unable to account for the observed rates and the lack of solvent dependance in quenching. Electron exchange induced relaxation was determined to be the most probable quenching mechanism. A good correlation was observed between k_q and the non-radiative relaxation rate. These results confirm that nitroxyl radicals are very non-selective in their quenching abilities, and suggest that the best analytical probe adducts will include a fluorophore with an appreciable non-radiative relaxation rate.

Chapter three. An important aspect of humic and fulvic acid geochemistry is the ability of these materials to influence metal ion speciation in natural waters. The modeling of these interactions has been hampered by the ill-defined chemical nature of humic substances. The most useful models would predict complex titration data on the basis of a few measurable "average" chemical parameters. A current approach incorporates the electrostatic interaction between metal ions and humic macromolecules to better predict the effects of ionic strength and pH on metal binding (*4*). The goal of the second chapter of this thesis was to provide an experimental basis for these models.

Diffusional quenching by charged and neutral nitroxides was employed to explore the electrostatic properties of fulvic (FA) and humic (HA) acids. Cationic nitroxides were found to be up to 16 times more effective than neutral analogues in quenching the fluorescence of humic materials. This result is attributed to the enhanced coulombic attraction of cations to the anionic FA or HA surface, and is interpreted as an estimate of surface electrostatic potential. Reduction of molecular charge at low pH and shielding of charge at high ionic strength (I) produced diminished enhancements, consistent with this interpretation. The potential was found to be especially sensitive to ionic strength, suggesting that this electrostatic effect should be of particular importance in transition zones, such as estuaries, where I increases from <5 mM to 0.7 M as river water and seawater mix. High molecular weight fractions of HA have a higher apparent surface potential than lower molecular weight fractions, indicating that larger humic molecules may have an enhanced ability to bind metal ions.

Chapter four. Optical properties of colored dissolved organic matter (COM) are of interest both because they may provide additional clues as to the sources and sinks of this material, and because of the interferences that can be caused by non-living light-absorbing material in remote estimates of phytoplankton populations. Absorbance and fluorecence characteristics of COM may vary with its source and age, but data are still too scarce to identify systematic variations in natural samples. In this chapter a survey was undertaken of optical spectra of water samples and of isolated organic matter from coastal Florida and the Gulf of Mexico. Absorption spectra were characterized by their log-linearized slopes (*S*) as well as by their absolute intensities. The slope, *S*, is found to be much greater (steeper decrease in absorbance with increasing wavelength) for blue-water samples than for riverine and coastal samples, indicating that the visible-light absorbing fraction of DOM may be preferentially removed from surface waters.

Chapter five. Complete fluorescence excitation/emission matrix spectra were collected for an array of natural samples. When normalized to their respective absorbance spectra, these provide a full 'map' of fluorescence quantum efficiency over the entire uv-visible range. This technique is showing promise as a way to identify important spectral regions in these complex chromophore mixtures. Fluorescence quantum yields show minor differences among samples, but exhibited a remarkably small range (1.2±0.1%) for a wide variety of samples. Changes in quantum yield with excitation wavelength within a single sample are an indication of the heterogeneity of the chromophore mixture present in these materials.

Chapter six. Chapter six examines some of the problems inherent in deriving optical infomation for natural water samples from material isolated on C-18 columns. DOM isolated on C-18 columns had different optical charateristics than whole water samples, suggesting selective isolation of light absorbing material.

Chapter seven and appendices. Chapter seven briefly summarizes the results of the previous chapters and offers some ideas for future work on these themes. Appendix A explains the correction applied to absorbance spectra of seawater as a result of its refractive index. A paper by Coble, et.al. (5) on fluorescence properties of Black Sea samples is provided in appendix B. Appendix C compiles the computer programs written to collect and manipulate 3D fluorecence spectra.

References

(1) Kieber, D.J. and N.V. Blough (1990). Determination of carbon-centered radicals in aqueous solution by liquid chromatography with fluorescence detection. *Anal. Chem.*, **62**: 2275-2283.

(2) Kieber, D.J. and N.V. Blough (1990). Fluorescence detection of carbon-centered radicals in aqueous solution. *Free Radical Res. Comm.*, **10**: 109-117.

(3) Green, S.A., D.J. Simpson, G. Zhou, P.S. Ho and N.V. Blough (1990). Intramolecular quenching of excited singlet states by stable nitroxyl radicals. *J. Amer. Chem. Soc.*, **112**: 7337-7346.

(4) Bartschat, B., S.E. Cabaniss, and F. M. M. Morel (1992),*Environ. Sci. Technol.* **26**, 284-294.

(5) Coble, P.G., S.A. Green, N.V. Blough and R.B. Gagosian (1990). Charaterization of dissolved organic matter in the Black Sea by fluorescence spectroscopy. *Nature*, **348**: 432-435.

Reprinted from the Journal of the American Chemical Society, 1990, *112* p. 7337-7346.
Copyright © 1990 by the American Chemical Society and reprinted by permission of the copyright owner.

Chapter Two Intramolecular Quenching of Excited Singlet States by Stable Nitroxyl Radicals

S. A. Green,[†] D. J. Simpson,[†,§] G. Zhou,[‡] P. S. Ho,[‡] and N. V. Blough[*,†]

Contribution from the Department of Chemistry, Woods Hole Oceanographic Institution, Woods Hole, Massachusetts 02543, and Department of Biochemistry and Biophysics, Oregon State University, Corvalis, Oregon 97331. *Received March 15, 1990*

Abstract: Absorbance and steady-state and time-resolved fluorescence measurements were employed to examine the mechanism(s) of excited singlet state quenching by nitroxides in a series of nitroxide–fluorophore adducts. This work establishes the following: (1) the absorption and emission energies of the fluorophores are unaffected by the presence of the nitroxide substituent(s), and the residual emission that is observed from the adducts arises from the locally excited singlet of the fluorophore, not from charge recombination; (2) rate constants for intramolecular quenching by the nitroxides (k_q) are high (10^8–10^{10} s^{-1}) and decrease significantly with increasing nitroxide to fluorophore distance—however, relatively high rates of quenching ($>10^8$ s^{-1}) are observed over distances as great as 12 Å; (3) *Förster energy transfer does not contribute significantly* to the quenching due to the low values for the spectral overlap integrals; (4) the k_q's do not increase proportionally to the solvent-dependent increases in the Dexter overlap integral, indicating that energy transfer by the Dexter mechanism is not responsible for the quenching; (5) the values of k_q show no obvious correlation with the calculated free energies for photoinduced electron transfer, suggesting that this quenching pathway is also unimportant; (6) for hematoporphyrin–nitroxide adducts, which contain a fluorophore whose singlet energy is below that of the first excited state energy of the nitroxide (thus precluding energy transfer), significant rates of quenching are still observed; (7) for compounds with similar nitroxide–fluorophore distance, an approximately linear correlation is observed between the k_q's of the paramagnetic compounds and the nonradiative rate constants of the diamagnetic reference compounds, suggesting that the nitroxide moiety catalyses a preexisting nonradiative pathway in the fluorophore. These results indicate that the quenching arises through electron exchange which causes relaxation of the (local) singlet state to the triplet and/or ground state of the fluorophore.

Introduction

Diffusional quenching by stable nitroxyl radicals of excited singlet,[1] doublet,[2] and triplet[1d,f,3-10] states and of excimers[11] has been studied extensively over the past 20 years. The goal of much of this work has been to understand the mechanism(s) through which excited states are quenched by paramagnetic species. Recently however, fluorescence quenching by nitroxides has also become an important tool with which to probe the structural and dynamical properties of membranes[12] and micelles.[13]

While it has been generally accepted that nitroxide quenching of singlet states can result from an electron exchange-induced[14] intersystem crossing to the triplet[1b,e] or internal conversion to the ground state,[1e-8] significant contributions to the quenching may also arise from charge[1f] and/or energy transfer.[1a,12d] Green et al.[1b] argued that charge (electron) transfer is unimportant owing to a lack of solvent dependence of the quenching rate constant. However, as noted by Chattopadhyay et al.,[1f] the quenching occurs at the diffusion limit and thus may not be differentiated by solvent polarity.[15] Green et al.[1b] also suggested that Förster energy transfer[16] is insignificant because of the low extinction coefficients of the nitroxides in the 400–550 nm spectral region. Recent work by Puskin et al.[12d] suggests that energy transfer can be important and, in some cases, can extend the quenching radius to as much as 10 Å, approximately twice the interaction distance originally calculated by Green et al.[1b] Furthermore, energy transfer by electron exchange[17] cannot be excluded a priori for compounds having singlet energies greater than the lowest excited state energy of the nitroxide (~2.6 eV for the piperidinyl nitroxides).

Until recently, information on the efficiency of intramolecular quenching of excited states by nitroxide was unavailable. We have shown that intramolecular quenching of excited singlets is highly efficient[18] and that covalently linked, nitroxide-fluorophore adducts can be employed as very sensitive optical probes of radical/redox reactions.[18-21] These adducts also offer a means of studying the mechanism(s) of nitroxide quenching in more detail and of establishing the distance dependence and possible importance of "through-bond"[15] vs "through-space" interactions in the quenching. This information is essential for the construction of better optical

---

[*] To whom correspondence should be addressed.

[†] Woods Hole Oceanographic Institution.

[‡] Oregon State University.

[§] Present address: Life Sciences Division, Los Alamos National Laboratory, Los Alamos, NM 87545

(1) (a) Buchachenko, A. L.; Khloplyankina, M. S.; Dobryakov, S. N. *Opt. Specktrosk.* (USSR) 1967, *22*, 554–556. (b) Green, J. A.; Singer, L. A.; Parks, J. H. *J. Chem. Phys.* 1973, *58*, 2690–2695. (c) Darmanyan, A. P.; Tatikolov, A. S. *J. Photochem.* 1986, *32*, 157–163. (d) Watkins, A. R. *Chem. Phys. Lett.* 1974, *29*, 526–528. (e) Kuzmin, V. A.; Tatikolov, A. S. *Chem. Phys. Lett.* 1977, *51*, 45. (f) Chattopadhyay, S. K.; Das, P. K.; Hug, G. L. *J. Am. Chem. Soc.* 1983, *105*, 6205–6210. (g) Yee, W. A.; Kuzmin, V. A.; Kliger, D. S.; Hammond, G. S.; Twarowski, A. J. *J. Am. Chem. Soc.* 1979, *101*, 5104.

(2) Samanta, A.; Bhattacharyya, K.; Das, P. K.; Kamat, P. V.; Weir, D.; Hug, G. L. *J. Phys. Chem.* 1989, *93*, 3651.

(3) (a) Singer, L. A.; Davis, G. A. *J. Am. Chem. Soc.* 1967, *89*, 158. (b) Singer, L. A.; Davis, G. A.; Muralidharan, V. P. *J. Am. Chem. Soc.* 1969, *91*, 897.

(4) (a) Yang, N. C.; Loeschen, R.; Mitchell, D. *J. Am. Chem. Soc.* 1967, *89*, 5465. (b) Chapman, O. L.; Koch, T. H.; Klein, F.; Nelson, P. J.; Brown, E. L. *J. Am. Chem. Soc.* 1968, *90*, 1657.

(5) (a) Schwerzel, R. E.; Caldwell, R. A. *J. Am. Chem. Soc.* 1973, *95*, 1382. (b) Caldwell, R. A.; Schwerzel, R. E. *J. Am. Chem. Soc.* 1972, *94*, 1035–1037.

(6) Gijzeman, O. L. J.; Kaufman, F.; Porter, G. *J. Chem. Soc., Faraday Trans. 2* 1973, *69*, 727–737.

(7) Watkins, A. R. *Chem. Phys. Lett.* 1980, *70*, 262.

(8) (a) Kuzmin, V. A.; Tatikolov, A. S.; Borisevich, Y. E. *Chem. Phys. Lett.* 1978, *53*, 52. (b) Kuzmin, V. A.; Tatikolov, A. S. *Chem. Phys. Lett.* 1978, *53*, 606. (c) Borisevich, Y. E.; Kuzmin, V. A.; Renge, I. V.; Darmanyan, A. P. *Izv. Akad. Nauk. SSSR Ser. Khim.* 1981, 9, 2014. (d) Borisevich, Y. E.; Kuzmin, V. A.; Kokorin, A. I.; Sennikov, G. P.; Novozhilova, G. A.; Shapiro, A. B. *Izv. Akad. Nauk. SSSR Ser. Khim.* 1981, 9, 2019.

(9) Kuzmin, V. A.; Kliger, D. S.; Hammond, G. S. *Photochem. Photobiol.* 1980, *31*, 607.

(10) Chattopadhyay, S. K.; Kumar, C. V.; Das, P. K. *J. Photochem.* 1985, *30*, 81.

(11) Green, J. A.; Singer, L. A. *J. Am. Chem. Soc.* 1974, *96*, 2730.

(12) (a) London, E. *Mol. Cell. Biochem.* 1982, *45*, 181 and references cited therein. (b) Chattopadhyay, A.; London, E. *Biochemistry* 1987, *26*, 39. (c) Winiski, A. P.; Eisenberg, M.; Langner, M.; McLaughlin, S. *Biochemistry* 1988, *27*, 386. (d) Puskin, J. S.; Vistnes, A. I.; Coene, M. T. *Arch. Biochem. Biophys.* 1981, *206*, 164.

(13) (a) Atik, S. S.; Singer, L. A. *J. Am. Chem. Soc.* 1978, *100*, 3234. (b) Atik, S. S.; Kwan, C. L.; Singer, L. A. *J. Am. Chem. Soc.* 1979, *101*, 5696. (c) Atik, S. S.; Singer, L. A. *Chem. Phys. Lett.* 1978, *59*, 519. (d) Scaiano, J. C.; Paraskevopoulos, C. I. *Can. J. Chem.* 1984, *62*, 2351.

(14) (a) Hoytink, G. J. *Acc. Chem. Res.* 1969, *2*, 114. (b) Birks, J. B. *Photophysics of Aromatic Molecules*, Wiley-Interscience: London, 1970; pp 492–517. (c) Turro, N. J. *Modern Molecular Photochemistry*, Benjamin-Cummings Pub. Co. Inc.: Menlo Park, CA, 1978; Chapter 6.

0002-7863/90/1512-7337$02.50/0 © 1990 American Chemical Society

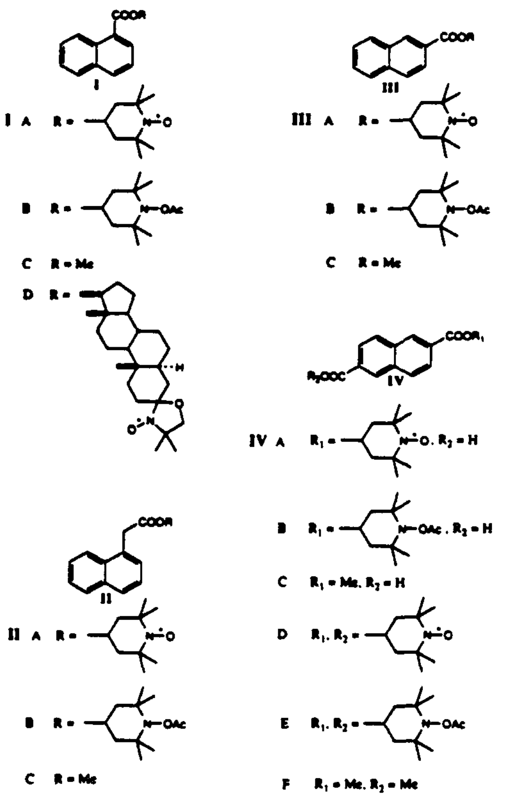

Figure 1. Naphthalene derivatives examined in this study.

radical sensors,[18-20] for a more complete analysis of nitroxide quenching in biophysical studies,[12,13] and for an understanding of the possible influence of stable or transient radicals on excited states in biological and chemical systems.

In this study, we examine the photophysical properties of a number of nitroxide-fluorophore adducts and their diamagnetic analogues. By employing compounds having fluorophores with differing singlet energies and a range of nitroxide-fluorophore distances, we attempt to assess the relative contributions of energy transfer, electron transfer, and electron exchange induced relaxation to the intramolecular quenching of singlet states by nitroxides.

Results and Discussion

A. Absorption, Excitation, and Emission Spectra. Table I summarizes the absorption and emission energies of I-IV (Figure 1) in various solvents. In water, methanol, acetonitrile, dioxane, and hexane, the absorption spectra of the nitroxide-fluorophore adducts were indistinguishable from the sum of the individual spectral contributions of the fluorophore and nitroxide substituents. Other than the loss of the weak nitroxide contribution in the visible (430-480 nm, $\epsilon \approx 10-13$ M^{-1} cm^{-1}) and ultraviolet (~246 nm, $\epsilon \approx 2 \times 10^3$ M^{-1} cm^{-1}), the spectra of the *O*-acetyl and methyl ester derivatives (Figure 1) were identical with those of the corresponding nitroxides. No evidence for optical charge transfer bands or enhanced ground to triplet absorption[14] by the fluorophore could be found in the spectra of the nitroxide adducts. While the absorption spectra of the fluorophores were largely insensitive to solvent polarity, the lowest energy band ($n - \pi^*$) of the nitroxides[22] shifted substantially to the blue with increasing solvent polarity as previously noted.[23] The influence of this shift on singlet state quenching will be addressed below (section D).

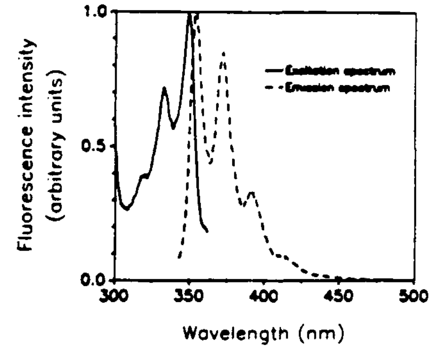

Figure 2. Fluorescence excitation and emission spectra of IVD in hexane.

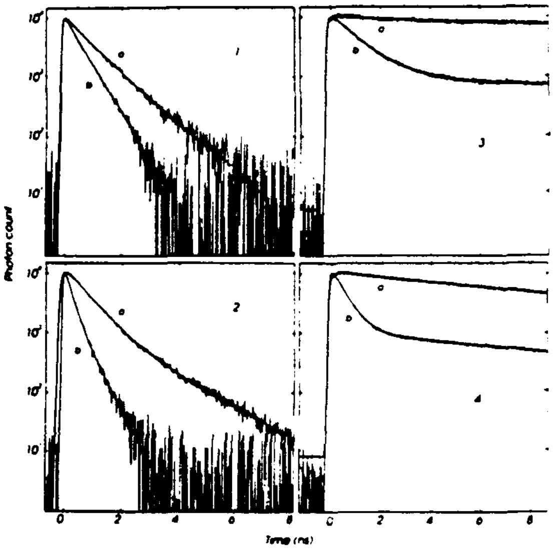

Figure 3. Fluorescence decays of nitroxide adducts (b) as compared to diamagnetic analogues (a): (1) ID and IB in acetonitrile; (2) ID and IB in hexane; (3) IIA and IIB in acetonitrile; and (4) IIIA and IIIB in acetonitrile. Excitation wavelength was 295 nm. Emission was monitored at the peak maximum for each compound (see Table I).

The fluorescence excitation spectra of the nitroxide adducts matched the absorption spectra of the fluorophore substituents and were indistinguishable from the excitation spectra of the corresponding diamagnetic derivatives.

The line shapes of the emission spectra were identical for the nitroxide adducts and the corresponding diamagnetic derivatives and generally showed a mirror-image relationship to the excitation spectra (Figure 2). With increasing solvent polarity, identical red shifts in the emission maxima were observed for the nitroxide

---

(15) (a) Closs, G. L.; Calcaterra, L. T.; Green, N. J.; Penfield, K. W.; Miller, J. R. *J. Phys. Chem.* 1986, *90*, 3673. (b) Oevering, H.; Verhoeven, J. W.; Paddon-Row, M. N.; Cotsaris, E.; Hush, N. S. *Chem. Phys. Lett.* 1988, *143*, 488. (c) Kroon, J.; Oliver, A. M.; Paddon-Row, M. N.; Verhoeven, J. W. *J. Am. Chem. Soc.* 1990, *112*, 4868.

(16) Förster, T. *Ann. Phys.* (*Leipzig*) 1948, *2*, 55.

(17) Dexter, D. L. *J. Chem. Phys.* 1953, *21*, 836.

(18) Blough, N. V.; Simpson, D. J. *J. Am. Chem. Soc.* 1988, *110*, 1915.

(19) (a) Kieber, D. J.; Blough, N. V. *Anal. Chem.*, in press. (b) Kieber, D. J.; Blough, N. V. *Free Radical Res. Commun.* 1990, *10*, 109.

(20) Gerlock, J. L.; Zacmanidis, P. J.; Bauer, D. R.; Simpson, D. J.; Blough, N. V.; Salmeen, I. T. *Free Radical Res. Commun.* 1990, *10*, 119.

(21) Blough, N. V. *Environ. Sci. Technol.* 1988, *22*, 77.

(22) (a) Kikuchi, O. *Bull. Chem. Soc. Jpn.* 1969, *42*, 47. (b) Salotto, A. W.; Burnelle, L. *J. Chem. Phys.* 1970, *53*, 333.

(23) (a) Briere, R.; Lemaire, H.; Rassat, A. *Bull. Soc. Chim. Fr.* 1965, 3273. (b) Mukerjee, P.; Ramachandran, C.; Pyter, R. A. *J. Phys. Chem.* 1982, *86*, 3189-3197.

Table I. Absorption and Fluorescence Maxima of I–IV[a]

	absorbance in methanol		fluorescence emission maxima, nm			
compd	abs max, nm	ϵ, M^{-1} cm^{-1}	hexane	acetonitrile	methanol	water
series I	222	4.2×10^4	332	361	369	390
	300	7.1×10^3	343			
			358			
series II[b]	228		328	326	326	325
	274		340	335	337	335
	284		318	353		
	294		352	371		
series III	242	1.9×10^4 (8.9×10^4)	336	344	364	376
	276	7.9×10^3	352	359	351	
	284	9.6×10^3 (1.3×10^4)	367	375		
	296	6.8×10^3 (9.7×10^3)	388			
	324	1.6×10^3 (2.2×10^3)				
	338	1.9×10^3 (2.7×10^3)				
series IVA–C	248	7.0×10^4	355	359	359	360
	288	1.2×10^4	373	377	374	381
	298	1.1×10^4	393	397	396	
	334	1.8×10^3	416	426		
	348	2.0×10^3				
series IVD–F	246	8.3×10^4 (8.4×10^4)	354	360	363	
	286	1.4×10^4	372	378	380	
	296	1.4×10^4 (1.3×10^4)	391	400		
	338	2.1×10^3 (2.3×10^3)		425		
	352	2.4×10^3 (2.8×10^3)				

[a] Absorption spectra and extinction coefficients measured in methanol. Values in parentheses are extinction coefficients for methyl esters (IIIC and IVF) for which the coefficient differs slightly from that of the nitroxide derivative. The nitroxide contributions to the absorption of I–IVA and I,IVD are described in the text and Figure 4. [b] Series II compounds were isolated as oils; extinction coefficients were not measured.

Table II. Fluorescence Lifetimes and Quantum Yileds of I–IV[a]

	hexane		acetonitrile		methanol[b]		water[c]	
	τ, ns	ϕ	τ, ns	ϕ	τ, ns	ϕ	τ, ns	ϕ
Series I								
A	(0.021)[d]	0.002	(0.033)[d]	0.004	(0.054)[d]	0.006	0.10	0.013 (0.009)[d]
B	0.73	0.05	1.7	0.22	2.8	0.31	7.1	0.66
C	1.00	0.06	1.8	0.20	2.9	0.28	7.3	0.57
D	0.48	0.03	1.1	0.14	1.1	0.12	-	-
Series II								
A	1.09	0.004 (0.006)	1.1	0.006 (0.004)	0.81	0.013 (0.004)	0.40	0.008 (0.002)
B	37.0	0.22	33.7	0.13	43.1	0.20	28.3	0.17
C	49.2	0.22		0.16	43.3	0.21		0.17
Series III								
A	0.52	0.017 (0.019)	0.50	0.016 (0.011)	0.65	0.026 (0.019)	0.46	0.031 (0.012)
B	9.0	0.33	12.4	0.28	11.0	0.32	10.9	0.28
C	9.8	0.38		0.30	11.0	0.30		0.32
Series IV								
A	0.29	0.009 (0.008)	0.33	0.013 (0.012)	0.54	0.010 (0.014)	0.70	0.029 (0.016)
B	14.1	0.40	13.2	0.52	1.1	0.028	12.2	0.28
C	11.5	0.48	13.7		1.2	0.046	12.3	
D	0.21	0.005 (0.006)	0.22	0.006 (0.007)	0.27	0.008 (0.009)	-	-
D	15.3	0.46	13.8	0.46	13.9	0.45	-	-
F	16.1	0.54	15.0	0.50	14.1	0.40	-	-

[a] Values in parentheses were calculated from eq 3. [b] Values in methanol are ~30% lower than those previously reported[18] due to correction of undocumented normalization and conversion routines in the SLM-Aminco software. [c] "Water" measurements for IVA–C were done in pH 8, 50 mM phosphate buffer; ID and IVD–F are not water soluble. [d] Calculated lifetimes only are reported for IA, except in water, because they were below the time resolution of the instrument. Values were calculated from quantum yields of IA and lifetimes of IB by using eq 3.

and diamagnetic adducts of a given substitution. These results indicate that the residual emission from the nitroxide adducts is arising from the same locally excited singlet state of the fluorophore substituent as in the diamagnetic derivatives and is not produced through charge recombination.[24] No evidence for exciplex emission from the paramagnetic adducts could be found in either polar (acetonitrile) or nonpolar (hexane) solvents.

B. Quantum Yield and Lifetime Measurements. While the presence of the nitroxyl radical substituent(s) did not influence the absorption and emission energies of the fluorophores in the adducts, the fluorescence quantum yields and lifetimes of the nitroxide adducts were reduced substantially relative to their corresponding diamagnetic derivatives in both polar and nonpolar solvents (Table II, Figure 3). The fluorescence decay of the nitroxide adducts could be well-fit to a sum of two exponentials but was dominated by the short-lived component (Figure 3). The small, long-lived component usually represented ≤5% of the total amplitude. We attribute this component to minor diamagnetic contaminants, on the basis of assessments of compound purity.

With few exceptions, the fluorescence decay of the diamagnetic derivatives could be fit as a single exponential process (Figure 3). The *O*-acetyl and methyl ester derivatives of a given substitution showed very similar lifetimes and quantum yields (Table II). These results indicate that the rate constants for radiative and nonradiative decay of the singlet do not differ significantly between the *O*-acetyl and the methyl ester derivatives (Figure 1). This leads us to conclude that, unlike the situation for aliphatic and aromatic amines,[25] intramolecular quenching (via electron

---

(24) Kosower, E. M.; Huppert, D. *Ann. Rev. Phys Chem.* **1986**, *37*, 127.

(25) Davidson, R. S. *Adv. Phys. Org. Chem.* **1983**, *19*, 1a.

Table III. Rate Constants for Intramolecular Quenching in the Naphthalene–Nitroxide Adducts[a]

	$k_q \times 10^{-9}$ s^{-1}			
compd	hexane	acetonitrile	methanol	water
IA	45	30	18	9.7
ID	0.7 ± 0.3	0.3 ± 0.1	0.5 ± 0.1	-
IIA	0.9	0.9	1.2	2.5
IIIA	1.8	1.9	1.4 ± 0.2	2.1
IVA	3.4	3.0	0.9	1.3
IVD	4.7	4.5 ± 0.5	3.7 ± 0.4	-

[a] Rate constants were calculated from fluorescence lifetimes (or quantum yields, in the case of compound IA, see Table II) by using eq 4. Uncertainties are ±10% except where otherwise noted.

transfer) by the hindered, O-substituted hydroxylamines is unimportant. Preliminary work on other O-substituted hydroxylamines is consistent with this conclusion.[19] In contrast, the unsubstituted hydroxylamine does appear to quench partially.[19,26]

The steady-state and time-resolved fluorescence measurements of the paramagnetic and diamagnetic forms can be related by

$$\phi_d = \frac{k_r}{k_r + k_{nr}} \qquad k_r + k_{nr} = \frac{1}{\tau_d} \tag{1}$$

$$\phi_p = \frac{k_r}{k_r + k_{nr} + k_q} \qquad k_r + k_{nr} + k_q = \frac{1}{\tau_p} \tag{2}$$

where $\phi_d(\phi_p)$ and $\tau_d(\tau_p)$ are the quantum yields and lifetimes of the diamagnetic (paramagnetic) compounds, respectively, k_r and k_{nr} are the rate constants for radiative and nonradiative decay of the diamagnetic compounds, and k_q is the intramolecular (nonradiative) quenching rate constant attributable to the nitroxide moiety. If k_r and k_{nr} are unaltered by the presence of the nitroxide, then

$$\phi_d/\phi_p = \tau_d/\tau_p \tag{3}$$

$$k_q = 1/\tau_p - 1/\tau_d \tag{4}$$

The measured ratios τ_d/τ_p and ϕ_d/ϕ_p are equal within the uncertainties (Table II), indicating that this condition applies. Errors are largest in the determination of ϕ_p, since traces of highly fluorescent impurities can produce significant overestimates of such low quantum yields, leading to low ϕ_d/ϕ_p ratios. For this reason, rate constants for intramolecular quenching, k_q (Table III) were calculated from the lifetime data employing eq 4, except in the case of compound IA where lifetimes were too short to be resolved by the instrument. For this compound the expected lifetimes were computed from eq 3 with use of the quantum yield data and the lifetime of the diamagnetic *O*-acetyl (IB). Lifetime data show <3% of a long-lived component for IA.[27]

In aprotic solvents such as acetonitrile and hexane, k_q increased from $\approx 10^8$ to 10^{10} s^{-1} in the order ID < IIA < IIIA < IVA < IA. This sequence reflects not only the differences in nitroxide–fluorophore distance but also the type, number and position of the naphthalene–nitroxide linkage(s) (vide infra). With the exception of compounds IA and ID, no significant differences were observed between k_q's measured in polar (acetonitrile) and nonpolar (hexane) solvents. Surprisingly, the k_q's for compounds IA and ID actually increased slightly with decreasing solvent polarity (Table III).

C. Dependence of k_q on Distance, Linkage Position, and Type. Because the distance and orientation of the nitroxide with respect to the fluorophore are not rigidly fixed in these compounds, the molecular mechanics program AMBER[28] was employed to search for the conformations of IA, IIA, and IIIA most likely to exist in solution. The strategy for this search is described in the Experimental Section.

Table IV. Total Energies, Nitrogen Atom–Naphthalene Ring Distances, and κ^2 for Lowest Energy Conformations of IA, ID, IIA, and IIIA

compd	energy,[a] kcal/mol	distance[b] R, Å	κ^2/[c]
IA	22.25	8.24	0.18
	22.30	8.26	0.11
	22.39	8.25	0.12
av[d]	**22.31**	**8.25**	**0.14**
ID[e]		12.2	
IIA	14.64	6.55	0.01
	15.01	7.81	0.03
	15.02	7.41	0.16
	15.18	7.94	0.07
	15.42	8.32	0.21
	15.47	8.66	2.01
	15.54	8.83	0.01
	15.80	7.59	0.17
av[f]	**15.12**	**7.59**	**0.26**
IIIA	16.67	9.04	0.21
	16.68	8.94	0.18
	16.74	9.04	0.33
av[d]	**16.70**	**9.01**	**0.24**

[a] Energy for each conformation is the sum of contributions for bond lengths and angles, and dipole and van der Waals interactions. [b] Distances were measured from the nitrogen atom to the center of the C9–C10 bond of the naphthalene ring. [c] κ^2 was calculated[29] from the emission (naphthalene) and absorption (nitroxide) dipoles. Emission dipoles for 1- and 2-substituted naphthaldehydes (^1L_b transition) were obtained from ref 40. The absorption dipole for the nitroxide group was taken to be perpendicular to the NO bond and lying in the CNC plane, on the basis of the local C_s symmetry of the nitroxide group and the analogy to the $n \rightarrow \pi^*$ transition in carbonyls.[15b,22,23,41] $0 < \kappa^2 < 4$, allowed range. [d] *Numerical* averages of the energies, distances, and κ^2 for the conformations of each compound. [e] Distance for ID was estimated from molecular models by using the same relative orientation of the carbonyl group as that calculated for the lowest energy conformation of IA. [f] Averages for IIA were weighted according to the population in the lowest energy conformation (E = 14.64 kcal/mol) compared with the other seven states (E_{av} = 15.35 kcal/mol). The ratio of population in states 2–8 relative to state 1 is estimated by $N_{(2-8)}/N_{(1)} = g_{(2-8)}/g_{(1)} \times \exp(-\Delta E/RT) = 7 \exp(-(15.35 - 14.64)/RT) = 2.11$.

IA and IIIA were each found to have three unique minimal energy conformations (Table IV). However, the average energy of the low-energy conformations of IIIA was 5.6 kcal/mol lower than that of IA. The higher overall energy of IA can be attributed to a sterically induced distortion of the naphthalene ring and subsequent effects on the dihedral angles within the ring and between the ring and the carboxylate group. This distortion was a result of unfavorable steric interactions between the carbonyl oxygen of the carboxyl group and the hydrogen at position 8 on the naphthalene ring. A rotation of the naphthalene ring by 180° relative to the carboxylate group resulted in greater steric interactions and a more distorted structure. Neither of the other compounds studied displayed this distortion.

In contrast to IA and IIIA, IIA exhibited eight low-energy conformations (Table IV). A single conformer exhibited both the lowest energy and shortest ring to nitrogen distance. Seven other conformers had an average energy that was only 0.7 kcal/mol higher. Because these conformers constituted a large set of thermally accessible states, we were forced to include them in the calculation of average distances. The energies and center-to-center distances of the energetically significant conformations of IA, IIA, and IIIA are summarized in Table IV. Coordinates for each of these conformations are provided in the supplementary material.

The fact that the short-lived fluorescence component of each of these three compounds could be well-fit as a single exponential decay suggests that these conformers interconvert rapidly on the time scale of the quenching (nanoseconds to sub-nanoseconds) or that conformations populated during the lifetime of the singlet do not differ significantly in their ability to quench the singlet state.

The Förster orientation factor, κ^2, was calculated for the conformers of IA–IIIA (Table IV) as a fairly simple means to com-

---

(26) Blough, N. V.; Kieber, D. J. Work in progress.

(27) A long-lived component present at a level of 3% could contribute as many as 50% of the photons to the measured quantum yield. This would result in an *underestimate* of k_q by a factor of 2. Quenching constants reported here, therefore, represent a lower limit for quenching rates in IA

(28) Weiner, P. K.; Kollmann, P. A. *J. Comput. Chem.* 1981, *2*, 287

pare the relative orientations of naphthalene and nitroxide groups. The absence of large variations in κ^2 suggests that differences in the relative orientation of the two groups is probably not the primary factor controlling the variations in quenching rates among these compounds.

The rates of energy transfer (Förster or Dexter) and electron transfer have well-defined distance dependencies. While the rate of Förster energy transfer follows an R^{-6} distance dependence,[14,29] the rates of Dexter transfer and electron transfer are expected to decline exponentially with distance.[15,17,30,31] However, the quenching rates observed in aprotic solvents bear no simple relationship to the nitroxide–naphthalene distances (Tables III and IV), as is illustrated by the following points: (1) while a comparison between IA and ID suggests that increasing R by 4 Å causes k_q to decrease by about 2 orders of magnitude, simply shifting the site of substitution from the α(IA) and β(IIIA) position on the naphthalene ring produces an ~20-fold decrease in k_q, although the values of R for IA and IIIA differ by only 0.76 Å; (2) insertion of a methylene group into the linkage at the α position (IIA) decreases k_q by ~40-fold, although the greater flexibility of this linkage allows a shorter R than either IA or IIIA. As we show below, the rather large variations in k_q observed for compounds having similar nitroxide–naphthalene distances (e.g. IA–IVA) cannot be explained by the differences in the singlet energy of the naphthalenes or by variations in the free energy for photoinduced electron transfer. Instead these variations appear to result from a relationship between k_q and the nonradiative rate constant of the parent (diamagnetic) compound. The presentation and interpretation of this relationship is provided in section D 3.

D. Mechanisms of Quenching. Several mechanisms could contribute to singlet state quenching in these nitroxide adducts. We address here the possible contributions of Förster (dipole–dipole) and Dexter (electron exchange) energy transfer, electron transfer, and electron exchange induced relaxation to the quenching. In principle, k_q reflects the sum of rate constants for each of these potential relaxation pathways

$$k_q = k_{FT} + k_{DT} + k_{ET} + k_{EX} \tag{5}$$

1. Energy Transfer. In the light of conflicting reports[1a,1b,1f,12d] as to the importance of Förster and Dexter transfer in the quenching of singlet states by nitroxides, we have reexamined this question. Since no emission is observed from the first excited state of the nitroxide, direct spectroscopic evidence for energy transfer was not obtainable. Instead, we compared the observed quenching rates of IA, IIA, and IIIA to the Förster (J_F) and Dexter (J_D) overlap integrals calculated from the fluorescence spectra of IB, IIB, and IIIB and the absorbance spectrum of 4-hydroxy-2,2,6,6-tetramethyl-1-piperdinyloxy (TEMPOL)

$$J_F = \int_0^\infty F(\lambda)\epsilon(\lambda)\lambda^4 d\lambda \Big/ \int_0^\infty F(\lambda) d\lambda \tag{6a}$$

$$J_D = \int_0^\infty F(\lambda)\epsilon(\lambda) d\lambda \Big/ \int_0^\infty F(\lambda) d\lambda \int_0^\infty \epsilon(\lambda) d\lambda \tag{6b}$$

where $F(\lambda)$ is the corrected fluorescence intensity of the fluorophore and $\epsilon_a(\lambda)$ is the extinction coefficient of the acceptor (TEMPOL) at wavelength λ.

The weak nitroxide absorption band overlaps with the red edge of the singlet emission of the naphthyl group. This absorption is solvent dependent[23] (Figure 4), shifting to the blue with increasing solvent polarity and thus increasing the values of J_F and J_D. The degree of spectral overlap is further enhanced in polar solvents for compounds IA and IIIA whose emissions shift to the red with increasing solvent polarity (Table I).

We have used these solvent-dependent changes in the overlap integrals to assess whether the quenching rates vary in the manner expected for energy transfer. The rate constant for Förster transfer is given by[29]

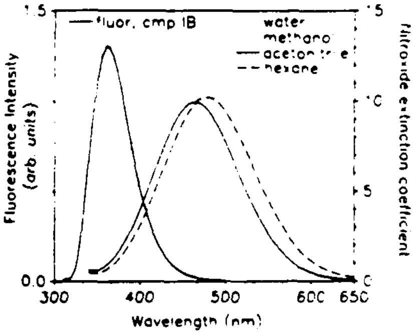

Figure 4. Absorption spectra of TEMPOL in a series of solvents showing the solvent–dependent shifts in the absorption maximum and extinction coefficients (M^{-1} cm^{-1}). Fluorescence emission spectrum of IB in methanol is included in order to illustrate the degree of spectral overlap between naphthalene emission and nitroxide absorption.

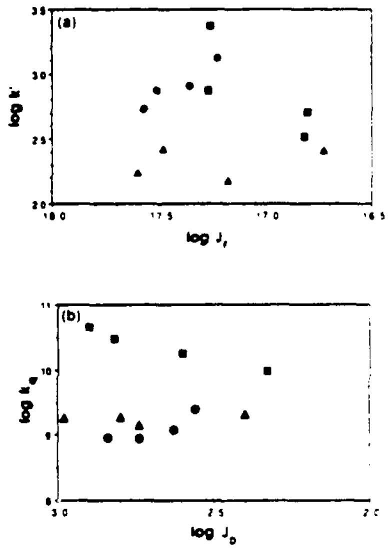

Figure 5. Intramolecular quenching constants vs spectral overlap integrals for IA (■), IIA (▲), and IIIA (●) (a) Förster spectral overlap integral, J_F (M^{-1} cm^3) (the rate constants have been normalized, $k' = k_q \tau d \eta^4 / \phi_d$, to account for solvent dependent variations in lifetime, quantum yield, and refractive index); (b) Dexter spectral overlap J_D (cm).

$$k_{FT} = \frac{J_F \kappa^2 \phi_d}{R^6 \eta^4 \tau_d} 8.71 \times 10^{23} \tag{7a}$$

where κ^2 is the orientation factor (Table IV), ϕ_d and τ_p are the quantum yield and lifetime, respectively, of the appropriate diamagnetic *O*-acetyl derivative (Table III), R is the donor–acceptor distance (Table IV), and η is the solvent refractive index.

The rate constant for Dexter transfer is given by[15b]

$$k_{DT} = \frac{4\pi H^2 J_D}{h} = \frac{4\pi^2 H_0^2 e^{-2R/L} J_D}{h} \tag{7b}$$

where H is the coupling matrix element, H_0 is the preexponential factor, and L is the Bohr radius.

Both of these theories predict that for constant donor–acceptor distance(s) (and orientation(s)) the rate constants for transfer will increase linearly with increasing values of the spectral overlap integrals. However, log plots of k_q vs J_F and J_D for IA, IIA, and IIIA (Figure 5) clearly do not show this relationship (with the possible exception of IIIA in the Forster plot (Figure 5a)).

---

(29) Lakowicz, J. R. *Principles of Fluorescence Spectroscopy*. Plenum Press: New York, 1983; p 305

(30) (a) Oevering, H.; Paddon-Row, M. N.; Heppener, M.; Oliver, A. M.; Cotsaris, E.; Verhoeven, J. W.; Hush, N. S. *J. Am. Chem. Soc.* 1987, *109*, 3258. (b) Kavarnos, G. J.; Turro, N. J. *Chem. Rev.* 1986, *86*, 401–449

(31) Marcus, R. A.; Sutin, N. *Biochim. Biophys. Acta* 1985, *811*, 265 and references cited therein.

Table V. Calculated Förster Energy Transfer Rates[a]

compd	$k_{FT} \times 10^{-9}\ s^{-1}$ hexane	acetonitrile	methanol	water
IA	0.016	0.081	0.014	0.150
IIA	0.005	0.004	0.008	0.014
IIIA	0.010	0.009	0.024	0.060
IVA	0.010	0.026	0.025	0.025

[a] k_{FT} calculated from eq 7a by using the average values of R and κ^2 (Table IV) and ϕ_d and τ_d values from Table II; J_F values generated from eq 6a.

Furthermore, equation 7a can be employed to calculate k_{FT} from R and κ^2 values (Table IV); these predicted Förster transfer rates (Table V) are more than an order of magnitude lower than the measured values of k_q. Moreover, choosing a value of $^2/_3$ for κ^2, corresponding to randomized donor–acceptor orientations,[29] increases k_{FT} to a maximum of only ~15% of the observed k_q values. Even in the case of anthracene, where the spectral overlap with TEMPOL is maximal for the family of linear aromatic ring systems, we calculate that the quenching radius for Förster energy transfer extends to only 9 Å (in ethanol).

We conclude that energy transfer through either a Förster or Dexter mechanism cannot account for the observed magnitude and (lack of) variation in the intramolecular quenching rate constants.

2. Electron Transfer. For electron transfer to be operative, the energy of the excited singlet must be sufficient to drive the relevant redox couple.[30,31] In the absence of Coulombic interactions, the thermodynamic driving force, ΔG_∞, is given by[30]

$$\Delta G_\infty = -E_{00} + E_{ox} - E_{red} \qquad (8)$$

where E_{00} is the 00-excitation energy of the fluorophore, and E_{ox} and E_{red} are the oxidation potential of the electron donor and the reduction potential of the acceptor, respectively.

Assuming a simple continuum model for solute-solvent interaction, additional terms for the Coulombic attraction between the separated charges, ΔG_{Coul}, and for the free energy of solvation of the ion pair, ΔG_{solv}, must be included. The total change in free energy is then given by[30,31]

$$\Delta G_{ET} = \Delta G_\infty + \Delta G_{Coul} + \Delta G_{solv} \qquad (9)$$

$$\Delta G_{Coul} = -e^2/\epsilon R \qquad (10a)$$

$$\Delta G_{solv} = \frac{-e^2}{2}\left(\frac{1}{r_d} + \frac{1}{r_a}\right)\left(\frac{1}{\epsilon_{MeCN}} - \frac{1}{\epsilon}\right) \qquad (10b)$$

and e is the electron charge, ϵ is the solvent dielectric constant, ϵ_{MeCN} is the dielectric constant of acetonitrile in which the redox potentials were measured, R is the distance between donor and acceptor (Table IV), and r_d and r_a are donor and acceptor radii respectively. Coulombic and solvation adjustments to ΔG_∞ are greatest (up to +0.8 eV) in hexane (ϵ = 1.88) and increase steeply with distance in this solvent. For the polar solvents acetonitrile and water, $\Delta G_{Coul} + \Delta G_{solv} < 0.1$ eV and exhibits little distance dependence.

For IA–IVA, the naphthalene moiety may act as either an electron acceptor or donor resulting in oxidation or reduction, respectively, of the nitroxide; these reactions are shown diagramatically in eqs 11 and 12

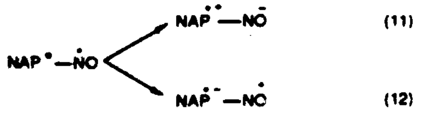
(11)

(12)

We calculated ΔG_{ET} for these reactions by employing eqs 8 and 9; results for the most favorable electron transfer route (eq 11 or 12) are given in Table VI. These calculations indicate that in acetonitrile both reduction and oxidation of the nitroxide are thermodynamically feasible but that the oxidative pathway (eq 12) is preferred in all cases by >0.15 eV. In hexane, the lack of solvent stabilization makes reduction of the nitroxide (eq 11) energetically unfavorable and reduces the driving force for the oxidative pathway ($\Delta G_{ET} > -0.4$ eV). In aqueous solution, nitroxide reduction (eq 11) has the greater driving force. Although these calculations suggest that the direction of electron transfer would reverse in water, the quenching rate constants do not differ greatly. If electron transfer is the dominant pathway for quenching, transfer in both directions must be occurring with equal facility.

Table VI. Singlet Energies (E_{00})[a] and Calculated Thermodynamic Driving Forces (ΔG_{ET}) for Electron Transfer[b]

	hexane[c,d]		acetonitrile[b]		water[e]	
compd	E_{00}	ΔG_{ET}	E_{00}	ΔG_{ET}	E_{00}	ΔG_{ET}
IA	3.82	−0.25	3.43	−0.90	3.18	−1.03
ID[f]	3.82	+0.03	3.43	−0.90		
IIA	4.00	+0.07	4.00	−0.87	4.00	−1.85
IIIA	3.72	−0.07	3.65	−1.12	3.30	−1.14
IVA	3.54	−0.29	3.51	−1.33	3.44	−1.28
IVD	3.54	−0.29	3.52	−1.34	-	-

[a] Singlet energies (E_{00}) were obtained experimentally from the intersection points of fluorescence excitation and emission spectra. [b] Calculated from eq 8 in text; units are eV. [c] Favored charge-separated product is (Nap⁻Nap⁺). Oxidation potential of TEMPOL (+0.63 V vs SCE) in acetonitrile from ref 2; reduction potentials for 1-,[35] 2-,[35b,c] and 2,6-[35a] substituted naphthoates (−1.92 V, −1.95 V, and −1.55 V, respectively), and 1-methylnaphthalene[35b] (−2.5 V) in dimethylformamide, acetonitrile or 75% dioxane/water were employed to calculate ΔG_∞ for IA, IIIA, IVA, and IIA, respectively. [d] Values in hexane adjusted for solvation (see text) by using eq 10 and the approximation $r_d = r_a$ = 3.8 Å. [e] In water the favored charge-separated product is (Nap⁺NO⁻). The reduction of TEMPO gives an irreversible wave in cyclic voltammetry (−0.62 V).[32,33] The oxidation potentials of 1-[35b] and 2-[35b] methyl-naphthalenes (+1.53 and +1.55 V, respectively) in acetic acid solution were used as the best available estimates for potentials of compounds substituted at the 1 and 2-positions. [f] Redox potentials for DOXYL were unavailable; the values for TEMPOL were assumed.

Within individual series of compounds our measured values of k_q do not show any obvious correlation with ΔG_{ET}. For example, the values of k_q for IIA are equal in acetonitrile and hexane, although electron transfer is calculated to be exergonic in the first solvent and endergonic in the latter. Other discrepancies are also apparent. In particular, the k_q's for IIIA and IVA do not vary significantly between acetonitrile and hexane despite the large (~0.8 eV) differences in ΔG_{ET} in these two solvents. Additionally, in polar solvents quenching of IIIA (β-substituted) is slower than IA (α-substituted) by an order of magnitude although its driving force is greater.

Overall, these data are inconsistent with the notion that electron transfer acts as the dominant pathway for singlet quenching.[15a,30,31] The lack of solvent dependence does not, by itself, rule out electron transfer since the rate of transfer is a function of the activation energy, ΔG^*, which includes an additional solvent dependence in the form of the solvent reorganization energy, λ_S.[30,31] Oevering et al.[30a] have demonstrated that the effect of solvent reorganization on ΔG^* may in some cases largely compensate for the solvent dependence included in ΔG_{ET}. We were unable to calculate ΔG^* precisely for these compounds owing to uncertainties in sensitive parameters such as the internal (nuclear) reorganization energy and the effective radius of the nitroxide group. Nevertheless, no reasonable values for these parameters lead to a prediction of faster rates in hexane than in acetonitrile as we have observed for several compounds (IA,D). On the basis of these observations, we tentatively conclude that electron transfer does not play a major role in the quenching. The complete lack of radical ion formation during singlet state quenching by nitroxides in polar solvents[1f,4] provides additional support for this view. However, owing to the uncertainties in the simple continuum model and the redox potentials for the nitroxides,[2,32,34] as yet, we are hesitant to exclude

---

(32) Fish, J. R.; Swarts, S. G.; Sevilla, M. D.; Malinski, T. *J. Phys. Chem.* **1988**, *92*, 3745.

(33) Tsunaga, M.; Iwakura, C.; Tamura, H. *Electrochim. Acta* **1973**, *18*, 241.

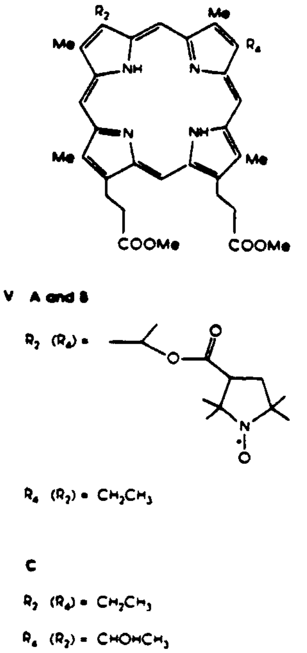

Figure 6. Hematoporphyrin derivatives examined in this study. The two isomers (VA and B) with the nitroxide at either the 2 or 4 position were separated, but were not uniquely identified.

unequivocally a contribution of electron transfer to the quenching.

3. Electron Exchange. Electron exchange between the naphthoate singlet and nitroxide doublet can produce rapid relaxation of the excited state.[1,14] Available relaxation routes are as follows:[1] (Dexter) energy transfer (13a), intersystem crossing to triplet (13b), or internal conversion (13c)

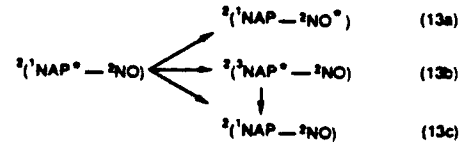

As discussed above Dexter energy transfer is an unlikely relaxation pathway. However, to eliminate energy transfer from consideration and focus on exchange-induced intersystem crossing (13b) or internal conversion (13c), preliminary data were collected on several hematoporphyrin–nitroxide adducts (Figure 6). For these compounds, the energy of the porphyrin singlet (~2.0 eV) is well below that of the pyrrolidinyl nitroxide doublet (~2.9 eV) thus eliminating the possibility of Dexter (or Förster) energy *transfer. ΔG_{ET} for these adducts is also calculated to be small* (−0.18 eV, nitroxide oxidation).[36] Nevertheless, in methanol, the rate constants for quenching in the A isomer, 6.6 × 10^8 s^{-1}, and the B isomer, 7.2 × 10^8 s^{-1}, are comparable to those of IIA. These results suggest that an electron exchange induced intersystem crossing to the triplet or internal conversion to the ground state is occurring.

Further support for an exchange-induced "local" relaxation is provided by the correlation presented in Figure 7. Here we have plotted the k_q's of the paramagnetic compounds against the nonradiative rate constants of their corresponding diamagnetic *O*-acetyl and methyl ester derivatives. With the exception of IVA in methanol, compounds having similar nitroxide–fluorophore distances (e.g. IA, IIA–IVD) exhibit an approximately linear relationship between these parameters. This correlation is interpreted to result from a fixed enhancement (~55-fold) by the nitroxide of a preexisting, nonradiative relaxation pathway in the fluorophore. Because nonradiative decay in most aromatic hydrocarbons proceeds almost exclusively through intersystem crossing (Ermolev's rule[14c]), this enhancement probably reflects a lifting of the spin restriction to singlet–triplet transition brought about through the coupling of the doublet and excited singlet states.[14] We suspect that the relatively minor deviations from this correlation result from variations in the degree of coupling among these derivatives due to small differences in distance, orientation, and structure (Figures 1 and 6).

If intersystem crossing (13b) competes effectively with triplet quenching by the nitroxide (13b → 13c),[3-10] one might expect to see an enhanced phosphorescence signal in nitroxide-substituted compounds as compared with their diamagnetic forms. Observations do not bear this out (Figure 8); triplet (480 nm) and singlet emission bands are both clearly visible for *IA*, *IB*, and *ID* at 77

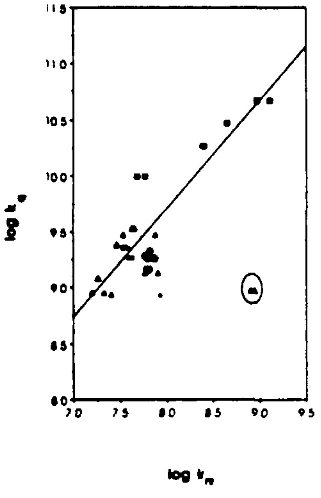

Figure 7. Intramolecular quenching constants (k_q) of nitroxide adducts IA (■), IIA (▲), IIIA (●), IVA (△), IVD (×), and VA (*) vs nonradiative rate constants (k_{nr}) of the corresponding diamagnetic *O*-acetyl and methyl ester derivatives. k_q values for IVD are divided by 2 to account for the presence of two nitroxide groups in this compound. The line represents a linear regression (slope = 0.96, r^2 = 0.76) of all data excluding IVA in methanol (circled) and VA. k_{nr} for VA in methanol was estimated from data of Andreoni et al.[43]

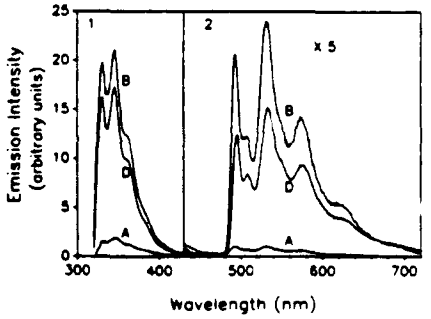

Figure 8. Fluorescence (1) and phosphorescence (2) emission spectra of IA, IB, and ID: excitation wavelength, 300 nm; bandpass, 2 nm; concentration, 15 μM in EPA glass, 77 K. Phosphorescence intensities are expanded by a factor of 5.

---

[34] While the oxidation potential of TEMPOL exhibits only a slight solvent dependence, its reduction is apparently more favorable by as much as 1 eV in protic solvents, perhaps due to stabilization of the reduced species by protonation (ref 32).

[35] (a) DeLuca, C.; Giomini, C.; Rampazzo, L. *J. Electroanal. Chem. Interfacial Electrochem.* 1986, *207*, 161. (b) Siegerman, H. In *Technique of Electrorganic Synthesis Part II*; Weinberg, N. L., Ed.; John Wiley and Sons, Inc.: New York, 1975. (c) Klopman, G.; Nasielski, J. *Bull. Soc. Chim. Belg.* 1961, *70*, 490.

[36] Driving force calculation is based on porphyrin reduction potential of −1.34 V vs SCE (ref 39) and PROXYL oxidation potential of +0.62 V (ref 32). Driving force for porphyrin oxidation/nitroxide reduction is +0.4 V.

K (EPA glass), but for the nitroxide adducts (IA, ID) the triplet emission is diminished to a greater extent than that of the singlet. Thus we cannot distinguish between pathway 13c and a rapid, two-step relaxation via 13b.

Conclusions

For all adducts examined in this study, absorption and fluorescence emission spectral shapes and energies were identical with those of the parent fluorophore. There was no evidence for charge-transfer absorption or charge-recombination emission. We conclude that the emission arises from the same locally excited singlet state in the presence or absence of nitroxide substituents.

Intramolecular quenching of excited singlet states by nitroxyl radicals is very efficient; rate constants are in the range of 10^8–10^{10} s^{-1}. At distances as great as 12 Å, the quenching can occur at rates > 10^8 s^{-1}.

Förster energy transfer cannot account for more than a small fraction of the observed rates, even assuming larger values for κ^2. The rates do not show the dependence on overlap integrals predicted by theories of Förster or Dexter energy transfer. There is no clear correlation of k_q values with calculated values of ΔG_{ET}, suggesting that photoinduced electron transfer is also unimportant. Significant quenching rates are obtained in hematoporphyrin–nitroxide adducts which contain a fluorophore whose singlet energy is below that of the lowest excited state of the nitroxide. Since the driving force for electron transfer is also small, this result suggests that the nitroxide moiety facilitates either intersystem crossing to the triplet or internal conversion to the ground state. Further support for exchange-induced relaxation is provided by the linear correlation between k_{nr} and k_q, indicating a fixed enhancement of a preexisting pathway. Thus we conclude that the quenching arises primarily through electron exchange. This conclusion is consistent with earlier studies of diffusional quenching of aromatic hydrocarbons by nitroxides.[1b]

This work provides the first preliminary evidence for long-range quenching by electron exchange *that proceeds via the local relaxation of the singlet and not energy transfer*. That this pathway also appears to out compete or to occur in preference to exergonic electron transfer is somewhat surprising, given current thinking on the relationship between electron-exchange and electron-transfer processes.[15b,30b,42] While compounds containing fluorophores with different structures, singlet energies, and redox potentials could, in principle, exhibit a number of different quenching mechanisms, data from this and previous studies[1] have failed to provide unequivocal evidence for the operation of mechanisms other than electron exchange in the quenching of excited singlet states by nitroxides. Further work employing a series of differing nitroxides and fluorophores combined within a rigid structural framework[15] could provide additional insight concerning the factors controlling the possible relaxation pathways.

Experimental Section

Optical Measurements. Solutions for optical measurements in all solvents were prepared from concentrated (~10 mM) stock solutions in methanol. All solvents were HPLC grade (Aldrich) used without further purification. Absorption spectra were measured on solutions in 1- or 5-cm quartz cells with a Hewlett-Packard 8451A diode array spectrophotometer (spectral resolution, 2 nm).

Quantum yield measurements were made on an SLM-Aminco SPF-500C spectrofluorometer linked to an IBM PC-XT for data collection and processing. Freshly made solutions had optical densities of ≤0.02 at the excitation wavelength, chosen as the absorbance maximum in the range of 280–300 nm. Excitation and emission bandpasses were 2 nm in most cases; 4-nm bandpasses were used to measure some of the very low quantum yields. Samples were thermostated at 20 °C. Solutions were deoxygenated through bubbling with N_2; emission scans were repeated until bubbling caused no further increase in fluorescence intensity. Any signal due to the solvent was removed by subtraction. Spectra were corrected for instrumental response and integrated by using correction factors and software provided by the manufacturer. (A modified correction procedure was used to avoid arbitrary normalization and conversion steps in the standard routines).

Quantum yields were calculated with respect to quinine sulfate in 0.1 N H_2SO_4 (OD = 0.02) and corrected for refractive index differences between solvents, by using

$$\phi = \frac{F_s A_{qs} \eta_s^2 \phi_{qs}}{A_s F_{qs} \eta_0^2} \qquad (14)$$

where the subscript s refers to the sample, qs refers to quinine sulfate, ϕ is quantum yield, A is absorbance at the excitation wavelength, F is the integrated, corrected fluorescence, η_s is the refractive index of the sample solvent, and η_0 is the refractive index of water. ϕ_{qs} is 0.55.

Fluorescence lifetimes were measured by time-correlated single-photon counting, on an instrument generously made available through the Laser Biomedical Research Center at MIT. Excitation was provided by a cavity-dumped tunable dye laser, synchronously pumped with the second harmonic of a mode-locked Nd-YAG (Coherent, Antares 76-S). For the naphthalene derivatives the dye pulses (5 ps fwhm, 20 MHz) were frequency doubled with a phase matched KTP crystal to 295 nm. The porphyrin derivatives were excited directly with the dye laser, tuned to 580 nm. Fluorescence from deoxygenated samples was collected at 90° (naphthalene derivatives) or 180° (porphyrin derivatives) and focused into a Spex monochrometer; entrance and exit slits were adjusted to obtain a counting rate of 4000–5000 photons per second impinging on the PMT.

A Canberra 2143 time-amplitude converter (TAC) received start pulses directly from the cavity dumper and stop pulses from the PMT. The TAC signal was passed to a multichannel analyzer and the data were saved in an IBM PC-XT for later analysis with a Sun microcomputer. The instrumental response limit for this system is about 70 ps.

Determination of Minimal-Energy Conformations of IA–IIIA. The general strategy for this search was to allow the functional groups of each compound to freely rotate around all nonconjugated bonds that were not in constrained ring structures. There were two degrees of rotational freedom in IA and IIIA: (1) the bond between the carboxyl carbon and oxygen atoms of the ester linkage; and (2) the carboxyl oxygen and carbon C1 of the nitroxyl ring. The functional groups were rotated through 360° around each of these two bonds in 5° increments. The structures after each rotation were energy-minimized by using AMBER[28] to optimize the bond distances, bond angles, dihedral angles of the bonds, and dipole and van der Waal's interactions. The structures were allowed to minimize to a convergence of 1.0 × 10^{-1} kcal/mol difference in overall energy, and 0.10 kcal/mol Å in the gradient of the overall energy. An analysis of the energies associated with each rotation versus the angle of rotation around each degree of freedom showed that the local energy wells were greater than ±10° in width relative to the angles of the minimized conformations. Thus a smaller rotational increment was not necessary in searching for the global energy minima.

The addition of a methylene group between the naphthalene ring and the carboxylate introduces two additional degrees of rotational freedom to IIA. To simplify this system, the structure was allowed to energy minimize in terms of only the naphthalene ring and the intervening methylene group. This fixes the methylene hydrogens in orientations that are not sterically hindered by the aromatic ring. The structure was then treated in the same fashion as IA and IIIA through rotations around the two carbon–oxygen bonds in the ester linkage, but also including the additional rotation about the methylene–carboxylate bond.

Preparation of Nitroxide Derivatives. General. All starting materials and reagents were obtained from Aldrich and used as received. High purity grade Burdick and Jackson solvents were used following distillation over CaH_2 in all preparations. Chromatographic separation was obtained on a flash column using 30μm silica (Amicon or Davisil) under positive N_2 pressure; solvents are indicated where appropriate. Melting points, which are uncorrected, were measured on a Mel-temp apparatus (Laboratory Devices). Infrared (IR) spectra were recorded as a thin film on a Mattson Sirrus 100 infrared spectrophotometer at 4 cm^{-1}. Mass

---

(37) Hassner, A., Alexanian, V. *Tetrahedron Lett.* 1978, *46*, 4475–4478.

(38) Smith, K. M., Ed. *Porphyrins and Metalloporphyrins*; Elsevier Scientific Publishing Co.: Amsterdam, 1975.

(39) Felton, R. H. In *The Porphyrins*; Dolphin, D., Ed.; Academic Press: New York, 1978.

(40) Suzuki, S., Fujii, T.; Ishikawa, T. *J. Mol. Spectrosc.* 1975, *57*, 490.

(41) Orchin, M., Jaffe, H. H. *Symmetry, Orbitals and Spectra*; John Wiley and Sons, Inc.: New York, 1971; pp 204–230.

(42) (a) Closs, G. L., Piotrowiak, P., MacInnis, J. M., Flemming, G. R. *J. Am. Chem. Soc.* 1988, *110*, 2652. (b) Closs, G. L.; Johnson, M. D.; Miller, J. R.; Piotrowiak, P. *J. Am. Chem. Soc.* 1989, *111*, 3751.

(43) Andreoni, A., Cubeddu, R., De Silvestri, S., Jori, G.; Laporta, P., Reddi, E. *Z. Naturforsch.* 1983, *38*, 83.

spectra (MS) were obtained by thermal desorption from a copper probe, in either an electron impact (EI) or chemical ionization (CI) mode on a Finnigan 4510 spectrometer interfaced with an INCOS 2300 data system. CI mass spectra of nitroxide derivatives gave an $(M + 2)^+$ molecular ion, suggesting the nitroxide derivative is chemically reduced prior to ionization in the mass spectrometer. This was not observed in the spectra of nitroxides obtained by EI or in the spectra of the nitroxide–acetyl derivatives by CI. Nuclear magnetic resonance (NMR) spectra of the acetyl derivatives were obtained on either a Bruker AM-250 or Varian XL-300 at Massachusetts Institute of Technology and measured in $CDCl_3$.

1-Oxy-2,2,6,6-tetramethylpiperidin-4-yl 1-Naphthoate (IA). 1-Naphthoyl chloride (950 mg) was dissolved in methylene chloride (10 mL). 4-Hydroxyl-TEMPO (860 mg in 2.0 mL of methylene chloride) was added dropwise to the stirred solution. After 20 h this solution was diluted with methylene chloride, washed with water, dried (Na_2SO_4), and evaporated to an orange oil which later crystallized on standing. Column chromatography (Bio-Rad.Bio-Sil A 100–200 mesh) eluting with methylene chloride and recrystallization from methanol afforded the desired product as orange needles: 962 mg; mp 100–102 °C; IR 1713 cm^{-1}; MS (EI) *m/e* 326 (M^+, 18), 155 (100); MS (CI) 328 ($[M + 2H]^+$, 25), 312 (M − 14, 35), 310 (M − 16, 45), 156 (100).

2-(1-Oxy-2,2,6,6-tetramethylpiperidin-4-yl) 6-Hydrogen Naphthalenedicarboxylate (IVA) and 2,6-Bis(1-oxy-2,2,6,6-tetramethylpiperidin-4-yl) Naphthalenedicarboxylate (IVC). 2,6-Naphthalenedicarboxylic acid (3.5 g) was suspended in methylene chloride (100 mL) and pyridine (3.0 mL). Thionyl chloride (3.0 mL) was then added dropwise, and the resultant solution was stirred until no suspension remained and the solution was clear. The intermediate diacid chloride was evaporated to dryness in an effort to remove extraneous thionyl chloride then dissolved in methylene chloride (150 mL) and pyridine (3.0 mL). 4-Hydroxy-TEMPO (1 g) in a small amount of methylene chloride was added and this mixture stirred overnight. Water (3.0 mL) was added and the precipitated diacid was filtered off and washed with excess methylene chloride. The combined filtrate was washed with water, dried with anhydrous sodium sulfate, and evaporated to a dark orange oil. The desired products were separated and purified by flash chromatography (eluting with 3% methanol/methylene chloride) and recrystallized from methanol giving compound IVA (90 mg) and compound IVD (220 mg). Compound IVA: mp >200 °C dec); IR 3200–2200 cm^{-1} (b), 1715, 1622 cm^{-1}; MS (EI) *m/e* 370 (M^+), 199 (80), 124 (100). Compound IVD: mp >225 °C dec; IR 1712 cm^{-1}; MS *m/e* (EI) 524 (M^+, 30), 370 (20), 124 (100).

1-Oxy-2,2,6,6-tetramethylpiperidin-4-yl 2-Naphthoate (IIIA). 2-Naphthoyl chloride (380 mg) and 4-Hydroxy-TEMPO (345 mg) were dissolved in cold pyridine and stirred overnight (20 h). This mixture was diluted with methylene chloride, washed with water (1 × 25 mL) and 1N HCl (3 × 25 mL), dried over anhydrous sodium sulfate, and evaporated to dryness. The desired product was purified by flash chromatography (methylene chloride), obtained as a solid and recrystallized from methylene chloride/*n*-hexane: 235 mg; mp 122–123 °C; IR 1713 cm^{-1}; MS *m/e* 328 ($(M + 2)^+$, 75), 312 (M − 14, 70), 310 (M − 16, 50), 156 (100).

1-Oxy-2,2,6,6-tetramethylpiperidin-4-yl* Naphth-1-ylacetate *(IIA). 1-Naphthylacetic acid (500 mg) was combined with dicyclohexylcarbodiimide (DCC, 610 mg), (dimethylamino)pyridine (DMAP, 32 mg), and 4-Hydroxy-TEMPO (462 mg) and dissolved in methylene chloride and stirred overnight under an atmosphere of N_2.[37] The solid dicyclohexyl urea was filtered off and further rinsed with methylene chloride. The combined filtrate was washed with 1 N HCl (2 × 75 mL) and water (3 × 75 mL), dried (Na_2SO_4), and evaporated. The product was purified by flash chromatography (methylene chloride) and evaporated to an orange oil which did not crystallize: IR 1733 cm^{-1}; MS (CI) *m/e* 342 ($(M + 2)^+$, 25), 326 (M − 14, 40), 324 (M − 16, 38), 156 (100).

17β-Hydroxy-4′,4′-dimethylspiro(5α-androstane-3,2′-oxazolidin)-3′-yloxy, Naphthoate (ID). Compound ID was prepared by the DCC coupling described above with use of 1-naphthoic acid and 3-DOXYL-17β-hydroxy-5 α-androstane (Aldrich). The desired product was purified by TLC on a 1-mm-thick plate (20 × 20 cm, Whatman) eluted with methylene chloride and obtained as a yellowish solid: mp 153–154 °C; IR 1714 cm^{-1}; MS (EI) *m/e* 530 (M^+, 1), 444 (DOXYL fragment loss, 2), 155 (100).

Preparation of Nitroxide–Acetyl Derivatives. 1-Acetoxy-2,2,6,6-tetramethylpiperidin-4-yl 1-Naphthoate (IB). Compound IA (50 mg) dissolved in tetrahydrofuran (3 mL) in the presence of 5% palladium/carbon (5 mg) was stirred under an atmosphere of hydrogen for 3 h. After this time the solution was filtered directly (with minimal exposure to air) into a solution of acetic anhydride/pyridine (1:10) which had been previously deoxygenated with nitrogen. This solution was stirred for 20 h under N_2 then diluted with methylene chloride, washed with water, dried, and evaporated to a yellowish oil. After chromatography on silica (eluting with methylene chloride) fractions containing product crystallized after solvents were removed. The final product was recrystallized from methanol to remove a small amount of compound IA and gave a snowy white solid: 20 mg; mp 86–87 °C; IR 1712, 1770 cm^{-1}; MS (EI) *m/e* 369 (M^+), 327 (M^+ − 42), 155 (90), 140 (100); NMR (250 MHz) δ 8.80 (d), 8.14 (d), 8.02 (d), 7.88 (d) 7.55 (m) (7 H, 2,3,4,5,6,7,8-H), 5.45 (m, 11-H), 2.13 (s, OCOMe), 2.20–2.00 (m, 4 H, 12-CH_2), 1.35, 1.17 (s, 12 H, 13a-Me).

2-(1-Acetoxy-2,2,6,6-tetramethylpiperidinyl-4-yl) 6-Hydrogen Naphthylenedicarboxylate (IVB), 2,6-Bis(1-acetoxy-2,2,6,6-tetramethylpiperidin-4-yl) Naphthalenedicarboxylate (IVE), 1-Acetoxy-2,2,6,6-tetramethylpiperidin-4-yl 2-Naphthoate (IIIB), and 1-Acetoxy-2,2,6,6-tetramethylpiperidin-4-yl Naphth-1-ylacetate (IIB). These compounds were prepared in a fashion analogous to compound IB. However, the hydroxylamine produced in the catalytic reduction of compound IVA precipitated upon its formation and excess tetrahydrofuran and pyridine was added in order to filter off the catalyst. Compound IVB was not purified chromatographically but was obtained as a white solid from crystallization in methanol. Compound IVB: IR 1769, 1753, 1715 cm^{-1}; MS (EI) *m/e* 413 (M^+), 371 (M^+ − 42), 140 (100); NMR (250 MHz) δ 8.74, 8.61 (s, 1,5-H), 8.22 (d), 8.18 (m, 4 H 3,4,7,8-H), 5.45 (m, 12-H), 2.16 (s, OCOMe), 2.11 (m, 4 H, 13-CH_2), 1.34, 1.18 (s 12 H, 14-Me). Compound IVE: IR 1766, 1703 cm^{-1}; MS (EI) *m/e* 610 (M^+, 5), 568 (M^+ − 42, 30), 124 (100); NMR (250 MHz) δ 8.58 (s, 1,5-H), 8.04 (m, 3,4,7,8-H), 5.43 (m, 12-H), 2.13 (s, OCOMe), 2.03 (m, 4 H, 13-CH_2), 1.33, 1.16 (s, 12 H, 14-Me). Compound IIIB: mp 115–116 °C; IR 1732 cm^{-1}; MS (CI) *m/e* 398 (M + 29, 5), 370 ($(M + 1)^+$, 100), 310 (M − CH_3CO_2H, 95), 198 (30); NMR (250 MHz) δ 8.54 (s, 1 H, 1-H), 8.00 (d), 7.94 (d), 7.86 (d), 7.55 (m) (6 H, 3,4,5,6,7,8-H), 5.39 (m, 11-H), 2.11 (s, OCOMe), 2.15–1.90 (m, 4 H, 12-CH_2), 1.31, 1.14 (s, 12 H, 13a-Me). Compound IIB: IR 1767, 1732 cm^{-1}; MS (CI) *m/e* 412 (M + 29, 5), 384 ($(M + 1)^+$, 100), 324 (M − CH_3CO_2H, 100), 198 (45); NMR (250 MHz) δ 7.96 (d), 7.84 (d), 7.77 (d), 7.49 (m), 7.38 (m) (7 H, 2,3,4,5,6,7-H), 5.06 (m, 11-H), 4.02 (s, 2 H, 1a-CH_2), 2.06 (s, OCOMe), 1.90–1.67 (m, 4 H, 12-CH_2), 1.17, 1.04 (s, 12 H, 13a-Me).

Preparation of Methyl Esters. Methyl 1-Naphthoate (IC) and Methyl 2-Naphthoate (IIIC). 1-Naphthoyl chloride (500 mg) 1 or 2-naphthoyl chloride was dissolved in cold pyridine (3 mL), methanol (2 mL) was added, and the resultant mixture was stirred in an ice bath for 2 h and at room temperature for an additional 4 h after which time the reaction mixture was diluted with methylene chloride, washed with water (1 × 25 mL), 1 M HCl (3 × 25 mL), dried (Na_2SO_4), and evaporated to dryness. The product was purified by flash chromatography (methylene chloride). Compound IC: obtained as a colorless oil; IR 1711 cm^{-1}. Compound IIIC: obtained as a solid and recrystallized from methylene chloride/*n*-hexane; mp 72–73 °C; IR 1711 cm^{-1}; MS (CI) *m/e* 215 ($(M + 29)^+$, 15), 187 ($(M + 1)^+$, 100), 155 (10).

2-Methyl 6-Hydrogen Naphthalenedicarboxylate (IVC), 2,6-Dimethyl Naphthalenedicarboxylate (IVF), and Methyl Naphth-1-ylacetate (IIC). Compounds IVC and F were prepared by the procedure used in the synthesis of compounds IVA and D substituting methanol for 4-Hydroxy-TEMPO. Compound IVC: mp >200 °C dec; IR 1721, 1682 cm^{-1}; MS (CI) *m/e* 259 (M + 29, 15), 231 ($(M + 1)^+$, 100); NMR (250 MHz, $CDCl_3$ and d_5-pyridine) δ 8.69, 8.61 (s, 1,4-H 8.20 (dd), 8.08 (dd),7.98 (d) (4 H, 3, 4,7,8-H), 3.96 (s, 3 H, 2a-OMe). Compound IVF: mp 188 °C (lit.[44] mp 186 °C), IR 1707 cm^{-1}. Compound IIC was prepared by the procedure used for the synthesis of compound IIB substituting methanol for the nitroxide, obtained as a colorless oil, IR 1736 cm^{-1}; MS (CI) *m/e* 229 ($(M + 29)^+$, 8), 201 ($(M + 1)^+$, 100), 169 ($(M + 1)^+$ −OMe, 65).

Preparation of Hematoporphyrin IX Carboxy-PROXYL Derivatives. 2(4)-Vinylhematoporphyrin IX DME was obtained from commercial hematoporphyrin IX (Aldrich) by the H_2SO_4/methanol procedure reported by Smith.[38] The product was purified by flash column on silica (3–5% methanol/methylene chloride) and obtained as a solid from methylene chloride/*n*-hexane. At this point, no effort was made to resolve the isomeric mixture of 2(4)-Vinylhematoporphyrin IX DME.

Vinylhematoporphyrin IX DME. IR 3442 (bd, O–H), 3319 (m, N–H), 1734 (s, ester C=O) cm^{-1}; MS (CI) *m/e* 637 ($(M + 29)^+$, 8), 609 ($(M + 1)^+$, 70), 591 ($(M + 1)^+$ − H_2O, 100); NMR (300 MHz) δ 10.18, 10.06, 10.01, 9.93, 9.91, 9.88 (4 H, a, b, g, and d meso-H), 8.20 (m, 1 H, 2a- and 4a-H of vinyl), 6.35, 6.17 (m, 3 H, 2a- and 4a-H of hydroxyl ethyl and 2b- and 4b-CH_2), 4.31 (4 H, 6a- and 7a-CH_2), 3.65, 3.61, 3.55, 3.53, 3.50, 3.43, 3.42 (overlapping s's, 18 H, 1,3,5,8-Me and 6,7-OMe), 3.23 (t, 4 H, 6b- and 7b-CH_2), 2.12 (d, 3 H, 2a- and 4a-Me).

2(4)-1-(Hydroxyethyl)-4(2)-ethyl-6,7-bis[2-(methoxycarbonyl)ethyl]-1,3,5,8-tetramethylporphyrin (VC). 2(4)-Vinylhematoporphyrin IX DME dissolved in tetrahydrofuran in the presence of 5% palladi-

---

(44) Buckingham, J., Ed. *Dictionary of Organic Compounds*, Chapman and Hall: New York, 1982; Vol 4.

um/carbon (5 mg) was stirred under an atmosphere of hydrogen overnight. After the catalyst was filtered off, the desired product was purified on a flash column (3% methanol/methylene chloride) and obtained as a solid: IR 3454 cm^{-1} (bd, O–H), 3318 (m, N–H), 1735 (s, ester C=O); MS (CI) *m/e* 639 ($(M + 29)^+$, 10), 611 ($(M + 1)^+$, 100), 593 ($(M + 1)^+ - H_2O$, 95); NMR (300 MHz) δ 10.34, 10.03, 10.01, 10.00, 9.99, 9.97 (4 H, a, b, g, and d meso-H), 6.32 (q, 1 H, 2a- and 4a-H of hydroxy ethyl), 4.34 (m, 4 H, 6a- and 7a-CH_2), 4.05 (m, 2 H, 2a- and 4a-CH_2), 3.66, 3.65, 3.64, 3.57, 3.56, 3.55 (overlapping s's, 18 H, 1,3,5,8-Me and 6,7-OMe), 3.25 (t, 4 H, 6b- and 7b-CH_2), 2.14 (d, 3 H, 2a- and 4a-Me of hydroxy ethyl), 1.84 (t, 3 H, 2a- and 4a-Me of ethyl).

2(4)-[1-[[(1-Oxy-2,2,5,5-tetramethylpyrrolidin-3-yl)carbonyl]oxy]ethyl]-4(2)-ethyl-6,7-bis[2-(methoxycarbonyl)ethyl]-1,3,5,8-tetramethylporphyrin (VA,B). The nitroxide derivative was prepared by the DCC coupling reaction with 3-carboxy-PROXYL and the hydroxy porphyrin. A and B isomers were separated by TLC (3% methanol/methylene chloride) but were not uniquely identified as to substituant position (2 or 4). *2(4)-carboxy-PROXYL-4(2)-ethylhematoporphyrin IX DME (VA)*: IR 3316, (m, N–H), 1735 (s, ester C=O) cm^{-1}; MS (CI) *m/e* 807 ($(M + 29)^+$, 1), 779 ($(M + 1)^+$, 3), 764 ($(M + 1)^+ - 15$, 8), 593 ($[M + 1]^+ - H_2O$, 100).

Acknowledgment. This work was supported by the Office of Naval Research under ONR Contract N00014-87-K-007 and Grant N00014-89-J-1260 (N.V.B.), and ONR Contract N00014-88-K-0388 (P.S.H.). Partial support for SG was provided by the Environmental Protection Agency. Fluorescence lifetime measurements were made possible through MIT's Laser Biomedical Research Center, an NIH funded facility at the George R. Harrison Spectroscopy Laboratory. We also thank K. An for help with the lasers and data deconvolution. This is contribution No. 7348 from the Woods Hole Oceanographic Institution.

Supplementary Material Available: A listing of atomic coordinates for low-energy conformations of IA, IIA, and IIIA (8 pages). Ordering information is given on any current masthead page.

The work described in chapter two was accomplished with the help of Dan Simpson (Los Alamos), who synthesized the nitroxide-fluorophore adducts. G. Zhou and P. Ho (Oregon State) calculated conformations and energies of compounds IA, IIA, and IIIA (table IV). Fluorescence lifetimes were measured using instruments made available through the Laser Biomedical Research Center at MIT, a facility funded by the National Institutes of Health at the George R. Harrison Spectroscopy Laboratory.

Reprinted from ENVIRONMENTAL SCIENCE & TECHNOLOGY, Vol. 26, 1992 p. 294-302.
Copyright © 1992 by the American Chemical Society and reprinted by permission of the copyright owner.

Chapter Three

Investigation of the Electrostatic Properties of Humic Substances by Fluorescence Quenching

Sarah A. Green,[*,†] **François M. M. Morel,**[*,‡] **and Neil V. Blough**[*,§]

Department of Chemistry, Woods Hole Oceanographic Institution, Woods Hole, Massachusetts 02543, and Ralph M. Parsons Laboratory, Department of Civil Engineering, Massachusetts Institute of Technology, Cambridge, Massachusetts 02139

■ A fluorescence quenching technique was employed to explore the electrostatic properties of fulvic acid (FA) and humic acid (HA). Cationic nitroxides were found to be up to 16 times more effective than neutral analogues in quenching the fluorescence of humic materials. This result is attributed to the enhanced Coulombic attraction of cations to the anionic FA or HA surface and is interpreted as an estimate of surface potential. Reduction of molecular charge at low pH and shielding of charge at high ionic strength produced diminished enhancements, consistent with this interpretation. High molecular weight fractions of HA have a higher apparent surface potential than lower molecular weight fractions, indicating that larger humic molecules may have an enhanced ability to bind metal ions.

Introduction

Humic substances play an important role in controlling trace-metal speciation in natural waters. As the prevalent chromophores in most aquatic environments, they are also responsible for initiating numerous photochemical transformations of both organic compounds (*1*, *2*) and trace metals (*3*). With the goal of better understanding these processes, a great deal of effort has gone toward modeling the interactions between metal ions and humic materials (*4*, *5*). Recently the electrolyte character of fulvic acids and humic acids has been considered in terms of its impacts on both cation binding (*6*, *7*) and rates of photochemical reactions (*8*).

A current approach to modeling metal binding by humic acids over variable pH and ionic strength regimes explicitly includes a Coulombic term in addition to intrinsic binding constants (*6*, *7*, *9*, *10*). In these models, intrinsic binding constants remain invariant with pH and ionic strength while the Coulombic term is allowed to vary as predicted by electrostatic theory. Initial application of this type of model has been successful in this laboratory (*6*) in fitting copper titration data without relying on such physically unsatisfying concepts as binding constants that vary with ionic strength.

Natural humic substances are oligoelectrolytes which are predicted to have a large negative surface potential, primarily due to deprotonated carboxylic acid groups. This negative potential is expected to result in increased cation concentrations near the humic surface. Experimentally this has been confirmed indirectly by Blough (*8*), who has shown that radicals produced by irradiation of humic acid are more efficiently scavenged by a cationic species than by analogous neutral or anionic compounds. Thus, electrostatic effects can influence the competition between charged and neutral species (e.g., oxygen) for photoproduced radicals. Similarly, this region of enhanced cation concentration around humic molecules may be an important zone for thermal and photoinduced metal reduction/oxidation, since an ion here may be sufficiently close to act as an electron acceptor/donor, yet be able to diffuse away before undergoing back electron transfer.

In this work our goal is to provide an experimental basis for models that require information about the electrostatic characteristics of humic materials. We have employed a fluorescence quenching technique to explicitly examine the local excess of cations around fulvic acid molecules and

---

[†] MIT-WHOI Joint Program in Oceanography.
[‡] Massachusetts Institute of Technology.
[§] Woods Hole Oceanographic Institution.

0013-936X/92/0926-0294$03.00/0 © 1992 American Chemical Society

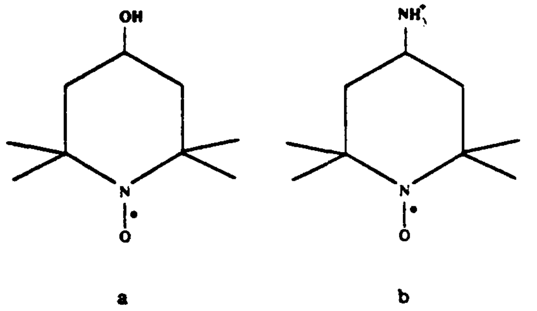

Figure 1. Quenchers employed in this study: (a) 4-hydroxy-tempo (tempol) and (b) 4-amino-tempo (tempamine).

to place limits on the effective fulvic acid surface potential as a function of pH and ionic strength. Also, the relative surface potentials of different size classes of the humic molecules are compared. Suwannee River fulvic acid (FA) and Suwannee River humic acid (HA) were selected as representitive humic substances.

Experimental Rationale

Among species known to be effective quenchers of fluorescence, paramagnetic compounds such as Cu^{2+}, O_2, and stable nitroxide radicals are particularly useful. Static quenching, produced by direct coordination of Cu^{2+}, Fe^{3+}, and other metal ions, has been employed in previous studies of cation binding to humic substances (*11–14*). Unlike these metals, nitroxides do not coordinate to these materials and may therefore be employed as dynamic quenchers to investigate weaker nonbonding interactions. Stable nitroxide radicals are, like oxygen, effective quenchers of excited singlet states (*15*), but have the advantage of a higher aqueous solubility. In addition, they are available in a variety of charged forms, making them especially well suited to studies of electrostatic effects. In these experiments we employ principally the neutral 4-hydroxy-tempo (tempol), the cationic 4-amino-tempo (tempamine) (Figure 1) and, to a lesser extent, the anionic 3-carboxy-proxyl and the cationic quaternary amine 4-(trimethylamino)-tempo to probe the anionic character of humic substances.

To interpret the data, we employ a simple physical model developed within the framework of the standard Stern–Volmer analysis (*16*):

$$F \xrightarrow{h\nu} F^{*} \qquad (1)$$

$$F^{*} \xrightarrow{k_r} F + h\nu \qquad (2)$$

$$F^{*} \xrightarrow{k_{nr}} F \qquad (3)$$

$$F^{*} + Q \underset{k_{-dif}}{\overset{k_{dif}}{\rightleftharpoons}} [F^{*}Q] \xrightarrow{k_{quen}} F + Q \qquad (4)$$

In the presence of quencher, Q, the excited fluorophore, F^{*}, can undergo three fates: (1) radiative relaxation to the ground state (F) with emission of a photon (eq 2), (2) nonradiative relaxation to the ground state (eq 3), or (3) a diffusional encounter to form a collision complex that provides a rapid, nonradiative relaxation pathway to the ground state (eq 4). Under constant illumination, the ratio of the fluorescence intensities in the absence (F_0) and presence (F) of quencher is given by the Stern–Volmer equation

$$F_0/F = 1 + k_q\tau[Q] \qquad (5)$$

where

$$k_q = k_{quen}k_{dif}/(k_{quen} + k_{-dif}) \qquad (6)$$

and

$$\tau = 1/(k_r + k_{nr}) \qquad (7)$$

is the excited state lifetime of the unquenched fluorophore. If $k_{quen} \gg k_{-dif}$, then $k_q = k_{dif}$ and the quenching becomes diffusion controlled. Because nitroxides quench excited singlet states at or near the diffusion-controlled limit (*17*), we consider k_{quen} to be large with respect to k_{-dif} throughout this discussion.

In practice, the ratio, F_0/F, is determined at a series of quencher concentrations and the slope, equal to $k_q\tau$, is determined from the plot of F_0/F vs [Q]. As we show below, this slope is substantially larger for the cationic, as compared to the neutral, quenchers. Because $k_q \approx k_{dif}$ this increased slope cannot result from a change in the efficiency of quenching within the collision complex (k_{quen} or k_{-dif}, eq 6). Instead, this result indicates that the cationic quencher is not homogeneously distributed in solution, but rather is attracted by Coulombic forces to the vicinity of the anionic FA. In the kinetic analysis, the increased slope obtained for the cationic quenchers is attributed to an enhanced diffusion-controlled rate constant (vide infra). A simpler, though less precise, interpretation is the pseudostatic model in which the increase is ascribed to an excess concentration of quenchers at the FA surface. In either case, the observed effects may be quantified by defining the term λ_{meas} as the measured electrostatic enhancement factor, such that

$$[Q]_L = \lambda_{meas}[Q]_B \qquad (8)$$

where $[Q]_B$ is the bulk quencher concentration, $[Q]_L$ is the apparent "local" quencher concentration around the fluorophore, and λ_{meas} is defined to be unity for neutral quenchers. Thus, $[Q]_L$ is the concentration of neutral quenchers which would be required to obtain the same degree of quenching as is measured for a concentration of cationic quenchers equal to $[Q]_B$. Equation 5 can then be reformulated as

$$F_0/F = 1 + k_q\tau\lambda_{meas}[Q] \qquad (9)$$

A Stern–Volmer plot for the neutral quencher has a slope of $K_N = k_q\tau$, while for a cationic quencher the slope is $K_C = K_N\lambda_{meas}$; the ratio of slopes from the two plots gives λ_{meas}. In this study, we use λ_{meas} to make relative comparisons among several samples and then invoke the more detailed analyses, described below, to study the ionic strength dependence of λ_{meas} for FA.

Pseudostatic Analysis. The interpretation of the parameter λ_{meas} is not necessarily straightforward, although it is clearly related to the electrostatic characteristics of the fluorophore. In its simplest interpretation (*18*), the local quencher concentration in the vicinity of the fluorophore is related to $[Q]_B$ through the Boltzmann equation

$$[Q]_L = [Q]_B \exp(-\Psi'/k_BT) \qquad (10)$$

which gives

$$\lambda_{meas} = \exp(-\Psi'/k_BT) \qquad (11)$$

where Ψ' is the apparent attractive electrostatic potential, k_B is the Boltzmann constant, and T is the absolute temperature. This is equivalent to defining a sphere around F, in which all possible quenchers are contained and are subject to an average potential, Ψ'. This simple approach has the advantage of being intuitively accessible, but it is important to acknowledge that it is a rough approximation because it neglects the dynamic nature of the quenching and the distance dependence of Ψ.

Diffusional quenching is accomplished not only by quenchers immediately adjacent to an excited fluorophore, but also by those that can reach one during its excited-state lifetime. Since Ψ decreases as a function of distance, $[Q]_L$ also decreases radially from the surface. Thus, neither Ψ' nor $[Q]_L$ in eq 10 are well-defined entities, but they actually represent distance-weighted averages along the gradient from the surface to some distance away. This effect is moderated somewhat by geometric considerations since the probability that a quencher will diffuse to a fluorophore decreases very rapidly with their separation distance. The overall result is that $\lambda_{\max}$ does not directly represent the potential at the surface, as is suggested by eq 11, but is smaller than that limiting value due to participation by more distant quenchers (subject to a lower potential).

$\Psi(r)$ is a function of the size and charge of the macromolecule, and of the ionic strength, I (M), through the Debye length, $\kappa = 0.327\sqrt{I}$ (Å^{-1}). For small, spherically symmetrical potentials, the Debye–Hückel equation gives (*19*)

$$\frac{\Psi(r)}{k_BT} = zr_0\,\frac{\exp[\kappa(R-r)]}{r(1+\kappa R)} \qquad (12)$$

where z is the product of charges on the macromolecule and quencher, R is the radius of closest approach of counterions to the macromolecule, and r is the distance from the center of the macromolecule; r_0 (Onsager length) is equal to 7.1 Å in water at 25 °C. For large Ψ, eq 12 is not valid and numerical calculations must be employed (*6*).

Kinetic Analysis. A simple kinetic analysis (*20*) includes the dynamics of the problem, and in cases where the Debye–Hückel equation is applicable, an analytical expression for the steady-state quenching rate is obtained. In this approach the Stern–Volmer constant, k_q (eq 5), is given by

$$k_q = 4\pi D\beta \qquad (13)$$

where

$$\beta^{-1} = \int_R^{\infty} \frac{\exp(\Psi(r)/k_BT)}{r^2}\,dr \qquad (14)$$

and D is the sum of diffusion coefficients for Q and F, and R is the sum of their radii. For $\Psi = 0$ (e.g., neutral quencher), $\beta = R$. With $\Psi(r)$ defined by eq 12, an attractive potential results in

$$\beta = -zr_0\exp(zr_0\kappa') \qquad (15)$$

with

$$\kappa' = \kappa/(1 + R\kappa) \qquad (16)$$

Then we have

$$\lambda = \beta/R = \frac{-zr_0}{R}\exp(zr_0\kappa') \qquad (17)$$

This predicts that a plot of ln λ vs κ' will be linear with slope zr_0. κ' is a function of molecular radius (eq 16), so R remains an adjustable parameter.

The static definition of λ, described by eq 11, and the kinetically derived expression (eq 17) represent two limiting cases. The first case, in which dynamics are ignored, is equivalent to assuming that the product $D\tau$ is small, so that only quenchers that are very close to a fluorophore can reach it before it emits a photon. The second case relies on the assumption of a steady-state distribution of quenchers around each excited fluorophore, which is only obtained for large values of $D\tau$. The pseudostatic model predicts fairly large values for λ because it only accounts for the participation of those quenchers most strongly affected by the attractive potential. The dynamic model predicts quite small values for λ because at long times, when a steady state has been achieved, the probability that an excited fluorophore will still have a quencher in close proximity is small and the rate of quenching is therefore governed by more distant quenchers (see Appendix). At intermediate times, applicable to most fluorophores, we expect $\lambda_{\max}$ to fall somewhere between these two extremes, and so we do not expect either model to exactly describe the quenching data. We take two approaches to modeling fulvic acid quenching as a function of ionic strength. First, we apply the pseudostatic model, but account for distance averaging by choosing Ψ' (eq 11) equal to the potential at a distance, r' (instead of at the surface), where Ψ' is given by eq 12 and r' is treated as a fitting parameter. In the second model, we graph ln λ vs κ' according to eq 17 and discuss our results in this context.

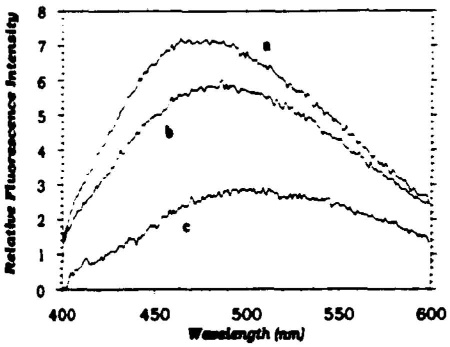

Figure 2. Fluorescence spectra of HA fraction C, in 10 mM borate buffer: (a) no quencher added, (b) with 8.2 mM tempol, and (c) with 8.2 mM tempamine. Spectra have been corrected for dilution, but not for inner filter effect, which leads to an apparent red shift in peak maxima (b and c) due to light absorption by the nitroxides in the range 400–460 nm.

Fluorescence of Humic and Fulvic Acids. Absorption of light by humic substances decreases approximately exponentially throughout the ultraviolet and visible wavelength regime (*21*). Light absorption in the range 300–400 nm results in fluorescence emission having a broad maximum near 460 nm (Figure 2); with longer wavelength excitation the emission peak decreases in intensity and shifts to the red. For Suwannee River fulvic acid, the overall fluorescence maximum occurs with excitation at 350 nm and emission at 460 nm. This is also the case for bulk Suwannee River humic acid, although individual size fractions of this material show slightly different fluorescence characteristics (vide infra). Broad, overlapping excitation and emission spectra and shifts in emission maxima with excitation wavelength are indicative of multiple fluorophores in these materials. This is confirmed through the measurement of complex, multiexponential fluorescence decay kinetics which suggest a minimum of three fluorescing species with lifetimes ranging from <1 to 6 ns (*22*).

In principle, the Stern–Volmer equation strictly applies only to species exhibiting a monoexponential fluorescence decay, a possible complication in the quenching of humic samples. In practice, however, significant nonlinearity in these plots would be detectable only if fluorescence lifetimes of the several species present differed by over 1 order of magnitude and at very high quencher concentrations (>50 mM); neither condition applies in this study. (It follows that a linear Stern–Volmer plot does not necessarily indicate the presence of a single, unique fluorophore.) The measured lifetimes of humic and fulvic acid fluorophores are in the range of <1 to ~7 ns (*22–25*); fewer than 5% of the fluorophores present have lifetimes longer than 2.5 ns (*22, 25*). In eq 1, τ becomes a weighted average of the true lifetimes. Because we do not rely on τ explicitly, only its constancy, its actual value is of secondary importance to this discussion.

A detailed theory of fluorescence quenching, incorporating time dependence and multiple lifetimes, has been derived by Szabo (*26*). However, for our purposes it makes little sense to apply such in-depth theories to a system that includes ill-defined values of τ, diffusion coefficients, and R. Indeed, if we are to retain generality for natural samples, it is reasonable to neglect differences in detail among individual molecules and to focus on what can be learned from these heterogeneous samples. In this spirit we shall first compare λ_{mean} values for FA and several size fractions of HA, at a fixed ionic strength of 5 mM (10 mM borate buffer). Then for FA we measure λ_{mean} as a function of ionic strength and make comparisons with a model compound, perylenetetracarboxylic acid. We then examine our measured values in the context of the pseudostatic (eq 11) and kinetic (eq 17) models using some reasonable assumptions about the average size and charge on humic molecules.

Experimental Section

General Procedures. Standard Suwannee River fulvic acid and humic acid were obtained from the International Humic Substance Society (IHSS). Fulvic acid was used as received; humic acid was acid washed to remove labile metals, as recommended by Hering (*27*), with the exclusion of the drying step. Perylenetetracarboxylic acid (PTC) was obtained from Aldrich as the dianhydride and was hydrolyzed in 25 mM NaOH. An NMR spectrum of PTC in D_2O/NaOD did not reveal any impurities or (partial) anhydride in solution. Water was from a Millipore Milli-Q system. 4-Hydroxy-tempo (tempol) and 4-amino-tempo (tempamine) were obtained from Aldrich; 4-(trimethylamino)-tempo(I^-) (trimethyl-tempamine) and 3-carboxy-proxyl were purchased from Sigma or Molecular Probes. Trimethyl-tempamine was passed through an anion-exchange column to replace I^- with Cl^-; the other compounds were used as received. Concentrated stocks (0.2–0.4 M) of these were made in water and their precise concentrations determined by absorption at 434 nm (ϵ = 12.6 M^{-1} cm^{-1}). In the experiments using tempamine and 3-carboxy-proxyl, the pH of stock solutions was adjusted to match that of the fulvic or humic sample being titrated.

Absorbance spectra were measured on an HP 8451A diode array spectrophotometer with 2-nm resolution. Fluorescence data were collected on an SLM Aminco SPF-500C fluorometer in ratio mode; the excitation and emission bandpasses were typically 4 and 5 nm, respectively. A 1-cm quartz cell was used for all optical measurements. Reported emission spectra have been corrected for instrument response with the software provided by the company.

Size Fractionation. HA was separated into 10 size fractions by gel chromatography using Sephadex G-50 (Sigma) eluted with 10 mM borate buffer (pH = 9.1). HA was not retained on either Sephadex G-10 or G-25 columns, indicating that chemical interactions with the gel do not occur in this buffer system. The column was 21.5 cm in length, with internal diameter 1.5 cm; flow rate was 0.56 mL/min. A sample of HA was preequilibrated in the eluting buffer and 0.5 mL of solution was applied to the column. Nine fractions of 0.9 mL each, and a tenth of 5.9 mL, were collected. Five samples, A–E, were chosen for quenching experiments, where A corresponds to fraction 2, B to 4, C to 6, D to 8, and E to 10. Fractions (except E) were diluted in buffer to an OD at 350 nm of 0.072, 0.063, 0.030, 0.013, and 0.013 for A–E, respectively.

Quenching. Concentrated stock solutions (~0.5 g/L) of FA were prepared in water, filtered (0.2 μm), and kept refrigerated in the dark. No difference in absorbance, fluorescence, or quenching properties was observed between fresh and stored samples. Solutions for quenching experiments were made by dilution of stocks into 10 mM acetate or borate buffers, providing an initial ionic strength of 5 mM. Ionic strength was increased, when required, by addition of the appropriate volumes of 0.4 or 4.0 M NaCl. The contribution of probe nitroxides is not included in the reported ionic strengths. Fulvic acid concentrations were approximately 5 mg/L; absorbance at 350 nm was 0.03 ± 0.005 (1-cm cell).

In quenching experiments, 2-mL solutions of fulvic or humic acids, or PTC, were titrated with 5–10-μL increments of nitroxide stock solutions to a final quencher concentration of ~10 mM. Fluorescence emission of FA was monitored at 460 nm with excitation at either 350 or 365 nm. HA fractions were excited at 350 nm with emission measured at 520 (A), 500 (B), 475 (C), or 465 nm (D and E). Excitation and emission wavelengths for PTC were 468 and 511 nm, respectively. Samples were illuminated only during actual measurement to avoid possible photobleaching or other photoinduced reactions. No change in fluorescence was observed when solutions were deoxygenated through bubbling with N_2, so no further attempt was made to exclude oxygen. The pH did not change by more than 0.1 pH unit during any titration.

Fluorescence data were corrected for dilution, weakly fluorescent impurities in the nitroxide stocks, and inner filter effect (*28*). Inner filter corrections did not exceed 25% for the highest nitroxide concentration employed and were nearly equivalent for both tempol and tempamine due to their almost identical absorption spectra. Data were graphed according to the Stern–Volmer equation (eq 5). Plots were linear with an intercept of 1.00 ± 0.02, except in a few cases where a decrease in slope was observed at high quencher concentrations. These deviations were observed primarily during titrations with trimethyl-tempamine and may be due to steric effects associated with the bulk of the three methyl groups surrounding the positive charge on this quencher. Initial slopes for trimethyl-tempamine were the same as those for tempamine, indicating that the primary amine in the latter compound is not contributing to the observed quenching. Tempamine was employed for subsequent experiments.

In a second set of experiments, solutions containing fulvic acid, either alone, with tempol (~4 mM), or with tempamine (~4 or 7 mM), were titrated in parallel with 0.4 or 4.0 M NaCl. The salt titration in the absence of nitroxide was used to correct for (small) changes in fulvic acid fluorescence due to ionic strength alone; other corrections were as noted above. From these data, λ was calculated for each addition from the rearranged Stern–Volmer equation:

$$\lambda = [(F_0/F) - 1]/K_N[Q]_B$$

where K_N is obtained from quenching by tempol (λ = 1).

Results and Discussion

Suwannee River fulvic and humic acid fluorescence was effectively quenched by the neutral and cationic nitroxides employed in this study (Figure 2). Emission appeared to be uniformly suppressed from 370 to 650 nm (excitation at 350 nm) although light absorption by the nitroxide itself

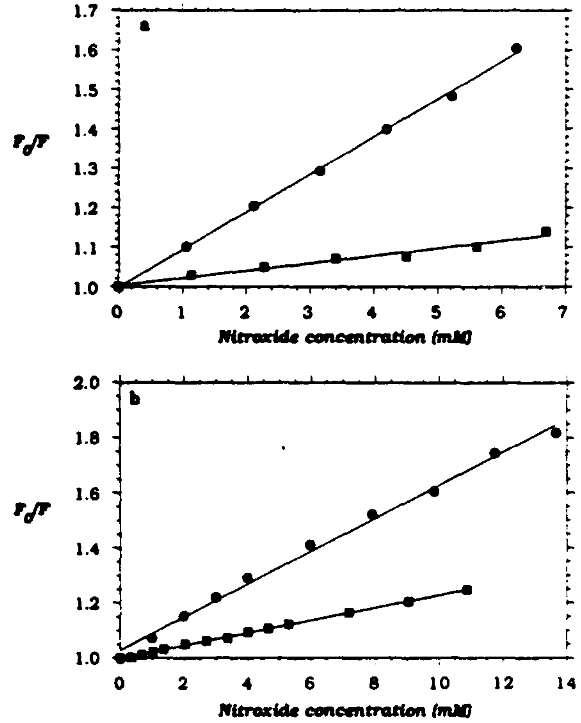

Figure 3. Stern–Volmer plots of quenching of fulvic acid fluorescence by tempol (squares) or tempamine (circles): (a) pH = 8.8, I = 5 mM; (b) pH = 4.6, I = 12 mM.

Table I. Fluorescence Peak Maxima and Relative Efficiencies, Measured Stern–Volmer Quenching Constants K_N (Tempol) and K_C (Tempamine), and Ratios (λ_{meas}) for FA and HA Fractions and PTC

sample	fluor max, nm	F_0/abs[a]	K_N, M^{-1}	K_C, M^{-1}	λ_{meas}
FA					
pH = 9.1	460	11.7	18.6	94.9	5.1
pH = 4.6	460	11.6	18.6	65.1	3.5
HA fractns[b]					
A	530	0.49	9.5	160.4	16.9
B	510	0.99	15.4	159.1	10.3
C	477	2.5	14.0	136.4	9.7
D	467	4.5	10.8	84.9	7.9
E	470	5.7	20.5	61.2	3.0
perylenetetra-carboxylic acid	511		32.2	122.3	3.8

[a] Fluorescence at peak maximum divided by absorbance at 350 nm, background subtracted. [b] HA fraction A contains the largest molecular weight molecules, E the smallest.

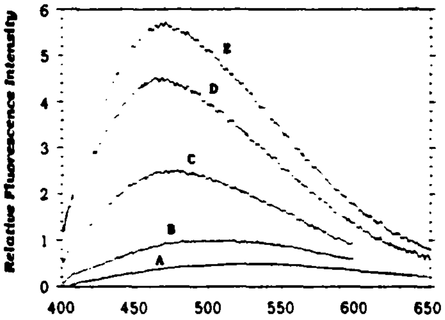

Figure 4. Fluorescence emission scans of HA size fractions A–E. Intensity has been normalized to absorbance at the exciting wavelength (350 nm); excitation and emission bandpasses were 5 nm.

(peak maximum at 435 nm) makes this difficult to ascertain. No new emission or absorption bands, which would indicate specific excited- or ground-state interactions between humics and nitroxides, were observed.

Suwannee River Fulvic Acid. FA solutions were titrated with tempol under a variety of pH and ionic strength conditions. Stern–Volmer plots (Figure 3) were linear and reproducible to within 4%. No systematic change in the slope (K_N) was observed over the pH and ionic strength range studied (pH = 4–9, I = 5–300 mM), indicating that the local concentration of neutral quencher is not significantly influenced by these factors. A value of K_N = 18.6 M^{-1}, an average of 50 determinations (including both slopes from Stern–Volmer plots and single-point measurements from NaCl titrations), represents the baseline, dynamic quenching coefficient and was used as a point of comparison for the charged quenchers. Quenching of FA fluorescence by cationic nitroxides, tempamine and trimethyl-tempamine at pH = 9.1 and I = 5 mM, resulted in linear Stern–Volmer plots with slopes 5.1-fold greater than those obtained for tempol (Table I). A smaller increase (3.5-fold) was measured at pH = 4.6. The anionic nitroxide, 3-carboxy-proxyl, was an ineffective quencher, giving Stern–Volmer plots with a slope of 0 within experimental uncertainty. Since in each case the identical nitroxide moiety is responsible for quenching, there should be no intrinsic differences in quenching efficiency among these compounds. All observed variations are therefore attributed to Coulombic interactions.

Suwannee River Humic Acid. HA, which is more polydisperse than the FA (*29, 30*), was used to examine changes in surface potential with molecular size. An empirical size separation was accomplished by gel permeation chromatography. Because gel filtration does not provide accurate molecular weight values for humic substances when calibrated against globular proteins (*30–32*), we refrain from estimating precise molecular weights of our fractions. This technique does, however, give a qualitative separation by size (*31, 32*). Molecular weight ranges estimated by analytical ultracentrifugation (*30*) are 2000–10000 for HA and 1000–2000 for FA from this source. Other workers report somewhat lower molecular weight values for FA: 860 by flow field-flow fractionation (*29*), and 740 by vapor-pressure osmometry (*33*).

For all fractions, fluorescence efficiency (F_0/absorbance) decreased with increasing size (Figure 4, Table I), a trend which has been previously observed (*34, 35*). In addition, emission spectra for the large-sized HA fractions were red-shifted relative to FA emission. Some variation in K_N was observed among the humic samples, which, along with the shifts in emission wavelength, could indicate the dominance of different fluorophores or different fluorophore microenvironments in each fraction. To a first approximation, differences in fluorescence yield or energy do not affect determinations of λ_{meas} because quenching by neutral and cationic nitroxides is compared for each sample. This can pose a problem when fluorescence is extremely low because quenching by the neutral nitroxide, tempol, becomes difficult to measure accurately. For this reason, more concentrated solutions (higher absorbance) were employed for quenching experiments with fractions A and B.

Quenching by the cationic nitroxide increased significantly with molecular size (Table I). Fraction A, containing the highest molecular weight species, exhibited

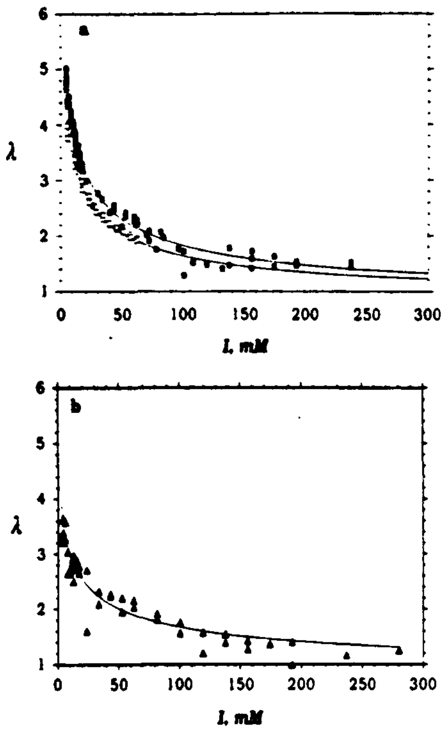

Figure 5. λ vs ionic strength for FA (■) and PTC (□) at pH = 9.1 (a) and pH = 4.6 (b). The lines are plots of the Debye–Hückel potential at 5 Å from the surface, for R = 8 Å, and z = −4.3 (a) or z = −3.0 (b).

both the highest degree of quenching by tempamine and the lowest by tempol, giving it the largest λ_{max} of any sample in this study. Fraction E, containing the lowest molecular weight species, showed the lowest λ_{max} in this group. If molecular charge increases proportionally to volume, then the potential at the surface, $\Psi(R)$, increases as $R^2/(1 + \kappa R)$ (eq 12, with $z \propto R^3$, $r = R$). Our data show a strong correlation between λ_{max} and R, consistent with this prediction.

Data suggest that acid content per carbon, specific volume, and therefore charge per volume do not differ greatly between humic and fulvic acids. Total (carboxyl and phenolic) acidity per gram (*36*) is nearly identical for FA (7.6 mmol/g) and HA (7.8 mmol/g), and their molar volumes (*30*) (0.46 and 0.51 cm^3/g, respectively) are within 10% of each other. However, carboxyl groups are relatively more important in FA (6.1 mequiv/g) than in HA (4.9 mequiv/g) (*36*). Thus, at pH = 9.1, HA should have a smaller overall charge per gram than FA; their higher molecular weights give HA a larger charge per *molecule* than FA. These data represent whole HA; there are no independent data available on possible variation of these parameters among size fractions.

Ionic Strength Effects. FA solutions were titrated with NaCl to examine the effect of ionic strength on quenching by cationic quenchers. At pH = 9.1, λ_{max} decreased rapidly in the range of 5–50 mM NaCl, with more gradual decreases at higher salt concentrations (Figure 5). The trend is the same at pH = 4.6, but the magnitude of λ_{max} is lower throughout this ionic strength range. Thus, sodium ions can effectively shield the electrostatic interactions between the cationic nitroxide and the fulvic acid and thus decrease the apparent surface potential of fulvic acid molecules.

Overall, these data fit our expectations for the behavior of oligoanionic macromolecules. At high pH all carboxyl (and perhaps some of the phenolic) groups are dissociated and the molecular charge is large, while at pH 4.6 some of these groups are protonated and the total charge is lower. The lack of complete charge neutralization at this pH is consistent with the carboxylic acid (pK_a < 3–5) content of these materials. In addition, the HA data confirm the expectation that large humic molecules have a greater surface potential than small ones.

These dramatic changes in λ_{max} lend support to models that incorporate electrostatic terms to account for variations in acidity or metal binding constants with ionic strength. Electrostatic terms should be of particular importance in transition zones, such as estuaries, where I increases from <5 mM to 0.7 M as river water and seawater mix. Size distributions in humic substances may also influence the transport and ultimate fates of some metal species which may be preferentially bound to the larger organic molecules.

Model Compound: Perylenetetracarboxylic Acid. PTC was employed as a model compound because its charge (−4) and size (R = 6.5 Å) are comparable to those estimated for FA. Quenching of PTC by tempol gave a K_N approximately 2-fold larger (32.2 M^{-1}) than that measured for FA (18.6 M^{-1}). This result is expected (eq 5) based on the longer fluorescence lifetime of PTC (~5.4 ns) as compared with FA. The Stern–Volmer plot obtained from quenching by tempamine showed upward curvature; this is predicted when the degree of quenching is high and the steady-state limit is not reached (*28, 37*). Higher order corrections to the Stern–Volmer equation predict nonlinearity, but the curvature is slight so we may safely neglect this correction. We therefore concentrate on the linear portion of the plot, which leads to $K_N\lambda$ = 122.3 M^{-1}. The ionic strength dependence of quenching by tempamine was remarkably similar to that of FA (Figure 5), with λ_{max} values for PTC falling slightly lower for ionic strengths of 5–60 mM.

Pseudostatic and Kinetic Model Fits

The qualitatively reasonable behavior of our results encouraged an attempt to extract more quantitative information about FA from these data, using the pseudostatic and kinetic analyses presented under Experimental Rationale.

Although it ignores important aspects of the quenching process, we observe that the pseudostatic model (eq 11) accurately reproduces the shape of the plots of λ vs ionic strength, with Ψ' taken as the Debye–Hückel potential at a distance (r') of 11 Å from the center of the FA molecule (Figure 5). For this fit we chose z = −4.3 and R = 8 Å, in accordance with Aiken et al. (*33*). PTC data can be fit with z = −4, R = 6.5, and r' = 15 Å.

While the kinetic model is not expected to accurately predict absolute quenching rates, the relative change in rate with ionic strength may still be examined. Because κ' must be calculated from R, which is not well constrained, determination of z from eq 17 is not unambiguous. Thus, the model compound, PTC, was used to aid in choosing the appropriate range of values for R. Figure 6a shows plots of ln λ vs κ' for PTC, with R equal to 6.5, 8, and 11 Å. The resulting z values are −3, −3.3, and −4.0, respectively. Estimates of the molecular dimensions of PTC suggest a radius of 6.5 Å, whereas the correct charge of −4 is obtained only when a larger radius of 11 Å is chosen. There could be several causes for this discrepancy: (i) molecular radius and Debye–Hückel radius may not be

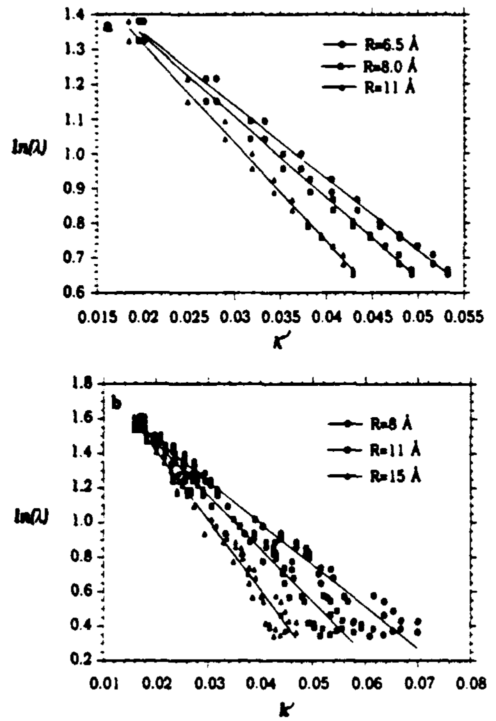

Figure 6. (a) Plot of ln λ vs κ' for PTC with R set to 6.5, 8.0, and 11.0 Å. (b) ln λ vs κ' for FA with R set to 8.0, 11.0, and 15.0 Å.

identical, especially where a substantial hydration sphere is expected; (ii) a breakdown of assumptions implicit in the Debye–Hückel analysis, e.g., a small, spherically symmetric potential and a continuous solvent; (iii) application of a steady-state theory to dynamic, molecular-scale interactions (*37*). It appears unlikely that impurities in the PTC solution (e.g., semianhydride) decreased the average charge per fluorophore in this solution since no such compounds were detected by NMR.

Despite these limitations, this analysis can provide useful information about the charge on FA. Molecular weight considerations require that FA (MW > 750) have a radius at least as large as that of PTC (MW = 424). Plots of ln λ vs κ' are shown in Figure 6b for R equal to 8, 11, and 15 Å. The slopes give z values of −3.4, −4.3, and −5.7, respectively.

Some further limits may be placed on R and z from current data on FA. Charge per molecule is based on accurate measurements of acidity equivalents per gram, and less well constrained determinations of molecular weight. For our purpose, number-average molecular weight, M_n, is more appropriate than the higher weight-averaged values; charge equivalents·M_n gives the average charge per molecule. Taking 6.1 mequiv of carboxylic acid/g (*38*) for FA, and recent M_n measurements of 711 (*39*), 829 (*33*), and 860 (*29*), gives z equal to −4.3, −5.0, or −5.2, respectively. Our data show that if PTC (R = 11 Å) is a good size analogue for FA, then z is equal to −4.3. If FA is larger than this, then a higher charge is predicted (z = −5.7 for R = 15 Å). The radius of gyration (R_g) for this material has been measured (*33*) by small-angle X-ray scattering to be 7.7 ± 0.6 Å (average of two measurements, pH = 9); other fulvic acid samples from the Suwannee River have given R_g values of 7.0 ± 0.3 and 8.8 Å (*33*). For a spherical molecule, R_g underestimates the molecular radius by ~30% (*40*).

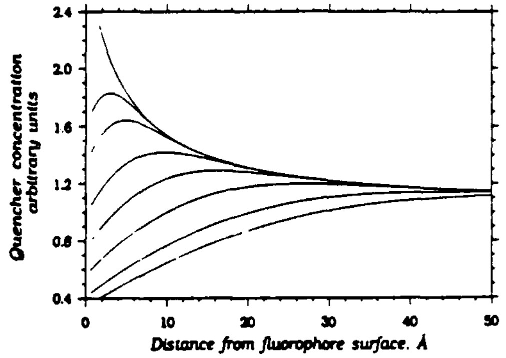

Figure 7. Schematic representation of the time evolution of the probability that a quencher with charge +1 will be within distance r of a fluorophore with charge −1. The times represented are 0, 0.05, 0.1, 0.25, 0.5, 1, 2, and 3 ns after excitation, based on the equation of Flannery (*43*) with intrinsic quenching rate equal to 5 times diffusional encounter rate.

Effect of Sample Heterogeneity. Fulvic and humic acids are heterogeneous mixtures of compounds, so the inevitable biases which this can introduce must be considered. A general question is whether the fluorescent molecules in a sample of humic material are representative of *all* molecules present; specific to quenching techniques is the question of how the results are affected by an uneven distribution of fluorescence among the molecules.

We are not aware of any technique that has successfully isolated a nonfluorescent fraction of any humic or fulvic acid, nor have any simple, free fluorophores been identified in these substances. (For example, in our work all size fractions of HA were fluorescent, but no pure fluorophores were detected.) This is a strong indication that the observed fluorescence originates from within diverse HA molecules and is not due to a few unique, separable compounds. We therefore assume, as do those who employ static quenching to measure binding coefficients (*11–14*), that the fluorescent molecules are representative of the total humic sample. Additionally, because there is no intrinsic reason why fluorescence and charge should be linked, we may assume that each fluorescent molecule contains the same charge as nonfluorescent molecules of the same size and neglect this as a significant source of error.

Neither static nor dynamic quenching depends on the number of fluorophores present; if all molecules were otherwise identical, results would not depend on what percentage of them were fluorescent. However, in a mixture of variously sized molecules, each with identical fluorescence and surface potential, the fluorescence quenching technique measures the number-averaged λ (i.e., it depends on the number of molecules present, not their mass), which tends to emphasize the smaller sized species (*41*). This bias is enhanced because large humic molecules are, as demonstrated above (Table I), less highly fluorescent than are small ones; this leads to a smaller loss of overall solution fluorescence in quenching of a large molecule than in quenching of a small one. Thus, despite its higher surface potential, the high molecular weight fraction is underrepresented in measurements of both F_0 and F, and the bias in our results should be toward the smaller and less charged molecules in each sample.

Conclusions

These experiments have demonstrated that cations are present at the surface of humic and fulvic acids in significant excess over their concentrations in bulk solution. This effect is more pronounced at high pH where a larger fraction of acid groups are dissociated. It is also very sensitive to ionic strength, consistent with shielding of potential by electrolyte ions. Surface potential increases with molecular size in Suwannee River humic acid, as is reasonable if acid content per mass remains constant in this material. Because highly charged metal ions will be particularly susceptible to attractive potentials, this observation is of particular importance for those attempting to incorporate electrostatic effects into models of metal binding to humic substances (*6*). The surface charge calculated by a kinetic analysis of quenching data is in good agreement with predictions based on acid content and molecular weight measurements.

Acknowledgments

We thank B. Bartschat for help with theoretical aspects of humic acid electrostatics.

Appendix

The difficulties encountered in applying the steady-state kinetic model to fluorescence quenching data result from the time evolution of the probability of finding a quencher near an excited fluorophore (see, e.g., Hong and Noolandi (*42*), Flannery (*43*), Szabo (*26*), Eads et al. (*37*)) (Figure 7). At $t = 0$, corresponding to the absorption of a photon by the fluorophore, the concentration of neutral quenchers near the (negatively charged) fluorophore surface is identical to that in the bulk solution, while the concentration of cationic quenchers is higher (eq 10). At $t > 0$, the concentration of quenchers in contact with an excited fluorophore is zero because all such fluorophores have been quenched. With increasing time after excitation, the probability of finding a quencher and excited fluorophore in close proximity decreases, until, at long times, a steady state is reached. Equations 13–17 describe the steady-state situation. Thus, if the natural lifetime of the excited fluorophore is shorter than the time required to reach steady state, the measured quenching rate will be greater than that predicted by eq 13. The relevant time scale for this process can be approximated by the mean time a molecule takes to traverse a distance equal to the Debye length, $1/\kappa$, estimated from the mean diffusion time:

$$t = (\kappa^2 D)^{-1}$$

With $1/\kappa = 20$ Å ($I = 25$ mM) and $D = 10^{-5}$ cm^2 s^{-1}, this gives $t = 4$ ns. Because the time scales of fluorescence decays in solution are generally in the nanosecond range, the steady-state solution is unlikely to apply to quenching in the presence of a strong, attractive potential.

Registry No. Tempol, 2226-96-2; tempamine, 14691-88-4.

Literature Cited

(1) Zepp, R. G.; Schlotzhauer, P. F.; Sink, R. M. *Environ. Sci. Technol.* **1985**, *19*, 74–81.

(2) Faust, B. C.; Hoigné J. *Environ. Sci. Technol.* **1987**, *21*, 957–964.

(3) Waite, T. D.; Wrigley, I. C.; Szymczak, R. *Environ. Sci. Technol.* **1988**, *22*, 778–785.

(4) Dzombak, D. A.; Fish, W.; Morel, F. M. M. *Environ. Sci. Technol.* **1986**, *20*, 669–675.

(5) Fish, W.; Dzombak, D. A.; Morel, F. M. M. *Environ. Sci. Technol.* **1986**, *20*, 676–683.

(6) Bartschat, B.; Cabaniss, S. E.; Morel, F. M. M. *Environ. Sci. Technol.*, preceding article in this issue.

(7) Tipping, E.; Backes, C. A.; Hurley, M. A. *Water Res.* **1988**, *22*, 597–611.

(8) Blough, N. V. *Environ. Sci. Technol.* **1988**, *22*, 77–82.

(9) Tipping, E.; Reddy, M. M.; Hurley, M. A. *Environ. Sci. Technol.* **1990**, *24*, 1700–1705.

(10) de Wit, J. C. M.; van Riemdijk, W. H.; Nederlof, M. M.; Kinniburgh, D. G.; Koopal, L. K. *Anal. Chim. Acta* **1990**, *232*, 189–207.

(11) Saar, R. A.; Weber, J. H. *Anal. Chem.* **1980**, *52*, 2095–2100.

(12) Ryan, D. K.; Weber, J. H. *Anal. Chem.* **1982**, *54*, 986–990.

(13) Waite, T. D.; Morel, F. M. M. *Anal. Chim. Acta* **1984**, *162*, 263–274.

(14) Cabaniss, S. E.; Shuman, M. S. *Anal. Chem.* **1986**, *58*, 398–401.

(15) Green, S. A.; Simpson, D. J.; Zhou, G.; Ho, P. S.; Blough, N. V. *J. Am. Chem. Soc.* **1990**, *112*, 7337–7346.

(16) Turro, N. J. *Modern Molecular Photochemistry*, 1st ed.; Benjamin/Cummings: Menlo Park, CA, 1978; p 246.

(17) Green, J. A.; Singer, L. A.; Parks, J. H. *J. Chem. Phys.* **1973**, *58*, 2690–2695.

(18) Winiski, A. P.; Eisenberg, M.; Langner, M.; McLaughlin, S. *Biochemistry* **1988**, *27*, 386–392.

(19) Tanford, C. *Physical Chemistry of Macromolecules*, 1st ed.; John Wiley and Sons: New York, 1961; p 465.

(20) Weston, R., Jr.; Schwartz, H. A. *Chemical Kinetics*, 1st ed.; Fundamental Topics in Physical Chemistry; Prentice Hall: Englewood Cliffs, NJ, 1972; pp 151–171.

(21) Zepp, R. G.; Schlotzhauer, P. F. *Chemosphere* **1981**, *10*, 479–486.

(22) Lochmüller, C. H.; Saavedra, S. S. *Anal. Chem.* **1986**, 58, 1978–1981.

(23) Milne, P. J.; Odem, D. S.; Zika, R. G. In *Photochemistry of Environmental Aquatic Systems*; Zika, R. G., Cooper, W. J., Eds.; ACS Symposium Series 327, American Chemical Society: Washington, DC, 1987; pp 132–140.

(24) Milne, P. J. Ph.D. Thesis, University of Miami, Miami, FL, 1989.

(25) Lappen, A. J.; Seitz, W. R. *Anal. Chim. Acta* **1982**, *134*, 31.

(26) Szabo, A. *J. Phys. Chem.* **1989**, *93*, 6929–6939.

(27) Hering, J. G. Ph.D. Thesis, MIT-WHOI Joint Program in Oceanography, 1988.

(28) Lakowicz, J. R. *Principles of Fluorescence Spectroscopy*, 1st ed.; Plenum Press: New York, 1983; p 44.

(29) Beckett, R.; Jue, Z.; Giddings, J. C. *Environ. Sci. Technol.* **1987**, *21*, 289–295.

(30) Reid, P. M.; Wilkinson, A. E.; Tipping, E.; Jones, M. N. *Geochim. Cosmochim. Acta* **1990**, *54*, 131–138.

(31) Reuter, J. H.; Perdue, E. M. *Geochim. Cosmochim. Acta* **1981**, *45*, 2017–2022.

(32) De Nobili, M.; Ghessing, E.; Sequi, P. In *Humic Substances II: In Search of Structure*; Hayes, M. H. B., MacCarthy, P., Malcolm, R. L., Swift, R. S., Eds.; John Wiley and Sons Ltd.: West Sussex, UK, 1989; pp 561–592.

(33) Aiken, G. R.; Brown, P. A.; Noyes, T. I.; Pinkney, D. J. In *Humic Substances in the Suwannee River, Georgia: Interactions, Properties, and Proposed Structures*; Averett, R. C., Leenheer, J. A., McKnight, D. M., Thorn, K. A., Eds. *Open-File Rep.—U.S. Geol. Surv.* **1989**, *No. 87-557*, 163–178.

(34) Stewart, A. J.; Wetzel, R. G. *Limnol. Oceanogr.* **1980**, *25*, 559–564.

(35) Hayase, K.; Tsubota, H. *Geochim. Cosmochim. Acta* **1985**, *49*, 159–163.

(36) Thorn, K. A. In *Humic Substances in the Suwannee River, Georgia: Interactions, Properties, and Proposed Structures*; Averett, R. C., Leenheer, J. A., McKnight, D. M., Thorn, K. A. Eds. *Open-File Rep.—U.S. Geol. Surv.* **1989**, *No. 87-557*, 251–309.

(37) Eads, D. D.; Dismer, B. G.; Fleming, G. R. *J. Chem. Phys.* **1990**, *93*, 1136–1148.

(38) Bowles, E. C.; Antweiler, R. C.; MacCarthy, P. In *Humic Substances in the Suwannee River, Georgia: Interactions, Properties, and Proposed Structures*; Averett, R. C., Leenheer, J. A., McKnight, D. M., Thorn, K. A., Eds. *Open-File Rep.—U.S. Geol. Surv.* **1989**, *No. 87-557*, 205–229.

(39) Aiken, G. R.; Malcolm, R. L. *Geochim. Cosmochim. Acta* **1987**, *51*, 2177–2184.

(40) Haschemeyer, R. H.; Haschemeyer, A. E. V. *Proteins: A Guide To Study by Physical and Chemical Methods*, 1st ed.; John Wiley and Sons: New York, 1973; p 206.

(41) Wershaw, R. L.; Aiken, G. R. In *Humic Substances in Soil, Sediment, and Water*; Aiken, G. R., McKnight, D. M., Wershaw, L. R., MacCarthy, P., Eds.; John Wiley: New York, 1985; pp 477–492.

(42) Hong, K. M.; Noolandi, J. *J. Chem. Phys.* **1978**, *68*, 5172–5176.

(43) Flannery, M. R. *Phys. Rev. A* **1982**, *25*, 3403–3406.

Received for review May 9, 1991. Revised manuscript received September 9, 1991. Accepted October 8, 1991. This work was supported by the Environmental Protection Agency under Grant CR-815293-01, by the National Science Foundation under Grant OCE-8917688, and by the Office of Naval Research under Grant N00014-89-J-1260. This is contribution No. 7734 from the Woods Hole Oceanographic Institution.

Note of clarification:

The technique of gel chromatography separates molecules by size, not molecular weight. Therefore the HA fractions examined in this chapter contain molecules of similar size, not molecular weight. However, size fractions separated by gel chromatography have been found to correlate with molecular weight as determined by uv ultracentrifugation (31).

Chapter Four: Absorbance of waters of coastal South Florida and the Gulf of Mexico

Introduction

Study of the optical properties of colored organic matter (COM) in the sea has several motivations. Light absorption is a predominant characteristic of humic substances, which are ubiquitous in the environment, and thus, absorption measurements provide a straightforward method for tracking the sources and sinks of this important component of the global carbon cycle. In addition, an understanding of light absorption and emission of COM is proving to be crucial to interpretation of data and images in the rapidly expanding field of remote sensing, especially in the highly colored waters of coastal regions. Ultimately, careful study of COM absorption and fluorescence spectra, combined with detailed photochemical studies, may lead to identification of the key chromophores present in this material, giving us new insights as to COM behavior in the diverse environments in which it is found.

Color has long been recognized as one indicator of the organic content of soil and water. Colored substances were first extracted from peat in 1786, and from natural waters as early as 1839 (*1*). Indeed, color is a defining characteristic of aquatic humic substances which are variously known as "Gelbstoff," "yellow substance," colored organic matter (COM) or "dissolved fluorescence." Organic-rich rivers are often described as having "black water," e.g. the Rio Negro, a major tributary of the Amazon, and the Black River of North Carolina. The characteristic yellow-brown color of these waters is due to the strong absorption of short-wavelength visible radiation by COM. In seawater, fluorescence, rather than absorbance, of COM has commonly been employed as an estimate of dissolved organic matter. This is due, in part, to the much lower COM content of seawater compared with many freshwaters and the relatively high sensitivity of fluorescence techniques. Although the colored material in natural waters is undoubtedly organic, all dissolved organic matter (DOM) is not colored.

Large-scale surveys of pigment concentrations in the ocean are rapidly expanding our understanding of the spatial and temporal distributions of photosynthetic organisms. Extensive data sets of optical parameters can be collected from satellites or airplanes, but care is required in their analysis. For example, pigment concentrations are typically calculated from ratios of water-leaving radiance at several wavelengths (e.g. 443 or 520 and 550 nm (2)) and are assumed to reflect the living plankton population. However, the presence of non-living light-absorbing material can seriously distort these determinations, necessitating modification of standard algorithms for observations of coastal regions (3-6). Further analysis of the attenuation of light due to absorption by phytoplankton, non-living detrital particles, and dissolved organic matter is required for interpretation of these measurements (7). Light absorption by dissolved organic matter, is the subject of the present study.

A more thorough understanding of the nature of chromophores encountered in the ocean may eventually help to clarify the distinctions between "old" oceanic DOM having an apparent radiocarbon age of up to 5000 yr before present, "fresh" DOM produced *in situ* by marine organisms, and terrestrial DOM delivered by rivers or coastal runoff. The relative contributions of these sources to the vast pool ($\approx 1.7 \times 10^{17}$ g) of organic carbon in the oceans are not well understood. Although sufficient organic matter is delivered by rivers each year to account for the DOM content of the seas, measured characteristics (e.g. $\delta^{13}C$, H/C and C/N ratios) of oceanic and terrestrial DOM are different. Based on such data, it is thought that terrestrial DOM must either be lost or significantly transformed upon its arrival in the oceans (*8*).

Both marine and terrestrially derived COM may be altered or destroyed by photochemical processes in the photic zone. Photochemical reactions of COM result in generation of carbon radicals (*9-11*), reactive oxygen species (*12-14*), and reduction of associated trace metals (*15*). In order to estimate the impact that such reactions may have on the global distribution of organic carbon, much more work is required on the optical properties of marine surface waters and of riverine source waters, and on how these relate to the photodegradation pathways of COM.

Background

Light absorption in the aquatic environment is dominated by organic chromophores. Many of these, of course, reside within, and are synthesized by photosynthetic (and other) organisms. This work is not concerned with these generally well-characterized compounds, but rather, with the ill-defined, non-living, dissolved organic substances that are ubiquitous in natural waters. In focusing on these, it is important to be aware that inorganic ions and complexes can also be significant absorbers of uv and visible radiation. Absorption by nitrate (313 nm) and nitrite (280, 360 nm) is unlikely to cause interferences because concentrations and absorption coefficients are relatively small in most instances. However, the overwhelming presence of sodium chloride in seawater precludes any meaningful optical measurements in this medium at wavelengths below 240 nm.

Absorption by organic species in the range of 250-600 nm most likely arises from $\pi \rightarrow \pi^*$ and $n \rightarrow \pi^*$ transitions of conjugated alkenes and extended, or heavily substituted, aromatic structures. Charge transfer interactions, either within metal fig. 1. Absorption spectrum of sample I-12, collected in spring, 1991, at 25.51°N 81.32°W. Both field-collected and lab-collected spectra are shown.

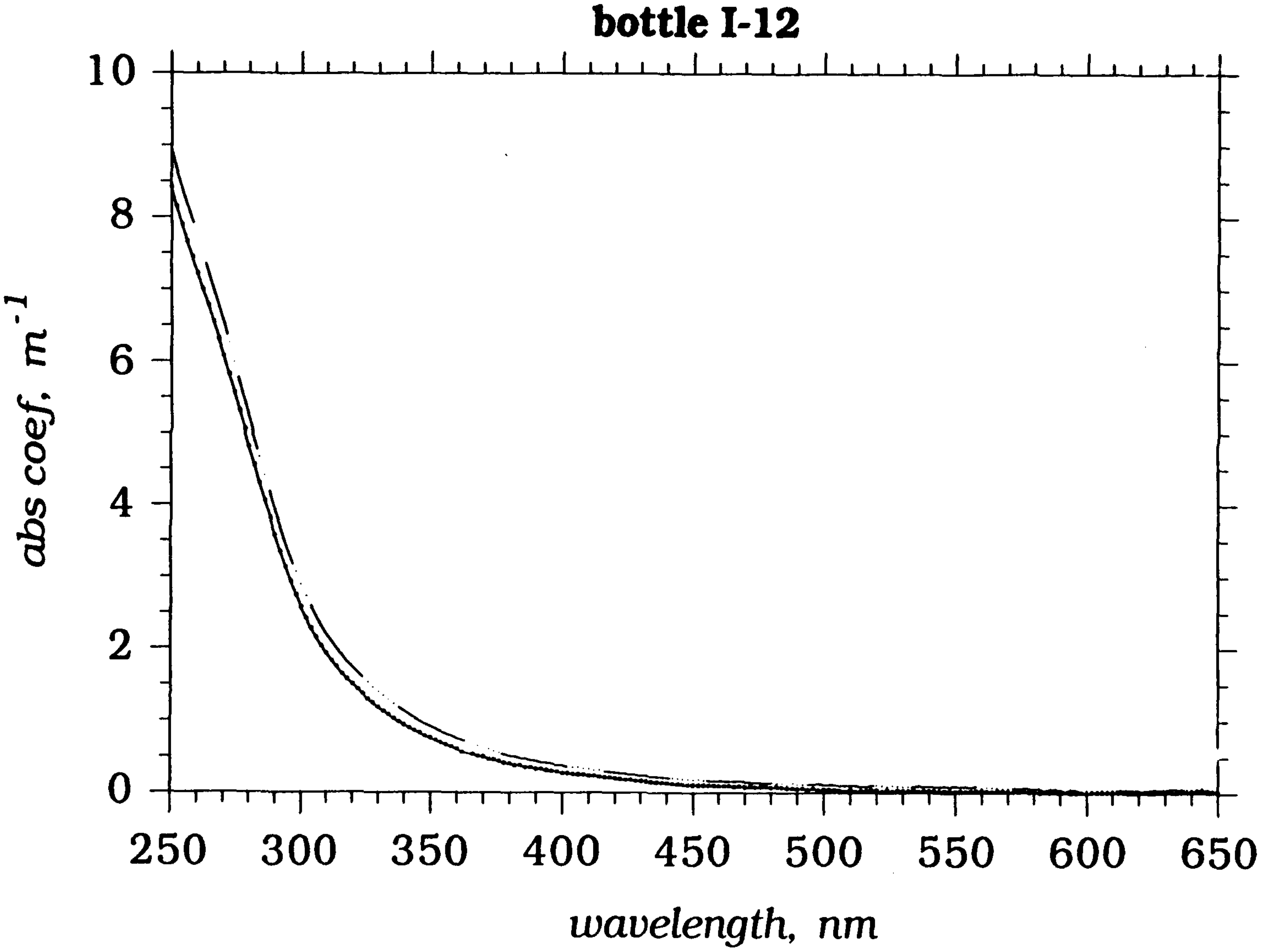
bottle I-12
abs coef, m^{-1}
10
8
6
4
2
0
250
300
350
400
450
500
550
600
650
wavelength, nm

-ligand complexes or between adjacent organic groups, may also contribute to this absorption signal. For natural water samples no well-defined absorption or emission peaks attributable to distinct compounds are observed. Only a small fraction (10-15%) of the DOM in any natural sample has been uniquely identified, and of the known compounds, many do not absorb significantly in the uv-visible region (e.g. carbohydrates, aliphatic amino acids, lipids). Of the large pool of unidentified DOM in the oceans, we do not know what fraction absorbs light in any spectral region, i.e. what subset of DOM constitutes COM.

The shapes of absorption spectra of COM from soil, freshwater, and saltwater are quite similar, exhibiting a roughly exponential decrease with increasing wavelength from the uv-B region (290-320 nm) into the visible (*16-19*). An example is shown in figure 1. The absorbance at a given wavelength can therefore be taken as a measure of COM "concentration"; absorbance at 300 nm ($a(300)$) was chosen for this study. Specific (mass normalized) absorption coefficients ($l\bullet(\text{g carbon}\bullet\text{m})^{-1}$) can vary greatly depending on the sources of COM (*20, 21*), so $a(300)$ is not necessarily proportional to the *mass* of organic carbon present in a sample, especially when several carbon sources contribute to the signal. Nevertheless, it provides a useful, first-order comparison among samples.

The observed exponential decay of absorption coefficients with increasing wavelength can be quantified by fitting spectra to an equation of the form

$$(1) \qquad a(\lambda)=a(r)exp[S\bullet(\lambda-r)]$$

where $a(\lambda)$ is the absorption coefficient at wavelength λ, and r is a reference wavelength (usually 450 nm). In general, this relationship provides a reasonable fit to absorbance data, and there have been several attempts to use the slopes (S) of plots of $ln(a)$ vs λ to characterize optical properties of natural waters (5, *17-19*). The parameter S is a logical extension to the use of ratios of absorbance at selected wavelengths, E_4/E_6, commonly employed by soil scientists (*22, 23*). (E_4/E_6 is the ratio of absorbances at 465 and 665 nm). S, like E_4/E_6, gives an indication of the rate of decrease in absorption with increasing wavelength. There is, however, no *a priori* reason for absorbance spectra of natural samples to display this type of empirical relationship. Thus, while slopes of such plots can be used as a qualitative measure of similarities among samples, in some cases deviations from linearity are severe, and may themselves communicate useful information.

Because light absorption in natural waters cannot be easily attributed to identifiable chromophores, absorption spectra cannot be described as sums of distinct components. Instead, an empirical approach is taken and an effort is made to characterize COM using a few, easily measured spectral parameters. The absorption coefficient at 300 nm ($a(300)$) and the slope (S) of the log-linearized spectrum are employed here to describe obvious spectral features. A more qualitative comparison of spectral characteristics can reveal more subtle variations, perhaps providing clues as to the origin of COM at a given site.

Several caveats must be considered in the use of the parameter S. It is calculated from a linear fit to a semilog plot and therefore gives exaggerated weight to the low $a(\lambda)$ values at wavelengths at the red edge of the spectrum. Thus, when graphs exhibit curvature, S will be strongly influenced by even a small absorbance at long wavelengths. Most spectra do show some curvature when plotted in this manner, therefore S values depend to some degree on the wavelength range over which they are calculated. In addition, an exponential factor, such as S, does not behave as a linear parameter in mixing of different water masses. Mixing of waters with n distinct S values (S_i) gives a spectrum exhibiting multiexponential decay:

$$(2) \qquad a(\lambda)=\sum_{1}^{n} a_i(r)exp[S_i\bullet(\lambda-r)]$$

which will be continuously curving when plotted as *ln(a)* vs λ. In theory, if *n* is small (2 or 3), non-linear fitting protocols could be used to determine S_i values. In practice, however, even for *n*=2, differences between S_1 and S_2 in natural waters are rarely large enough to distinguish curvature due to mixing from that observed in many "pure" natural samples. In this example, the apparent *S* value measured for a mixture will be strongly weighted towards the smaller of S_1 and S_2.

Besides curvature in semilog plots of absorption spectra, there can be other obstacles to an unambiguous determination of S. Measurement of large *S* values poses some difficulty; the samples with the largest values of *S* invariably have very low absorbance, with *a(λ)* often falling below detection limits at <320 nm. This means that *S* must be determined from as few as 10-15 points, and it also becomes quite sensitive to errors in correcting for baseline offsets (see Appendix A). An additional consideration, related to the general problem of nonlinearity in semilog plots, is the possibility of calculating a non-representative slope because of curvature in the spectrum of a weakly absorbing sample. This problem is illustrated by the fact that many samples in this work showed a distinct upward curvature at wavelengths below ~310 nm. If this material is diluted such that only a small portion on the blue edge of the spectrum remains within detection limits, *S* will appear anomalously large compared with *S* values determined from solutions containing higher concentrations of the same material.

Despite these shortcomings, the parameter *S* retains simplicity as its primary advantage. It provides a straightforward device for categorizing gross differences in optical absorbance among water samples. When the fit is good, the whole spectrum may be predicted from measurements at just a few wavelengths, a result which has been suggested for potential application to remote sensing (4-6). In order for this parameter to be of general utility, we must have some understanding of how it varies with factors such as source, 'age', and history of the absorbing organic matter. If we are to study this material in the laboratory, it is also important to ascertain how sample collection and storage procedures may bias measurements of optical properties.

Methods

Study sites and sample collection The major study area investigated in this work was along the southern coast of Florida (fig 2). Samples representing both oligotrophic "blue water" and terrestrially-derived "brown water" from this region were studied. Blue water samples were obtained at several stations in the Gulf of Mexico and in the Gulf Stream. Coastal samples were collected in and around Oyster Bay, located at 24°22'W 81°6'N. The area was visited in both May and August 1991, in order to assess seasonal variations in optical properties. Freshwater samples, representing the terrestrial source water, were collected from the Tamiami Canal.

Florida samples were collected aboard the R.V. Columbus Iselin out of Miami, along the south-eastern side of the Florida Keys and into the Gulf of Mexico to 85.4° W in spring and 86.0° W in fall (fig 2). On the fall cruise, the Iselin followed a direct path from this western-most point back east to Oyster Bay; in the spring the ship reached the shore somewhat further north and followed the coast ≈100 km down to the Bay.

For samples from South Florida, absorption spectra were measured both at sea and in the lab. In the field, water was drawn with a 20 ml syringe directly from the surface pumping system on the R.V. Columbus Iselin. This system draws water from ~2 m fig. 2. Map of sampling locations around South Florida and the Gulf of Mexico. Absorbance spectra were collected in the field at each surface site indicated. Bottled samples and COM isolates came from selected sites along the cruise tracks. Samples were collected during two cruises of the R/V Columbus Iselin in May (x) and August (O) 1991.

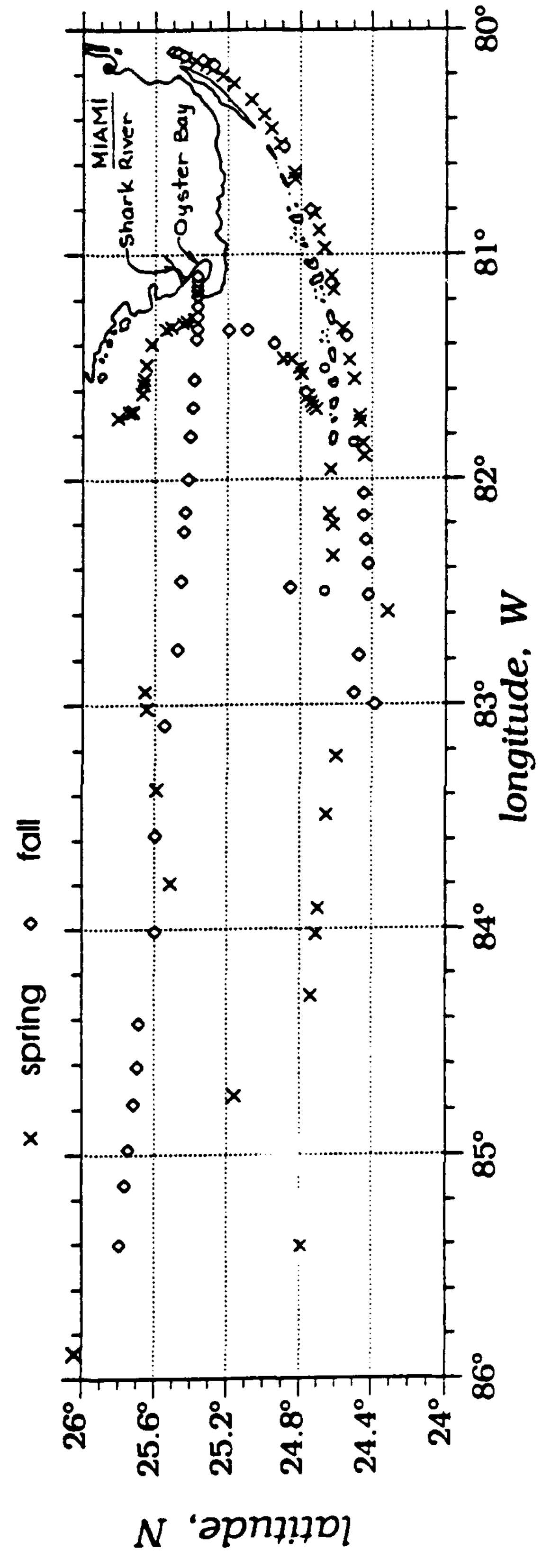

× spring
◇ fall
MIAMI
Shark River
Oyster Bay
80°
81°
82°
83°
84°
85°
86°
longitude, W
26°
25.6°
25.2°
24.8°
24.4°
24°
latitude, N

below the surface through a Teflon inlet, located forward of the ship's bow; seawater is continually flushed through Teflon lines which deliver it directly to the shipboard laboratory. Water was immediately filtered through a pre-rinsed 0.2 µm nylon filter, and its absorbance was measured within 10 minutes. Water samples were collected in clean glass bottles for fluorescence and absorbance measurements in Woods Hole. They were refrigerated at 4° C immediately after collection.

Optical data. Absorption spectra, both on shipboard and in the lab, were measured on an HP 8451A diode array spectrophotometer with 2 nm resolution. Purified water from a Millipore "Milli-Q" system was used as a reference. Spectra were stored on floppy disks for later replotting and analysis. The estimated sensitivity limit of the spectrophotometer is 0.002 absorbance units, corresponding to an absorption coefficient of about 0.1 m^{-1} (5 cm cell).

Spectral data were transfered from the HP-85 computer internal to the spectrophotometer to a Macintosh computer. Several steps were required in this procedure: (i) conversion of HP-85 'spectral data format' to regular HP-basic format, (ii) conversion of HP-basic format to standard IEEE ASCII. For the first step I wrote an HP basic program (TRANS and variations) to recall spectral files and store them in HP standard format, with or without wavelength values, background subtraction, or other manipulations. Commercial software (A Gentle Wind, Inc.) was used to convert the HP data to standard ASCII. From this point data were easily imported into DOS or Macintosh programs, including worksheet and graphing software, or the SLM-Aminco fluorometer software.

Data were manipulated and graphed using Kaleidagraph, running on a Macintosh SE-30. The baseline was adjusted, either during or after transfer from the HP-85 computer, to be zero over the range of 700 to 800 nm (see Appendix A). The absorption coefficient, $a(\lambda)$, in units of m^{-1}, is given by:

$$a(\lambda)=2.303\, A(\lambda)/l = 46.06\, A(\lambda) \tag{4}$$

where A is the measured optical density and l is the cell length (0.05 m). Spectra were graphed as $ln(a)$ vs λ, and slopes were determined by use of a standard linear regression routine provided with Kaleidagraph software.

Results

Geographical distribution of absorbance As a first approximation, the optical absorption coefficient at 300 nm ($a(300)$) is taken as a measure of the amount of COM in a sample. Seasonal and spatial variations of $a(300)$ in the waters studied are employed to investigate the transport of organic material in these systems. Values of $a(300)$ ranged from a high of 84.3 m^{-1} (Tamiami Canal, August, 1991) to a low of 0.1 m^{-1} (central Gulf of Mexico, May, 1991). The data are listed in tables I (May data) and II (August data). Because most of the samples were collected along an east-west path, it is convenient to plot $a(300)$ as a function of longitude, as shown in figures 3 and 4 for the spring and fall data, respectively. Three regions are defined in these plots. The southeastern region extends from Miami to 82.0° W and includes all samples collected south of the Keys. The Gulf of Mexico region is everything west of 82.0° W. The Florida Bay region includes the area along Florida's west coast, north of the Keys and extending to 82.0° W. The Shark River flows into Oyster Bay, and thence into Florida Bay, at about 81.0° W. Freshwater samples, collected inland, and the most highly absorbing samples collected within Oyster Bay are not included on these plots.

Table I. Absorption coefficients, slopes, and positions of surface samples collected in May 1991.

sample# disk 1	a(300) m^{-1}	slope $x10^3 nm^{-1}$	position, decimal degrees	
			latitude, N	longitude, W
freshwater				
50	60.08	17	Everglades (0.2 mm filtered)	
49	63.48	17	Everglades (0.45 mm filtered)	
seawater				
3	0.44	22	25.431°	80.122°
7	0.51	27	25.378°	80.137°
9	0.40	27	25.321°	80.155°
13	0.52	26	25.290°	80.172°
14	0.34	24	25.230°	80.202°
16	0.32	33	25.168°	80.238°
21	0.48	28	25.072°	80.314°
22	0.48	[19]*	25.002°	80.381°
25	0.33	45	24.961°	80.442°
28	0.63	[13]	24.914°	80.510°
31	1.00	21	24.837°	80.636°
33	1.26	19	24.832°	80.663°
35	0.38	23	24.725°	80.816°
38	1.16	20	24.698°	80.891°
39	0.77	22		
41	0.41	26	24.669°	80.968°
43	0.57	[13]	24.629°	81.093°
45	0.46	29	24.615°	81.154°
47	0.70	20	24.564°	81.326°
53	0.59	27	24.528°	81.465°
55	0.75	20	24.502°	81.550°
57	0.56	22	24.471°	81.712°
59	0.29	32	24.465°	81.741°
61	0.52	44	24.452°	81.836°
63	0.35	32	24.444°	81.895°
65	0.52	29		
67	0.26	47	24.602°	83.229°
71	0.23	43	24.653°	83.489°
75	0.16	62	24.700°	83.909°
77	0.25	33	31.027°	84.023°
79	0.23	48	24.739°	84.299°
81	0.44	19		
83	0.10	87	25.515°	83.795°
85	0.26	39	25.589°	83.374°
87	0.21	48	25.649°	83.016°
89	0.11	85	25.657°	82.940°
91	1.56	24	25.807°	81.721°

Table I. (continued) Absorption coefficients, slopes, and positions of surface samples collected in May 1991.

sample#	a(300)	slope	position, decimal degrees	
disk 2	m^{-1}	$x10^2\ nm^{-1}$	latitude, N	longitude, W
1	0.73	36	25.747°	81.697°
3	1.03	21	25.725°	81.697°
5	0.89	23	25.725°	81.689°
7	0.87	27	25.672°	81.611°
9	1.02	17	25.667°	81.571°
11	1.06	18	25.662°	81.548°
13	1.34	21	25.651°	81.486°
15	2.04	21	25.620°	81.394°
17	2.74	21	25.541°	81.330°
19	2.75	20	25.511°	81.320°
21	2.39	19	25.447°	81.304°
23	2.63	18	25.424°	81.297°
27	2.62	20	25.384°	81.283°
34	36.21	20	Oyster Bay	
44	1.21	[13]	24.849°	81.461°
46	1.35	[14]	24.804°	81.497°
48	1.23	20	24.792°	81.526°
50	1.22	17	24.756°	81.622°
52	1.06	21	24.742°	81.650°
54	1.24	19	24.731°	81.669°
57	1.60	20	24.713°	81.684°
60	0.65	[16]	24.639°	82.156°
62	0.68	[16]	24.620°	82.207°
64	0.59	[15]	24.621°	82.345°
66	0.33	35	24.316°	82.591°

• Values in parenthesis represent spectra with strong curvature.

Table II. Absorption coefficients, slopes, and positions of surface samples collected in August 1991.

sample	a(300)	slope	position, decimal degrees	
disk 1	m^{-1}	$x10^3 nm^{-1}$	latitude	longitude
freshwater				
30	84.3	17	Tamiami River	
seawater				
1	0.31	38	25.505°	80.096°
2	0.39	25	25.505°	80.096°
3	0.24	48	25.472°	80.102°
4	0.48	23	25.442°	80.115°
5	0.25	40	25.339°	80.133°
6	0.31	29	25.276°	80.154°
7	0.31	36	24.893°	80.522°
8	0.90	17	24.747°	80.799°
9	0.67	20	24.632°	81.125°
10	1.16	20	24.632°	81.125°
11	0.26	65	24.545°	81.358°
12	0.95	20	24.448°	82.067°
13	0.54	20	24.450°	82.166°
14	0.45	23	24.439°	82.274°
15	0.45	23	24.425°	82.382°
16	0.56	15	24.425°	82.518°
17	0.40	34	24.474°	82.783°
18	0.62		24.859°	82.487°
19	0.33	36	24.502°	82.950°
20	0.47	23	24.388°	82.998°
22	0.48	30	26.008°	85.932°
31	1.09	26	25.797°	85.402°
32	0.69	22	25.767°	85.135°
34	0.83	20	25.749°	84.978°
35	0.50	16	25.717°	84.776°
36	0.29	47	25.698°	84.611°
37	0.38	33	25.688°	84.421°
38	0.31	28	25.601°	84.011°
39	0.45	35	25.598°	83.580°
40	0.16	72	25.548°	83.089°
41	0.20	62	25.477°	82.755°
42	0.40	25	25.460°	82.457°
43	0.47	23	25.441°	82.235°
44	0.43	33	25.435°	82.147°
45	0.46	31	25.417°	81.998°
46	0.78	17	25.403°	81.803°
47	1.07	19	25.392°	81.676°
48	1.13	18	25.385°	81.551°
49	4.44	18	25.373°	81.373°

Table II. (continued) Absorption coefficients, slopes, and positions of August 1991 samples.

	salinity	sample	abs	slope	position, decimal degrees	
	‰	disk 1	m^{-1}	x10^{2} nm^{-1}	latitude	longitude
coast station		50	5.38	18	25.367°	81.332°
transect	35.3	53	4.17	18	25.367°	81.327°
"	34.5	54	5.29	18	25.367°	81.273°
"	33.8	55	6.51	18	25.367°	81.227°
"	32.2	56	8.47	20	25.367°	81.182°
"	32.0	57	13.71	17	25.367°	81.158°
"	35.3	58	34.13	17	25.367°	81.138°
"		59	39.87		25.367°	81.115°
"	23.4	60	40.36	17	25.367°	81.115°
Shark R.	19.2	61	53.58	17	25.367°	81.093°
		62	1.77	14	25.192°	81.334°
		63	1.18	29	25.092°	81.333°
		64	1.09	17	24.946°	81.395°
		65	0.97	19	24.772°	81.608°

fig. 3. Absorption coefficients (*a(300)*) vs longitude for spring samples. (×) indicates the south-eastern region, (□) indicates the Gulf of Mexico samples, and (■) represents the Florida Bay area.

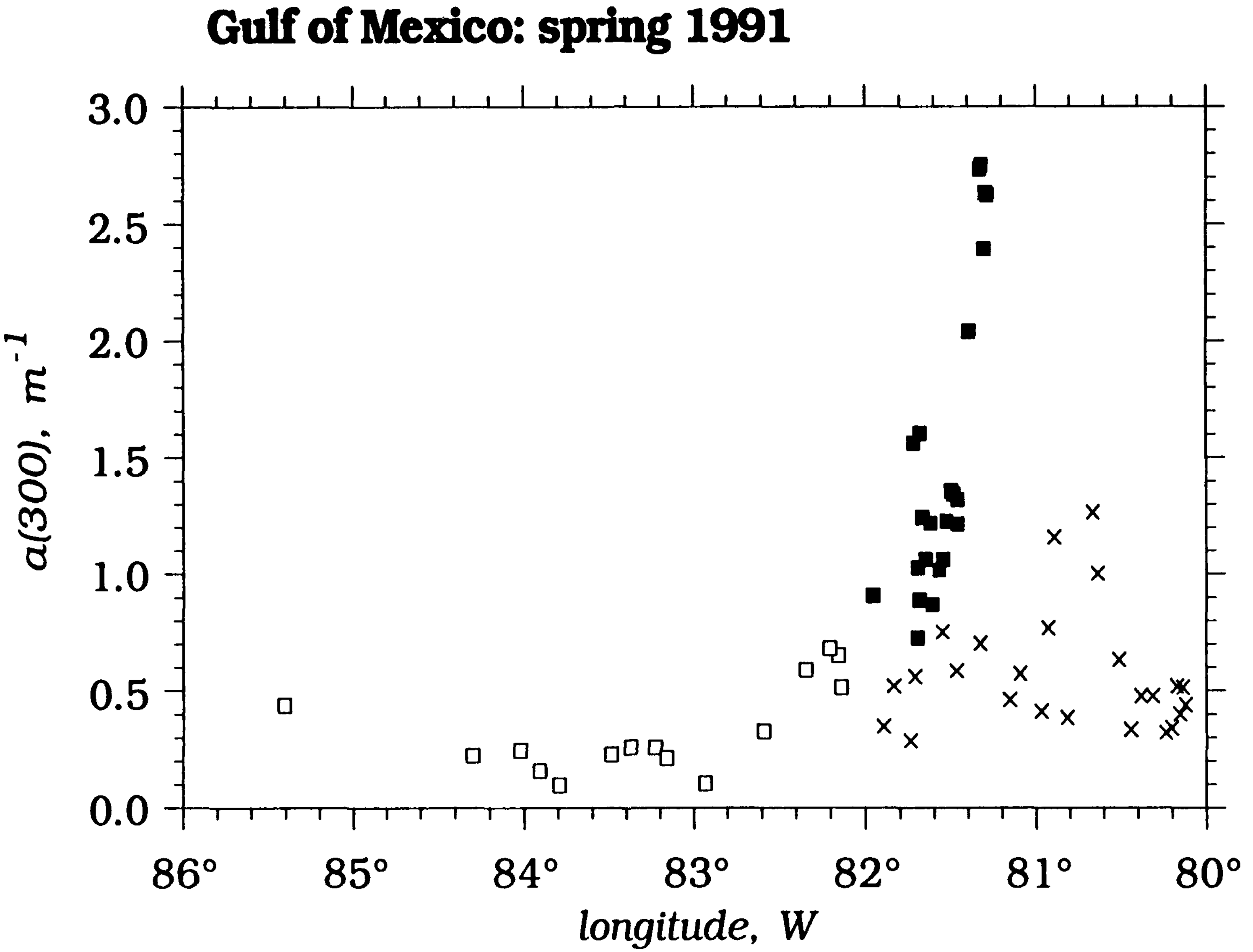
Gulf of Mexico: spring 1991
3.0
2.5
2.0
1.5
1.0
0.5
0.0
a(300), m-1
86°
85°
84°
83°
82°
81°
80°
longitude, W

fig. 4. Absorption coefficients (*a(300)*) vs longitude for fall samples. (×) indicates the south-eastern region, (□) indicates the Gulf of Mexico samples, and (■) represents the Florida Bay area.

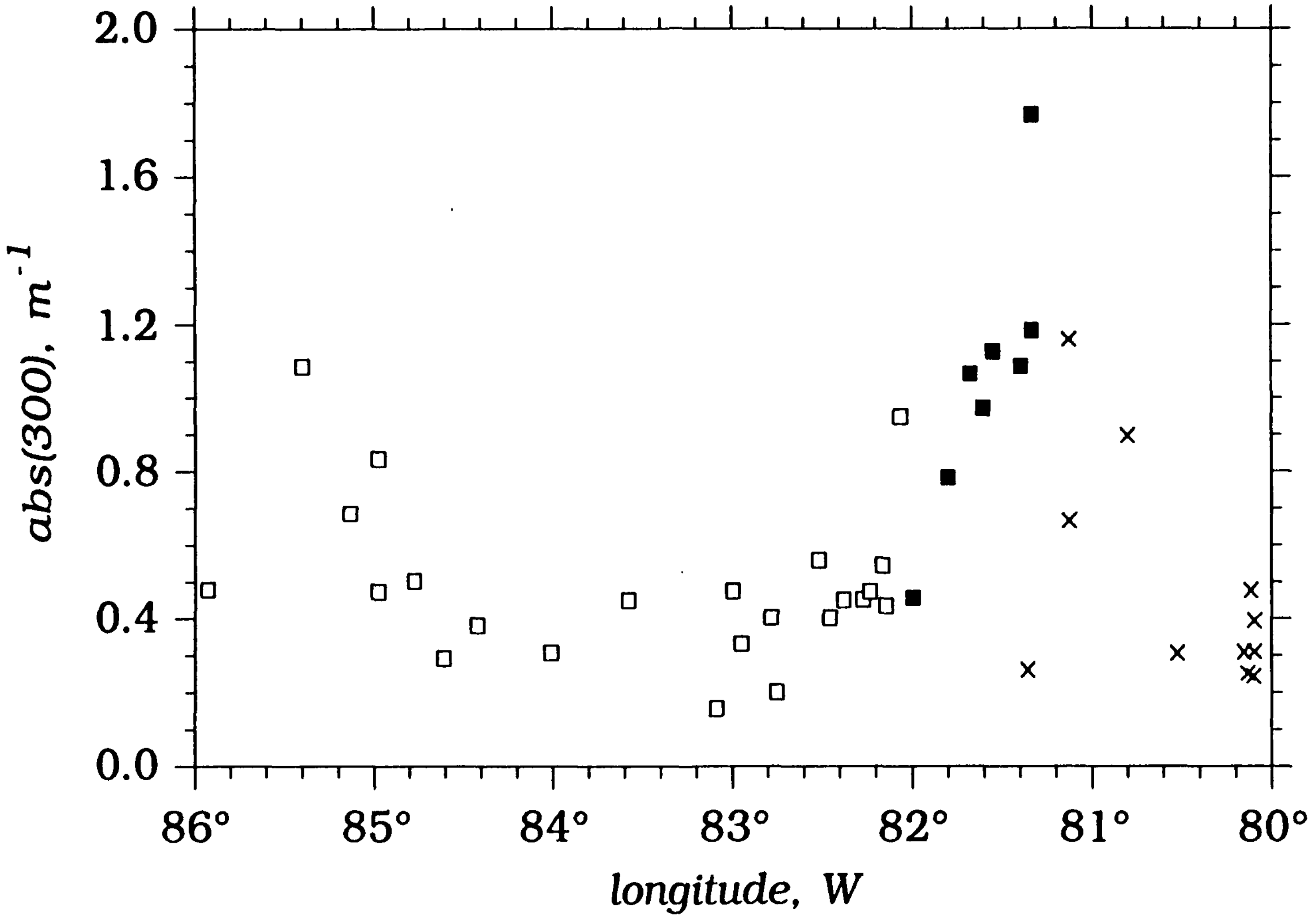

Gulf of Mexico: fall 1991

fig. 5. Absorption coefficients (*a(300)*) vs longitude for spring(x) and fall (O) samples.

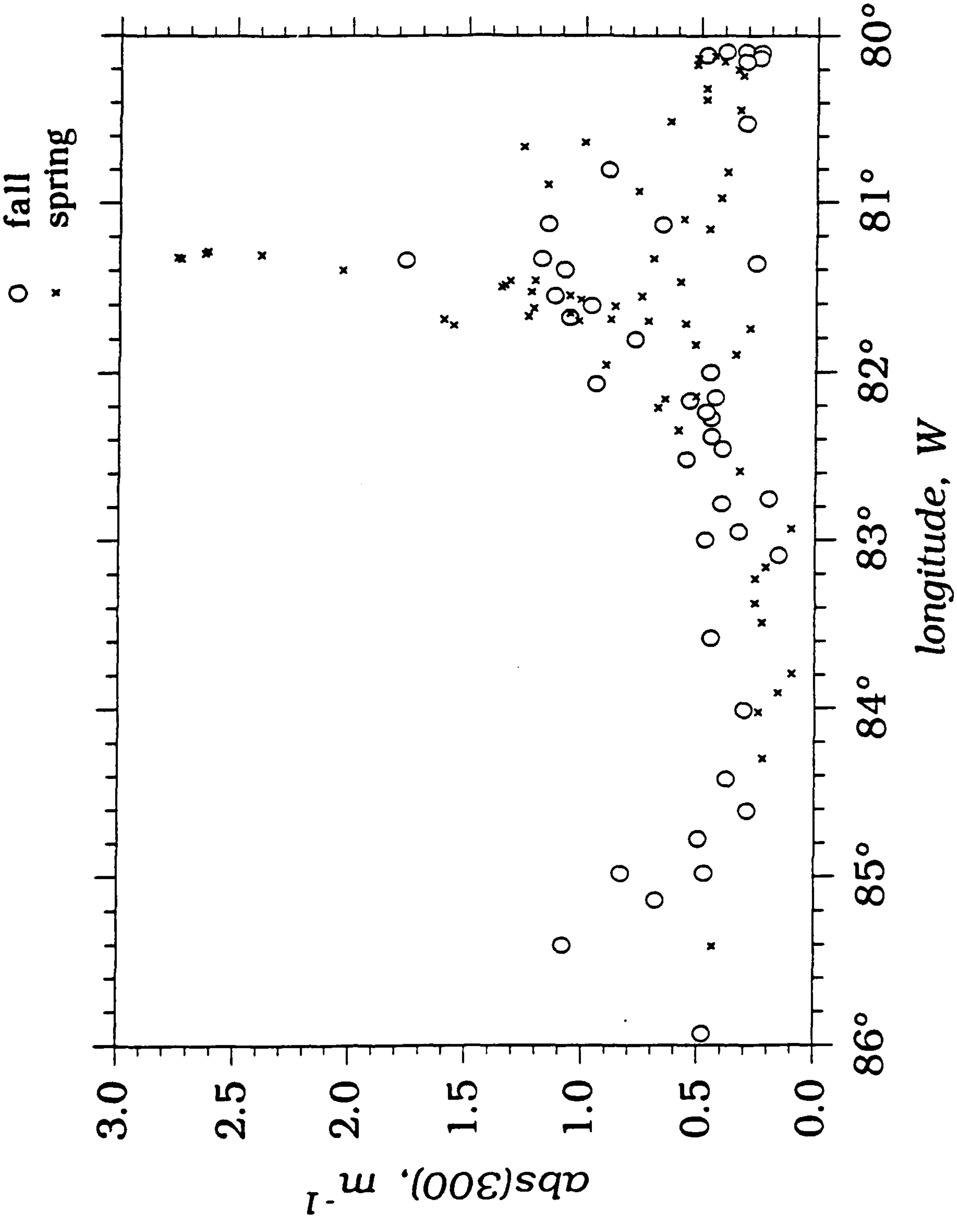
fall
spring
abs(300), m-1
3.0
2.5
2.0
1.5
1.0
0.5
0.0
longitude, W
80°
81°
82°
83°
84°
85°
86°

The most obvious feature in the absorbance data, apparent in both spring and fall, is the pronounced maximum due to the Shark River inflow to Oyster Bay (see fig. 2). In contrast, both the Gulf and south-east blue water regions have *a(300)* values less than 1 m^{-1}. There was considerable variation in *a(300)* values in the south-east region between 80.5° W and 81.5° W in both seasons sampled. This area is just south of the Keys which separate Florida Bay from the Straits of Florida; waters originating in the Everglades, with their characteristic high absorbance, flushing through between these islands probably produce the observed scatter in the *a(300)* data. Data from both wet and dry seasons are compared in figure 5. While there are no striking seasonal differences, there is some suggestion that *a(300)* may have been slightly higher in the Gulf of Mexico (west of 82° W) during the fall cruise. Not shown on these plots are the samples collected within Oyster Bay itself, which had *a(300)* values in excess of 30 m^{-1} in both seasons (tables I and II).

Spectral Characteristics. Figure 6 shows the log-linearized spectra of a series of water samples collected on a transect from "blue water" (26° 00.48' N 85° 55.9' W) into Oyster Bay in August 1991. This figure demonstrates several general features common to many of the spectra collected in this region. The plots are quite linear in the range of 290-500 nm (over which *S* was calculated) but some deviations from linearity are apparent. In particular, an obvious bump is noticeable in the region 260-300 nm. This feature is most distinct in waters with a low overall absorbance where it may be responsible for the large values of S calculated for these samples. In addition, spectra which extend beyond 550 nm sometimes show a small increase in *a(λ)* around 560 nm. A definite trend towards steeper slopes with lower absorbance is evident from these data.

S was calculated from absorbance spectra plotted as *ln(a)* vs λ; the portion from 290 nm to the point where absorbance decreased to the detection limit of the spectrophotometer was fit to a line by a standard linear regression. In most cases the fit was quite good; some typical examples, with fits, are shown in figure 7. Reliable values of *S* measured on field-collected spectra varied from $\approx$0.015 to >0.030 nm^{-1}. The lowest slopes corresponded to inland and coastal samples, while offshore "blue waters" generally exhibited larger values of *S*. Very large *S* values measured for several samples are included in the tables (I and II), although the weak absorbance of these samples makes these values suspect.

Absorption spectra of bottled samples were remeasured after transportation to Woods Hole to determine whether their optical properties had been retained during storage and handling. *a(300)* values of bottled samples measured in the lab are plotted against those measured in the field in fig. 8. The correlation is excellent and the slope is within 5% of unity. The slight decrease in absorbance in some of the bottled samples may be due to minor losses of absorbing material, perhaps to the glass walls of the bottles.

The correlation of *S* values measured in the field and on bottled samples is not as good as that of *a(300)* values (fig 9). This primarily reflects the greater uncertainty in *S*, estimated to be $\approx$15%, and greater for larger *S* values. A substantial decrease in *S* after collection may be indicative of contamination of the bottles. Several bottled samples (fall: #36-39) were discarded due to the appearance of an obviously new absorption band at $\approx$330 nm. For the remaining bottles, variations in *a(300)* and *S* were within the estimated errors; we therefore assume their fluorescence to be equally representative of that in the field.

fig. 6. A series of absorbance spectra plotted as the natural log of the absorption coefficient (m^{-1}). Samples were collected in August, 1991 along the transect between the central Gulf of Mexico and Oyster Bay.

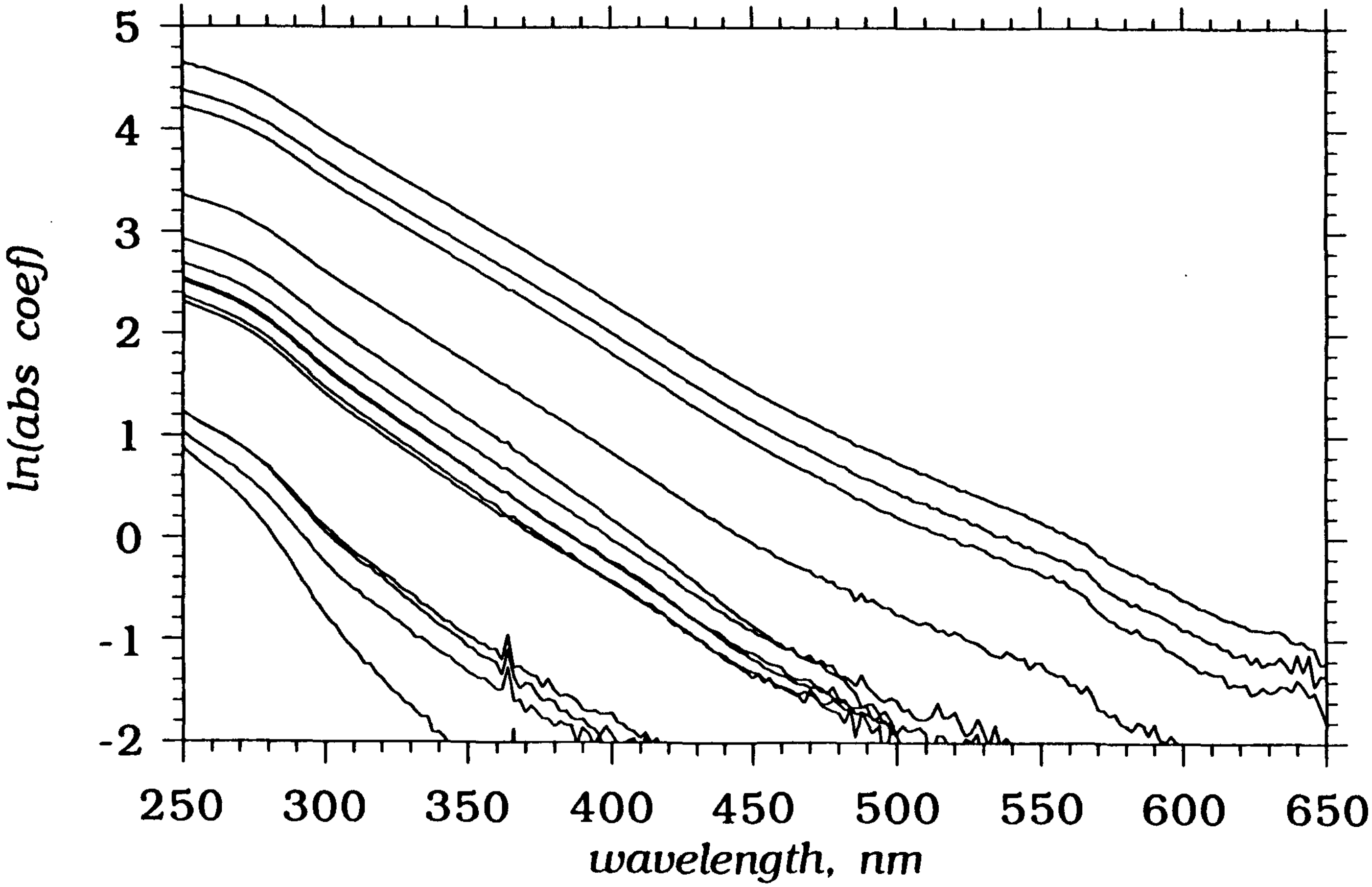

Blue water to Shark River: fall 1991

fig. 7 Example of good and not so good linear fits to log-linearized absorbance spectra. The pronounced increase in slope at wavelengths <310 nm is apparent in several spectra. These spectra were all collected on shipboard in August, 1991.

Gulf of Mexico: fall 1991

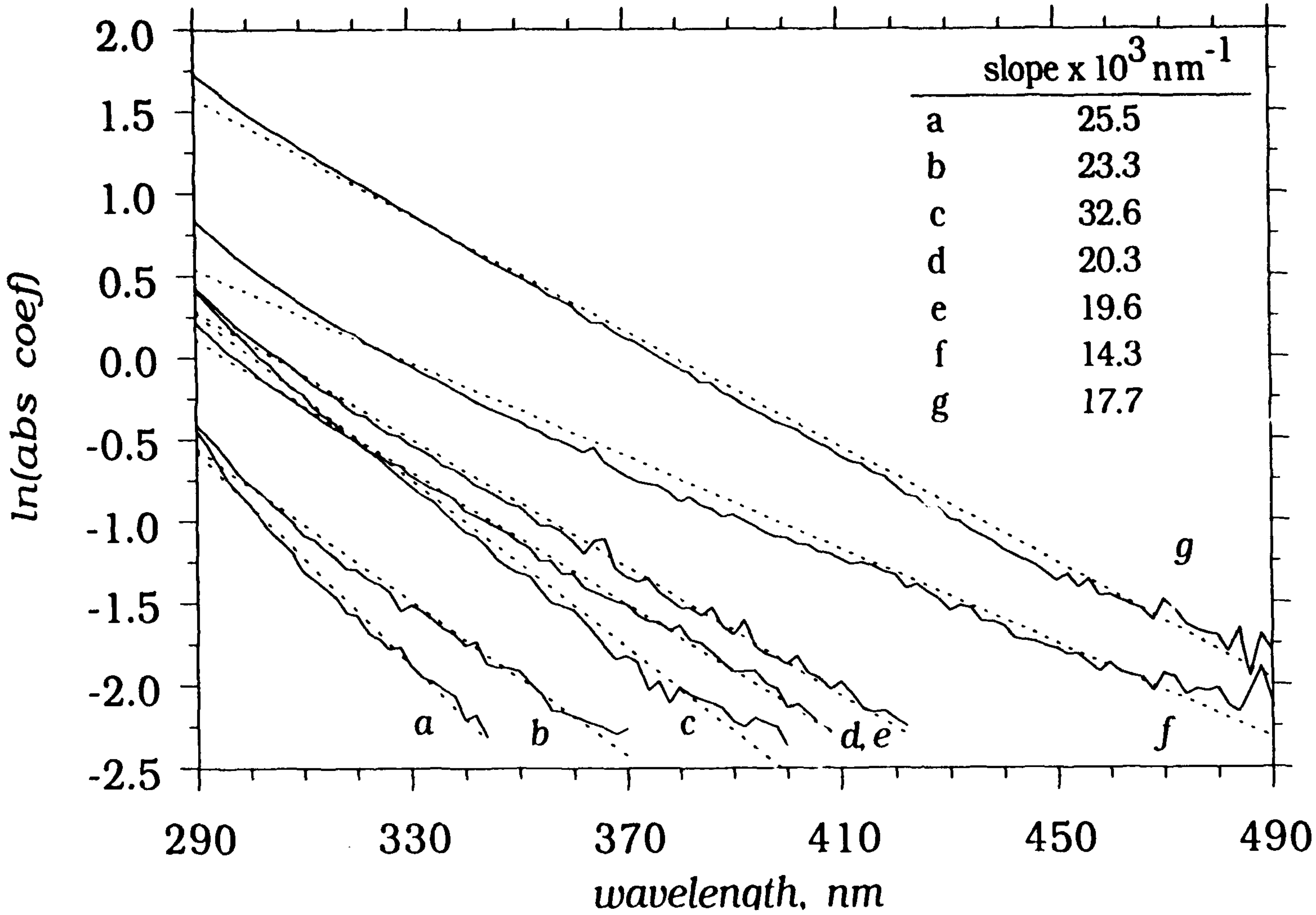

fig. 8 Correlation between *a(300)* values measured on field and stored samples. Linear correlation is shown. The lower plot shows an expanded scale.

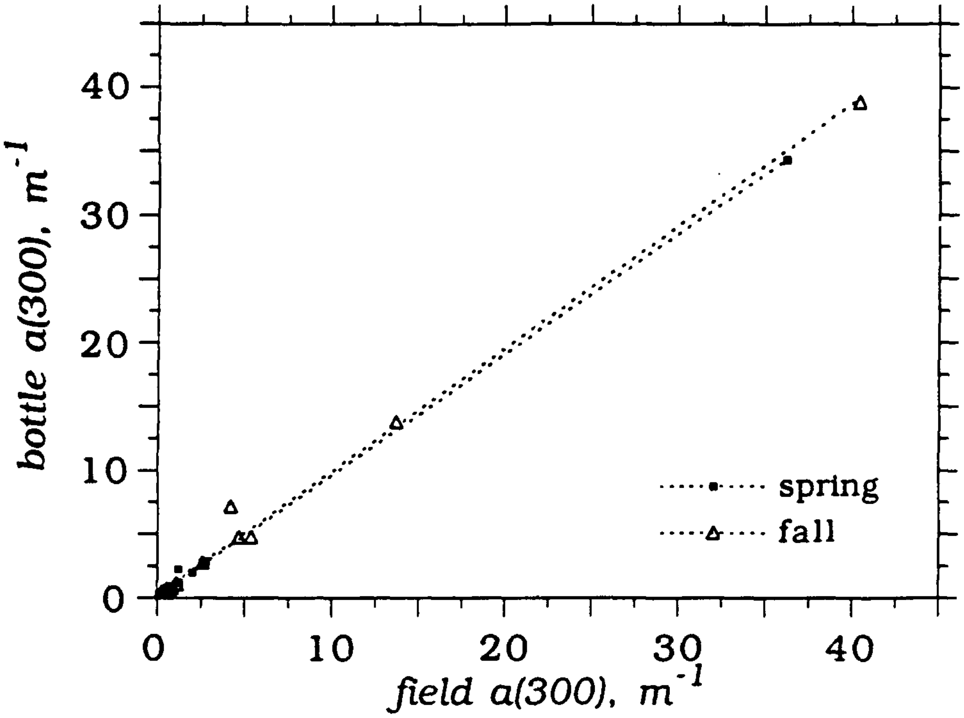
bottle a(300), m^{-1}
field a(300), m^{-1}
0
10
20
30
40
spring
fall

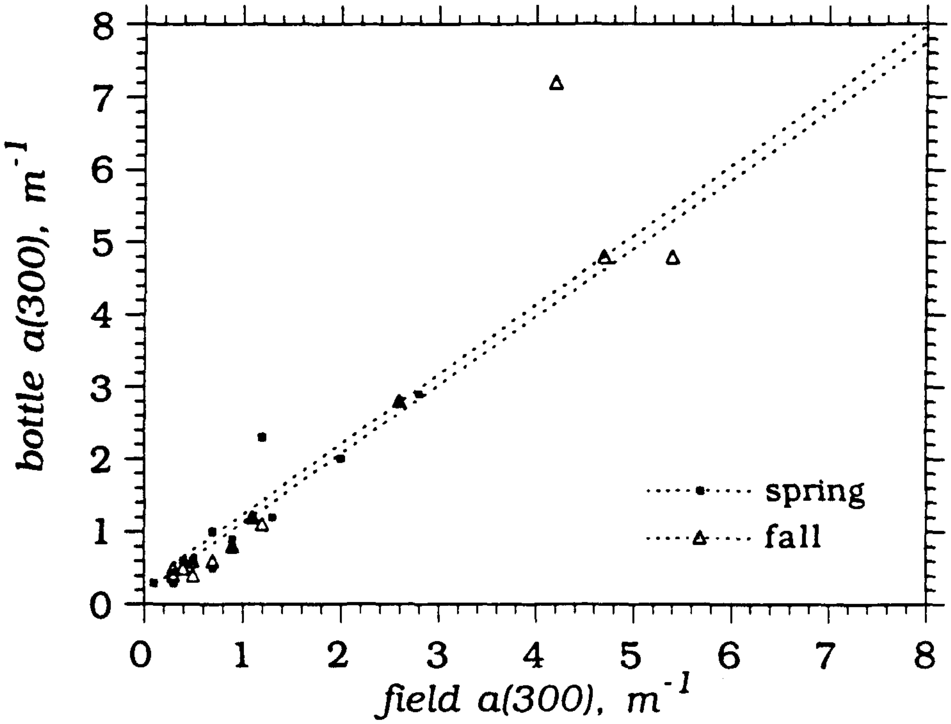
bottle a(300), m^{-1}
field a(300), m^{-1}
0
1
2
3
4
5
6
7
8
spring
fall

fig. 9 Comparison of spectral slopes measured on shipboard and in the lab; the 1:1 line is shown for reference.

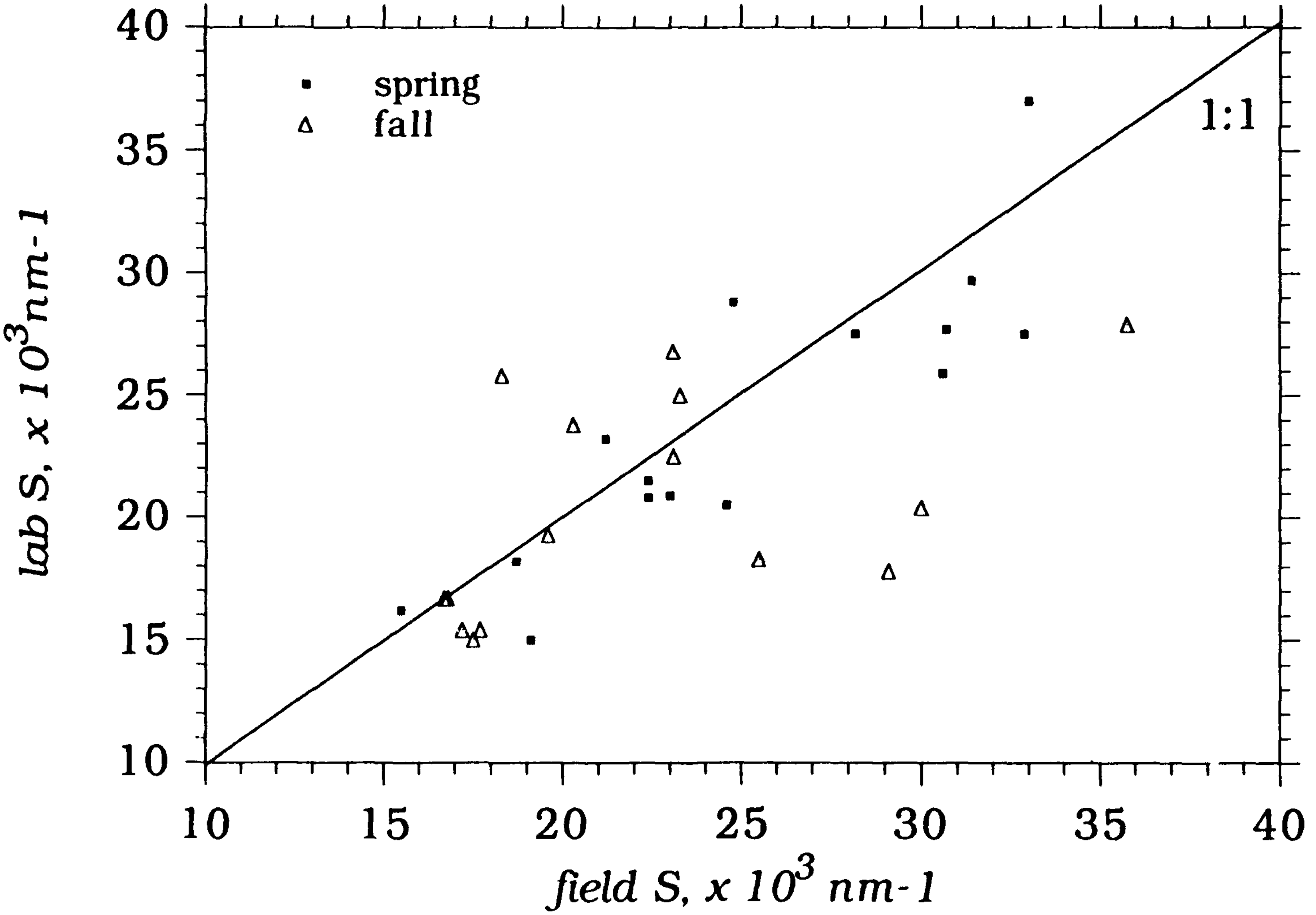
spring
fall
1:1
lab S, x 10^3nm-1
field S, x 10^3 nm-1
10
15
20
25
30
35
40
10
15
20
25
30
35
40

Discussion

Many *S* values for Gulf waters were significantly larger than previously recorded log-linearized slopes, with values >0.030 nm^{-1} observed for some blue-water samples. Few values were as low as the average slopes reported for seawater by Bricaud et al. (0.014 nm^{-1}) (*16*) and for freshwaters by Zepp and Schlotzhauer (0.014 nm^{-1}) (*19*). They agreed more closely with slopes measured by Carder et al. (0.0190 nm^{-1}) (*5*) for fulvic acid extracts from the Gulf of Mexico, and by Davies-Colley (0.0187 nm^{-1}) (*18*) for a series of freshwater lakes. Blough et al. (*17*) measured values ranging from 0.0137 to >0.0190 nm^{-1} for the Orinoco Estuary and Caribbean Sea. A comparison of the sparse data collected thus far indicates that there is more variability in this parameter than was originally believed.

The samples examined by Bricaud et al. (*16*) had been filtered through glass-fiber filters only, and substantial corrections for scattering by residual particles were applied to the absorbance spectra before *S* could be determined. Very long pathlength cells (1.1 m) were employed which may accentuate the apparent scattering signal due to the refractive index difference between seawater and the distilled water reference solution (see appendix B). *S* values for their 105 samples ranged from 0.010 to 0.020 nm^{-1}, with an overall mean of 0.014±0.003 nm^{-1}.

Zepp and Schlotzhauer (*19*) used centrifugation to remove scattering particles from their solutions. No corrections for scattering were applied. Their measured slopes ranged from 0.010 to 0.0175 nm^{-1}. If significant scatterers are present, *S* values for dissolved material tend to be underestimated.

Carder et al. (5) isolated humic (HA) and fulvic acids (FA) on XAD columns from the Gulf of Mexico. *S* values were measured on reconstituted samples and were found to be 0.011 and 0.019 nm^{-1}, for marine humic and fulvic acids, respectively. For material isolated on C-18 columns, absorption spectra of reconstituted COM extracts do not necessarily mirror those of the water from which they were obtained (see chapter 6). It is not known whether XAD isolates exhibit similar discrepancies. It has been pointed out (5) that choosing HA and FA to represent the whole of marine COM absorption may result in an underestimate of attenuation coefficients, however this choice may also cause underestimates of *S* values.

The correlation of *a(300)* and *S* is shown on a semi-log scale in figure 10. The general inverse relationship between *a(300)* and *S* is apparent, but it does not appear to be a simple relationship. Points on this graph fall into three regions: (i) samples with $S>0.020$ nm^{-1}, and $a(300)<1$ m^{-1}, (ii) samples with large *a(300)* values and $0.016<S<0.020$ nm^{-1}, and (iii) those with $a(300)\approx 1$ m^{-1} and $S<0.016$ nm^{-1}. Spectra of samples in the last category were the most likely to exhibit noticeable curvature. Region (i) shows the most monotonic decrease in *a(300)* with increasing *S*. This region is the least important for remote sensing applications because the absorbance is too low at wavelengths ≥ 440 nm^{-1} to interfere with estimations of chlorophyl concentration. Regions (i) and (ii) exhibit a lot of scatter; it does not appear that a useful relationship between *a(300)* and *S* can be derived for this location.

Application to remote sensing. Absorption by COM affects both the depth of light penetration into the water column and the spectral qualities of the light received and reflected at each depth. It is intuitively clear that the photons detected above optically clear waters originate from a greater depth range than those detected from highly fig. 10 Absorption coefficients ($a(300)$) vs S for spring (●) and fall (□) data. on a semi-log scale.

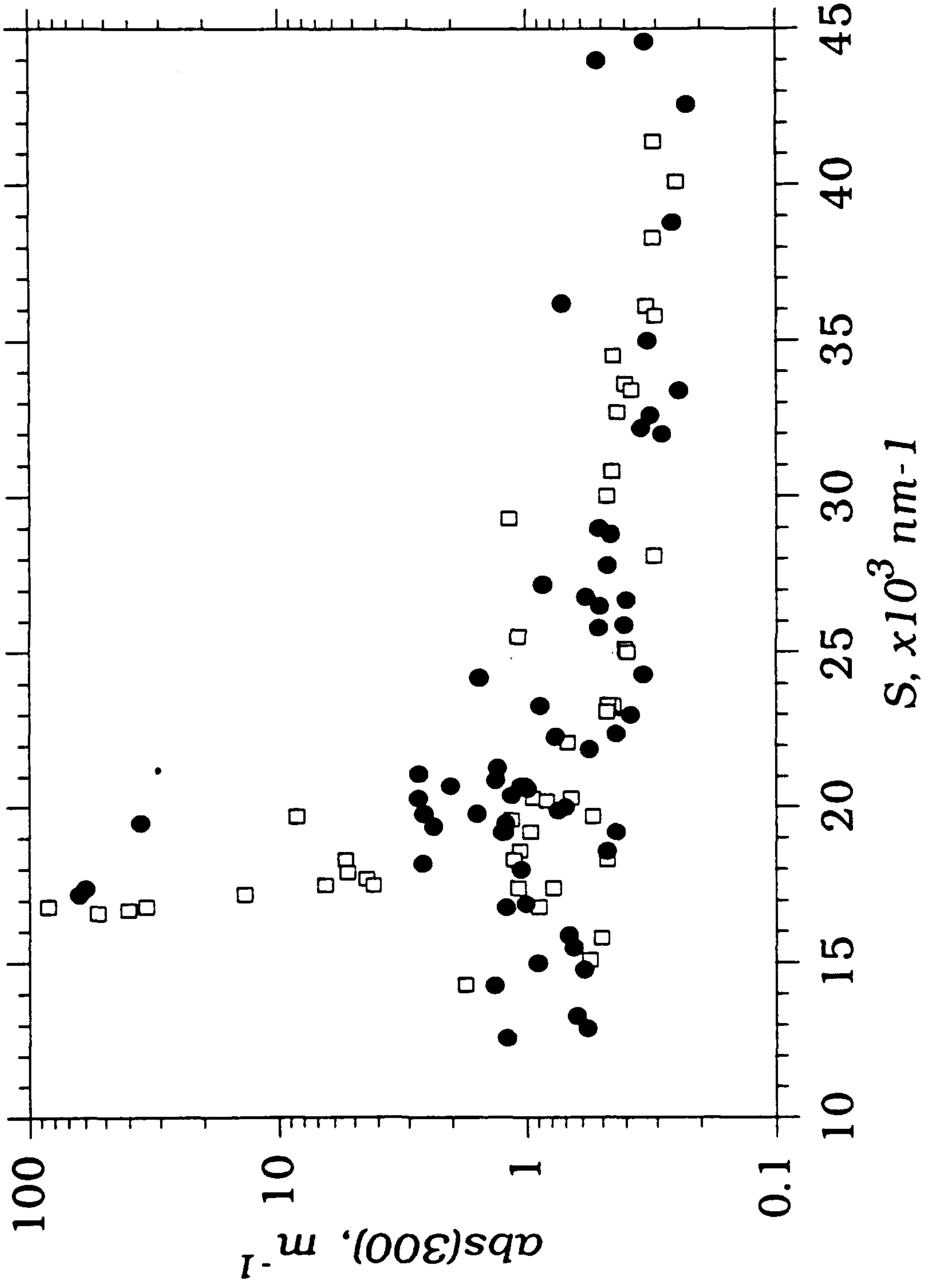
100
10
1
0.1
abs(300), m-1
10
15
20
25
30
35
40
45
S, x10^3 nm-1

colored waters. Some theoretical and practical aspects of light penetration depth have been discussed by Kirk (*24*).

The first-order problem of COM absorbance in remote sensing concerns its ability to interfere with determinations of chlorophyll concentrations, which are used to estimate phytoplankton populations. The link between color sensors on satellites or remotely moored buoys and the optical properties of these important ocean components can be expressed in terms of the irradiance reflectance, R(λ) (*6*). This parameter can be formulated Carder, 1991 #60} as

$$R(\lambda) \approx 0.33(b_w' + b_p')/(a_w + a_{COM+d} + a_\phi^*[Chl\ a]),$$

where b_w' and b_p' are backscattering coefficients for water and particles, a_w is the absorption coefficient of water, a_ϕ^* and [Chl *a*] are, respectively, the specific absorption coefficient and concentration of chlorophyll in living phytoplankton, and a_{COM+d} is the combined absorption coefficient of COM and detrital particles. All terms (except [Chl *a*]) are wavelength dependent. [Chl *a*] is determined by comparing the ratios *R(412)/R(443)* and *R(443)/R(565)*, so each parameter must be known at three wavelengths. Values of b_w' and a_w are available in tables, and b_p' is calculated via empirical relationships. a_ϕ^* is derived from studies of phytoplankton under various environmental and growth conditions. Data on the function $a_{COM+d}(\lambda)$ are still quite sparse; the present study aims to help remedy this dearth.

The next generation of color-scanning satellite will survey a wavelength band near 410-415 nm, in addition to the chlorophyll absorption bands at ≈440 and 560 nm. The goal is to determine the contribution of COM absorbance to the chlorophyll signal by measuring absorbance near 410 nm (where there is only a small contribution from chlorophyll) and then extrapolating to longer wavelengths. The accuracy of this procedure depends on the accuracy of S values which are required for wavelength extrapolation, and, if this method is to be generalized, on the degree of variability of *S* in different regions of the ocean.

In assessing $a_{COM+d}(\lambda)$, Roesler et al. observed that the absorption spectra of both COM and detrital material could be fit as exponential functions, with $\overline{S}$ =0.016 and 0.011 nm^{-1}, respectively. Using these values they attempted to describe the total combined absorbance as a single exponential decay. Carder et al.(6), more logically, combined the above-noted detrital and HA terms which have identical S values (0.011 nm^{-1}), and included a second exponential term for the FA fraction of COM(S=0.019 nm^{-1}). An adjustable parameter was required to account for the relative contributions of the HA-detrital and FA absorbances.

The present survey of absorbance spectra indicates that *S* varies from ≈0.014 to >0.03 nm^{-1} in waters in the South Florida/Gulf of Mexico region. Thus, in this region, an *S* value of 0.019 nm^{-1} may either over or underestimate the COM contribution to chlorophyll absorbances. Carder et al. (6) suggested that variations in the ratio between humic and fulvic acids could be important in coastal regions. This could account for apparent S values between 0.011 (HA) and 0.019 nm^{-1} (FA). The curvature observed in several of the log-linearized spectra may be attributable to a significant HA contribution to the signal. Values >0.019 nm^{-1} cannot be accounted for by FA/HA mixtures.

The impact of uncertainties in S values on assessments of phytoplankton populations depends on relative concentrations of COM and chlorophyll in the water of interest. If phytoplankton are sparse, then errors in estimating the contribution of COM to the signal become very important. If S is taken to be 0.014 nm^{-1} in an area where it is actually equal to 0.03 nm^{-1}, then, on extrapolation from 410 to 440 nm, fig. 11. Map of South Florida showing Oyster Bay and the Shark River Slough. The Tamiami Canal runs parallel to route 41. Map is from P.J. Gleason, in "Environments of South Florida: Present and Past II. (1984) Miami Geological Society, Coral Gables.

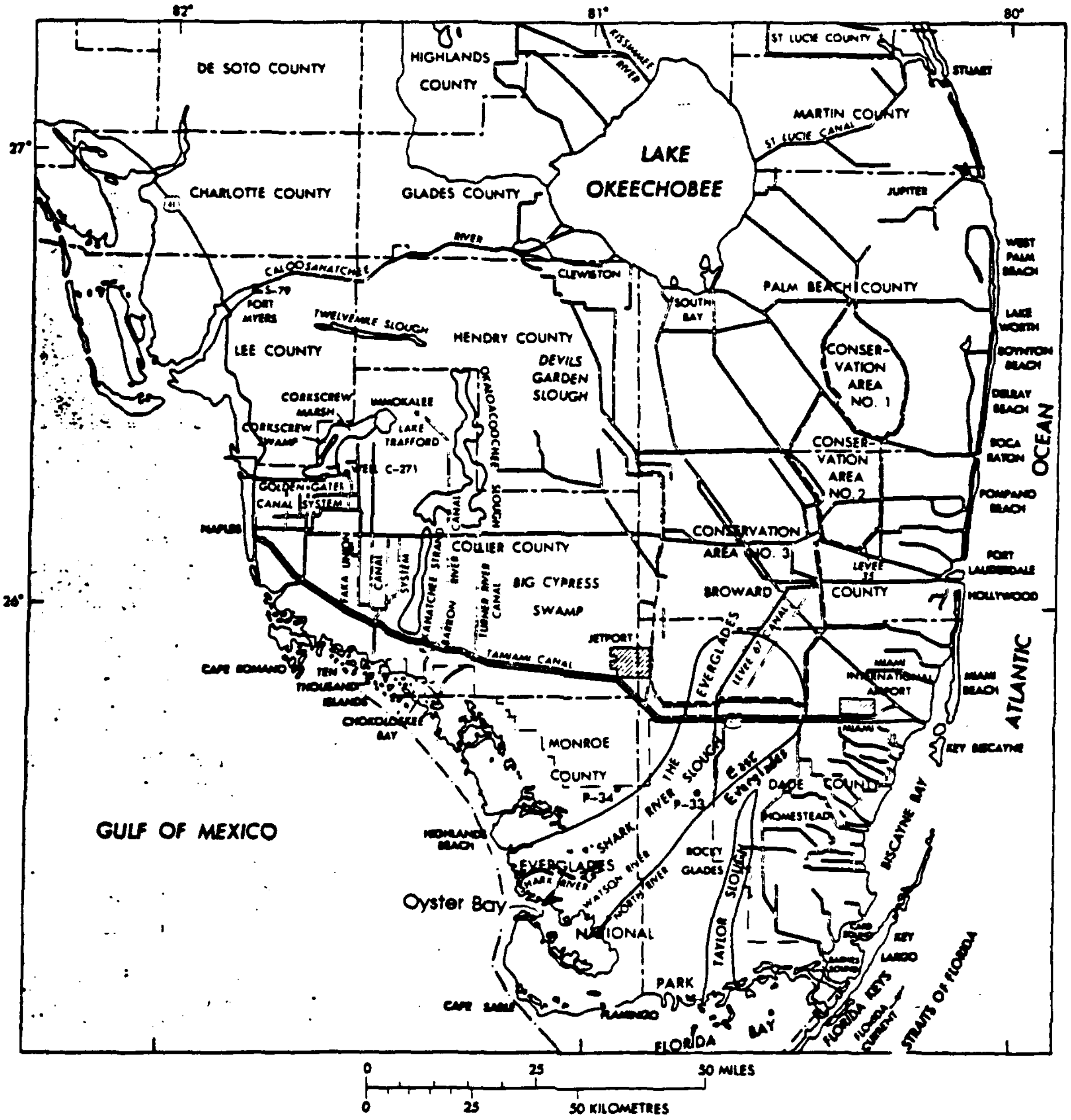
82°
81°
80°
27°
26°
DE SOTO COUNTY
HIGHLANDS COUNTY
KISSIMMEE RIVER
ST LUCIE COUNTY
STUART
MARTIN COUNTY
ST LUCIE CANAL
LAKE OKEECHOBEE
CHARLOTTE COUNTY
GLADES COUNTY
JUPITER
41
RIVER
CALOOSAHATCHEE
CLEWISTON
S-79
FORT MYERS
TWELVEMILE SLOUGH
HENDRY COUNTY
SOUTH BAY
PALM BEACH COUNTY
WEST PALM BEACH
LAKE WORTH
BOYNTON BEACH
LEE COUNTY
DEVILS GARDEN SLOUGH
CONSERVATION AREA NO. 1
DELRAY BEACH
CORKSCREW MARSH
IMMOKALEE
LAKE TRAFFORD
CORKSCREW SWAMP
OKALOACOOCHEE SLOUGH
CONSERVATION AREA NO. 2
BOCA RATON
WELL C-271
GOLDEN GATES CANAL SYSTEM
POMPANO BEACH
OCEAN
NAPLES
CONSERVATION AREA NO. 3
COLLIER COUNTY
FAKA UNION CANAL SYSTEM
FAKAHATCHEE STRAND
BARRON RIVER CANAL
TURNER RIVER CANAL
BIG CYPRESS SWAMP
LEVEE 35
FORT LAUDERDALE
BROWARD COUNTY
HOLLYWOOD
EVERGLADES
LEVEE 67 CANAL
JETPORT
TAMIAMI CANAL
CAPE ROMANO
TEN THOUSAND ISLANDS
MIAMI INTERNATIONAL AIRPORT
MIAMI BEACH
ATLANTIC
CHOKOLOSKEE BAY
MONROE COUNTY
MIAMI
KEY BISCAYNE
THE SHARK RIVER SLOUGH
P-34
P-33
DADE COUNTY
HOMESTEAD
BISCAYNE BAY
GULF OF MEXICO
HIGHLAND BEACH
EVERGLADES
SHARK RIVER
WATSON RIVER
NORTH RIVER
ROCKY GLADES
TAYLOR SLOUGH
Oyster Bay
NATIONAL
PARK
CARD SOUND
KEY LARGO
BARNES SOUND
CAPE SABLE
FLAMINGO
FLORIDA BAY
FLORIDA KEYS
FLORIDA CURRENT
STRAITS OF FLORIDA
0
25
50 MILES
0
25
50 KILOMETRES

the error in $a_{COM+d}(440)$ will be ≈60%. The observation that very steep slopes are primarily observed in waters with weak COM absorbance is consistent with the classification of such waters as "type I"; algorithms that neglect COM are generally applied, with good results, to these waters. The fact that absorbance parameters measured in this work differ from those measured in other regions supports the idea that these factors are site-dependent and may need to be determined individually for each site of interest. Since no major seasonal variations were observed, temporal factors do not seem to be of primary importance, at least not in this particular region.

Case Study: Variations in Absorbance in Oyster Bay

The collection of large data sets during two seasons from this area allows some specific observations to be made pertaining to the local environment of Oyster Bay. In this section I make a detailed comparison of absorption spectra among several samples collected in this region during spring and fall, 1991.

In South Florida, the dominant land feature is an extensive wetland region at the southwestern edge of the state. These wetlands once covered over 10,000 km^2; now the Everglades National Park occupies about 5,700 km^2 of this area(fig 11). The climate is subtropical and is characterized by a pronounced rainy season generally extending from June through September. Nearly 80% of the mean annual rainfall (132.5 cm) occurs during this period. Thus, summer is the wet season, and the dry season occurs during the months of October through May. In 1991 the effects of the dry season were probably accentuated due to an extended drought over the previous several years. The rains in the summer of 1991 were near normal.

The major freshwater drainage area to the Everglades is the Shark River Slough, which originates in Lake Okeechobee and flows south in a shallow sheet over an extensive area having an average gradient of only 2.8 cm km^{-1} (25). The Shark River empties into Oyster Bay, which communicates with the Gulf of Mexico. The estuary is shallow and tidally flushed; the water is visibly tea colored. The vegetation around Oyster Bay is primarily mangrove swamp, dominated by red mangroves *(Rhizophora mangle)*, with some black mangroves *(Avicennia germinans)* also present. Further inland, the major plants are sawgrass *(Cladium jamaicense)* and spikerush.

The possible sources of COM to Oyster Bay are (i) terrestrially-derived COM delivered by the Shark River, (ii) marine-derived COM delivered by tidal flow, and (iii) COM produced within the Bay itself. The relative importance of each of these sources is likely to vary seasonally. One reasonable scenario is that large amounts of COM are carried in runoff as summer rains flood areas that have remained relatively dry during the winter months. This arrives in Oyster Bay as a pulse of freshwater, rich in terrestrial COM. At the same time, tidal inundations of coastal areas also increase in frequency in late summer (26). At the start of the dry season, inputs of COM-rich freshwater are greatly diminished and tidal mixing is reduced. Over the drier winter period, concentrations of COM and seasalts within the Bay may increase due to evaporation and diminished circulation. Terrestrial COM travels through many miles of marshland before reaching Oyster Bay, so it is likely that most labile components are removed during transit. Marine-derived COM is probably present, as some fraction of the total, throughout the year.

Seasonal variations in a(300) and S within Oyster Bay. The major seasonal variation between spring and fall samples of 0‰ and 32‰ salinity are summarized in figure 12, and in the table III.

fig. 12 Spring and fall log-linearized absorbance spectra for waters with salinities of 0‰ and 32‰. From top to bottom: Tamiami River, fall (○), Everglades 0‰ water, spring (□), Oyster Bay water, 32‰, spring (■), Oyster Bay water, fall (●).

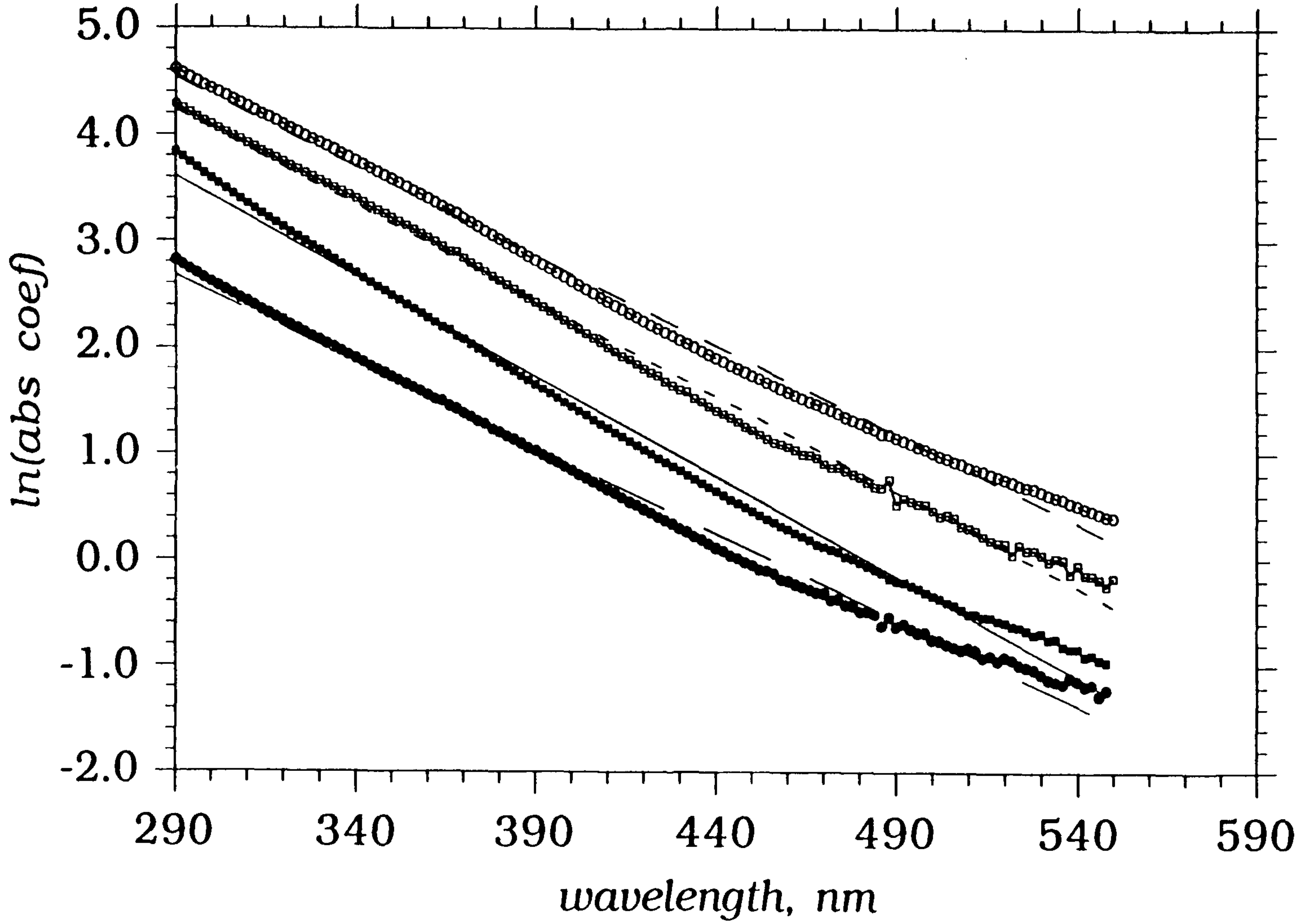
5.0
4.0
3.0
2.0
1.0
0.0
-1.0
-2.0
ln(abs coef)
290
340
390
440
490
540
590
wavelength, nm

Table III. a(300) and S values for 0‰ and 32‰ salinity samples.

	a(300) (m^{-1})		*S* (nm^{-1}), ±0.002		*QY** *% (355 nm)*	
Salinity	0‰	32‰	0‰	32‰	0‰	32‰
May	60.1	36.2	0.0180	0.0189	-	1.5±.1
August	84.3	13.7	0.0168	0.0162	1.90±.04	1.11±.04

* Fluorescence quantum yield, see chapter 5.

Spring and fall samples show markedly different values of *S* which persist in both fresh and salt waters. Thus, this difference cannot be attributed to processes within the estuary, but must be a result of either increased production of long-wavelength absorbing DOM during the rainy season, or faster degradation, or removal, of this fraction during the dry season. Increased DOM production might occur, for example, in seasonally flooded areas when they become inundated. Selective degradation, e.g. by photochemical processes, is an attractive idea because it can also provide a mechanism to explain the large values of S obtained for surface COM in blue-water regions of the ocean.

Fluorescence quantum yields (chapter 5) are significantly different among these samples. The anomalously high yield for the Tamiami River (fall, 0‰) is notable, hoever it is difficult to draw any conclusions from this single sample. The variation within Oyster Bay is confirmed by a number of samples. It may be an indication of seasonal biological processes in the estuary (e.g. leaf loss by mangroves), or it may be due to the relatively large contributions of terrestrial material present during the fall rainy season.

In May, at the end of the dry season, there is very little freshwater flowing into Oyster Bay and the flooded area of the Shark River Slough is reduced by nearly 40% (27). The lowest salinity we were able to measure in this season was 32.10 ‰. Along the coast, north of Oyster Bay, salinity reached 36.39 ‰. Insufficient samples of intermediate salinity were collected to allow extrapolation to a freshwater end member. Within the Bay the absorbance at 300 nm was 34.4 m^{-1} at a salinity of 32.2 ‰; this is nearly three times higher than the *a(300)* measured for the fall sample with identical salt content.

This large ratio of *a(300)* to salinity measured in the spring, as compared to fall, could have several explanations. (i) The concentration of COM in the freshwater source may have increased during the dry season. (ii) COM may be generated within Oyster Bay from *in situ* production of organic material. (iii) COM delivered throughout the year, and remaining trapped in the Bay, may become more concentrated due to evaporation during drier weather.

Assuming simple, direct mixing of seawater and fresh, terrestrially-derived water, the 32.2‰ sample would consist of about 90% seawater [(32.2‰-0‰)/36‰]. This would imply an *a(300)* of the freshwater end member of 290 m^{-1}, which is ≈3.5 times higher than the largest *a(300)* we measured in this region (84.3 m^{-1},Tamiami R., August 1991). In addition, freshwater samples collected during the dry season had lower *a(300)* values (60 m^{-1}) than those collected during the rainy period (84.3 m^{-1}), contrary to the seasonal variation in Oyster Bay.

Conservative mixing of fresh and salt water cannot explain the observed *a(300)* and salinity in Oyster Bay. The absorbance in Oyster Bay is much greater than would be predicted based on this simple model; it appears to contain a much larger fraction of fig. 13 Same spectra as shown in figure 10, but normalized to identical absorbance values at 400 nm, (■) 0‰, (△) 32‰, above: spring, below, fall.

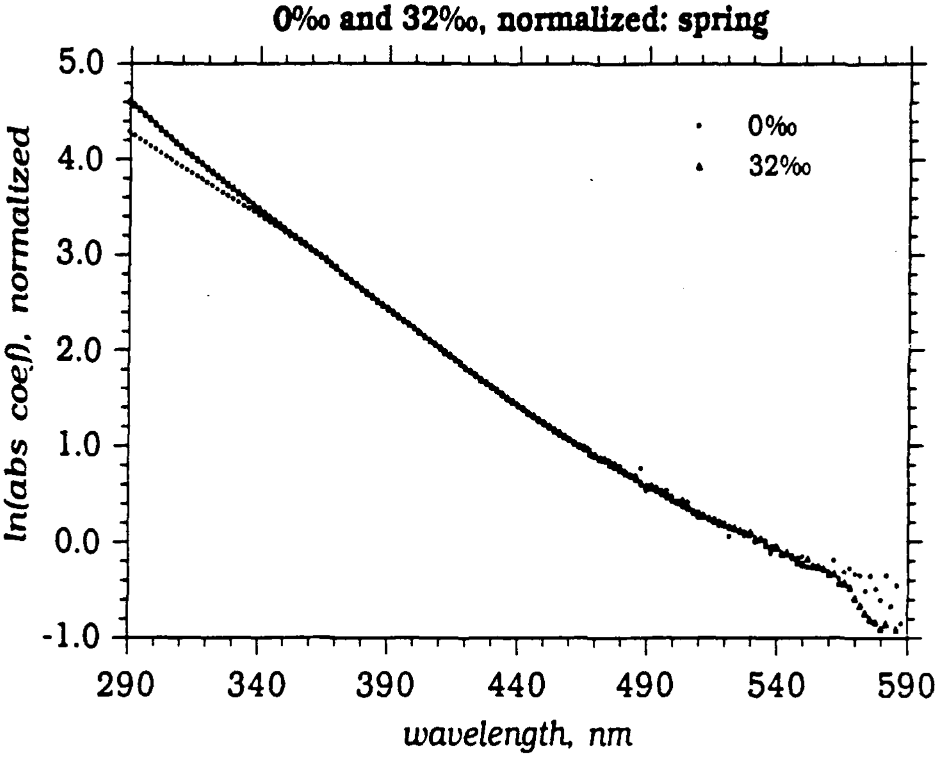

0‰ and 32‰, normalized: spring

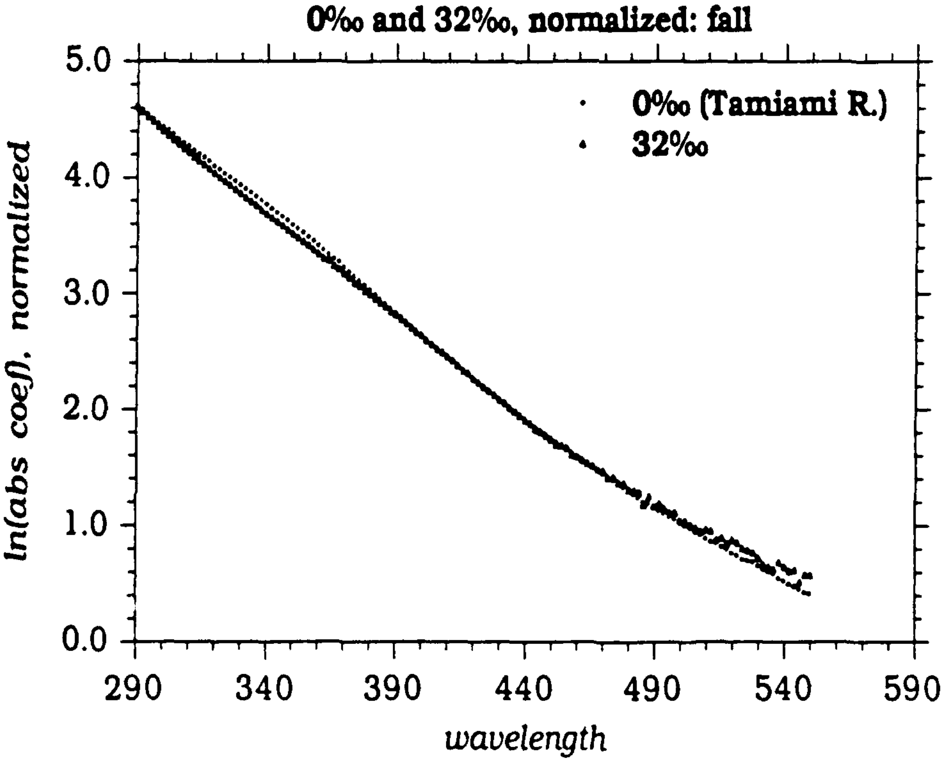

0‰ and 32‰, normalized: fall

terrestrially-derived material than is indicated from its salt content. Generation of COM within the salt water region will increase absorbance without changing the salinity; evaporation will increase both *a(300)* and salinity. On the basis of these *a(300)* measurements, it is not possible to differentiate between COM produced in saline water and that transported from freshwater and concentrated by evaporation. Qualitative differences in the optical properties of these materials may be used to estimate the relative importance of these two contributions.

The relatively restricted communication between Oyster Bay and the Gulf of Mexico and the high water temperatures in this climate (22-24°) suggest that evaporative water loss could be significant. Evaporation of freshwater concentrates salts within such a zone, increasing salinity and exaggerating the apparent seawater content.

To identify which process dominates during this season, we qualitatively compare 0‰ and 32.2‰ samples by normalizing the absorbance at 400 nm (fig 13). The normalized spectra show remarkable coincidence at wavelengths longer than 360 nm. Non-linearities in the freshwater spectrum are faithfully reproduced by 32‰ water. From 290 to 360 nm the 32.2‰ spectrum shows a marked positive deviation compared with the freshwater. This indicates either that absorbers responsible from the longer wavelength (>360 nm) signal are selectively removed during mixing with salt water, or that uv (<360 nm) absorbers are selectively added during this process. The latter explanation seems more plausible both because of the invariant shape of the spectra above 360 nm, and because seawater from the Gulf of Mexico absorbs sufficiently in the uv range to account for the observed increase at shorter wavelengths. This suggests that *in situ* production of COM within Oyster Bay is not significant during this season, although we cannot rule out the possibility that DOM produced within the estuary could be strongly absorbing at short wavelengths.

In August, surface samples (2 m) were collected on a transect through the mixing zone of fresh Shark River water with seawater. The salinity gradient measured was from 19.2 to 35.3 ‰ with *a(300)* values of 4.1 to 53.5 m^{-1}; a graph of *a(300)* vs salinity is shown in fig 14. A very good linear fit is obtained, indicating conservative mixing along this transect. On extrapolation to zero salinity, the intercept of this plot suggests that the freshwater end member should have an absorbance of 114 m^{-1} at 300 nm. We were unable to collect zero-salinity Shark River water during this season, but a freshwater sample from the Tamiami Canal had an absorbance of 84.3 m^{-1}. This water provides a reasonable approximation of the fresh source water to the Everglades (R. Jones, pers. com.). The high end-member *a(300)* value of 114 m^{-1} is consistent with the organic carbon content of the inland Everglades waters (which can exceed 60 mg•C/l). However, because this absorbance coefficient is ≈25% higher than measured freshwater values, the data does not rule out the possibility that some COM is introduced within the extensive salt and brackish wetlands of this region and is not derived solely from freshwater runoff.

Comparison of 0‰ and 32‰ wet season samples reveals very little change in spectral slope; *S* values are 0.0168 nm^{-1} and 0.0162 nm^{-1} respectively (fig 11). Normalization of these spectra shows excellent correspondence at all wavelengths, with the exception of a slight bulge at 340 nm in the 0‰ sample. It appears that, although the quantity of COM must increase in water traveling from the Tamiami Canal to Oyster Bay, its absorption parameters remain nearly constant. In contrast, the fluorescence quantum yield of this water decreases by 30% during transit.

fig. 14 Dilution transect into Oyster Bay: absorption coefficient is plotted against salinity from 19 to 35‰.

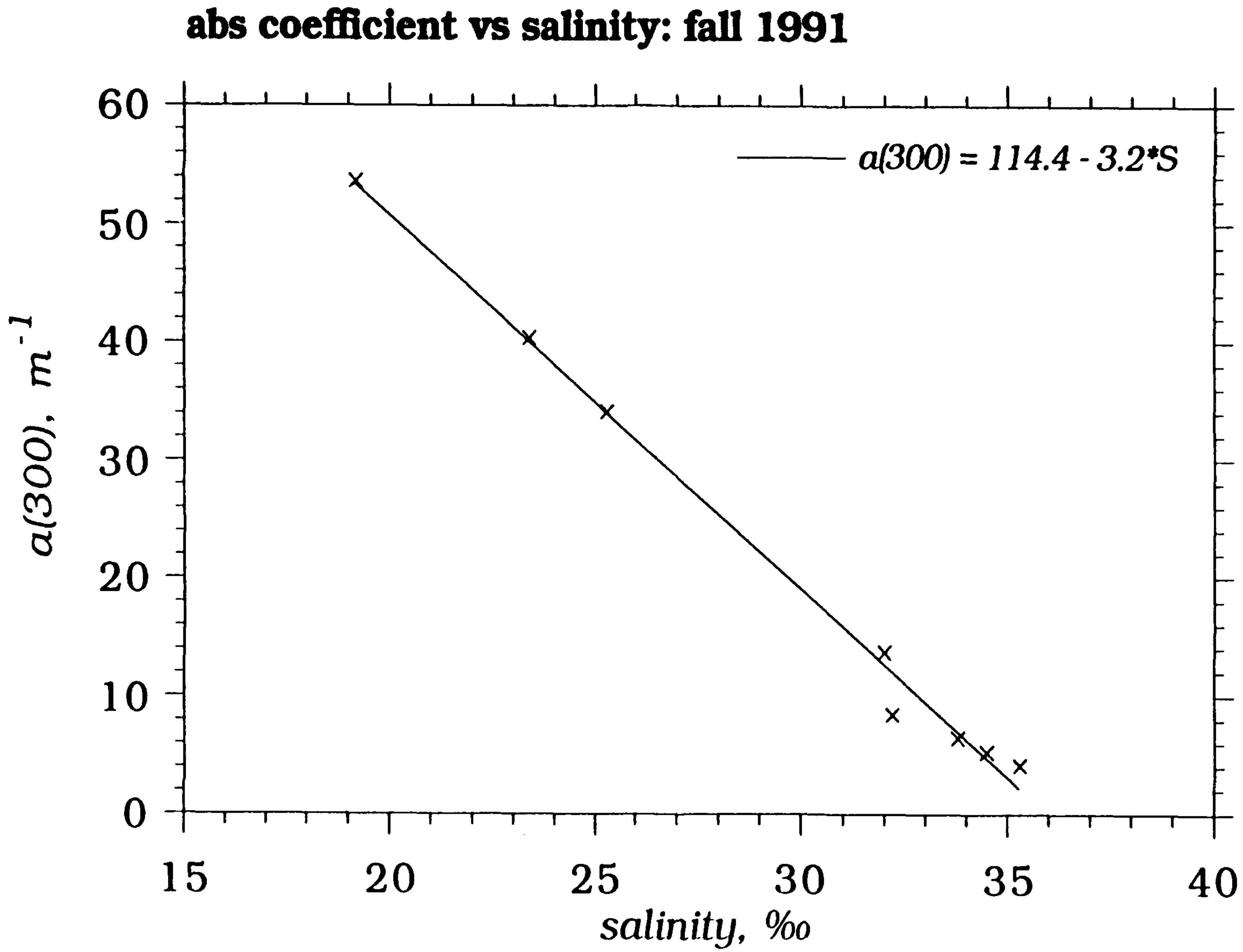
abs coefficient vs salinity: fall 1991
a(300) = 114.4 - 3.2*S
a(300), m^-1
60
50
40
30
20
10
0
15
20
25
30
35
40
salinity, ‰

Conclusions

Absorption coefficients in the South Florida region varied by nearly two orders of magnitude in the waters collected. *S* values ranged from a low of 0.014 nm^{-1} to >0.030 nm^{-1}. Blue, "type 1," waters (with weak absorbance) had the largest slopes, and the most consistent trend of increasing *S* with decreasing *a(300)*. In more highly absorbing coastal waters the correlation between S and *a(300)* was less clear. Temporal changes in absorption parameters were minimal outside of the estuary. These observations support the prediction (6) that COM corrections to remote sensing algorithms should be site-specific. Satellite-derived estimates of primary productivity may be confounded in a region such as this where substantial changes in absorbance and *S* occur over a relatively small area.

The variations in absorption parameters identified in a case study of the Oyster Bay region suggest that a more detailed investigation of seasonal and local flucuations of optical parameters could be useful. A survey of the optical properties of leachates from possible source materials, such as leaf-litter, soil, and sediments could help clarify their contributions to the COM released to the marine environment.

References

(1) Stevenson, F.J. (1985). Geochemistry of soil humic substances. In *Humic substances in soil, sediment, and water*; Aiken, G.R., D.M. McKnight, R.L. Wershaw and P. MacCarthy, ed.; John Wiley & Sons: New York; pp. 13-52.

(2) Müller-Karger, F.E., J.J. Walsh, R.H. Evans and M.B. Meyers (1991). On the seasonal phytoplankton concentration and sea surface temperature cycles of the Gulf of Mexico as determined by satellites. *J. Geophys. Res.*, **96**: 12645-12665.

(3) Bristow, M., D. Nielsen, D. Bundy and R. Furtek (1981). Use of water Raman emission to correct airborne laser fluorosensor data for effects of water optical attenuation. *Appl. Optics*, **20**: 2889-2906.

(4) Roesler, C.S., M.J. Perry and K.L. Carder (1989). Modeling in situ phytoplankton absorption from total absorption spectra in productive inland marine waters. *Limnol. Oceanogr.*, **34**: 1510-1523.

(5) Carder, K.L., R.G. Steward, G.R. Harvey and P.B. Ortner (1989). Marine humic and fulvic acids: their effects on remote sensing of ocean chlorophyll. *Limnol. Oceanogr.*, **34**: 68-81.

(6) Carder, K.L., S.K. Hawes, K.A. Baker, R.C. Smith, R.G. Steward and B.G. Mitchell (1991). Reflectance model for quantifying chlorophyll *a* in the presence of productivity degradation products. *J. Geophys. Res.*, **96**: 20599-20611.

(7) Smith, R.C., J. Marra, M.J. Perry, K.S. Baker, E. Swift, E. Buskey and D.A. Kiefer (1989). Estimation of a photon budget for the upper ocean in the Sargasso Sea. *Limnol. Oceanogr.*, **34**: 1673-1693.

(8) Williams, P.M. and E.R.M. Druffel (1988). Dissolved organic matter in the ocean: comments on a controversy. *Oceanogr.*, **1**: 14-17.

(9) Kieber, D.J. and N.V. Blough (1990). Fluorescence detection of carbon-centered radicals in aqueous solution. *Free Radical Res. Comm.*, **10**: 109-117.

(10) Kieber, D.J. and N.V. Blough (1990). Determination of carbon-centered radicals in aqueous solution by liquid chromatography with fluorescence detection. *Anal. Chem.*, **62**: 2275-2283.

(11) Blough, N.V. (1988). Electron paramagnetic resonance measurements of photochemical radical production in humic substances. 1. Effects of O_2 and charge on radical scavanging by nitroxides. *Environ. Sci. Technol.*, **22**: 77-82.

(12) Zafiriou, O.C. (1990). Chemistry of superoxide ion-radical (O_2^-) in seawater. I. $pK_a^*{}_{sw}$ (HOO) and uncatalyzed dismutation kinetics studied by pulse radiolysis. *Mar. Chem.*, **30**: 31-43.

(13) Faust, B.C. and J. Hoigné (1987). Sensitized photooxidation of phenols by fulvic acid and in natural waters. *Environ. Sci. Technol.*, **10**: 957-970.

(14) Haag, W.R. and J. Hoigné (1986). Singlet oxygen in surface waters. 3. Photochemical formation and steady-state concentrations in various types of waters. *Environ. Sci. Technol.*, **20**: 341-348.

(15) Waite, T.D. and F.M.M. Morel (1984). Ligand exchange and fluorescence quenching studies of the fulvic acid-iron interaction: effects of pH and light. *Anal. Chim. Acta.*, **162**: 263-274.

(16) Bricaud, A., A. Morel and L. Prieur (1981). Absorption by dissolved organic matter of the sea (yellow substance) in the uv and visible domains. *Limnol. Oceanogr.*, **26**: 43-53.

(17) Blough, N.V., O.C. Zafiriou and J. Bonilla (1992). Optical absorption spectra of waters from the Orinoco River outflow: terrestrial input of colored organic matter to the Caribbean. *J. Geophys. Res.*, : in press.

(18) Davis-Colley, R.J. and W.N. Vant (1987). Absorption of light by yellow substance in freshwater lakes. *Limnol. Oceanogr.*, **32**: 416-425.

(19) Zepp, R.G. and P.F. Schlotzhauer (1981). Comparison of photochemical behavior of various humic substances in water: III. Spectroscopic properties of humic substances. *Chemosphere*, **10**: 479-486.

(20) Hayase, K. and H. Tsubota (1985). Sedimentary humic acid and fulvic acid as fluorescent organic materials. *Geochem. Cosmochem. Acta.*, **49**: 159-163.

(21) Stewart, A.J. and R.G. Wetzel (1981). Asymmetrical relationships between absorbance, fluorescence, and dissolved organic carbon. *Limnol. Oceanogr.*, **26**: 590-597.

(22) Chen, Y., N. Senesi and M. Schnitzer (1977). Information provided on humic substances by E_4/E_6 ratios. *Soil Sci. Soc. Am. J.*, **41**: 352-358.

(23) Orlov, D.S. (1985). *Humus acids of soils [Gumusovye kisloty pochv]*, ; Oxonian Press Pvt. Ltd.: New Delhi; pp 126-176.

(24) Kirk, J.T.O. (1989). The upwelling light stream in natural waters. *Limnol. Oceanogr.*, **34**: 1410-1425.

(25) Hofstetter, R.H. (1983). Wetlands in the United States. In *Ecosystems of the World, vol 4B, Mires: Swamp, Bog, Fen, and Moor. Regional Studies*; Gore, A.J.P., ed.; 4B; Elsevier: New York; pp. 201-244.

(26) Twilley, R.R. (1985). The exchange of organic carbon in basin mangrove forests in a Southwest Florida estuary. *Estuarine, Coastal and Shelf Science*, **20**: 543-557.

(27) Bartlett, D.S., K.B. Bartlett, J.M. Hartman, R.C. Harris, D.I. Sebacher, R. Pelletier-Travis, D.D. Dow and D.P. Brannon (1989). Methane emissions from the Florida Everglades: patterns of variability in a regional wetland ecosystem. *Global Biogeochemical Cycles*, **3**: 363-374.

Chapter Five: Fluorescence of waters of coastal South Florida and the Gulf of Mexico

Introduction

Fluorescence of natural chromophores is of analytical interest for quantifying COM because it is more easily measured than absorbance at the low levels observed in the environment (*1*). Laser and solar-induced fluorescence signals are also amenable to measurement by airborne sensors that offer a rapid means of characterizing large areas of surface water (*2, 3*). The use of fluorescence intensity measurements to quantify COM concentrations, through either shipboard sampling or remote sensing techniques, ultimately depends on the assumption that fluorescence energies and quantum yields do not differ greatly among samples. Both these aspects of natural water fluorescence are examined in this chapter.

The wavelength of maximum emission intensity is a useful parameter in the characterization of pure chromophores. However, attempts to gain information about COM from the positions of peak maxima have not been very successful (*4*). One reason that fluorescence spectra of natural samples are difficult to interpret is that they represent mixtures, rather than pure chromophores. The absorption spectra of natural COM samples lack well defined peaks which would indicate favorable wavelengths for excitation of fluorescence. In addition, the energy of the emitted light, as well as its intensity, is dependent upon the excitation wavelength chosen. Because fluorescence yields are low, spectra in aqueous solution are sometimes dominated by Raman scattering from water. Due to these factors, the choice of excitation and emission wavelengths is often rather arbitrary and it is frequently impossible to interpret the resulting spectra, or to compare spectra collected in different labs. Three dimensional matrix spectra provide a complete plot of fluorescence intensities, and allow unambiguous identification of both excitation and emission energies corresponding to peak maxima.

It is essential to quantify the range of fluorescence quantum yields of COM in natural waters because variations in measured fluorescence intensity can be due to differences in either COM concentration or fluorescence yield. If the quantum yield is known, or well constrained, then COM concentrations can be determined directly from fluorescence intensity.

The yield of emitted photons from COM depends, of course, on the types of fluorescent chromophores present. However, because COM represents a mixture of light-absorbing components, the fluorescence yield also reflects the proportion of these that are fluorescent, i.e. the ratio of fluorescent to non-fluorescent chromophores. In general, of the photons absorbed by a typical COM sample, approximately 1% is re-emitted as fluorescence. A comparable fraction (estimated to be 0.4-1.5% (5)) of excited singlet COM molecules is converted to the triplet state. The majority of absorbed energy is dissipated as heat through non-radiative processes. Aging of COM may cause transformations of fluorescent to non-fluorescent components, or vice versa. Additionally, solution pH and ionic strength can affect quantum yields of many fluorophores. Only a small amount of data is available on how these parameters influence COM fluorescence in its natural environment (*6, 7*).

In this study I have measured the complete 3D fluorescence spectra of whole water samples collected in South Florida and the Gulf of Mexico, and of reconstituted COM extracts from several sources. I determined fluorescence quantum yields for all samples using excitation wavelengths of 337 and 355 nm. For several samples I also combined the fluorescence matrix spectra with absorption spectra in order to obtain plots of quantum yields as a function of excitation wavelength from 260 to 470 nm.

Background

Matrix spectra Fluorescence matrix spectra show the intensity of emission as a function of both excitation and emission wavelengths (*8*, *9*). In order to interpret matrix spectra of natural COM, it is useful to consider first the characteristics of a 3D spectrum for a pure fluorophore. Emission from the vast majority of solvated fluorophores results from relaxation of the first excited singlet state to the ground state. Because this energy difference is fixed, emission occurs at the same wavelength, regardless of excitation wavelength. "Excess" absorbed energy is rapidly dissipated through vibrational relaxation before emission of a photon. The intensity of the emission, however, is variable; it is predicted to be proportional to the amount of light absorbed at each excitation wavelength. Thus, the 3D spectrum of a single fluorophore reproduces its absorption spectrum along the excitation axis, with the energy of the emission maximum constant (with inhomogeneous broadening due to solvation effects) on that axis. On a contour plot this appears as a line parallel to the excitation axis and intersecting the emission axis at the peak maximum. An example, rhodamine B, is shown in figure 1. This type of plot is rarely employed in the study of pure compounds because it provides no information that is not easily accessible from single excitation and emission plots. However, for a mixture of unknown components, such plots are useful for defining the overall spectral qualities of a sample, and for estimating COM behavior under broad band radiation.

3D spectra may be reduced to two dimensions by integrating over each individual fig. 1a 3D fluorescence spectrum of a dilute aqueous solution of rhodamine B.

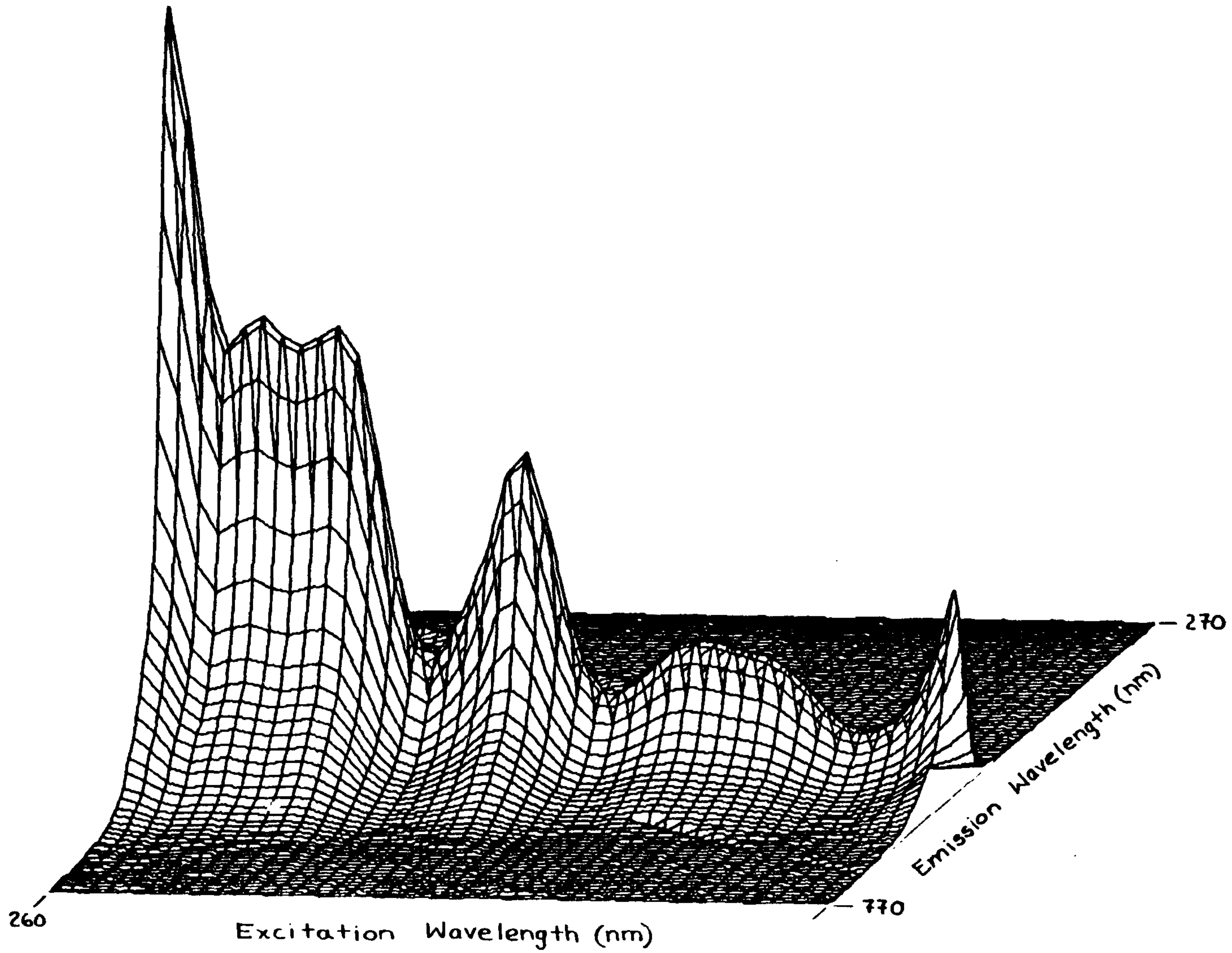
260
Excitation Wavelength (nm)
770
Emission Wavelength (nm)
270

fig. 1b. Contour view of figure 1a. Contour lines represent fluorescence intensity; each contour interval corresponds to 2% of maximum intensity.

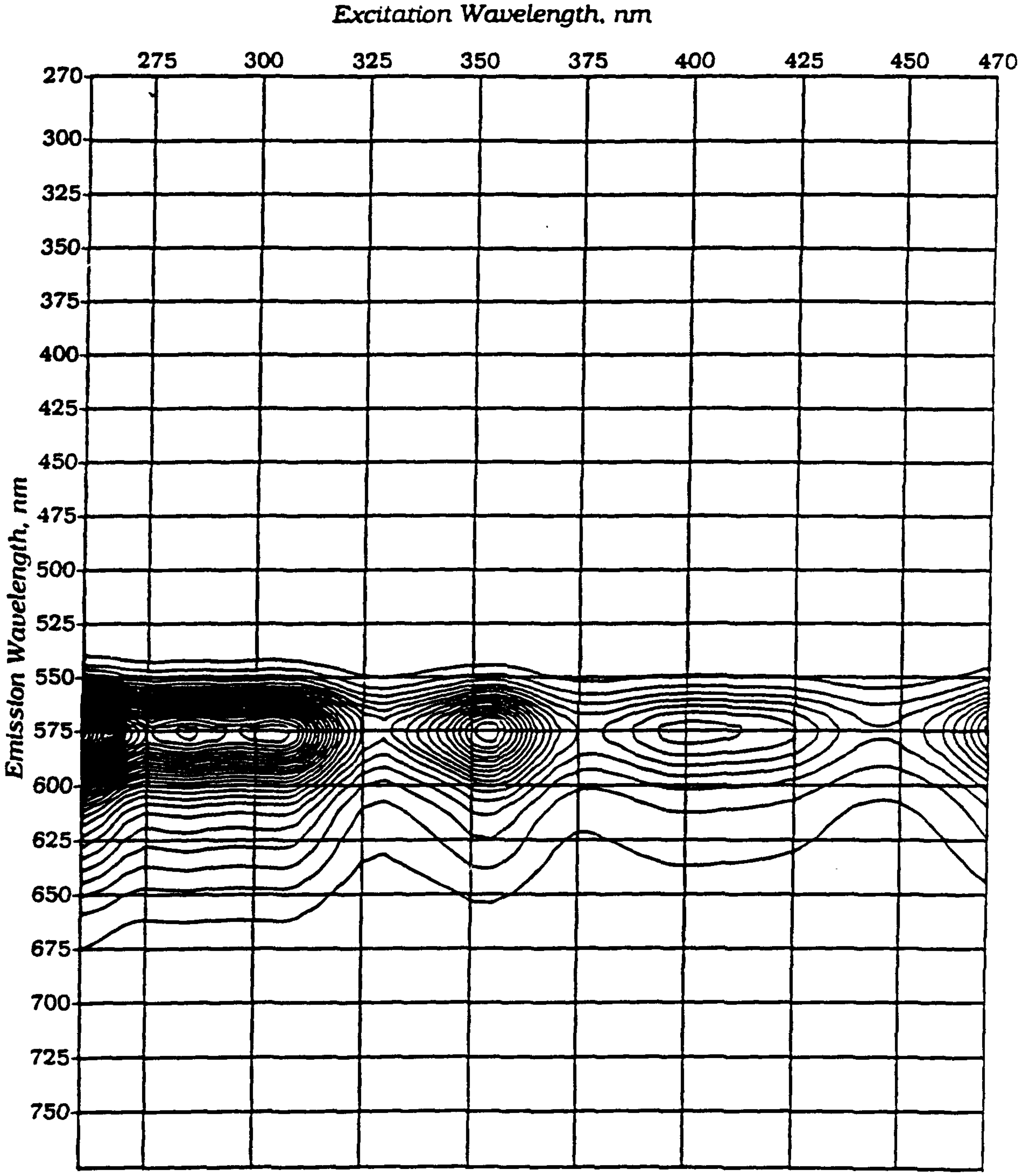
Excitation Wavelength, nm
275
300
325
350
375
400
425
450
470
Emission Wavelength, nm
270
300
325
350
375
400
425
450
475
500
525
550
575
600
625
650
675
700
725
750

emission (or excitation) spectrum and plotting the result against excitation (or emission) wavelength. This is rather like looking at the 3D plot from the "side," whereas in a contour plot it is seen from "above". It may be looked at from either the excitation or emission "edge." The result of integrating the series of emission spectra is a plot of the total (relative) number of photons emitted at each excitation wavelength. It is plotted as the integrated fluorescence intensity vs excitation wavelength. This gives a "combined excitation spectrum" which is equivalent to scanning the excitation monochrometer and recording the *total* fluorescence intensity at each point rather than the intensity at a fixed, single wavelength. Because they are analogous to standard excitation spectra, these plots might be expected to reproduce their respective absorption spectra. For a pure fluorophore in solution, photons absorbed at any energy have an equal likelihood of being re-emitted; thus fluorescence excitation spectra coincide with absorption spectra in energy and in relative intensities.

The complementary "combined emission spectrum," gives the wavelength distribution of emitted photons expected under broad band radiation (260-470 nm). One possible use of this type of spectrum is in predicting total surface irradiance emitted from organic-rich waters. In this application the spectra would be normalized to account for the change in intensity of solar radiation across the spectrum.

Quantum yields For a given chromophore the ratio of photons emitted to photons absorbed (fluorescence quantum yield, Q) is a constant under fixed solvent conditions. This relationship can be expressed as $F=aQC$, where F is the integrated fluorescence intensity, a is the absorption coefficient of the solution at the excitation wavelength, and C is a constant defined by instrumental parameters, and derived by measurement of a fluorescence standard. Fluorescence intensity has been used as a tracer with little regard to possible variations in Q (*1, 10-13*), but significant quantum yield differences have been reported for lake waters and for marine sediments.

"Dissolved fluorescence" has been used extensively as a water-mass and biological tracer in and around the North Sea (*12*), Japan (*14*), the North Pacific (*15*), Black Sea (*16*) and the South-Eastern coast of the US (*7*). It has generally been found to be high in rivers, consistent with a major terrestrial source of fluorescent chromophores. Behavior in mixing zones is generally conservative, although there are several reports of sources of fluorescent material in estuaries (*7*). Fluorescence of pore waters in the Santa Barbara Basin is reported to exceed that of overlying seawater by 10-500 times (*17*). Very few of these broad-scale studies have measured fluorescence and absorbance simultaneously.

Several reports have described correlations of fluorescence/absorbance ratios (*F/a*) with molecular weight for humic substances extracted from Lawrence Lake in Michigan (*18*), Tokyo Bay sediments (*19*), and Suwannee River humic acid (*20*). Stewart and Wetzel (*18*) observed a substantial decrease in *F/a* for high molecular weight material compared to smaller size fractions, and I discerned a similar trend (see chapter 3). Sedimentary HA isolated by Hayase and Tsubota (*19*) also showed decreased *F/a* values for the larger size fractions. Their humic material had very low energy excitation (480 nm) and emission (540 nm) maxima compared with any sample that I have examined.

In many studies, *F* is taken as the fluorescence intensity at a particular point rather than integrated over the whole emission range. This could distort the results if there were significant variations in spectral shape among samples, but these materials generally show very similar, broad, featureless emission bands, so this is unlikely to be a major problem. In my work I found that the emission peak for SRHA shifted to longer wavelengths for the larger molecular weight fractions although its shape remained relatively constant (fig 4, chap. 3). If the emission intensity had been measured at a fixed wavelength instead of at the peak maximum, F/a would have appeared to decrease to a greater degree for these samples. Stewart and Wetzel (*18*) compared absorption at 250 nm with fluorescence excited at 360 nm, so the differences they observed could be due to variation in the shape (S) of the absorption spectra, as well as to changes in fluorescent properties.

Despite the difficulties in directly comparing results from these diverse studies, they all suggest that, for a given humic sample, F/a ratios are generally lower for larger size fractions. Physically this is not unreasonable; larger molecules have more vibrational degrees of freedom than do smaller ones, and therefore, may more easily dissipate absorbed energy through non-radiative vibrational relaxation pathways.

The total fluorescence of a bulk sample containing a mixture of components with different quantum yields can be predicted mathematically. For a solution of n chromophores, the total absorption coefficient, a_T, is the sum of contributions from each component: $a_T = a_1 + a_2 + ... + a_n = \sum_1^n a_i$. If f_i is the fractional contribution of a_i to the total, such that $a_i = f_i a_T$, then $a_T = \sum f_i a_T = a_T \sum f_i$. The total fluorescence yield is therefore $F_T = a_T C \sum f_i Q_i$, where Q_i is the quantum yield of the i^{th} chromophore. From this equation it is can be seen that the apparent quantum yield ($Q_m = F_T/a_T C$) measured for a natural water sample will be equal to $\sum f_i Q_i$. It is clear, then, that variations in Q_m among samples can be due to differences in either the distribution of chromophores (f_i) or in their individual quantum yields (Q_i). Since dilution affects all components equally, mixing of colored water with water lacking COM (or with very low COM concentrations, e.g. rainwater) will yield a linear plot of F vs a, with a zero intercept.

This approach can be used to predict the form of F vs a plots obtained from mixing of two water masses. The two end members are taken to have total absorption coefficients and apparent quantum yields of a_1 (a_2) and Q_1 (Q_2), respectively. Then the relationship between F_T and a_T is:

$$F_T = \frac{a_1 a_2 (Q_1 - Q_2)}{a_2 - a_1} + \frac{a_2 Q_2 - a_1 Q_1}{a_2 - a_1} a_T. \tag{3}$$

The plot of F vs a_T is linear. It has a zero intercept if $Q_1 = Q_2$; otherwise the intercept may be either positive or negative, depending on the relative magnitudes of a and Q in each sample. Mixing of different water masses with the same Q_m value (but not necessarily the same *chromophores*) will give a plot identical to that for a simple dilution, also having a zero intercept; in both cases the slope is proportional to Q_m. Mixing of waters with different Q_m values will result in a plot with a non-zero intercept. Non-zero intercepts can also result from scattering by particles which affect both absorbance and fluorescence measurements in a non-linear fashion.

Methods

Collection of water samples is detailed in chapter four. COM samples from several other regions were compared with those from South Florida. Reference Suwannee River fulvic acid (SRFA) and humic acid (SRHA) originate in the drainage of the Okefenokee Swamp in southeastern Georgia. SRFA and SRHA samples were purchased from the International Humic Substance Society (IHSS). The Orinoco is an organic-rich river flowing north through Venezuela and entering the Caribbean Sea at about 10°S 60°W. Water samples and organic extracts from the Caribbean, the Gulf of Paria, and the Orinoco estuary were collected by N. Blough on a cruise to this region in fall 1988 (*21*). N. Blough has also shared his fluorescence and absorbance data on water collected by F. Hoge (NASA) in the Delaware Bight. Water samples from the Amazon estuary were collected by K. Ruttenberg in October 1991. COM isolated from the Sargasso Sea by P. M. Williams (Scripps) and E. Druffel was included in the fluorescence studies.

Fluorescence was measured on an SLM-Aminco 500C fluorometer, which is controlled via an IBM XT computer running version 2.4 of the SLM-supplied software. This software version corrects errors in the correction and integration routines which plagued earlier releases. Samples were contained in 1 cm square quartz cells and thermostated to 23±2° C. Bandpasses were typically 4 nm on both excitation and emission slits. For some samples (Orinoco and Delaware Bight) bandpasses were 4 and 2 nm for excitation and emission, respectively. For intercomparison of data sets, integrated fluorescence values were normalized to uniform instrumental parameters; normalization factors were determined by measurement of a quinine sulfate standard at each instrumental configuration. Absorption spectra were collected just prior to all fluorescence measurements for use in calculating quantum yields. To avoid inner filtering of light within the sample cell, highly absorbing water samples were diluted with Q-water or 0.05 M borate buffer, to an OD in a 1 cm cell, of ≈0.02 at 300 nm.

Quantum yields were measured with excitation wavelengths of 337 and 355 nm, corresponding to emission wavelengths of lasers commonly employed in remote sensing applications. Some quantum yields were also measured at an excitation wavelength of 385 nm. Emission spectra were corrected for instrumental configuration and integrated using software provided by the manufacturer. Solvent emission (primarily the Raman band of water) was subtracted from each spectrum. Quantum yields (ϕ) were calculated using a quinine sulfate reference (OD_{350}=0.02 in 0.1 N H_2SO_4, ϕ=0.55) from

$$\phi_s = \frac{F_s a_r \phi_r}{a_s F_r}, \tag{5}$$

where subscripts *s* and *r* refer to the sample and reference, respectively, *a* is the absorption coefficient of each at its excitation wavelength, and *F* is its integrated, corrected fluorescence intensity.

Matrix spectra. Forty-three emission spectra were concatenated to form each matrix spectrum. Excitation wavelengths (λ_{ex}) were varied in 5 nm increments from 260 nm to 475 nm; emission was measured at 5 nm intervals from λ_{ex}+ 10 nm to 770 nm. Emission spectra were collected sequentially by use of the programs "matblue," "matred," and "datblue," written in the SLM macro language. Each emission spectrum was itself collected in two parts: an initial "blue" part requiring no special treatment, and a "red" part collected with a long-pass optical filter (385-LP), placed between the sample and detector, in order to remove second order Raleigh scattering (at λ_{ex} x 2 nm). The emission intensities of spectra filtered in this way were corrected, in subsequent steps, for the small (2-5%) absorbance of the filter by dividing by its transmittance at each wavelength sampled.

To process the raw spectral data, first the 'blue' and 'red' parts of each spectrum were joined to form 43 integral spectra, with excitation range of 260 to 470 nm and emission from λ_{ex} + 10 to 770 nm. Correction for the filter was also included in this step. A macro program, "add," was written within the SLM software to accomplish both of these tasks.

An interactive fortran program, "matrix," was written to read and plot 3D spectra.

This program reads binary data from SLM-generated files and collects them into a single matrix. It calls a commercial fortran subroutine, "Plot88," in order to plot the data in either 3D or contour formats. This plotting subroutine allows 3D plots to be rotated to any viewing angle and contour intervals to be adjusted on contour plots. Home-written subroutines are used for various manipulations of spectra. One spectrum can be subtracted from another, in order to remove background Raman scatter peaks or fluorescence of a blank. Spectra can be normalized either to a fixed peak height, or by dividing by their absorption spectra. They may be integrated along excitation or emission axes; integration of absorbance-normalized spectra gives a listing of relative fluorescence yields at each excitation wavelength (*vide infra*). Matrices may be saved after background subtraction (and normalization) to avoid rereading and re-correction of original data. Copies of all computer programs for data collection and manipulation are included in Appendix C.

Results

Fluorescence spectra Figure 2 shows three corrected emission spectra of a surface water sample collected outside Oyster Bay in the fall of 1991 (bottle II-50). Excitation wavelengths were 337, 355, and 385 nm. These spectra are typical of most collected in this region, and resemble those of natural water samples from virtually any other waters examined in this project. The fluorescence yield of natural COM is low enough that the distinctively sharp Raman band (O-H stretch) of water is always apparent in dilute samples; it occurs at an energy of $\nu=\nu_{ex}-3400\ \mathrm{cm}^{-1}$, where ν_{ex} is the excitation energy in wavenumbers (cm^{-1}). Fluorescence emission is broad and unstructured, with peak maxima at 444 and 460 nm for excitation at 337 and 355 nm, respectively. With few exceptions, peak maxima at these excitation wavelengths varied by only ±5 nm of these energies for all samples from this region. The width of these emission peaks, and the fact that the peak maxima shift to the red with decreasing excitation energies, indicate that there are multiple emitting species present in this material.

Matrix spectra provide a complete picture of fluorescence emission but are somewhat difficult to compare with one another. Several presentations of these plots are used to highlight different aspects of the spectra. Gross differences in spectral shape are sometimes apparent through inspection of the 3D plots. Unfortunately, however, most spectra of natural waters are very similar and tend to resemble "potatoes under blankets" (*22*). Peak maxima and shoulders may be identified by their emission and excitation wavelengths; these are most easily determined on contour plots. Integrated spectra allow excitation and absorption spectra to be directly compared.

The spectrum of sample II-50 (fig 3 and 4) is taken as an example throughout the discussion. As is typical, the 3D spectrum of this sample shows its maximum fluorescence intensity at 260/450 (excitation/emission, in nm) at the blue edge of the excitation range. Excitation further into the uv was not possible because lamp intensity falls off rapidly in that region, and seasalt absorption begins to interfere with light penetration. The spectrum is dominated by a broad peak with maximum intensity at 300/430 and extending to 330/430. This spectrum, like most others, exhibits a distinct shoulder peak at 345/440, and a secondary shoulder at ≈390/480. The red shift of the emission with increasing excitation wavelength is clear from the diagonal slant of the contour lines. (Compare to contour plot of rhodamine b, fig 2.)

The II-50 spectrum has a distinct small peak at 280/310, which occurs in some samples and is virtually absent in others. Because it corresponds roughly to the energies of tryptophan absorbance and fluorescence, this has been designated "protein-like" by Coble et al. (*16*) and Mopper and Park (*23*). However, there is, as yet, fig. 2 Fluorescence emission spectra of sample II-50 with excitation at 337, 355, 385 nm (right to left). The prominent Raman scattering band of water has not been subtracted from these plots.

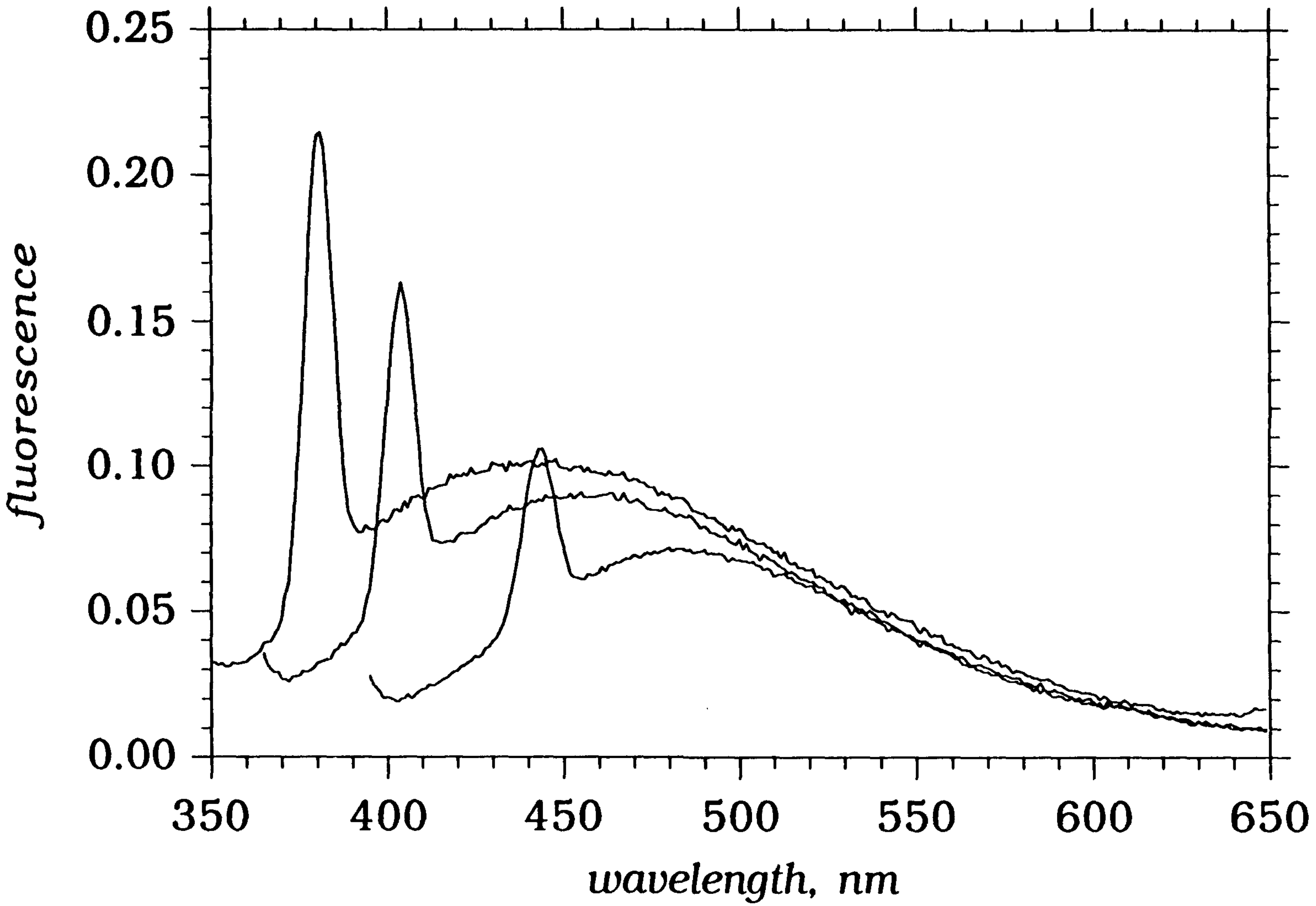
0.25
0.20
0.15
0.10
0.05
0.00
fluorescence
350
400
450
500
550
600
650
wavelength, nm

fig. 3 3D matrix spectrum of sample II-50. Excitation is from 260 to 470 and emission from 270 to 770 nm in 5 nm increments. The vertical scale is emission intensity; units are arbitrary. Lines parallel to the excitation axis are equivalent to single excitation spectra; lines parallel to the emission axis correspond to single emission scans at different excitation wavelengths.

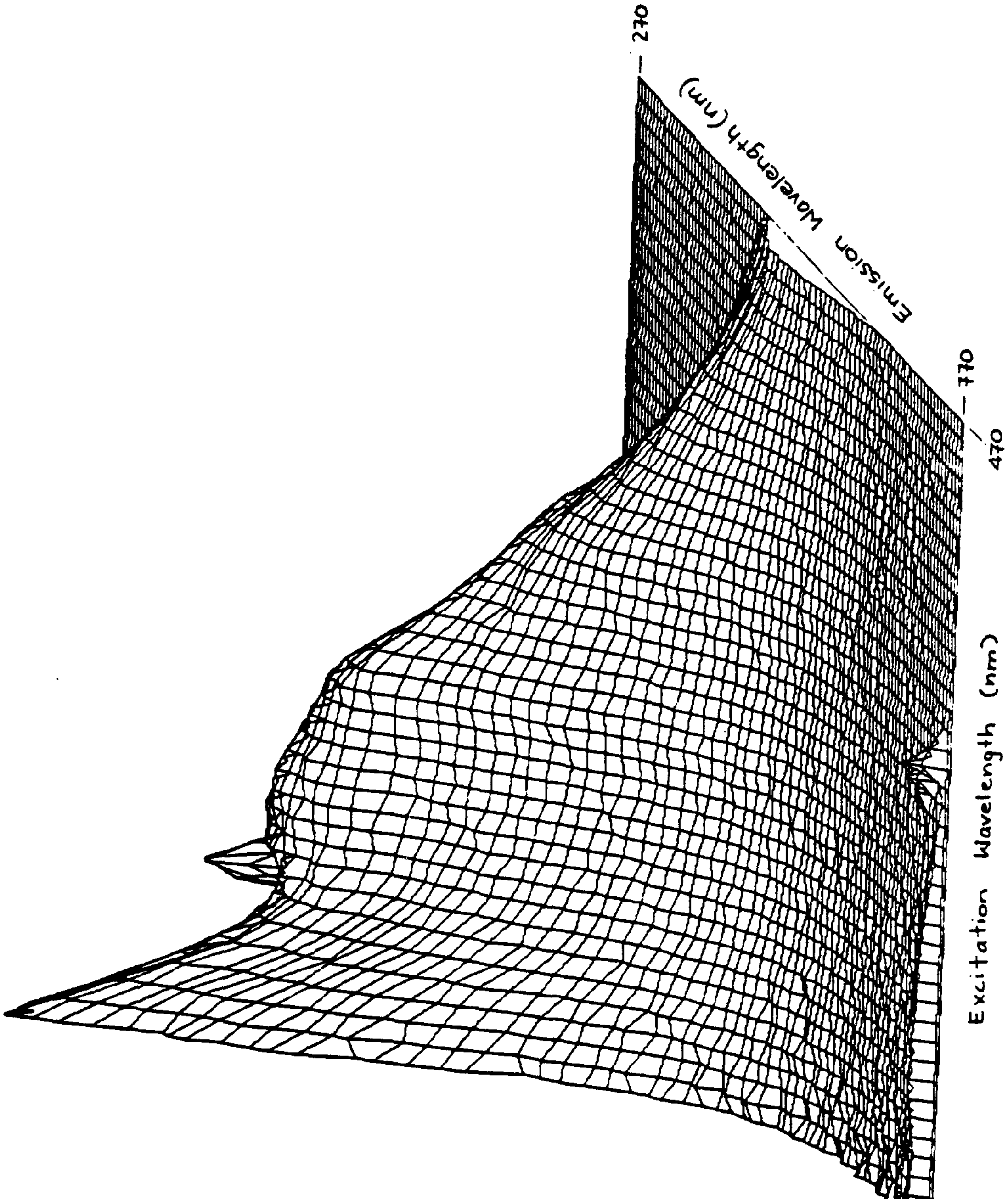
270
Emission Wavelength (nm)
770
470
Excitation Wavelength (nm)
260

fig. 4 Same spectrum as in previous figure, viewed in contour. Contour intervals are 2% of maximum intensity.

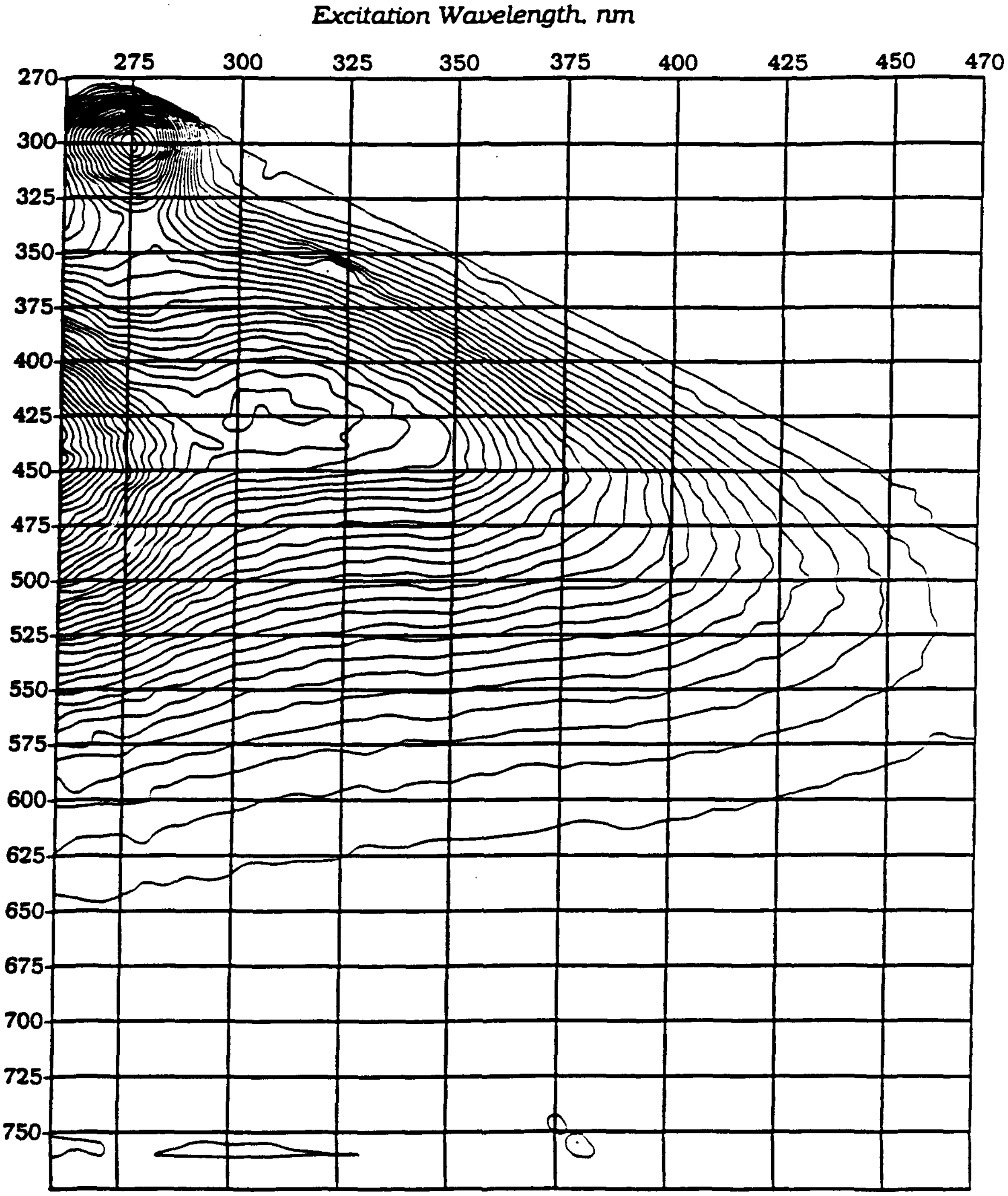
Excitation Wavelength, nm
275
300
325
350
375
400
425
450
470
270
300
325
350
375
400
425
450
475
500
525
550
575
600
625
650
675
700
725
750

no independent evidence for the presence of protein in these samples.

The shapes of the matrix spectra of water samples from Oyster Bay and the Gulf of Mexico were all nearly identical. Locations of their peak maxima and identifiable shoulders are shown in table I. All showed the same two, more or less distinct, peaks or shoulders at 305-315/420-435 and 350/445. The first of these tended to be blue-shifted (305/420) in blue-water as compared with Oyster Bay and Tamiami River waters (315/435). In SRFA, it is strongly red-shifted, appearing at 330/450.

Table I. Peak maxima in matrix spectra. Sample locations are given in chapter 4 tables I (May) and II (August).

sample #	peak maxima and shoulders (ex/em, nm)	
I-5	305/415	340/445
I-11	295/415	335/440
I-12	300/420	345/445
I-13	315/420	345/445
I-14	310/425	345/445
I-31	295/430	350/445
II-49	305/425	350/445
II-50	300/430	350/440
II-57	310/435	340/445
II-60	310/435	340/445
Tamiami River	315/435	350/445
SRFA	330/450	345/450

The 345/450 peak appears at nearly the same place in all natural water samples examined thus far. However, in blue-water, the sloping region between 310/435 and 345/445 is steeper, with the second peak more clearly defined than it is in brown-water spectra (fig. 5). In river samples, and in SRFA, these peaks almost merge into a single broad band.

Although the observed spectral variations do not seem large when viewed on a coarse grid of 210x500 nm, a 10 nm shift of a peak maximum represents a substantial change in excitation or emission energy. These results suggest that a more detailed look at the region of $290 \le \lambda_{ex} \le 410$ nm and $400 \le \lambda_{em} \le 500$ nm would be fruitful. This might take the form of either higher resolution spectra (i.e. 1 or 2, instead of 5, nanometer increments) or, possibly, synchronous spectra, which are equivalent to diagonal stripes across the 3D matrix. Synchronous spectra have been used to resolve mixtures of river waters (*6*) and may be more broadly applicable to environmental chemistry.

Integrated excitation and emission spectra, with corresponding absorption spectra, of a standard quinine sulfate solution and of sample II-50 are shown in figures 6 and 7, respectively. For quinine sulfate, the integrated excitation and absorption spectra are closely matched. This confirms that fluorescence is proportional to absorption for this compound, as expected for a pure, simple fluorophore. The two spectra become partially decoupled at $\lambda_{ex} \le 330$ nm due to optical factors intrinsic to the fluorometer (i.e. decreasing lamp intensity and changes in efficiency of the optics at short wavelengths). In the perpendicular direction, the integrated plot along the emission axis exactly reproduces (except for intensity) any single emission spectrum of quinine sulfate; the shape of the emission spectrum does not vary with excitation energy

In contrast to the quinine sulfate standard, the integrated fluorescence of the natural water sample (II-50) deviates significantly from its absorption spectrum. A comparison of the shapes of these two spectra (but not of their intensities, which are arbitrary in this plot) suggests that the fluorophores in this sample are not coincident with the absorbers; i.e. photons at 350 nm are more likely than those at 300 or 450 nm to provoke fluorescence. The integrated emission spectrum shows that photons from the seawater sample are emitted mainly at 450 nm. The shoulder fig. 5 Comparison between blue and brown water matrix spectra (II-31 and Oyster Bay)

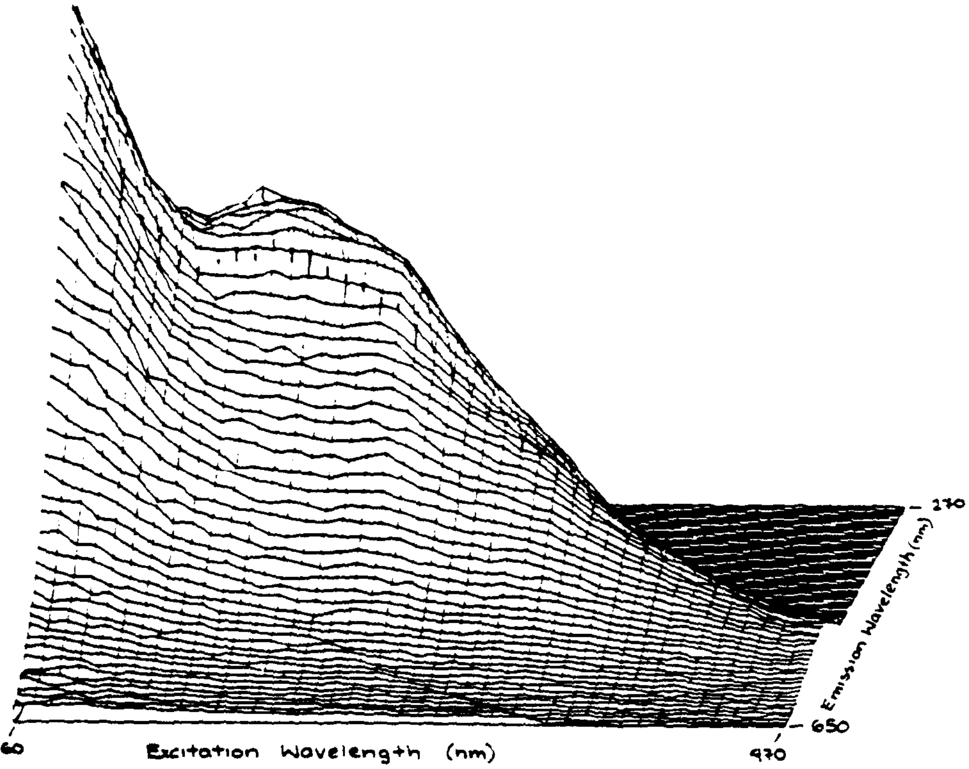
260
Excitation Wavelength (nm)
470
270
Emission Wavelength (nm)
650

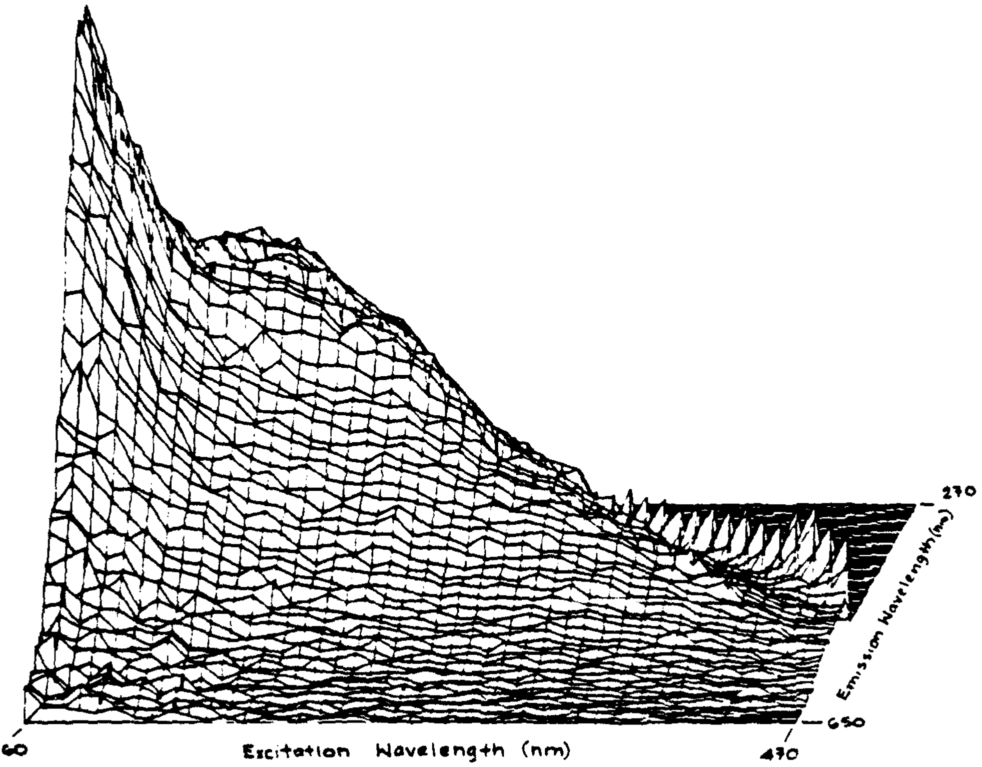
260
Excitation Wavelength (nm)
470
270
Emission Wavelength (nm)
650

fig. 6 Integrated spectra of quinine sulfate standard. Combined excitation spectrum, above, is plotted with the absorption spectrum (right axis). Intensity units are arbitrary. The combined emission spectrum is shown below.

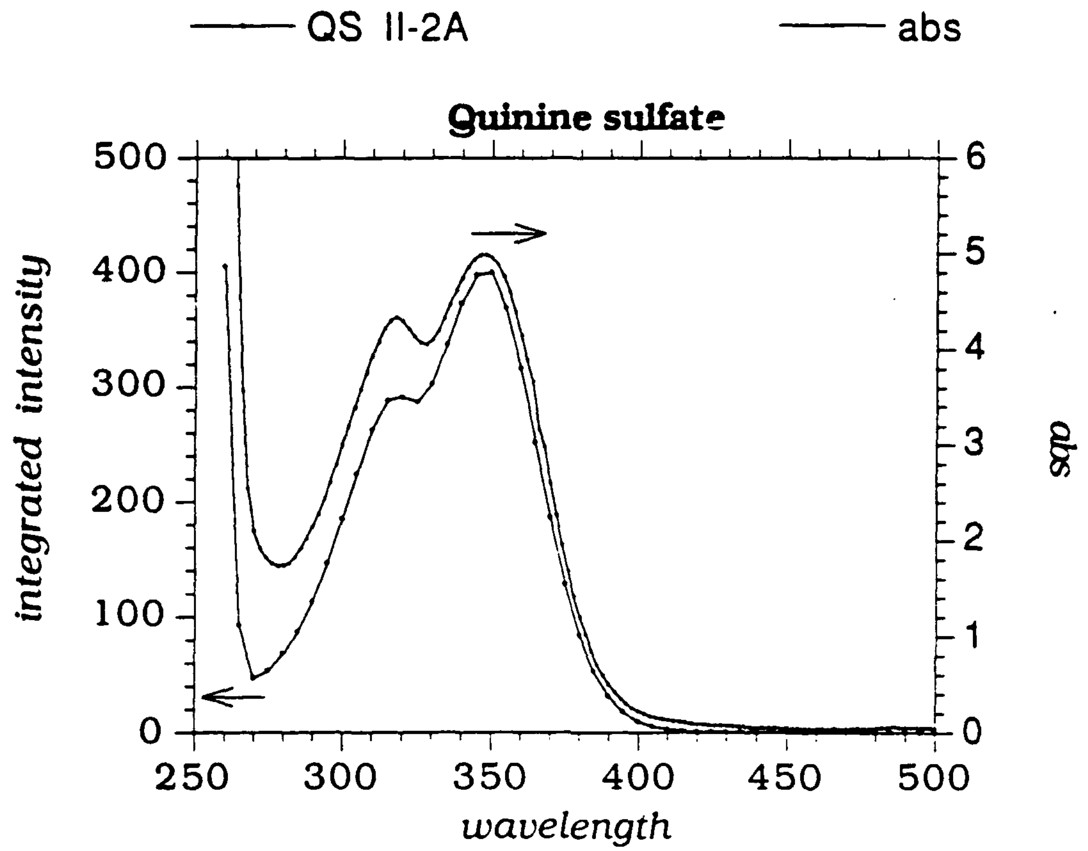
QS II-2A
abs
Quinine sulfate
500
400
300
200
100
0
integrated intensity
6
5
4
3
2
1
0
abs
250
300
350
400
450
500
wavelength

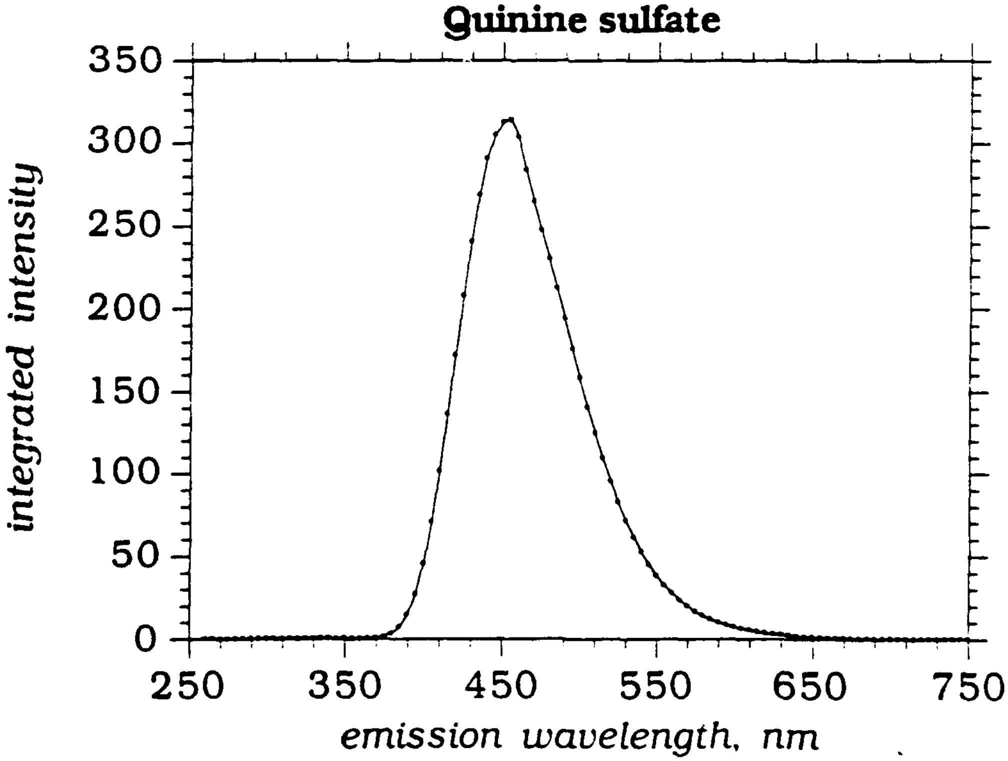
Quinine sulfate
350
300
250
200
150
100
50
0
integrated intensity
250
350
450
550
650
750
emission wavelength, nm

fig. 7 Integrated spectra of sample II-50. Combined excitation spectrum, above, is plotted with the absorption spectrum (right axis). Intensity units are arbitrary. The combined emission spectrum is shown below.

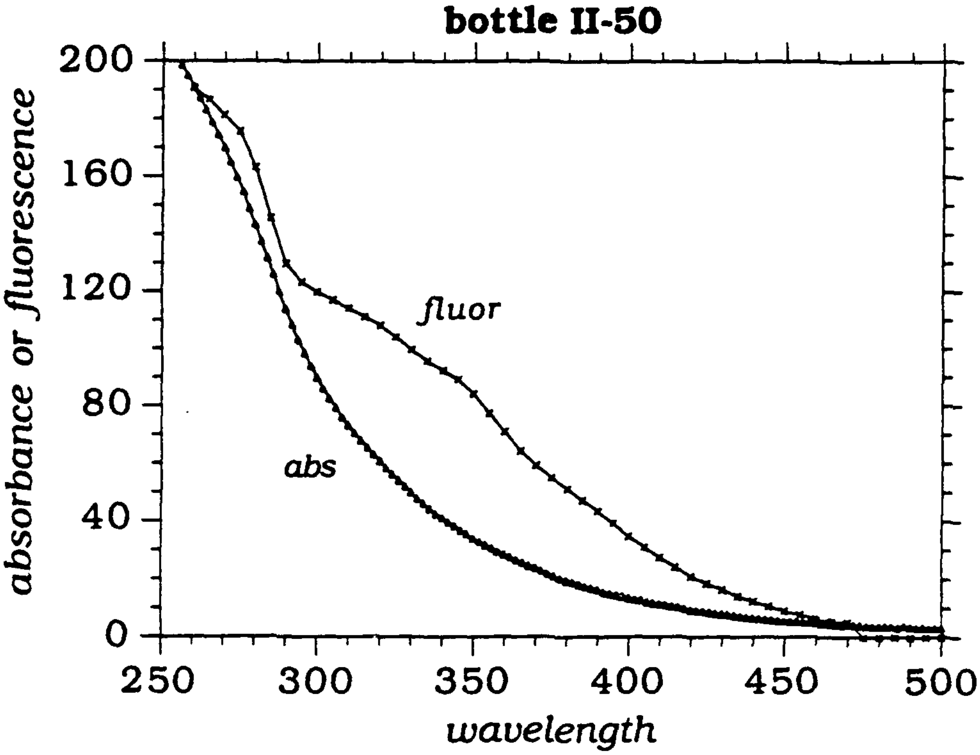

bottle II-50

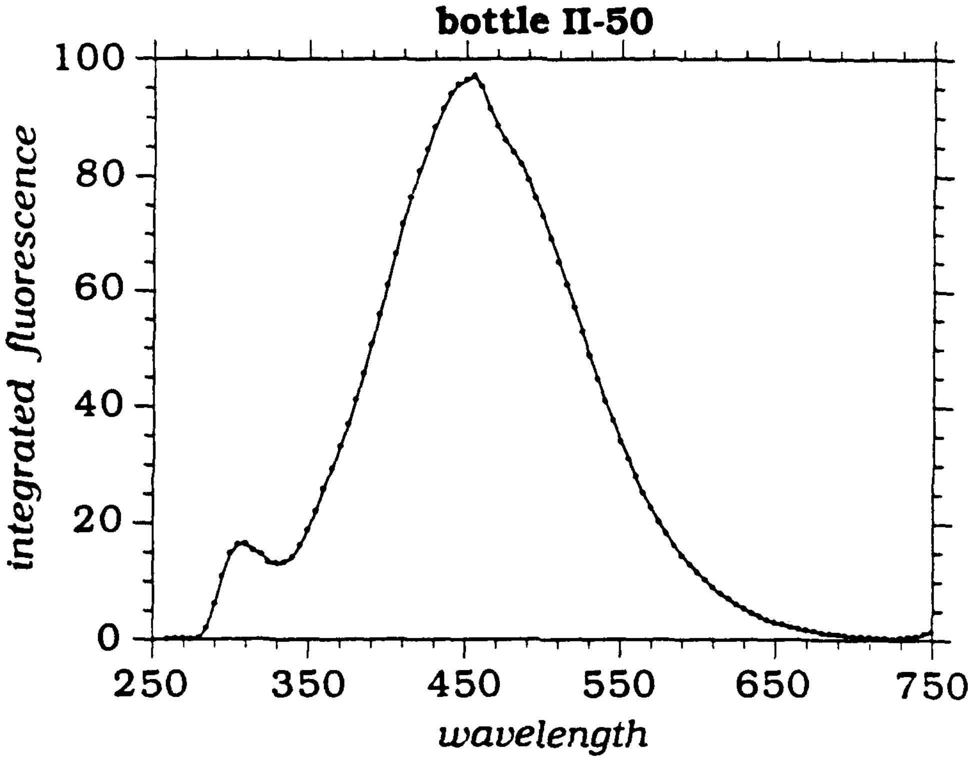

bottle II-50

Table II. Absorption coefficients, integrated fluorescence, and quantum yields for bottled samples collected in May 1991.

		337 nm			355 nm		
	sample	abs	fluor	QY (x 100)	abs	fluor	QY (x 100)
	2	0.23	1.81	0.93 ± 0.38	0.17		
	4	0.29	1.77	0.72 ± 0.23	0.20	1.56	0.92 ± 0.43
	5	0.26	0.78	0.35 ± 0.13	0.19	1.37	0.87 ± 0.43
	6	0.15	1.72	1.37 ± 0.85	0.10	2.34	2.73 ± 2.49
	7	0.10	0.78	0.89 ± 0.80	0.06	0.29	0.61 ± 1.00
	8	0.11	0.75	0.78 ± 0.64	0.07	0.50	0.81 ± 1.04
	9	0.50	5.25	1.25 ± 0.23	0.32	4.29	1.57 ± 0.45
	10	0.35	3.18	1.07 ± 0.28	0.24	2.72	1.32 ± 0.50
	11	0.84	8.43	1.18 ± 0.13	0.58	6.75	1.37 ± 0.22
	11	0.80	9.92	1.45 ± 0.17	0.54	7.30	1.60 ± 0.27
	12	1.23	12.54	1.20 ± 0.09	0.85	9.84	1.37 ± 0.15
	13	1.15	12.27	1.26 ± 0.10	0.79	9.90	1.48 ± 0.17
Oyster Bay	14	15.5	173.5†	1.32 ± 0.06	10.66	135.5†	1.51 ± 0.11
	14*	1.89	21.16	1.32 ± 0.06	1.30	16.52	1.51 ± 0.11
	20	0.53	4.75	1.06 ± 0.18	0.36	4.07	1.32 ± 0.33
	21	0.38	3.72	1.14 ± 0.27	0.26	3.01	1.37 ± 0.49
	22	0.45	5.67	1.48 ± 0.30	0.33	4.71	1.68 ± 0.46
	23	0.11	0.95	0.99 ± 0.81	0.08	0.63	1.00 ± 1.23

* Diluted with 50 mM borate buffer.

† Fluorescence and quantum yields calculated from diluted samples.

Table III. Absorption coefficients, integrated fluorescence, and quantum yields for bottled samples collected in August 1991.

		337 nm				355 nm				385 nm			
	sam#	abs	fluor	QY (x 100)		abs	fluor	QY (x 100)		abs	fluor	QY (x 100)	
	4	0.17	1.19	0.82	±0.43	0.10	0.92	1.06	±0.95	0.06	0.91	#	
	6	0.24	1.00	0.50	±0.19	0.17	0.45	0.31	±0.17	0.13	0.77	0.70	±0.49
	7	0.15	1.22	0.97	±0.60	0.09	0.82	#		0.05	0.67	#	
	8	0.39	2.87	0.89	±0.21	0.27	2.27	1.00	±0.34	0.17	1.65	1.14	±0.61
	9	0.26	2.16	0.98	±0.34	0.17	1.55	1.12	±0.62	0.08	1.41	#	
	10	0.53	4.90	1.11	±0.19	0.37	3.48	1.12	±0.28	0.21	2.75	1.54	±0.66
	15	0.19	1.39	0.88	±0.43	0.12	0.80	0.81	±0.64	0.07	0.86	#	
	20	0.16	1.06	0.80	±0.47	0.10	0.82	0.97	±0.90	0.05	0.53	#	
Gulf Station	22	0.26	1.92	0.89	±0.32	0.17	1.17	0.81	±0.43	0.10	0.99	1.13	±1.00
	31	0.52	4.48	1.02	±0.18	0.36	3.44	1.12	±0.28	0.21	2.12	1.22	±0.54
	49	2.42	25.10	1.15	±0.04	1.71	20.10	1.30	±0.07	1.01	12.40	1.36	±0.12
	50	2.21	21.84	1.17	±0.05	1.43	17.81	1.48	±0.10	0.69	11.37	1.96	±0.26
	53	3.67	28.84	0.94	±0.02	2.64	24.01	1.08	±0.04	1.56	16.47	1.25	±0.07
	57	7.26	59.85†	0.98	±0.03	5.29	49.48†	1.11	±0.04	3.13	30.07	1.14	±0.03
	57*	3.52	29.02	0.98	±0.03	2.55	23.85	1.11	±0.04	1.50	15.09	1.20	±0.07
	60	21.16	177.98†	1.00	±0.03	15.72	148.55†	1.12	±0.05	9.72	92.82†	1.14	±0.08
	60*	2.82	23.72	1.00	±0.03	2.09	19.75	1.12	±0.05	1.31	12.49	1.14	±0.08
Oyster Bay	61	41.70	352.87†	1.01	±0.03	31.20	291.25†	1.11	±0.05	18.91	204.61†	1.29	±0.10
	61*	2.77	23.44	1.01	±0.03	2.09	19.51	1.11	±0.05	1.24	13.42	1.29	±0.10
Tamiami R.	30	46.10	669.32	1.71	±0.03	33.70	555.38	1.90	±0.04	19.00	336.46	2.10	±0.01
	30*	3.43	49.80	1.71	±0.03	2.50	41.20	1.90	±0.04	1.44	25.50	2.10	±0.01

Absorption coefficient too low for accurate calculation. * Diluted with 50 mM borate buffer.

† Fluorescence and quantum yield values calculated from diluted samples.

visible at about 480 nm is an instrumental artifact which is removable (with difficulty) by correction routines. The emission peak maximum at 430 nm, visible on the 3D and contour plots, is overwhelmed by the signal at 450 nm.

Integrated spectra are shown for several additional coastal water samples in figure 8 The integrated excitation spectra exhibit more variability than do absorption spectra; e.g. the ratio of total emission at λ_{ex}=300 and λ_{ex}=350 is clearly different among these samples. The combined emission spectra, however, are nearly indistinguishable, apart from intensity. The only notable feature is the small peak at λ_{em}=300 for sample I-13. Peak maxima are all ≈455 nm.

Quantum Yields Quantum yields, for 337 and 355 nm excitation, were calculated for all bottled samples and COM isolates. The results are shown in tables II (spring samples), III (fall samples), IV and V (COM isolates). Integrated fluorescence intensities (*F*) have been normalized to the same instrumental conditions and so are directly comparable. Uncertainties in quantum yields were determined by a standard error propagation procedure (*24*). The major source of error is in the absorbance data; thus quantum yields are not very precise for weakly absorbing samples. The use of COM extracts is meant to alleviate this problem. However, reconstituted isolates were not always representative of the water from which they were obtained (*see chapter 6*).

Quantum yields of surface seawater samples fall in a narrow range between 0.8 and 1.9% for excitation at either 337 or 355 nm. In most cases, yields were slightly higher with 355 nm excitation. The highest values were observed for spring samples collected within Oyster Bay; values for fall samples from the same region were ≈20% lower. Reconstituted extracts generally exhibited slightly higher quantum yields than unconcentrated water samples (table IV).

Table IV. Absorption coefficients, integrated fluorescence, and quantum yields for extracts reconstituted into oligotrophic seawater.

		337 nm			355 nm	
extract#	*a(337)*	*F*	*QY*	*a(355)*	*F*	*QY*
spring						
1	1.27	10.50	0.98 ± 0.07	0.92	9.09	1.17 ± 0.12
2	2.17	16.74	0.91 ± 0.04	1.64	13.92	1.00 ± 0.06
3	1.57	15.39	1.16 ± 0.07	1.12	13.08	1.38 ± 0.11
4	1.56	16.59	1.26 ± 0.07	1.08	14.70	1.61 ± 0.14
5	2.29	31.8	1.48 ± 0.06	1.63	27.20	1.81 ± 0.09
6	2.31	27.72	1.42 ± 0.06	1.69	23.46	1.64 ± 0.09
7	4.46	64.9	1.64 ±0.03	3.22	54.9	1.94 ±0.06
8	4.05	35.9	0.96 ±0.02	3.09	31.6	1.12 ±0.03
9	3.22	30.5	1.01 +0.03	2.44	26.4	1.17 ±0.04
10	4.00	37.3	1.01 ±0.02	3.02	32.6	1.19 ±0.04
fall						
BWX	2.93	30.9	1.12 +0.04	2.07	25.9	1.35 ±0.06
II-50X	3.57	36.3	1.10 ±0.03	2.68	31.7	1.30 ±0.04

Quantum yields for deep Sargasso Sea COM extracts are given in table V.

Table V. Quantum yields of Sargasso Sea isolates.

		QY x10^{2}		
depth, m	•sample #	337 nm	355 nm	385 nm
50	PW-5-76-A50-2	1.86±0.08	2.2±0.1	2.8±0.3
850	PW-5-76-B850-2	1.47±0.05	1.6±0.1	1.9±0.2
1500	PW-5-76-C1500-2	1.81±0.06	2.1±0.1	2.5+0.2
3200	PW-5-76-D3200-2	1.81±0.06	2.1±0.1	2.5±0.2

•Samples provided and numbered by Williams and Druffel

With the exception of the 850 m sample, quantum yields are very similar to one another, but are higher than surface water values, for each excitation wavelength used. The uniqueness of the 850 m sample may be due its source in the oxygen minimum zone, or it may be a signature of the Antarctic Intermediate water found at this depth.

The fluorescence yields for a large number of samples can most easily be compared graphically by plotting *F* against the absorption coefficient at the excitation wavelength, *a(ex)*, as shown in figures 9 and 10, for 337 and 355 excitation. Also included on these graphs are data from the Delaware Bight, the Sargasso Sea, the Orinoco and Amazon Rivers, and SRFA and SRHA. Optically dense samples ($a(ex)$>4 m^{-1}) were diluted to obtain accurate fluorescence values; they were renormalized to original absorbance values for inclusion on these graphs. The highest values are not included on these linear plots in order to keep the scale manageable. COM isolates from the Gulf region have also been renormalized to their natural absorbance values. Isolates from the Suwannee River, Sargasso Sea and the Orinoco were not re-adjusted because optical data for their parent waters were unavailable.

With few exceptions, all points on these plots fall within an envelope roughly defined by lines through the origin with slopes of 6 and 12 for 337 nm data, and 7 and 16 for 355 nm data. These lines are shown on the graphs. No significant difference between spring and fall data is obvious in these data. Because of the difficulties associated with measuring absorption coefficients on very weakly absorbing solutions, there are large errors in the *a* values for the blue water samples, so this endmember is not well constrained on these plots.

In general, yields at 355 nm are ≈10-20% higher than those at 337 nm. This result is apparent in both weakly absorbing samples, despite the large errors inherent in the measurement of ϕ, and in more highly absorbing samples and reconstituted extracts. This may be taken as further indication of the presence of multiple fluorophores, since quantum yield should be independent of excitation wavelength for a single fluorophore.

Because the difference in quantum yield between 337 and 355 nm excitations for any one sample is smaller than the overall variation among samples, both data sets are plotted together in figures 11 (linear scale) and 12 (log-log scale). A linear regression (determined on a linear plot, $r^2=0.94$, N=137) gives the relationship: $F=1.2\pm1.4+a9.9\pm0.2$. It is rather remarkable that the F/a ratio is so tightly constrained for such a variety of samples. The observed slope on the F vs a plot gives an apparent quantum yield (Q_m) of 1.2±0.2% for this whole suite of waters. (Calculated from $\phi_s = \frac{F_s a_r \phi_r}{a_s F_r}$ (eq.5) with $F/a=9.9$ m and $a_r\phi_r/F_r = 0.118\text{x}10^{-2}\ m^{-1}$ for the instrumental setting employed on the fluorometer.)

Matrix and absorption spectra were combined to give 3D plots of fluorescence efficiency. The absorption-normalized 3D spectrum of sample II-50 is shown in figure 13. In this example the fluorescence efficiency is greatest in the range of 350 to 400 nm. Although the *overall* fluorescence intensity is greatest at shorter wavelengths, a smaller *fraction* of the high-energy photons absorbed are re-emitted.

Figure 14 shows the integrated, normalized spectra of II-50; for comparison, un-normalized spectra are also shown. The integrated intensity plotted against the excitation axis is proportional to the fluorescence quantum yield at each wavelength from 260 to 470 nm. For II-50, the maximum fluorescence efficiency is obtained with excitation at 395 nm. A prominent secondary peak occurs at 360 nm, and a smaller fig. 8 Integrated spectra of several coastal samples. From top to bottom, samples are: Oyster Bay (I-14), I-13, I-9 and I-11, all collected in May 1991.

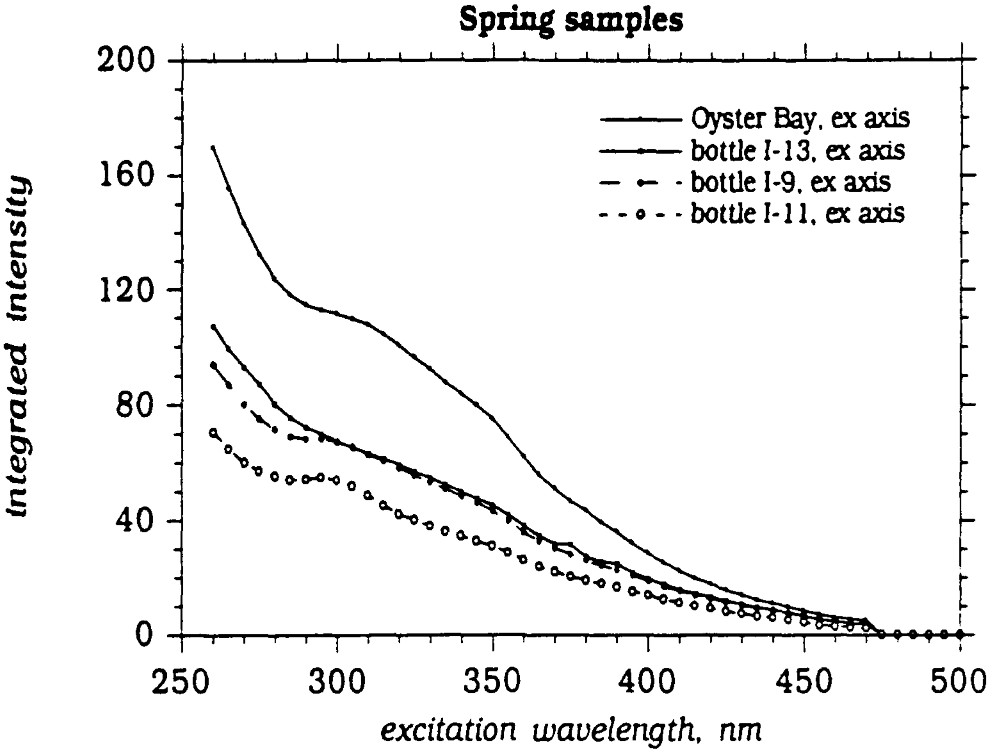
Spring samples
Integrated intensity
0
40
80
120
160
200
250
300
350
400
450
500
excitation wavelength, nm
Oyster Bay, ex axis
bottle I-13, ex axis
bottle I-9, ex axis
bottle I-11, ex axis

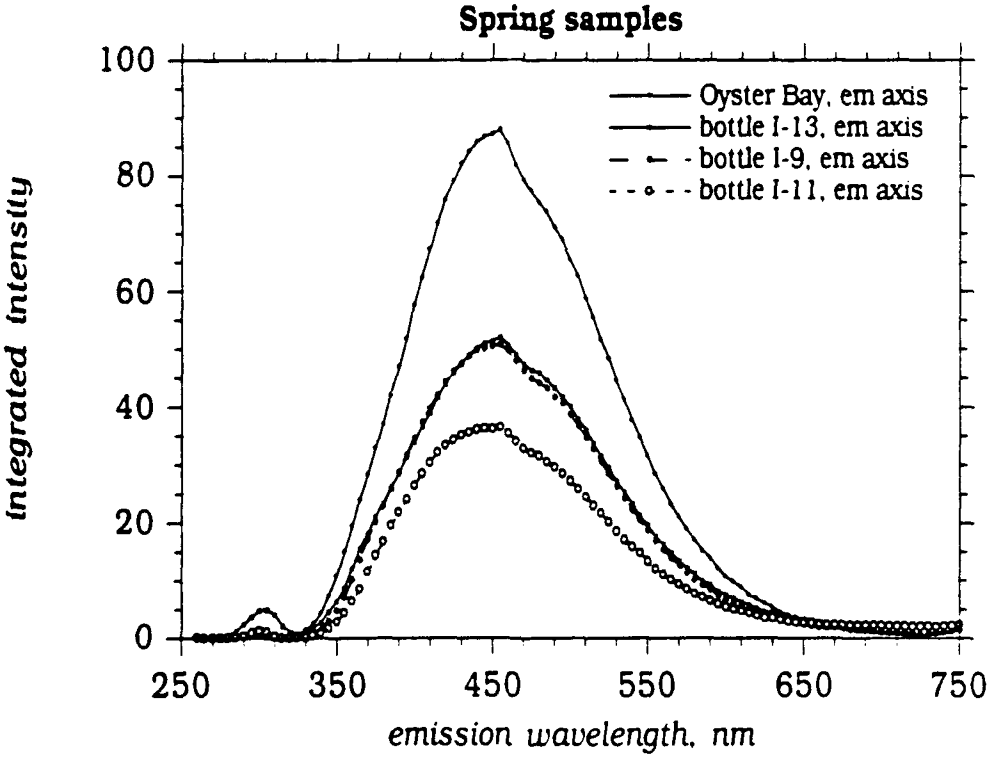
Spring samples
Integrated intensity
0
20
40
60
80
100
250
350
450
550
650
750
emission wavelength, nm
Oyster Bay, em axis
bottle I-13, em axis
bottle I-9, em axis
bottle I-11, em axis

fig. 9 Integrated fluorescence vs absorption coefficient at 337 nm. Data are from the Gulf of Mexico spring (○), fall (□), and COM isolates (●), the Delaware Bight (◇), Amazon (×) and Orinoco (+) Rivers, the deep Sargasso Sea (◆), and the Suwannee River (▲).

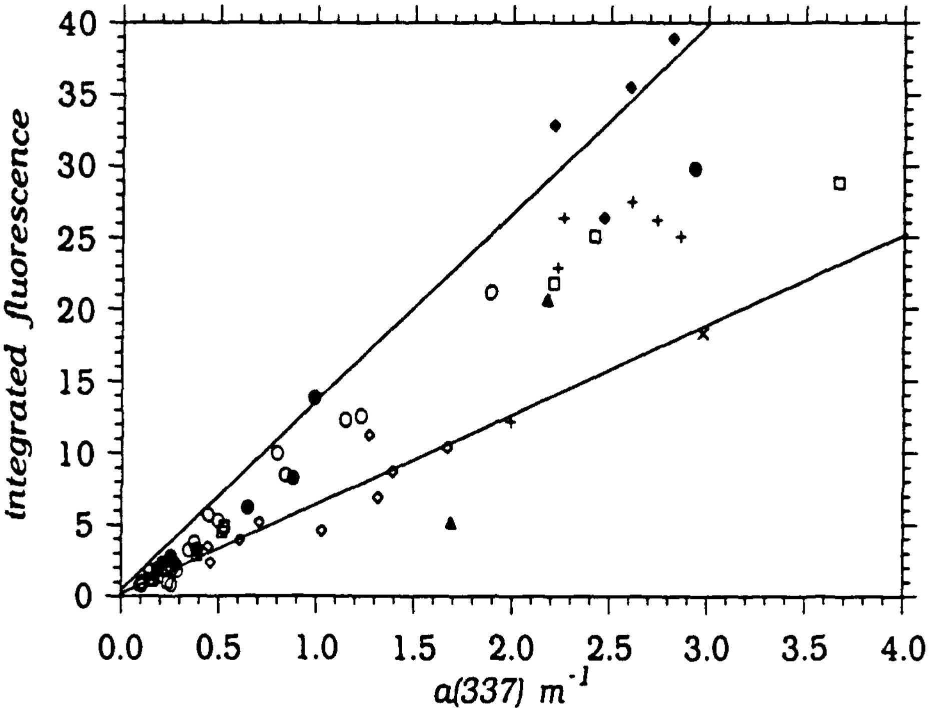
Integrated fluorescence
a(337) m^{-1}
0
5
10
15
20
25
30
35
40
0.0
0.5
1.0
1.5
2.0
2.5
3.0
3.5
4.0

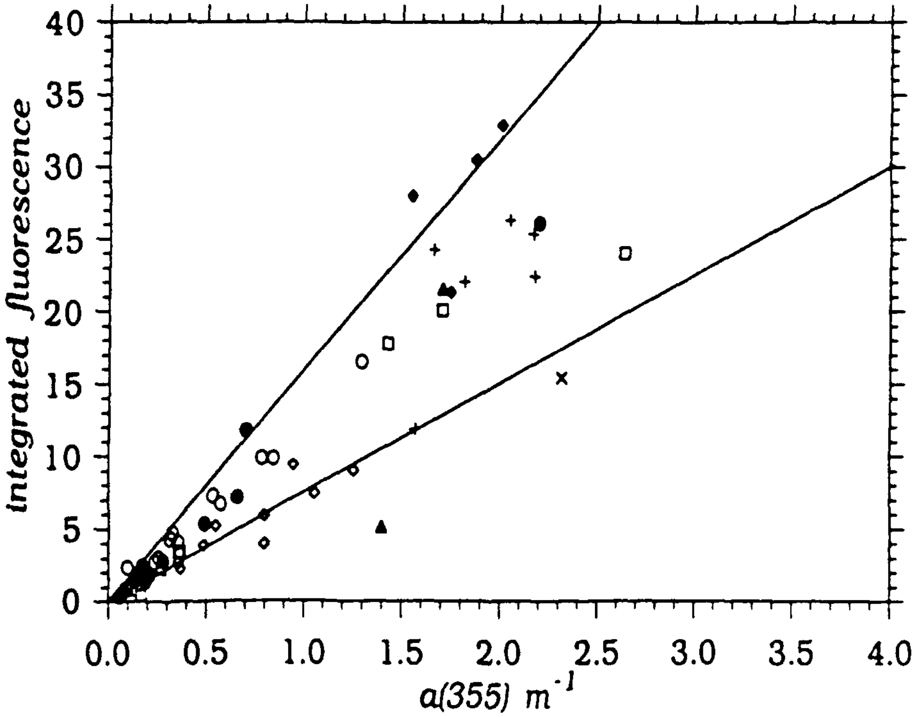
Integrated fluorescence
a(355) m^{-1}
0
5
10
15
20
25
30
35
40
0.0
0.5
1.0
1.5
2.0
2.5
3.0
3.5
4.0

fig. 10 Same as previous figure, on an expanded scale. Data are from the Gulf of Mexico spring (○), fall (□), and COM isolates (●), the Delaware Bight (◇), Amazon (X)and Orinoco (+)Rivers, the deep Sargasso Sea (◆), and the Suwannee River (▲).

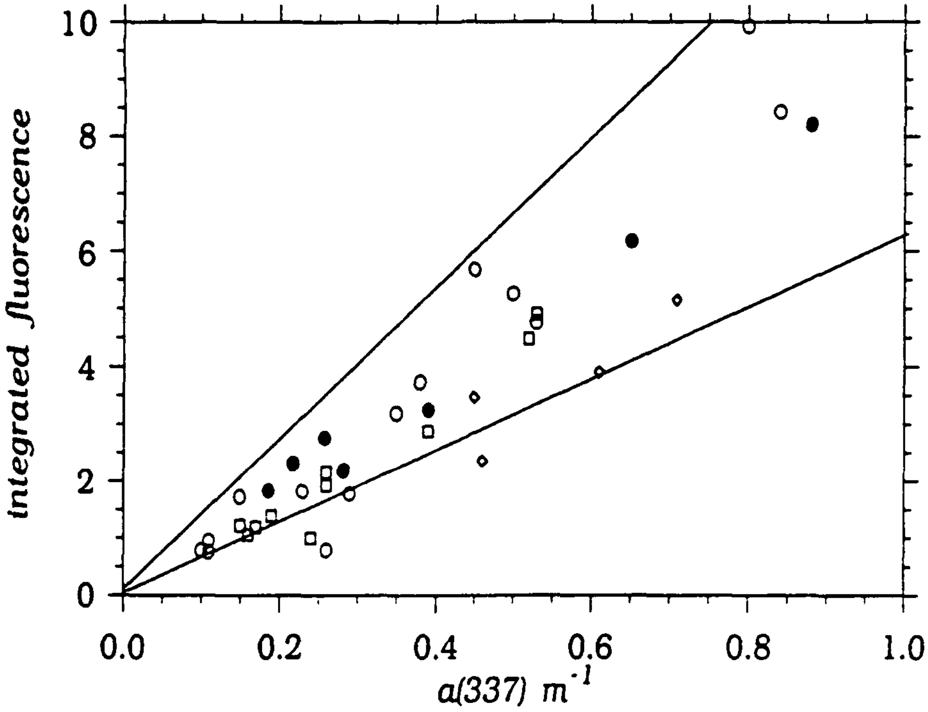
10
8
6
4
2
0
Integrated fluorescence
0.0
0.2
0.4
0.6
0.8
1.0
a(337) m^{-1}

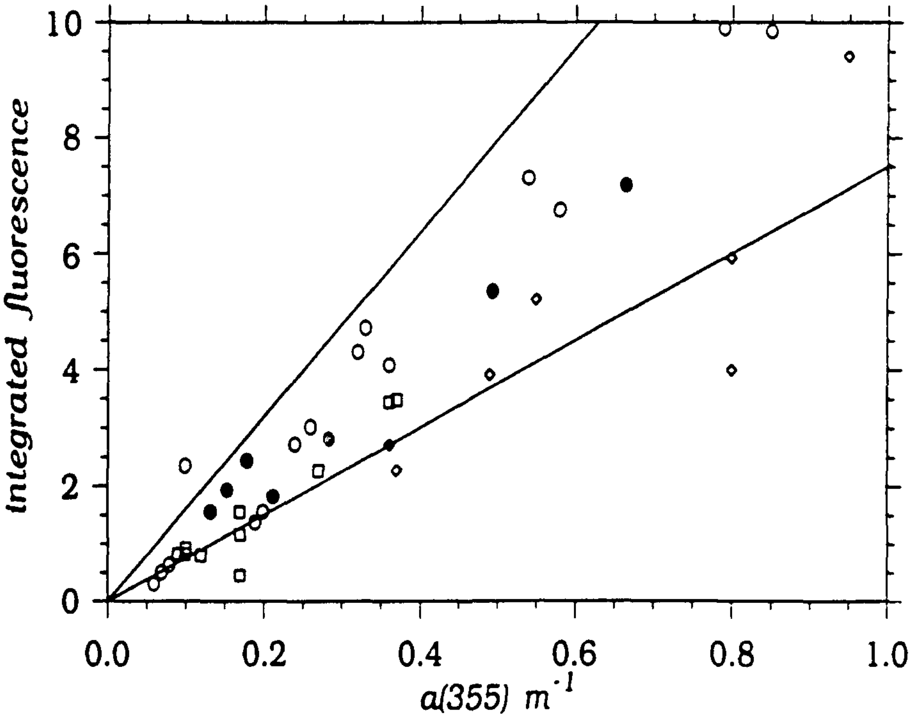
10
8
6
4
2
0
Integrated fluorescence
0.0
0.2
0.4
0.6
0.8
1.0
a(355) m^{-1}

one corresponds to the 280/310 emission. Peaks in the normalized spectrum are coincident with less distinct features that are apparent in the un-normalized version. The increasing intensity from 300 to 355 nm is in agreement with the difference in independently measured quantum yields at 337 and 355 nm.

Normalized, integrated spectra for several water samples are shown in figure 15. These represent strongly absorbing waters from in and around Oyster Bay; absorbance of blue-waters further into the Gulf was too low to allow adequate normalization for unconcentrated samples. The upper set of curves represent samples collected in May; the lower set are August samples from along a transect into the Bay. Within each group, spectra are very closely matched. The maximum efficiency is obtained with excitation at 380-390 nm for all samples, and they also share a distinct peak at 355 nm. At either edge, several spectra show indications of shoulder peaks at ≈305, 435, and 445 nm. In the region of 350 to 400 nm, the fluorescence efficiency of the spring samples is ≈20% greater than that of the fall samples. In the two seasons the efficiencies are nearly coincident for λ_{ex}=300 nm; below 290 nm their order seems to reverse. At the red edge, the spectra begin to approach one another by λ_{ex}≈460 nm.

The variability among the natural waters sampled is demonstrated in figure 16. Waters from the Amazon and Orinoco Rivers have substantially lower fluorescence efficiencies than the Tamiami River, and this difference extends across the spectrum. The two Oyster Bay samples fall between these extremes. SRFA, commonly used as a reference COM material, exhibits a dramatically different spectral shape from the others shown. Its fluorescence efficiency increases to a much greater extent in the region of 400-450 nm. In all cases the peak at 355 nm is clearly evident and does not exhibit any wavelength shifts. The longer wavelength band varies more in both position and intensity.

Discussion

The quantum yield data demonstrate a robust relationship between fluorescence and absorbance intensities and thereby suggest that measurement of fluorescence, which is inherently more sensitive than absorbance, can be used to determine optical attenuation coefficients in surface waters. Estimations of attenuation due to COM absorption are not likely to be in error by more than a factor of 2-3, when fluorescence is excited by light coincident with the absorption wavelength region of interest. If there are uncertainties in the absorption parameter, *S*, then extrapolation to other absorption energies could increase the potential error by several fold. This is still well within tolerable limits for many remote sensing applications. Ultimately, shipboard or airborne fluorometers may provide the optical parameters needed to accurately interpret satellite-derived data in regions where COM concentrations are important.

Raman emission has been suggested for use in calibrating airborne sensors to correct for optical attenuation within the water column (2, 3). This may prove to be a very useful "internal" standard for remote sensors, but in waters with high COM content, account must be taken of the fluorescence which may contribute significantly to the intensity measured at the chosen Raman wavelength. By contrast, in waters with very low COM concentrations, Raman emission may be the dominant contributor to measured solar-induced surface irradiance signals.

Variability within the relatively narrow range of quantum yields measured may ultimately be useful in disentangling sources and fates of organic carbon in the oceans. However, not enough quantum yield data from diverse sources have been fig. 11 Fluorescence vs absorption coefficient for all available data, 337 and 355 excitations, on a linear scale.

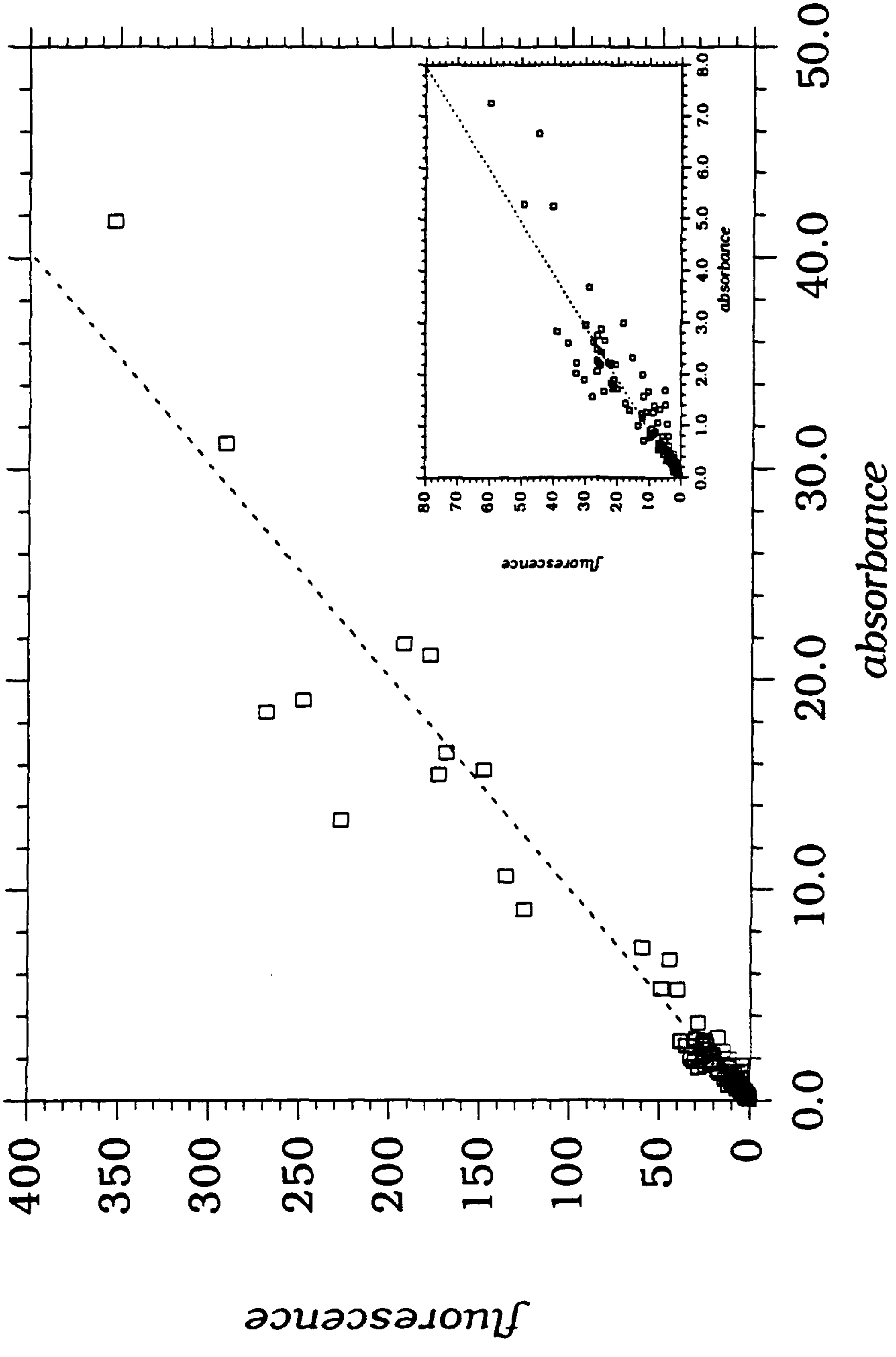
fluorescence
400
350
300
250
200
150
100
50
0
absorbance
0.0
10.0
20.0
30.0
40.0
50.0
fluorescence
80
70
60
50
40
30
20
10
0
absorbance
0.0
1.0
2.0
3.0
4.0
5.0
6.0
7.0
8.0

fig 12 Fluorescence vs absorption coefficient for all available data, 337 and 355 excitations, on a log-log scale.

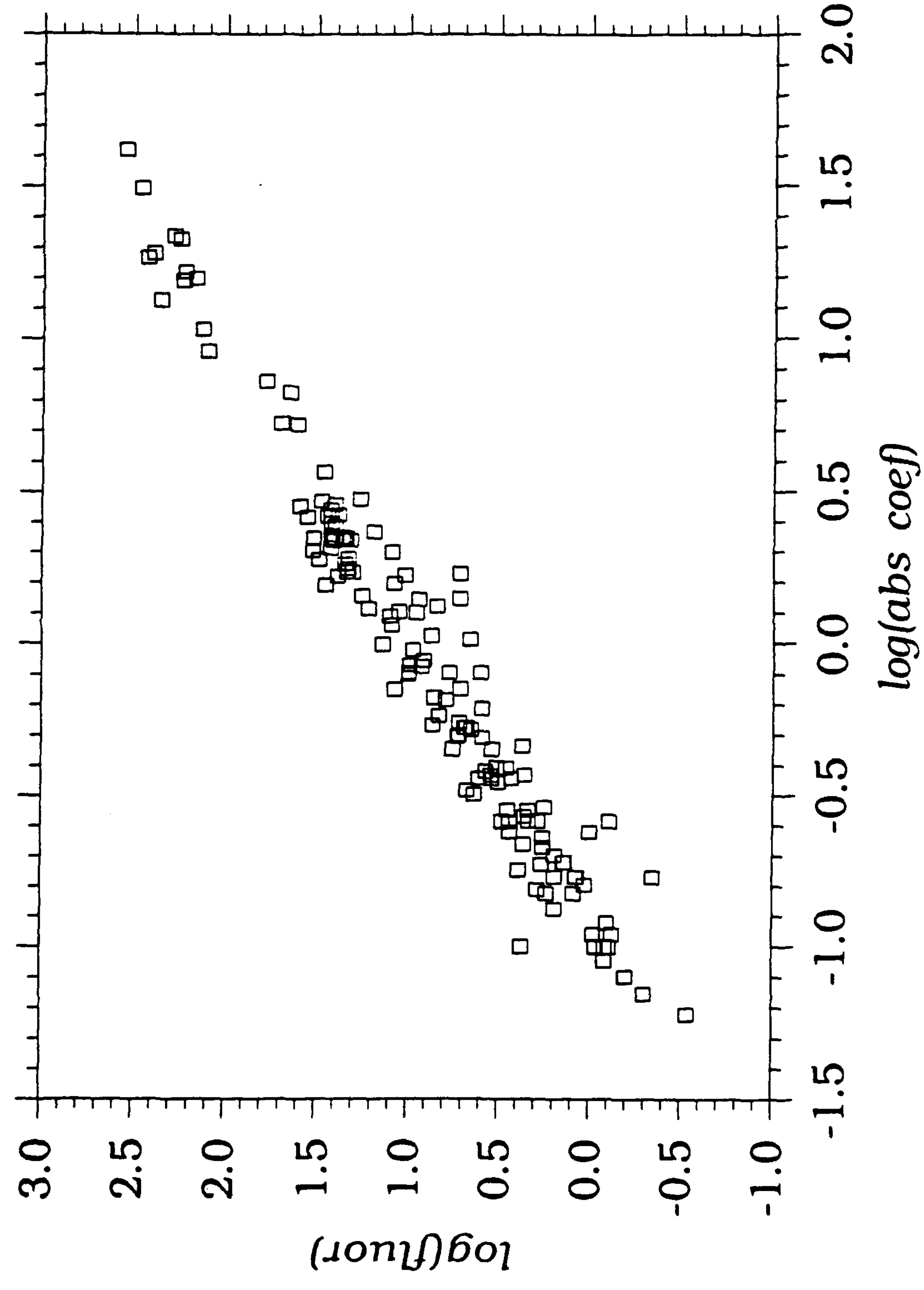
log(fluor)
3.0
2.5
2.0
1.5
1.0
0.5
0.0
-0.5
-1.0
log(abs coef)
-1.5
-1.0
-0.5
0.0
0.5
1.0
1.5
2.0

fig. 13 Normalized matrix spectrum of II-50. Peak maximum is at 395/480. (excitation/emission, in nm).

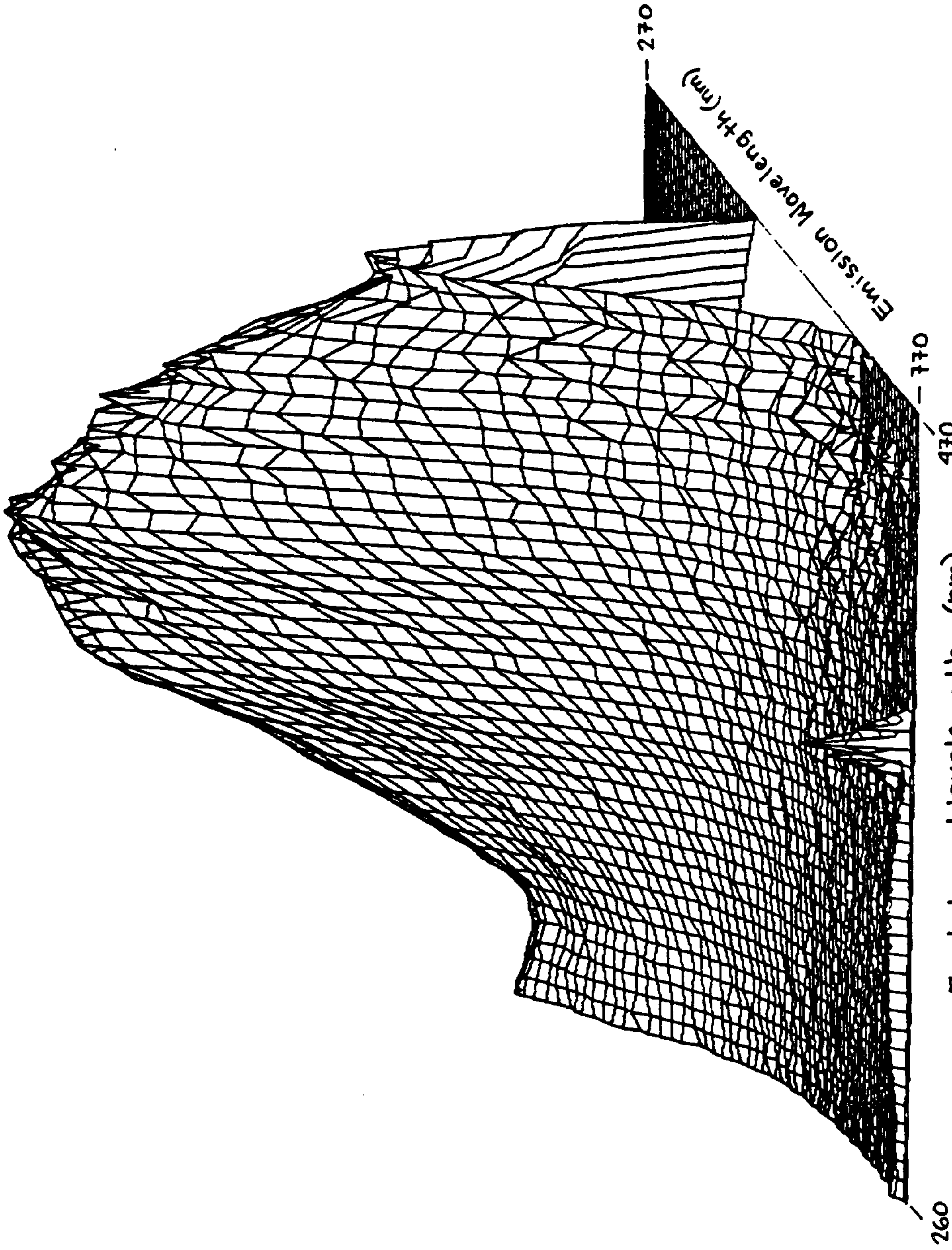
270
Emission Wavelength (nm)
770
470
Excitation Wavelength (nm)
260

fig. 14 Integrated, normalized spectra of II-50. Normalized spectra (right axes) are compared with un-nomalized versions (left axes).

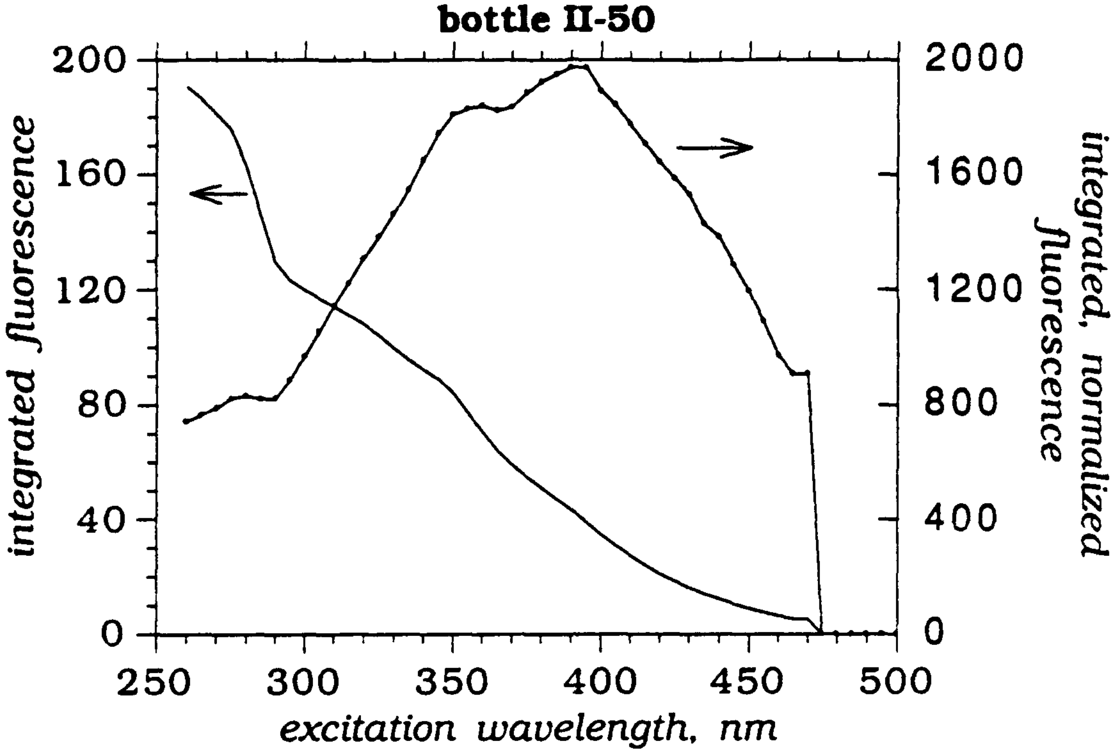
bottle II-50
integrated fluorescence
200
160
120
80
40
0
integrated, normalized fluorescence
2000
1600
1200
800
400
0
250
300
350
400
450
500
excitation wavelength, nm

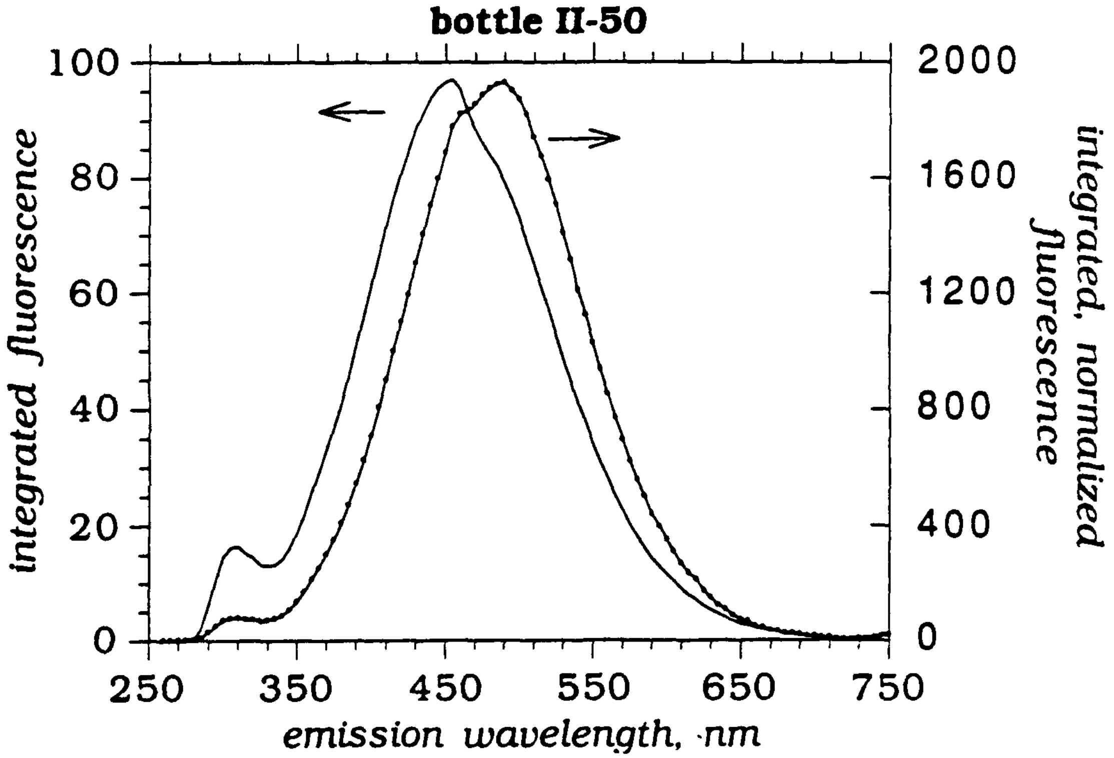
bottle II-50
integrated fluorescence
100
80
60
40
20
0
integrated, normalized fluorescence
2000
1600
1200
800
400
0
250
350
450
550
650
750
emission wavelength, nm

fig. 15 Integrated, normalized spectra of waters in and around Oyster Bay: I-12 (□), I-13 (○), I-14 (△) (spring samples) and II-49 (●), II-50, II-57 (■), II-60 (▲) (fall samples).

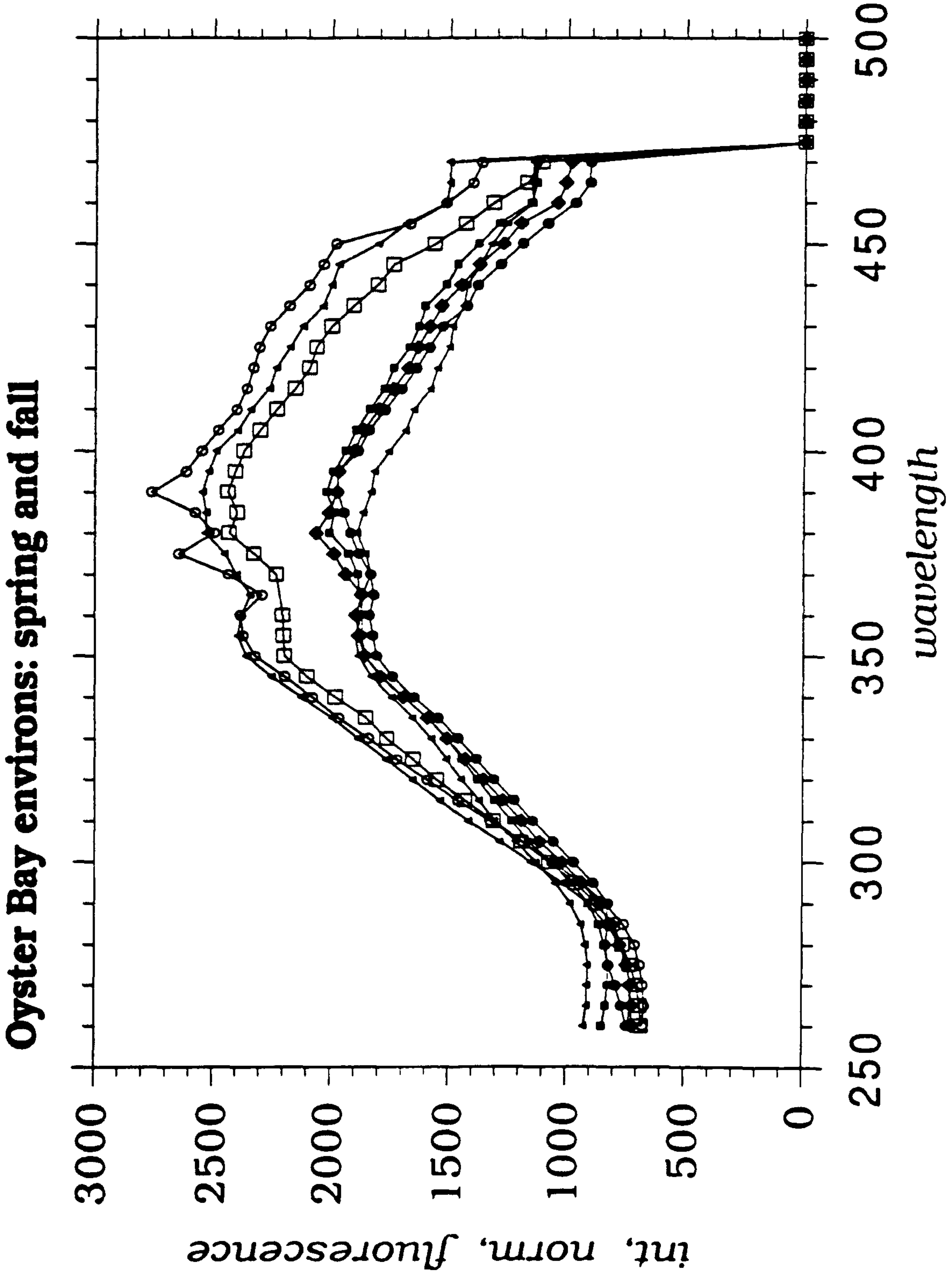
Oyster Bay environs: spring and fall
int, norm, fluorescence
0
500
1000
1500
2000
2500
3000
wavelength
250
300
350
400
450
500

fig. 16 Integrated, normalized spectra of various water and extracted COM samples. Sargasso Sea, 1500 m (□), SRFA (○), I-60 (△), Oyster Bay (I-14) (●), Tamiami River (▲), Orinoco estuary (sta 11) (I), Amazon River, 0‰ salinity (x).

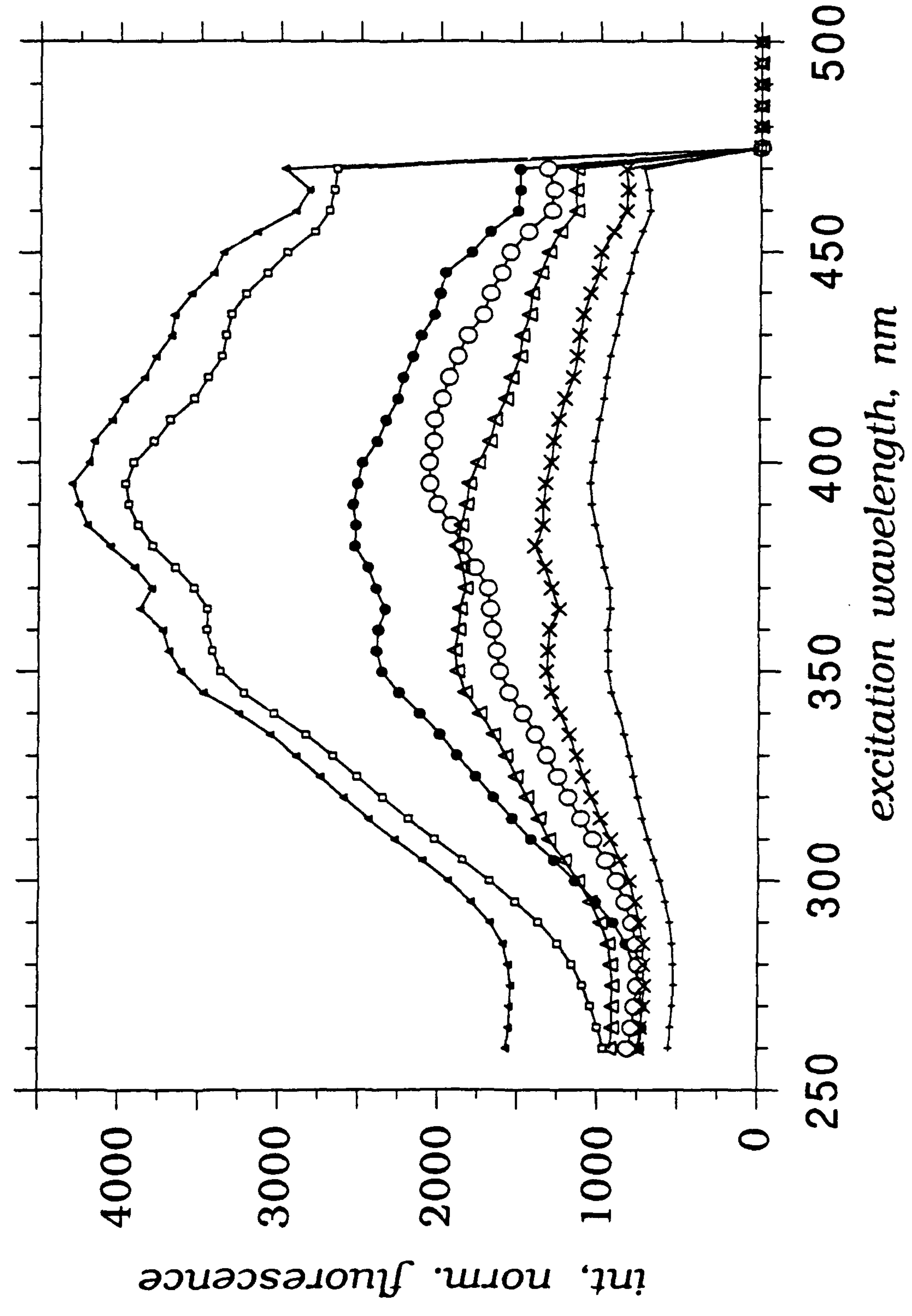
int. norm. fluorescence
0
1000
2000
3000
4000
excitation wavelength, nm
250
300
350
400
450
500

collected to permit any pattern to emerge. Several points on these plots stand out as having notably low or high *F/a(ex)* ratios. SRHA and the Amazon and Orinoco River samples are all below average, while three of the Sargasso Sea isolates lie somewhat above the norm. The Tamiami River exhibited a notably high fluorescence yield.

The samples with the lowest yields, the Amazon and Orinoco River waters, both drain large, seasonally flooded low-lying areas. These waters may carry a high load of humic-acid like DOM with low fluorescence efficiency. This is consistent with the very low quantum yields, in the range of 0.05 to 0.4%, that have been measured for soil fulvic acids and a series of terrestrial river and bog waters (25). SRHA (quantum yield=0.4%, at 355 nm) is probably closely related to these materials.

This generalization fails to account for the relatively high yields measured for Oyster Bay water, and the especially large value obtained for the Tamiami River (1.9% at 355 *nm*). Zepp and Schlotzhauer (25) also remarked that Everglades water had a high fluorescence yield of 1.2%, comparable to those I measured in Oyster Bay and nearby coastal waters. Perhaps specific vegetation or soil characteristics contribute to these differences.

The quantum yield (1.1% at 355 nm) measured for Oyster Bay water in August, while higher than the SRHA value, was 40% lower than the yield for Tamiami River water. The yield (1.5%) measured in Oyster Bay in May was 20% lower than the river water value, indicating that seasonal factors can be significant. Without additional data from waters in the intermediate salinity range (<19‰) it is not possible to determine whether terrestrial material is transformed as it travels to the Bay, or whether fluorescent material is lost during mixing with salt water. It is unlikely that ionic strength, natural quenchers, or pH changes could effect a 40% loss in quantum yield.

Quantum yields for deep sea COM have not, to my knowledge, previously been measured. So, inferences made on the basis of just four Sargasso Sea samples are purely speculative. The samples from 50, 1500, and 3200 m all exhibited quantum yields (2.1 at 355 nm) that were significantly larger than the yields of most surface samples. This observation could be accounted for by photobleaching of chromophores that reside in the surface mixed layer. Since fluorescence loss is more rapid than absorbance loss in humic materials, the effective fluorescence yield of COM brought to the surface would tend to decrease over time.

It is interesting to note that the 850 m sample from the Sargasso Sea showed a lower quantum yield than the others, particularly in light of the fact that "dissolved fluorescence" often shows a *maximum* in the oxygen minimum zone. This maximum has been attributed to *in situ* production of fluorescent material by bacteria (*16*), or to the release of organic matter from settling particles (*15*). If fluorescence and absorbance increase simultaneously, but not proportionally, then a zone of maximum fluorescence intensity could correspond with a minimum in quantum yield. Measurement of both parameters at the same location is required before any reasonable conclusions can be drawn.

Conclusions

Matrix spectra contain complete fluorescence information. However, they are somewhat unwieldy for comparison of fluorescence properties of multiple samples; a more detailed study of selected spectral regions may prove useful. Although 3D spectra do not exhibit large differences among samples, normalized, integrated plots reveal substantial variations in fluorescence quantum yield with excitation wavelength. Matrix plots may be most useful for identification of those spectral regions that allow maximum differentiation among samples, either in peak position, intensity, or quantum yield. In addition, they provide information on the wavelength distribution of fluorescence quantum yields that is required for the development of photon budgets for the surface oceans (*26*).

Fluorescence quantum yields with 337 or 355 nm excitation varied by no more than a factor of three for all samples examined. The overall average quantum yield was equal to 1.1±0.2%. This result is encouraging to researchers who would like to use laser or solar induced fluorescence to determine concentrations of COM. It indicates that measurement of fluorescence can provide a rapid and accurate means of estimating COM concentrations, light penetration depths, and thereby, light availability to photosynthetic organisms. Fluorescence may be the most sensitive means for measurement of local variations in COM absorption, which is required for interpretation of satellite data.

More detailed study of the relatively minor differences in fluorescence quantum yields among samples may provide clues about localized or seasonal changes in COM input to an area. Further study could also reveal the effects of biological degradation or sunlight exposure time on natural chromophores. To better understand these effects more data are required. In particular, it would be helpful to measure quantum yields of possible source materials (e.g. leaf litter, phytoplankton decay products, peat extracts) and to examine how they change under environmental conditions. For blue-water (open ocean) work, more precise determinations of absorption coefficients are required in order to accurately calculate quantum yields for very weakly absorbing waters, without employing time-consuming concentration procedures which may themselves bias optical measurements.

References

(1) Willey, J.D. and L.P. Atkinson (1982). Natural fluorescence as a tracer for distinguishing between Piedmont and Coastal Plain River water in the nearshore waters of Georgia and North Carolina. *Estuar. Coast. Shelf. Sci.*, **14**: 49-59.

(2) Ferrari, G.M. and S. Tassan (1991). On the accuracy of determining light absorption by "yellow subatance" through measurements of induced fluorescence. *Limnol. Oceanogr.*, **36**: 777-786.

(3) Bristow, M., D. Nielsen, D. Bundy and R. Furtek (1981). Use of water Raman emission to correct airborne laser fluorosensor data for effects of water optical attenuation. *Appl. Optics*, **20**: 2889-2906.

(4) MacCarthy, P. and J.A. Rice (1985). Spectroscopic methods (other than NMR) for determining functionality in humic substances. In *Humic substances in soil, sediment, and water*; Aiken, G.R., D.M. McKnight, R.L. Wershaw and P. MacCarthy, ed.; John Wiley & Sons: New York; pp. 527-559.

(5) Zepp, R.G., P.F. Schlotzhauer and R.M. Sink (1985). Photosensitized transformations involving electronic energy transfer in natural waters: role of humic substances. *Environ. Sci. Technol.*, **19**: 74-81.

(6) Cabaniss, S.E. and M.S. Shuman (1987). Synchronous fluorescence spectra of natural waters: tracing sources of dissolved organic matter. *Mar. Chem.*, **21**: 37-50.

(7) Willey, J.D. (1984). The effect of seawater magnesium on natural fluorescence during estuarine mixing, and implications for tracer applications. *Mar. Chem.*, **15**: 19-45.

(8) Coble, P.G., S.A. Green, N.V. Blough and R.B. Gagosian (1990). Charaterization of dissolved organic matter in the Black Sea by fluorescence spectroscopy. *Nature*, **348**: 432-435.

(9) Carder, K.L., R.G. Steward, G.R. Harvey and P.B. Ortner (1989). Marine humic and

fulvic acids: their effects on remote sensing of ocean chlorophyll. *Limnol. Oceanogr.*, **34**: 68-81.

(10) Laane, R.W.P.M. and L. Koole (1982). The relation between fluorescence and dissolved organic carbon in the Ems-Dollart estuary and the Western Wadden Sea. *Neth. J. Sea Res.*, **15**: 217-227.

(11) Laane, R.W.P.M. (1981). Composition and distribution of dissolved fluorescence substances in the EMS-Dollart estuary. *Neth. J. Sea Res.*, **15**: 88-99.

(12) Laane, R.W.P.M. and K.J.M. Kramer (1990). Natural fluorescence in the North Sea and its major estuaries. *Neth. J. Sea Res.*, **26**: 1-9.

(13) Laane, R.W.P.M. (1982). Sources of dissolved organic carbon in the Ems-Dollart estuary: the rivers and phytoplankton. *Neth. J. Sea Res.*, **15**: 331-339.

(14) Hayase, K., Yamamoto, M., Tsubota, H. (1987). Behavior of natural fluorescence in Sagami Bay and Tokyo Bay, Japan - vertical and lateral distributions. *Mar. Chem.*, **20**: 265-276.

(15) Hayase, K., Tsubota, H., Sunada, I. (1988). Vertical distribution of fluorescent organic matter in the North Pacific. *Mar. Chem.*, **25**: 373-381.

(16) Coble, P.G. PhD. thesis, (1990) Marine bacteria as a source of dissolved fluorescence in the ocean. MIT/WHOI Joint Program in Oceanography.

(17) Chen, R.F. and J.L. Bada (1989). Seawater and porewater fluorescence in the Santa Barbara Basin. *Geophys. Res. Lett.*, **16**: 687-690.

(18) Stewart, A.J. and R.G. Wetzel (1980). Fluorescence:absorbance ratios - a molecular-weight tracer of dissolved organic matter. *Limnol. Oceanogr.*, **25**: 559-564.

(19) Hayase, K. and H. Tsubota (1985). Sedimentary humic acid and fulvic acid as fluorescent organic materials. *Geochem. Cosmochem. Acta.*, **49**: 159-163.

(20) Green, S.A., F.M.M. Morel and N.V. Blough (1992). Investigation of the electrostatic properties of humic substances by fluorescence quenching. *Environ. Sci. Technol.*, **26**: 294-302.

(21) Blough, N.V., O.C. Zafiriou and J. Bonilla (1992). Optical absorption spectra of waters from the Orinoco River outflow: terrestrial input of colored organic matter to the Caribbean. *J. Geophys. Res.*, : in press.

(22) Morel, F.M.M. (1989). Personal Communication.

(23) Mopper, K. and Y.C. Park (1991). Origins of marine dissolved organic matter as revealed by fluorescence and amino acid racemization. *Deep Sea Res.*, **in press**: .

(24) Shoemaker, D.P., C.W. Garland, J.I. Steinfeld and J.W. Nibler (1981). *Experiments in physical chemistry*, 4th ; McGraw-Hill, Inc.: New York; pp 46-52.

(25) Zepp, R.G. and P.F. Schlotzhauer (1981). Comparison of photochemical behavior of various humic substances in water: III. Spectroscopic properties of humic substances. *Chemosphere*, **10**: 479-486.

(26) Smith, R.C., J. Marra, M.J. Perry, K.S. Baker, E. Swift, E. Buskey and D.A. Kiefer (1989). Estimation of a photon budget for the upper ocean in the Sargasso Sea. *Limnol. Oceanogr.*, **34**: 1673-1693.

Chapter Five: COM isolates.

Introduction

Concentrations of organic material in seawater are very low (≈50-150 µM-C/ℓ) and difficult to study at *in situ* levels. Much work, therefore, relies on the use of isolates of this material which can be studied in the laboratory at concentrations much higher than are encountered in nature.

In determining the optical properties of ocean and coastal waters, it is important to assess how the use of such isolates as a proxy for the whole water can bias results. I have therefore examined the absorbance and fluorescence spectra of water before and after DOM has been removed by extraction onto C-18 columns, as well as the spectra of samples reconstituted by dissolution of extracted DOM into oligotrophic seawater.

The goal of procedures for extraction of dissolved organic carbon from natural waters is to provide a concentrated sample, representative of the DOM originally present in the body of water. Ideally, this concentrate, when redissolved into organic-free water, would precisely reconstruct the organic carbon content of the original solution. Because DOM refers to the complex mixture of organic components found in the environment, extraction efficiency must be judged not only by the total *quantity* of material removed, but also by how well the *qualities* of the mixture are preserved during the isolation procedure, i.e. the relative extraction efficiencies of each of the many components. Numerous methods have been employed for the isolation of DOM from natural waters. These include freeze drying, vacuum distillation, coprecipitation with Ca^{+2}, Fe^{+3}, or Mg^{+2}, reverse osmosis, and an assortment of chromatographic methods (*1*). In general, the merits of a particular isolation method have been judged on the fraction of DOM removed from the water (although methods for measurement of DOM itself are still disputed), or by removal of absorbance or fluorescence at a given wavelength. The qualitative aspects of DOM isolation have rarely been examined. However, if the concentration procedure is selective for one or more specific fractions of the DOM present, then, even if the total quantity of material extracted is large, the reconstituted extracts may not be a very good match to the original water.

Several techniques commonly applied to highly colored freshwaters are not suitable for extraction of organic components from seawater. The two primary difficulties posed by seawater are its huge concentration of inorganic salts and its very low concentration of the organic substances of interest. These preclude methods based on the removal of water from the sample (e.g. freeze drying, vacuum evaporation) due to large volumes of water required and the co-isolation of NaCl with DOM. Solute concentration techniques requiring long processing times (e.g. dialysis) are also impractical, especially if samples are to be isolated on shipboard. The currently accepted technique for extraction of DOM from seawater is adsorption onto hydrophobic sorbants such as styrene-divinylbenzene resins (XAD-2) (2) or reverse-phase C-18 columns (Seppak, Mega-Bond Elutes) (3).

Methods

Organic material was concentrated from seawater by extraction onto solid phase C-18 columns following the procedures of Amador, et al. (3). Water was drawn from a 20 l glass carboy, through a large volume 0.2 μm Gelman filter, acidified to pH 2.3-2.5, and passed through a set of three Mega-Bond Elute (Analytichem International) columns, aligned in parallel. Volumes extracted ranged from 20 to 270 liters of seawater, depending on the organic content of the water. Salts were washed from the columns with ≈50 ml of Milli-Q water, and samples were eluted with 30-90 ml of HPLC grade methanol (Aldrich). The methanol eluates were stored in glass bottles with Teflon inner covers and were refrigerated at 4° C immediately after collection. They were transported to Woods Hole, where methanol was removed by roto-evaporation at 25°, and the organic isolates were redissolved in ≈6 ml of 50 mM borate buffer. They were filtered through washed, pre-combusted glass fiber filters (Gelman) and 0.2 µm nylon filters (Nalgene) to remove an insoluble, white residue. This was presumed to be column packing leached from the cartridges; it is produced during blank extraction of Q-water, as well as seawater, samples. The reconstituted isolates were stored at 4° C.

Results and Discussion

The assessment of extraction efficiency is dependent upon the definition of this term. Amador, et al. compared the extraction efficiencies of several columns, and an ultrafiltration technique employing filters of different nominal molecular weight cutoff. In their study, extraction efficiency was defined by the fractional loss of absorbance at 280 nm (a_{280}), fluorescence (broad band, excitation centered at 360 nm with emission centered at 490 nm), and H_2O_2 photoproduction capacity. Judging by these criteria, C-18 columns were determined to be more efficient than XAD resins, and comparable to ultrafiltration (molecular weight cut-off: 500). On extraction of five diverse seawater and estuarine samples, 23-81% of absorbance at 280 nm was retained on C-18 columns. On redissolution of isolates into the same water from which they had been removed, 90-100% of absorbance was restored, suggesting that little was irreversibly sorbed to the columns.

By the same criterion, my extractions of Oyster Bay and Gulf of Mexico water were slightly less efficient. *a(280)* values for four isolates and the percent absorbance retained for each are tabulated below (table I). Extracts 6 and 7 are both from Oyster Bay, but 6 was isolated without acidification; 7 was treated in the standard manner (pH=2.3).

Table I. Extraction efficiencies measured by *a(280)*.

	a(280)		
extract #	pre-column	post-column	fraction retained
1	1.29	0.86	0.33
5	3.56	2.66	0.25
6	58.01	49.62	0.14
7	51.93	30.34	0.42

I have conducted a more detailed study of extraction efficiencies for several samples collected in South Florida in May 1991. In particular, I have examined the full uv-visible absorption spectra (290-600 nm) of water before and after passage through C-18 columns, and of reconstituted extracts. In addition, absorption and 3D matrix spectra of extracted COM reconstituted into seawater were compared with spectra of unconcentrated waters.

Selective retention of absorbing material can alter the observed spectra, and there are several opportunities for fractionation to occur during the isolation procedure. Some light absorbing material always passes through these columns without sticking, some seems to remain on the column after elution of the sample, and some may be lost during drying, filtering, and reconstituting isolates. At each stage components with particular physio-chemical properties may be selected for or against. Comparison of spectra of unconcentrated water samples with those of isolated material reconstituted into oligotrophic seawater indicates that, with respect to optical properties, some fractionation is occuring during the isolation procedure. Fractionation is particularly significant for COM isolations from oligotrophic seawater.

The first point at which fractionation may occur is during passage through the columns. I have examined this possibility by comparing absorbance spectra of water before and after the DOM extraction. Pre-column samples were collected after filtration and acidification, directly from the extraction line. It is important that samples are compared at the same pH level because the absorption coefficient decreases slightly on acidification, as has been noted by Amador, et al (3) . Pre- and post-column spectra are shown in figures 1, 2and 3, for extracts I-1, I-2, I-5, II-50, I-6, and I-7. These spectra demonstrate that removal of absorbing material is not uniform across the uv-visible spectral region. Specifically, *S* values for post-column samples, except for 5, are higher than pre-column samples. Sample 5 does not exhibit a significant change in *S*, however curvature is somewhat increased in its post-column spectrum.

Sample 2 shows a pronounced absorbance 300 nm; this component does not appear in either the post-column sample or the reconstituted extract. Because it is the sole sample exhibiting this feature, I am unable to determine whether it is an artifact in the initial spectrum (perhaps due to a poor reference) or whether it represents a unique absorbing component which either adsorbed irreversibly to the column, or was destroyed during the elution and isolation procedure.

fig. 1 Log-linearized absorption spectra of acidified seawater before and after passage through a C-18 Mega-Bond Elute column. Samples 1 (above) and 2 (below). Linear fits and S values are also shown.

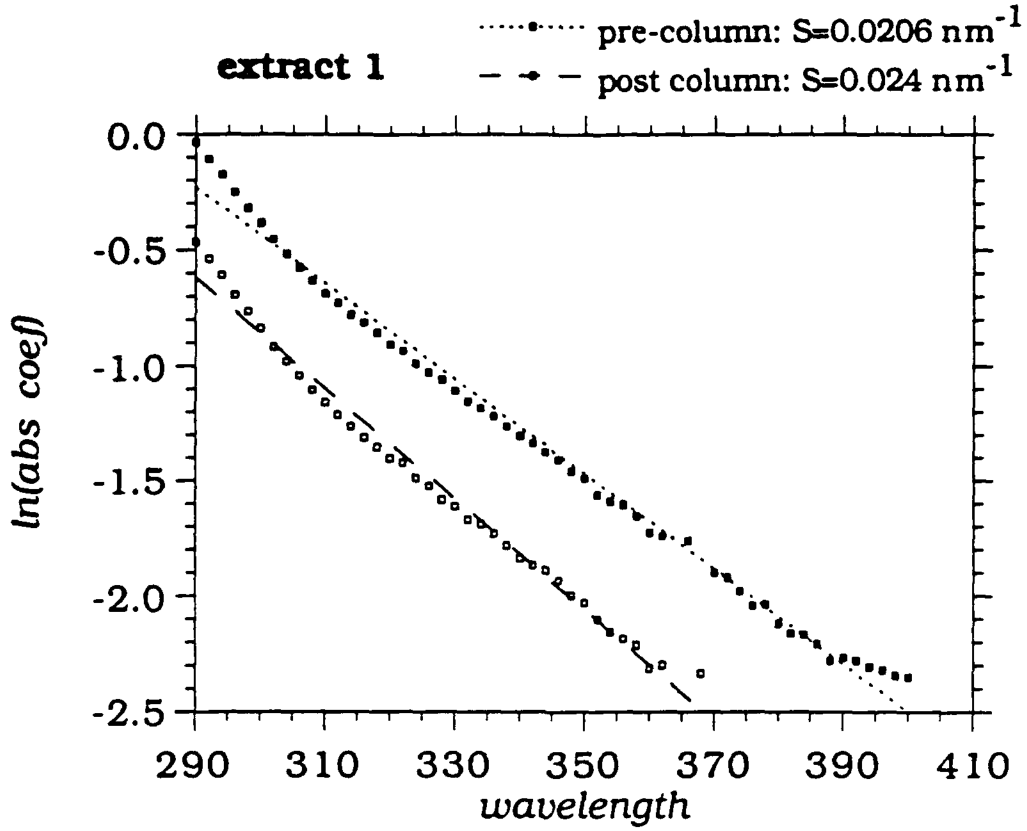
extract 1
pre-column: S=0.0206 nm^{-1}
post column: S=0.024 nm^{-1}
0.0
-0.5
-1.0
-1.5
-2.0
-2.5
ln(abs coef)
290
310
330
350
370
390
410
wavelength

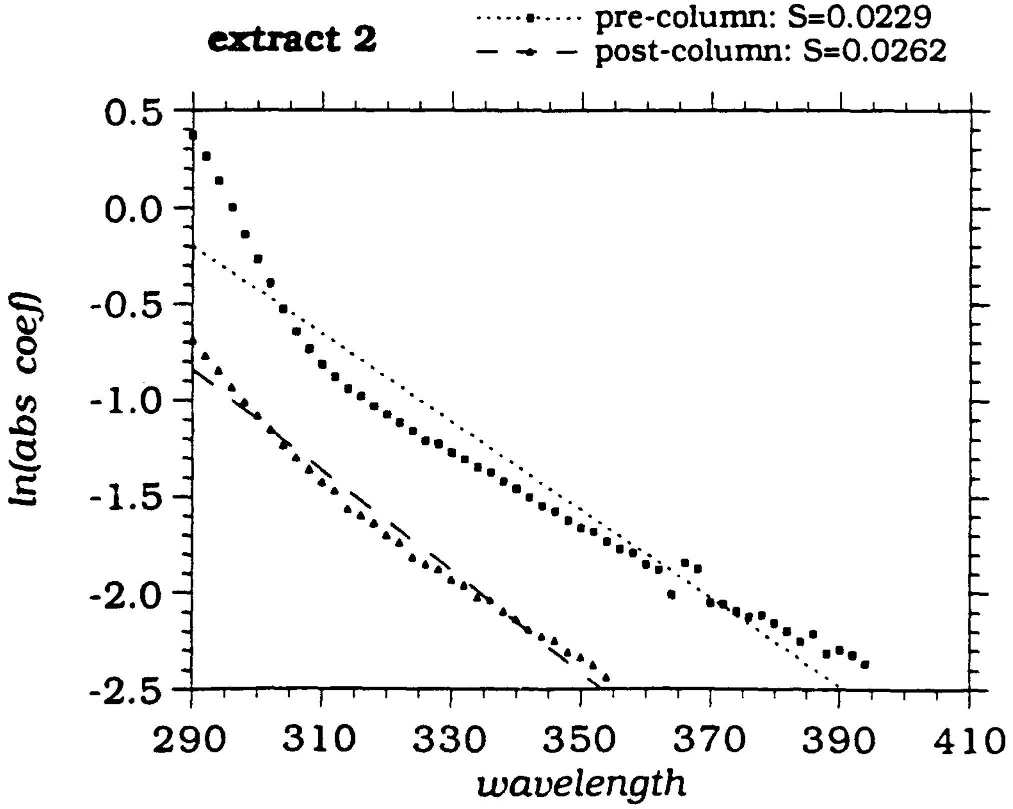
extract 2
pre-column: S=0.0229
post-column: S=0.0262
0.5
0.0
-0.5
-1.0
-1.5
-2.0
-2.5
ln(abs coef)
290
310
330
350
370
390
410
wavelength

fig. 2 Log-linearized absorption spectra of acidified seawater before and after passage through a C-18 Mega-Bond Elute column. Samples 5 (above) and II-50 (below). Linear fits and S values are also shown.

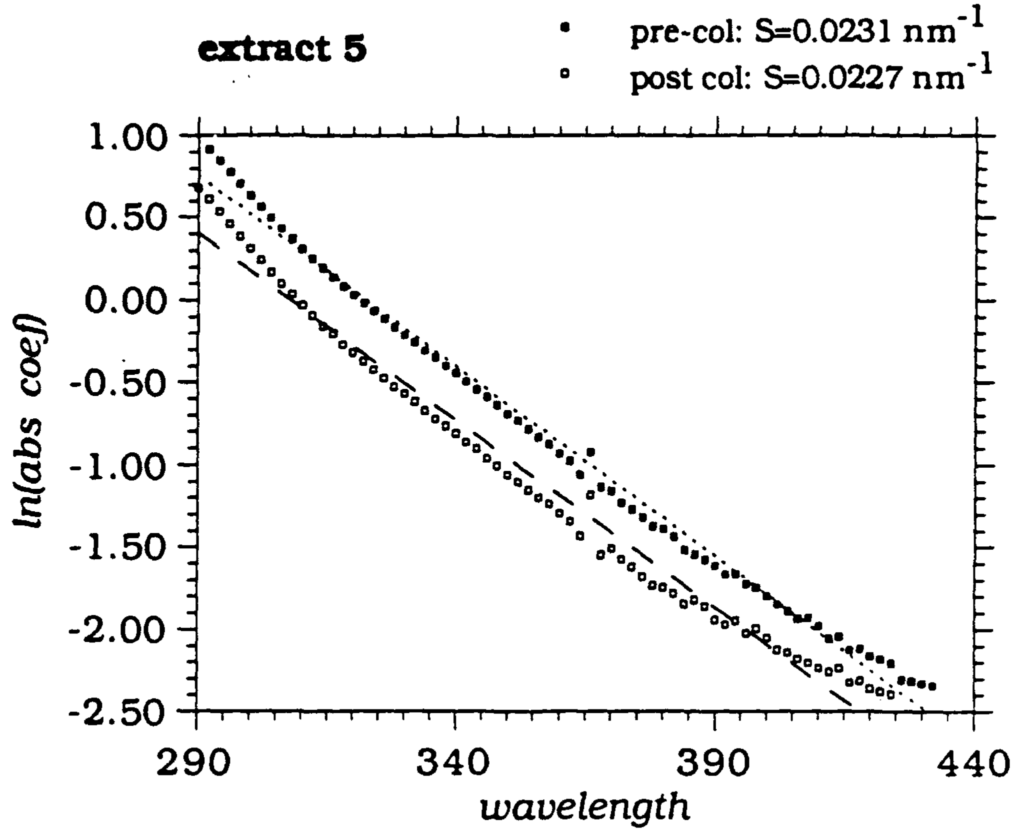
extract 5
● pre-col: S=0.0231 nm^{-1}
○ post col: S=0.0227 nm^{-1}
1.00
0.50
0.00
-0.50
-1.00
-1.50
-2.00
-2.50
ln(abs coef)
290
340
390
440
wavelength

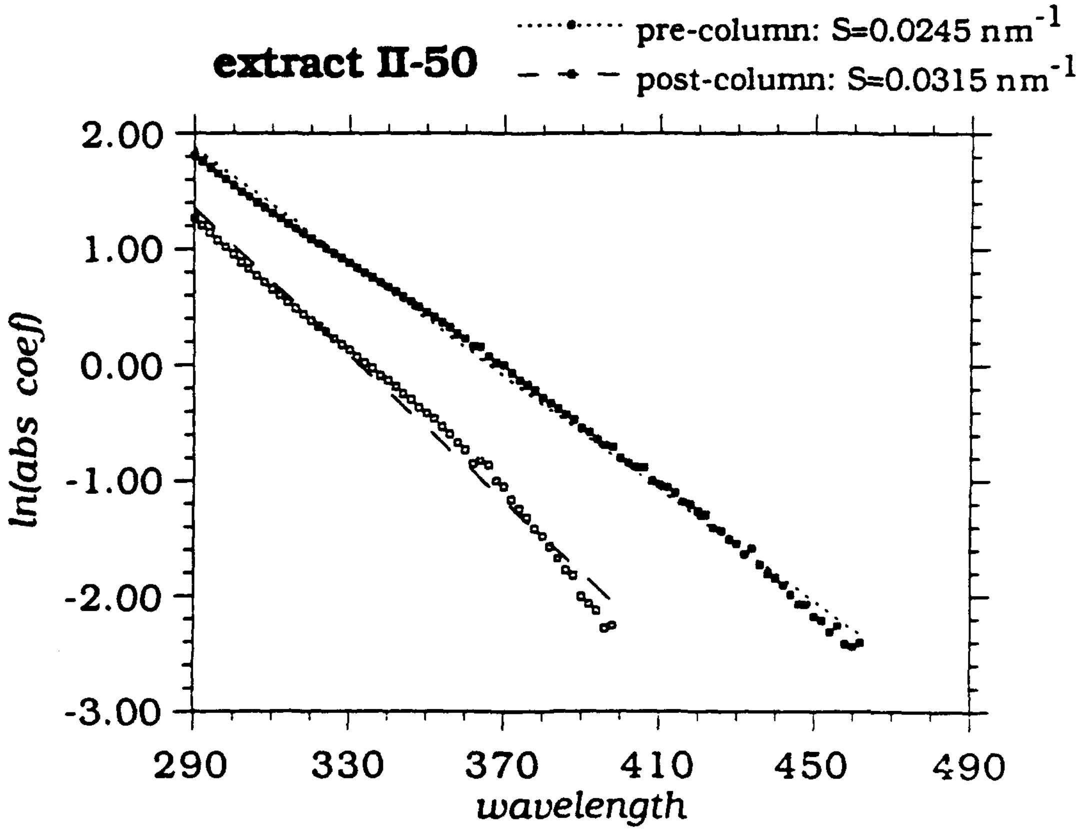
extract II-50
pre-column: S=0.0245 nm^{-1}
post-column: S=0.0315 nm^{-1}
2.00
1.00
0.00
-1.00
-2.00
-3.00
ln(abs coef)
290
330
370
410
450
490
wavelength

fig. 3 Log-linearized absorption spectra of acidified seawater before and after passage through a C-18 Mega-Bond Elute column. Samples 6 and 7 shown together Linear fits and S values are also shown.

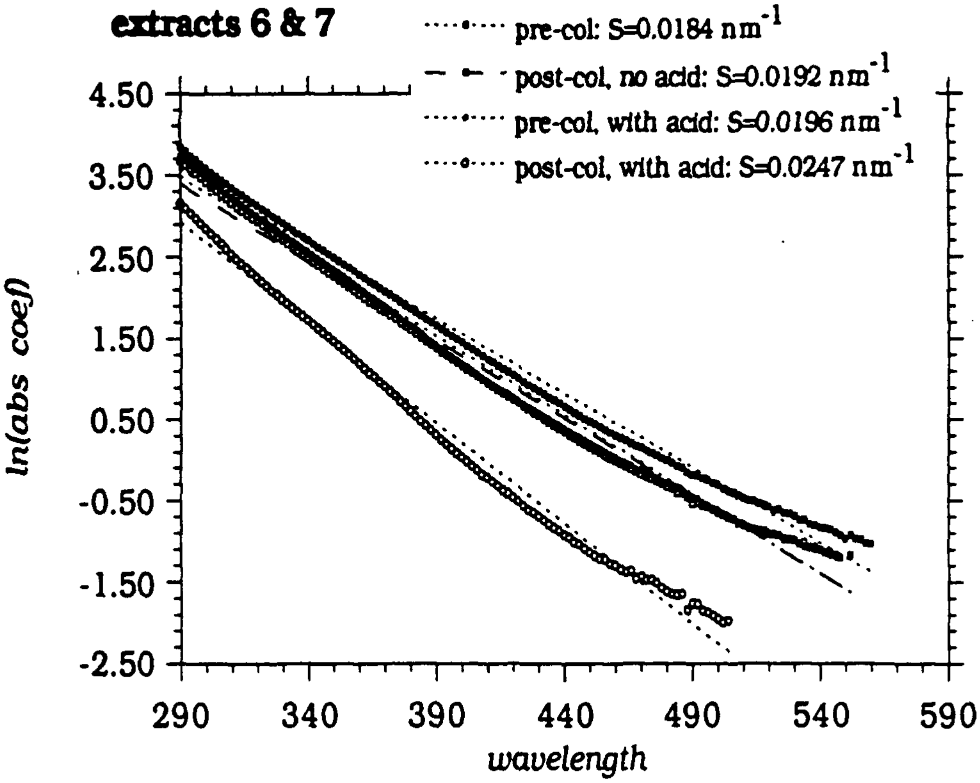
extracts 6 & 7
pre-col: S=0.0184 nm-1
post-col, no acid: S=0.0192 nm-1
pre-col, with acid: S=0.0196 nm-1
post-col, with acid: S=0.0247 nm-1
4.50
3.50
2.50
1.50
0.50
-0.50
-1.50
-2.50
ln(abs coef)
290
340
390
440
490
540
590
wavelength

fig. 4 Fraction of original absorbance retained (R(λ)) as a function of wavelength. Samples 1, 2, 5, and II-50.

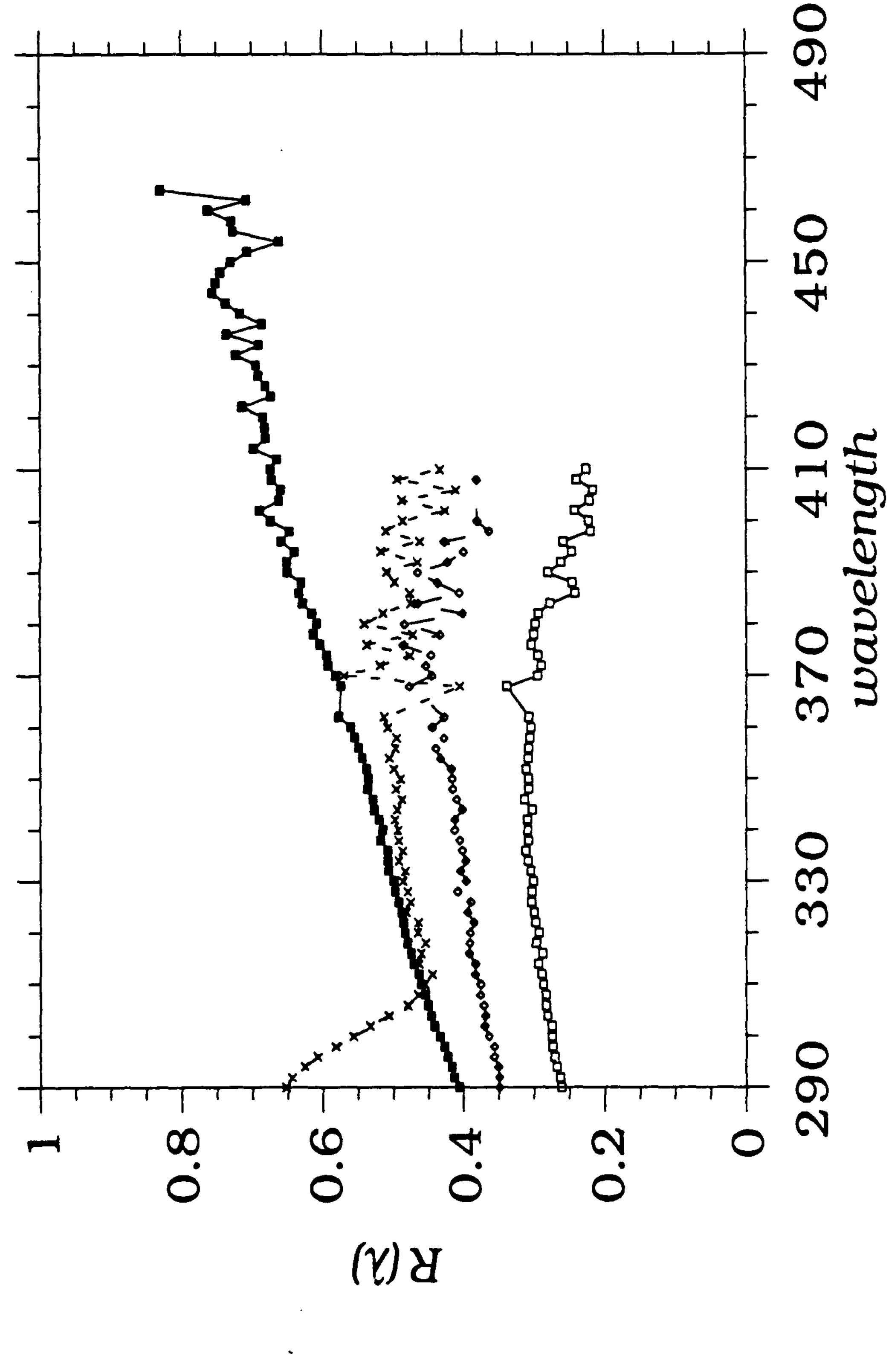
R(λ)
1
0.8
0.6
0.4
0.2
0
290
330
370
410
450
490
wavelength

fig. 5 Fraction of original absorbance retained (R(λ)) as a function of wavelength.

Samples 6 and 7.

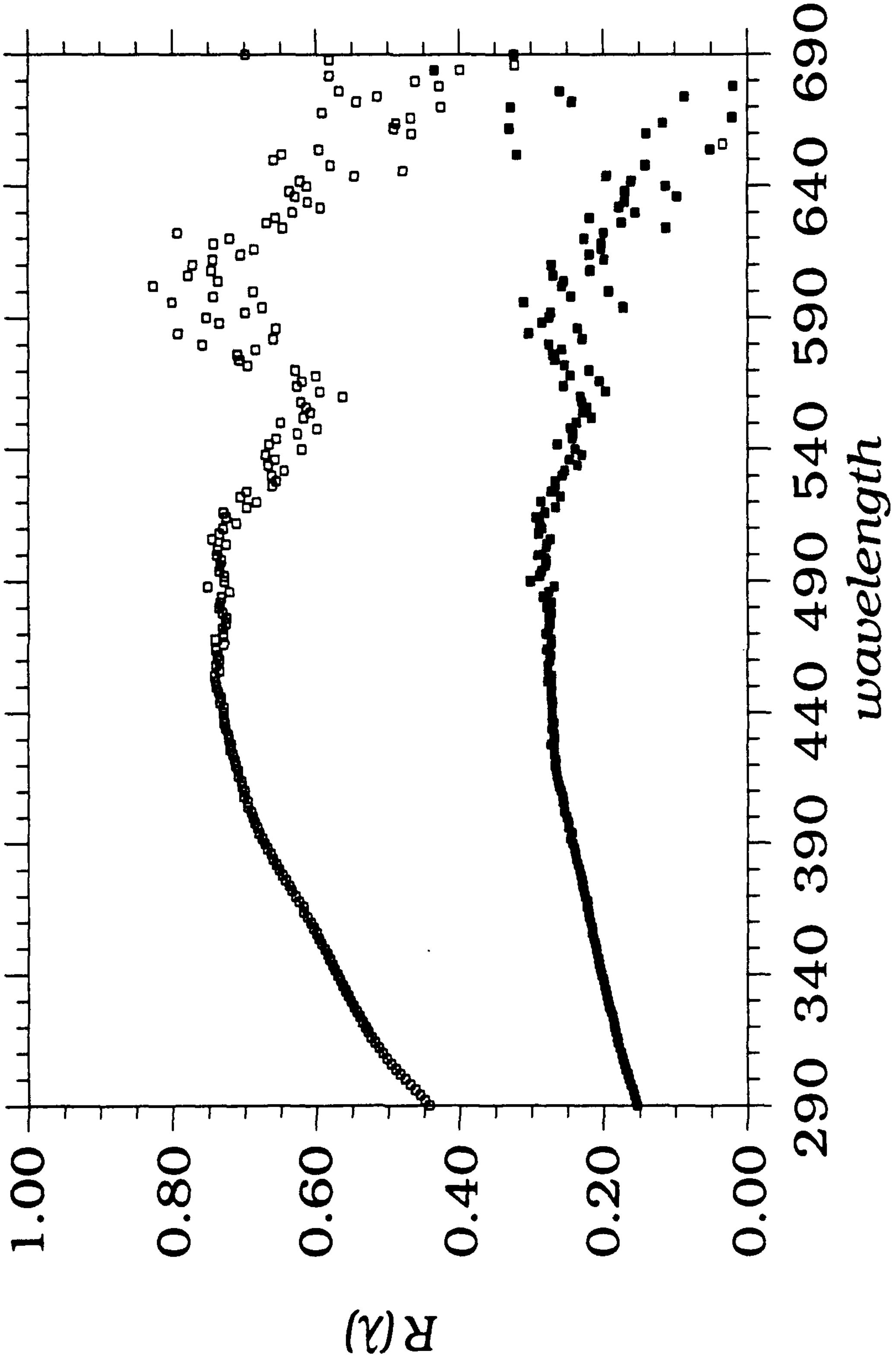
R(λ)
1.00
0.80
0.60
0.40
0.20
0.00
290
340
390
440
490
540
590
640
690
wavelength

The fraction of absorbers retained on the C-18 columns across the spectral range of interest may be calculated by:

$$R(\lambda) = \frac{T(\lambda) - P(\lambda)}{T(\lambda)}$$

where $R(\lambda)$ is the fraction retained, $T(\lambda)$ is the initial (pre-column) total absorbance, and $P(\lambda)$ is the post-column absorbance, at wavelength λ. Plots of $R(\lambda)$ vs λ are shown in figures 4 and 5. It can be seen that the overall extraction efficiencies are lower for blue-waters, 20-50% (samples 1, 2, and 5) than for brown waters (sample 7). In all cases, $R(\lambda)$ is increased for the red-absorbing fraction of COM. Sample 6 was extracted from Oyster Bay water (salinity 32‰) without being acidified. A comparison of 6 and 7 (same water, pH=2.3) indicates that acidification enhances COM removal at all absorption wavelengths, but that the effect is stronger for red-absorbers. Both of these highly absorbing samples show structure in the plots of $R(\lambda)$ vs λ. A component absorbing at 590 nm is removed with high efficiency, while there is a dip in efficiency for absorbers at 560 nm.

For one sample, II-50, acidified pre- and post-column water was saved and returned to the laboratory for fluorescence measurements. Matrix spectra were collected on both samples and integrated to determine which range of fluorophores was most efficiently retained by the C-18 columns. Figure 6 shows these integrated spectra as well as a plot of $R_f(\lambda)$, the fraction of fluorescence retained at each excitation wavelength. This is calculated analogously to $R(\lambda)$ for absorbance. $R_f(\lambda)$ exhibits a similar trend to $R(\lambda)$; by both measures extraction efficiencies increase for longer-wavelength absorbers. $R_f(\lambda)$ shows an additional dip in fraction extracted in the range of 300-350 nm.

Some possible reasons for differences in extraction efficiency among samples include poor pH stability and reduced efficiency due to overloaded columns. pH was monitored throughout the procedure; fluctuations were minor, generally within ±0.3 pH units. Amador, et al. (*3*) found that the fraction of COM retained (as measured by *a(280)*) on C-18 columns fell as the initial several hundred milliliters of water crossed them, but then it remained quite stable for the duration of the procedure. Pre- and post-column samples for the present study were drawn after several liters had passed through the Mega-Bond Elute cartridges, so this was probably not a factor here.

More fundamental reasons for selective extraction result from the physical properties of COM itself. Because C-18 columns select for the most hydrophobic material, the observation that they preferentially isolate absorbers towards the red edge of the spectrum suggests that these are also the most hydrophobic molecules. This is not inconsistent with some chemical generalizations: absorbance of long wavelength radiation tends to suggest the presence of extended conjugated systems or aromatic structures, and these also tend to be hydrophobic in nature.

fig. 6 Integrated fluorescence of acidified water (sample II-50) before and after passage through a C-18 column (above). Difference spectrum is also shown. Percent fluorescence retained for sample II-50 (below).

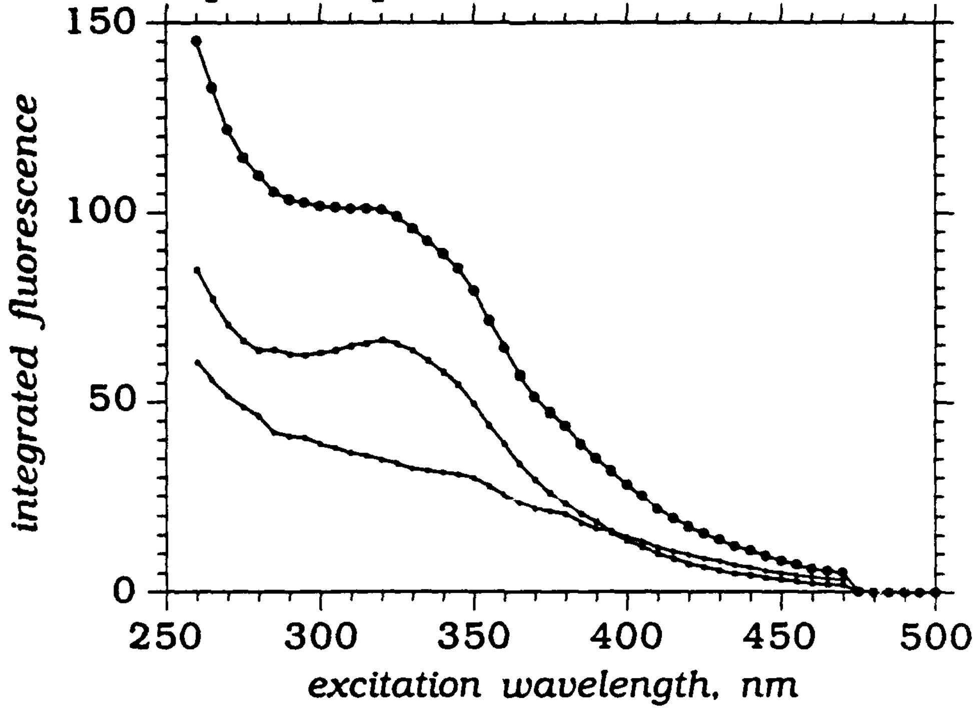
pre- and post column, and difference

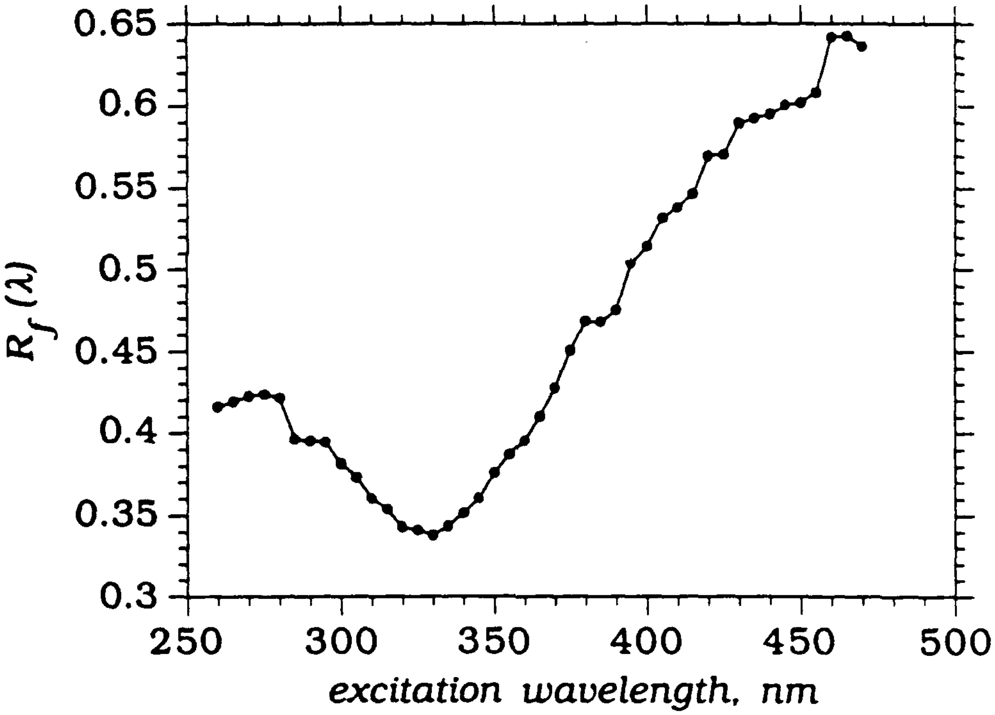
% fluorescence retained X II-50

Reconstituted isolates Extracted COM was redissolved in oligotrophic seawater (from the Sargasso Sea) in order to study its optical properties. Absorption spectra were taken against a seawater reference. Values of *S* are tabulated below for comparison with those measured at sea.

Table II. *S* values for extracts and unconcentrated seawater.

	S nm^{-1} x10^3	
extract#	water	extract
1	22	14
2	30	15
3	19	18
4	36	22
5	21	21
6	19	17
7	19	18
8	19	16
9	21	15
10	15	16
II-50	18	17
BWX	23	18

Slopes of the reconstituted samples are generally in reasonable agreement with those of the original water sampled, for waters with $S \leq 0.02$. For waters with $S \geq 0.02$, there was a significant discrepancy between the original and reconstituted samples. In cases where the two differ, the slope of the extract is invariably the smaller. This is consistent with evidence presented above suggesting that longer-wavelength absorbing material is isolated with the greatest efficiency.

Fluorescence As was noted in chapter four, the fluorescence quantum yields of isolates measured at 337 and 355 nm were generally slightly higher than those of the original waters. This indicates that fluorescent chromophores are extracted from seawater with somewhat greater efficiency than non-fluorescing COM.

Matrix spectra were measured on extracts reconstituted into seawater in order to better compare them with unconcentrated waters. In most cases, spectra of isolates were distinctly different from those of their parent waters. These differences were enhanced by normalization to absorption spectra. An example, extract I-4, is shown in figure 7. All extracts from this region exhibited a more or less distinct peak at 410/490 that was not apparent in the water samples. This feature was greatly enhanced, and slightly shifted to the red (430/500), by normalization (fig. 8). Integrated spectra of all extracts are shown in figure 9 along with that of the bottled sample II-50, for comparison. All clearly show enhanced intensity in the region of 400-450 nm. The prominence and consistent location of this peak suggest that it is a unique fluorophore with a relatively high quantum efficiency.

Because this feature was unique to the isolated COM, it was important to establish that it did not result from the isolation procedure itself. A series of control extractions were performed on purified (Milli-Q) laboratory water. First, 100 *l* of acidified Q-water was passed through a Mega-bond Elute column; this was then eluted and treated in an identical manner to field samples. To eliminate the possibility that the small material isolated in this experiment was due to contaminants in the Q-water rather than leachate from the C-18 column, a second sample of only 2 *l* of acidified Q-water was recirculated 50 times through a second column. This column was then replaced with a fresh one, and the same "pre-extracted" water was again passed through 50 times.

fig. 7 3D fluorescence spectrum of extract 4 reconstituted into oligotrophic seawater. Seawater fluorescence was very low and has been subtracted along with the Raman emission peaks.

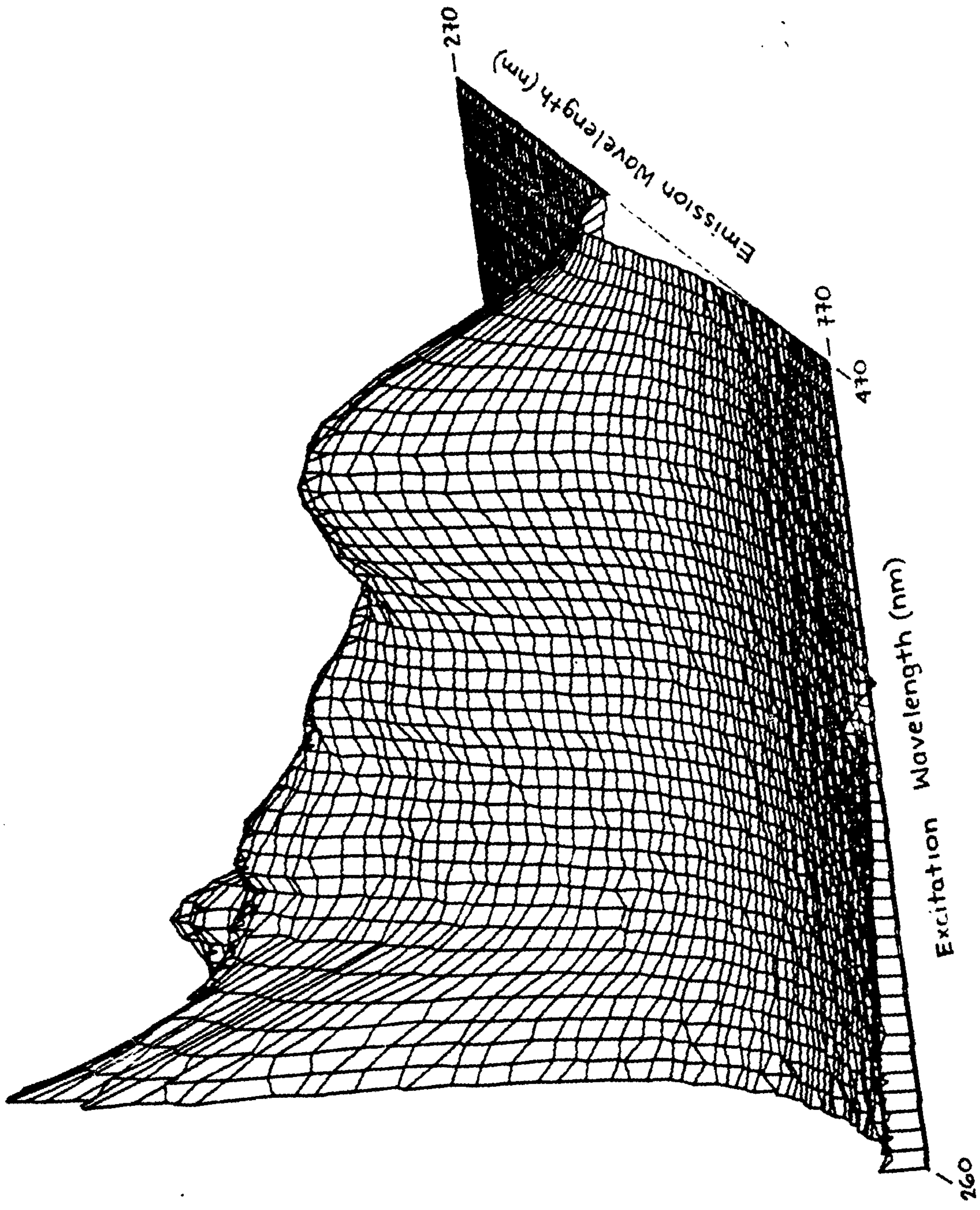
230
Emission Wavelength (nm)
770
470
Excitation Wavelength (nm)
260

fig. 8 Absorbance normalized 3D fluorescence spectrum of extract 4 reconstituted into oligotrophic seawater. Seawater fluorescence was very low and has been subtracted along with the Raman emission peaks.

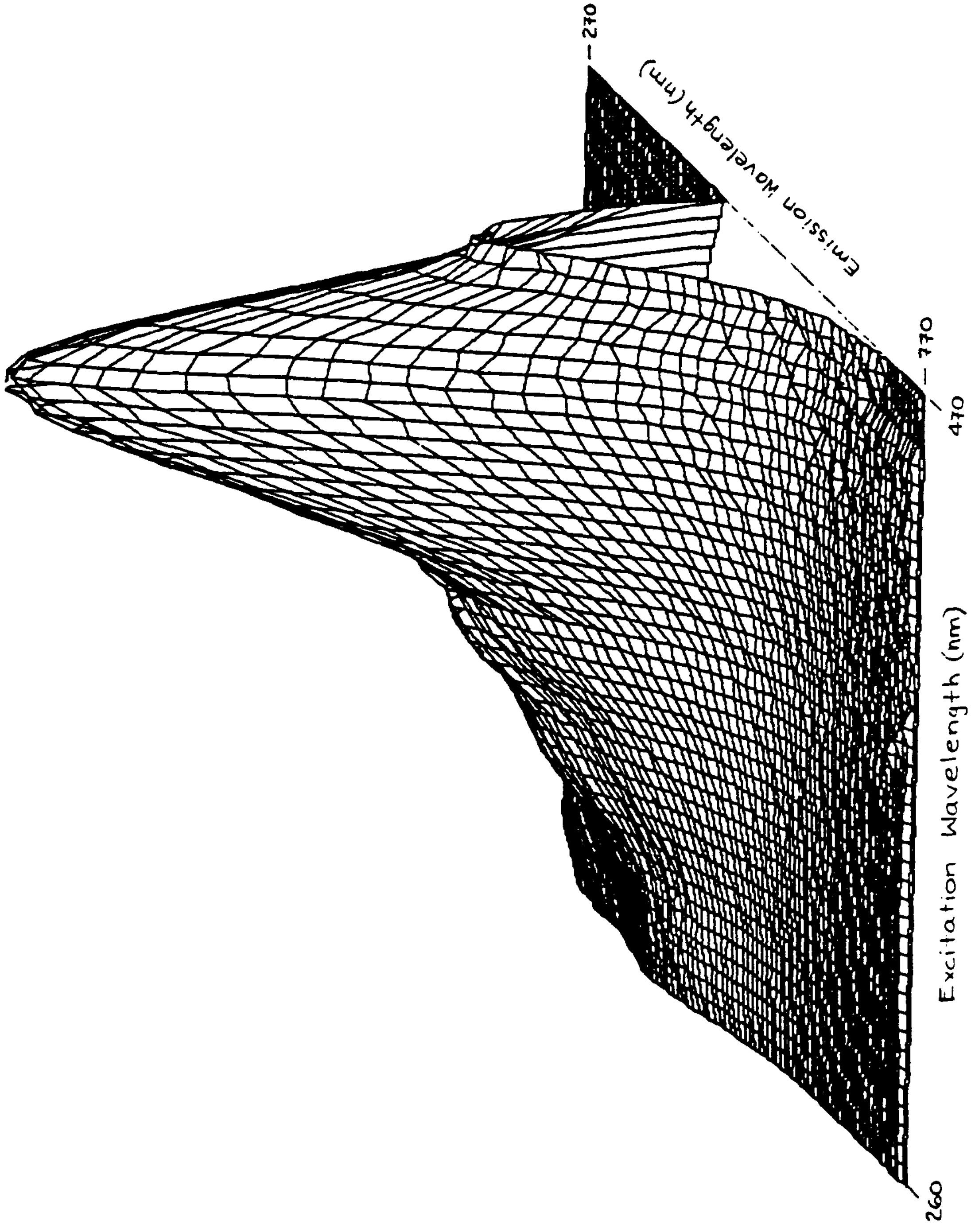
270
Emission Wavelength (nm)
770
470
Excitation Wavelength (nm)
260

fig. 9 (above) Integrated, normalized excitation spectra of riboflavin compared with spectrum of extract 4.

fig. 10 (below) Integrated, normalized emission spectra of riboflavin compared with spectrum of extract 4.

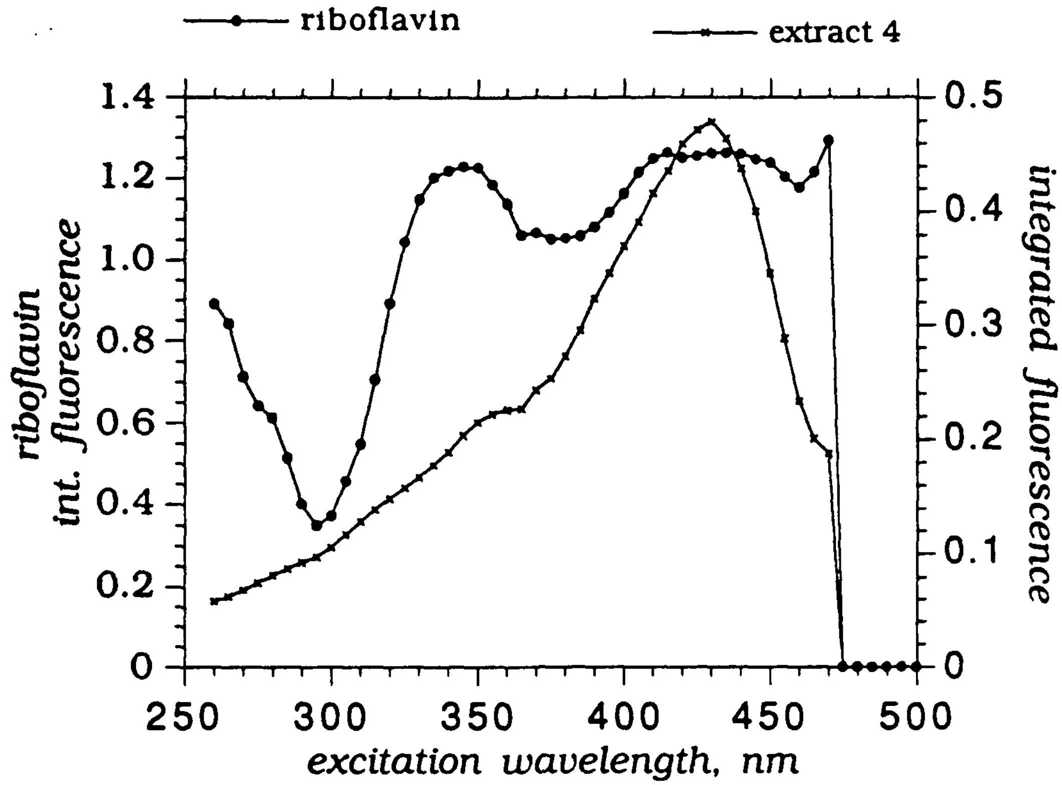
riboflavin
extract 4
riboflavin int. fluorescence
integrated fluorescence
excitation wavelength, nm
1.4
1.2
1.0
0.8
0.6
0.4
0.2
0
0.5
0.4
0.3
0.2
0.1
0
250
300
350
400
450
500

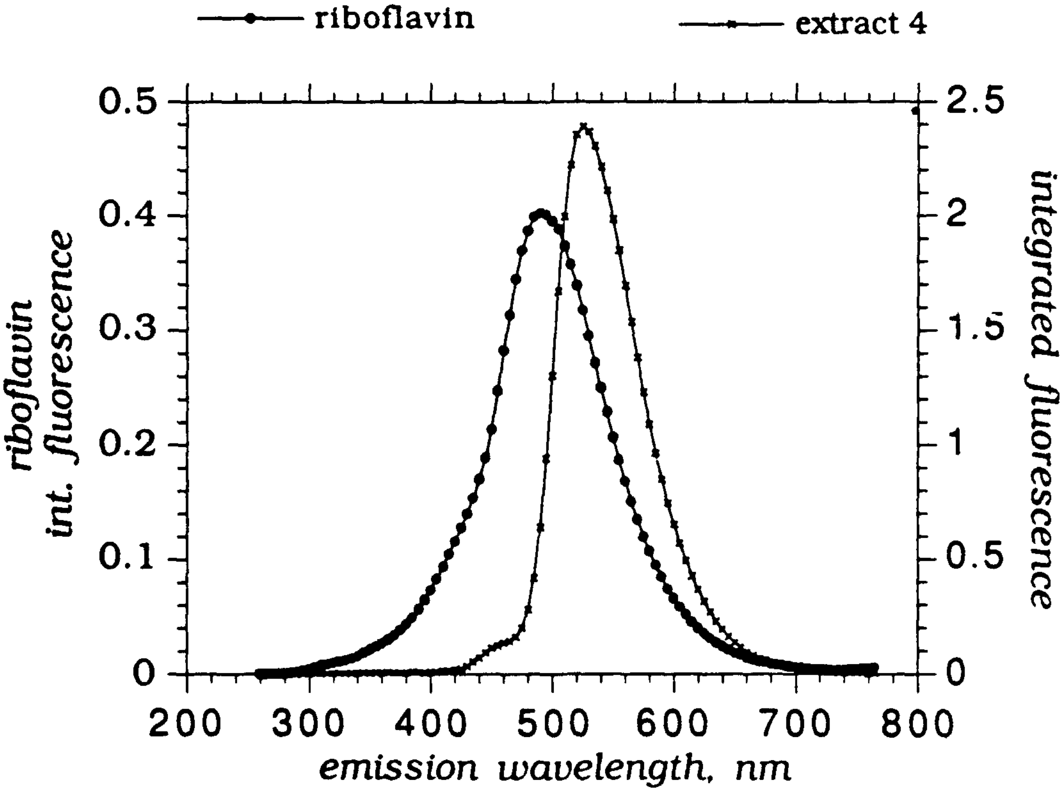
riboflavin
extract 4
riboflavin int. fluorescence
integrated fluorescence
emission wavelength, nm
0.5
0.4
0.3
0.2
0.1
0
2.5
2
1.5
1
0.5
0
200
300
400
500
600
700
800

Fluorescent material was recovered in each of these control experiments. However, in each case there was far too little to account for the signal observed in seawater extracts. The emission of these impurities was at wavelengths >500 nm, and its maximum contribution to the observed signals could not have been greater than about 1%.

Since it is not accounted for by the extraction procedure, the fluorescence peak at 430/500 must be due to a compound present in seawater. The most likely candidates to produce this signal are members of the flavin family. Riboflavin, and its photochemical decay products, lumiflavin and lumichrome, have all been detected in seawater, as have other related flavin compounds (4-6). The standard detection procedure for these compounds involves separation on a reverse phase HPLC column with fluorescence detection. So, it is not unexpected that they would be selectively sorbed to Mega-bond C-18 columns and show up as *higher fluorescent species in* reconstituted samples.

The integrated spectra of extract I-4 is compared to that of riboflavin in figure 10. The riboflavin solution, in borate buffer (pH=8.5) had been exposed to incandescent light and so is expected to have been partially converted to lumichrome. This is evident from the weak emission peak at 470 nm (lower plot). The emission and excitation spectra of extract I-4 do not correspond exactly to those of riboflavin, but the emission peak does match that of lumichrome. It would be instructive to examine spectra of pure lumichrome, and other flavins and decay products, in order to compare with spectra of isolates. HPLC analysis could unequivocally identify the isolated compounds.

These flavin-like peaks were more obvious in the blue-water samples than in brown-water isolates. This may be a result of the spatial distribution of these compounds, or their emission may be masked by other material in highly absorbing waters. Similar peaks were not observed in Orinoco isolates and are not visible in SRFA, which is isolated from terrestrial waters onto XAD columns. There is a hint of a peak at 435/500 nm in the Sargasso Sea sample from 850 m. This may be indicative of flavins produced by bacteria in the oxygen minimum zone, as proposed by Coble (7).

Conclusions

Significant fractionation with respect to optical properties occurs during isolation of COM on C-18 columns. Material absorbing at long wavelengths is more efficiently retained than the uv-absorbing fraction. Reconstituted isolates therefore have lower S values than the original water. Fractionation with respect to fluorescence components may be stronger than with respect to absorbance. Fluorescence quantum yields of reconstituted extracts were significantly higher than those of unaltered seawater samples. In addition, there is selective extraction of a highly fluorescent species (possibly a flavin-type compound) emitting at ≈500 nm.

References

(1) Aiken, G.R. (1985). Isolation and concentration techniques for aquatic humic substances. In *Humic substances in soil, sediment, and water*; Aiken, G.R., D.M. McKnight, R.L. Wershaw and P. MacCarthy, ed.; John Wiley & Sons: New York; pp. 363-385.

(2) Carder, K.L., R.G. Steward, G.R. Harvey and P.B. Ortner (1989). Marine humic and fulvic acids: their effects on remote sensing of ocean chlorophyll. *Limnol. Oceanogr.*, **34**: 68-81.

(3) Amador, J.A., C.A. Milne and R.G. Zika (1990). Extraction of chromophoric humic substances from seawater. *Mar. Chem.*, **29**: 1-17.

(4) Mopper, K. and R.G. Zika (1987). Natural photosensitizers in seawater: riboflavin and its breakdown products. In *In Photochemistry of environmental aquatic systems,*; Zika, R.G. and W.J. Cooper, ed.; Advancements in Chemistry Series 327; American Chemical Society: Washington, D.C.; pp. 175-190.

(5) Dunlap, W.C. and M. Susic (1986). Photochemical decomposition rates of pteridines and flavins in seawater exposed to surface solar radiation. *Mar. Chem.*, **19**: 99-107.

(6) Gentien, P. (1981). Fluorescent metabolites in coral reefs off Townville, Queensland. *Aust. J. Mar. Freshwater Res.*, **32**: 975-80.

(7) Coble, P.G. PhD. thesis, (1990) Marine bacteria as a source of dissolved fluorescence in the ocean. MIT/WHOI Joint Program in Oceanography.

Chapter Seven: Summary

The work presented in this thesis demonstrates that fluorescence techniques are powerful tools for investigating many chemical and environmental questions. Molecular scale photophysics are accessible through fluorescence measurements, and probes which perturb fluorescence emission provide information about both properties of natural organic macromolecules and their local solution environment. On a much larger scale, studies of the fluorescence properties of natural material from diverse sources may help to disentangle the cycling of DOM in the aquatic system.

Chapter two focused on the mechanism of intramolecular fluorescence quenching by nitroxide radicals. Quenching rates were not well explained by energy transfer or electron transfer mechanisms. The most likely quenching pathway was determined to be via an *electron-exchange mechanism.* There was a strong correlation between quenching rates an non-radiative relaxation rates of parent (unquenched) compounds. This suggests that the best probe fluorophores will have an appreciable non-radiative relaxation rate.

In chapter three a novel fluorescence quenching method was employed to study the electrostatic properties of natural organic matter. The experiments described in this chapter demonstrated that cations are present at the surface of humic and fulvic acids in significant excess over their concentrations in bulk solution. This effect is more pronounced at high pH and is also very sensitive to ionic strength. This is consistent with the dissociation of acid groups in basic solution, and the shielding of potential by electrolyte ions at high ionic strength. Surface potential increases with molecular size in Suwannee River humic acid, as is reasonable if acid content per mass remains constant in this material. Because highly charged metal ions will be particularly susceptible to attractive potentials, this observation is of particular importance for those attempting to incorporate electrostatic effects into models of metal binding to humic substances. The surface charge calculated by a kinetic analysis of quenching data is in good agreement with predictions based on acid content and molecular weight measurements.

Chapter four discuses the absorption parameters measured for a series of field samples collected around South Florida and the Gulf of Mexico. It is crucial to record absorption information if fluorescence data are to be properly interpreted. Slopes of the log-linearized absorbance spectra were found to vary more than has been previously reported. Data were discussed with respect to parameters of importance to remote sensing applications. A case study of Oyster Bay examined absorbance data in terms of *S* and *a(300)* values, and also compared the details of non-linear variations in spectral shape.

Fluorescence of natural water samples was investigated in chapter five. Fluorescence matrix spectra were quite similar in shape, but differences were revealed by integration of spectra. Quantum yields were remarkably similar for all samples examined; their maximum variation was a factor of three. Normalization of matrix spectra to absorbance provided a maps of fluorescence efficiency and integration of these maps resulted in plots of quantum yield as a function of excitation wavelength. Significant variations among samples were revealed on this type of graph.

Some of the difficulties inherent in determining optical properties of natural water from isolated COM samples are discussed in chapter six. Fractionation was observed with respect to both absorbance and fluorescence. COM absorbing at longer wavelengths was more efficiently extracted from seawater than the uv-absorbing fraction. Fractionation was most significant for weakly absorbing marine samples.

Future Work Each chapter of this work leads to myriad paths for further inquiry. In an effort to leave my trail open-ended, I set forth here a few ideas for future research. Some possibilities I have considered in detail, others have only fleetingly crossed my mind, all have been generated or elaborated upon through fruitful discussions with advisors and colleagues at MIT and WHOI.

Chapter two. Our initial study of nitroxide-fluorophore adducts begs the question of whether energy transfer can be unequivocally eliminated as a possible quenching mechanism. A planned study employing fluorophores whose emission energies are well below the absorption energy of the nitroxide will settle this question. A definite answer as to whether defined triplet or charge-transfer states exist at any time during the quenching process can be sought through use of transient absorption spectroscopy. Synthesis of compounds with different, well-defined nitroxide-fluorophore distances and orientations could clarify the distance and angular dependences of quenching rates. A study of the temperature dependence of quenching rates would elucidate the activation energy of this process.

Chapter three. Many questions were raised by my investigation of diffusional quenching in the presence of strong electrostatic attractions. Further studies of this type on humic and fulvic acids could investigate the effects of dications (e.g. Ca^{++}) on electrostatic potentials. It might be possible to use a static quencher such as copper to quench a few sites, then use nitroxides to investigate the potential of the remaining molecules. This may confirm the suggestion that humic molecules with the highest negative potential are the first to bind cations.

Some fundamental physical issues were raised by this work and I would hesitate to apply this technique to more complex systems until they are resolved. Quenching rates in this system exceeded the "diffusion-controlled limit" for bimolecular encounters. This suggests that steady-state fluorescence quenching techniques are surprisingly sensitive to the time-dependent kinetics expected at very short times for reactions between oppositely charged species. This observation bears further study; ideally the short-time kinetics and steady-state fluorescence quenching should be measured on the same, well-defined system.

Chapters four, five and six. Field studies always, by necessity, leave too many parameters unmeasured and too much of the globe unsampled. It is clear that much more information is required before generalizations can be made concerning the variability of optical properties of fresh and ocean waters. It is important to measure specific (mass-normalized) absorption coefficients in order to estimate the correlation between DOM and COM in natural waters. Additional work on samples already in hand will focus on their photochemical reactivity and rates of production of reactive transients. Laboratory experiments on the effects of sunlight exposure on optical properties of natural COM could help disentangle the processes of photobleaching and removal (e.g. by particles or biological consmption). Cultures of phytoplankton might also be used to determine what types of chomophores are released by marine organisms. Study of COM cycling before, during, and after seasonal phytoplankton blooms would be useful for the tracking of such blooms by remote sensing. My few deep-water samples hint that fluorescence yields for deep COM are significantly different than surface values; with further study, such differences may provide some clues about the global cycling of organic matter in the oceans.

Appendix A: Refractive Index Correction to Absorption Spectra

Absorbance measurements in seawater, especially those employing long pathlength cells, have frequently been plagued by baseline offsets, when measured against a pure, freshwater reference. In our HP 8451A diode array spectrophotometer this is manifest by an apparent optical density of ≈0.006 in the range 700-820 nm for seawater in a 5 cm cell. These offsets have been attributed to scattering by small particles or colloids which may pass through filters, leading some workers to employ substantial wavelength-dependent corrections for scattering.

Two observations argue against scattering being the cause of this baseline offset. First, the same offset is observed for a wide variety of 0.2 µm filtered seawater samples, and it is eliminated when the instrument is referenced against oligotrophic seawater as opposed to distilled water. If it were due to particle or colloid scattering, this would imply that all seawater samples tested have identical concentrations of scatterers.

Secondly, an offset of the same magnitude is observed for an 0.5 M NaCl solution in pure water, where no particles are expected. Instead, this effect is probably a result of the refractive index difference between the freshwater reference (n_D= 1.3330) and seawater (n_D= 1.3393, for salinity=34.8‰ (44)). This can be confirmed by comparing the apparent absorption spectra of other particle-free solvents of various refractive indices, referenced to Q-water. Methanol (n_D=1.326), ethanol (n_D=1.359) and 0.5 M NaCl (n_D=1.3381) showed spectral offsets of -0.0076, 0.0195, and 0.006, respectively. Both the direction and magnitudes of these offsets support the conclusion that, for the optical configuration of this instrument, refractive index is an important parameter.

Refractive index differences between solvents affect both the fraction of light reflected and the angle of refraction at the glass-solvent interface. The amount of light reflected at the interface is governed by : $(n_1-n_2)^2/(n_1+n_2)^2$, where n_1 and n_2 are the refractive indices of the quartz and solvent, respectively. The fraction of normal-incidence light reflected from a pure water- quartz interface is about 0.53% vs 0.50% for a seawater-quartz interface, so this is not a major contributor to the diminished intensity reaching the dectector through the seawater sample. However, the difference in refraction angle can produce this result. Because the output from the lamp is not collimated, light rays impinging on the cell face are not all normal to it. Thus, they are refracted according to the formula:

$$\sin\phi_1 = n_2 \sin\phi_2 / n_1$$

where ϕ_1 (ϕ_2) are the incident angles of the light ray. It is clear that a change in the angle of the light rays passing through the optical cell can result in defocussing of the beam, causing more or fewer photons reaching the detector. It is not possible to calculate the magnitude of this apparent absorption without knowing details of the optical configuration of the instrument, and specifically, the quality of the light beam focused onto the sample cell. Dispersion (change in refractive index with wavelength) could make the observed offset wavelength-dependant. In practice, though, dispersion is small for water (or seawater) in this spectral region, and we ignore it in correcting these results.

In treating our absorbance data, we have subtracted the apparent absorbance in the range 700-800 nm (normally $\approx$0.006) from the entire spectrum and assumed this offset is constant across the spectral region of interest. To test the validity of this correction, serial dilutions of a SRFA solution into seawater were performed. Absorbance spectra were collected using either a Q-water or seawater reference. After correction, slopes were indentical for both sets of samples.

Appendix B.

Characterization of dissolved organic matter in the Black Sea by fluorescence spectroscopy

by P.G. Coble, S.A. Green, N.V. Blough and R.B. Gagosian

Reprinted from *Nature*, (1990) **348**: 432-435.

Reprinted from Nature, Vol. 348, No. 6300, pp. 432–435, 29th November, 1990
© *Macmillan Magazines Ltd.*, 1991

Characterization of dissolved organic matter in the Black Sea by fluorescence spectroscopy

Paula G. Coble*, Sarah A. Green†, Neil V. Blough† & Robert B. Gagosian†

* School of Oceanography, University of Washington, Seattle, Washington 98195, USA
† Woods Hole Oceanographic Institution, Woods Hole, Massachusetts 02543, USA

THE natural fluorescence properties of sea water provide a means of elucidating the complex chemical composition and diverse sources of dissolved organic matter (DOM) in sea water[1–6]. The positions of excitation and emission maxima for a wide range of natural water samples show remarkable similarity[7]. High-sensitivity fluorescence spectroscopic studies[8] have shown recently that emission maxima for marine and coastal waters differ by 20 nm when the excitation wavelength is 313 nm. Here we present evidence from three-dimensional excitation emission matrix (EEM) spectroscopy that at least three fluorophores are present in waters of the Black Sea. Distinct changes in the relative abundance of these fluorophores are observed as a function of depth. We suggest that three-dimensional fluorescence spectroscopy can be used to distinguish between different types and sources of DOM in natural waters. These findings may have important applications in the field of remote sensing of phytoplankton pigments. For example, a better understanding of the sources of DOM components will help in correcting[9,10] remotely sensed data for the presence of gelbstoff (yellow-coloured DOM[11], which plays an important part in radiation absorption by surface waters).

We collected samples of dissolved organic matter during Leg 5 of the 1988 RV *Knorr* Black Sea Expedition (cruise 134-12, July 1988). The study site was located near the centre of the basin (43°5.0′ N, 34°00.0′ E) in 2,218 m of water. Dissolved oxygen was undetectable (<5 μM) below 100 m and hydrogen sulphide was present at all depths below 120 m (ref. 12). There was a constant increase in DOM fluorescence (Ex/Em = 320–390/475–530 nm) from the surface to 375 m, the maximum depth sampled[13,14].

DOM was concentrated from acidified (pH 3.2) sea water onto pre-cleaned octadecylsilane-bonded silica (Waters C18 Sep-Paks) at flow rates of 10–15 ml min^{-1}, eluted with methanol, concentrated by rotary evaporation at reduced pressure and redissolved in methanol[13,15]. Absorption spectra were measured on an HP-8451 diode array spectrophotometer. Fluorescence spectra were recorded on an SLM-Aminco SPF-500C spectrofluorometer in ratio mode. A procedural blank was prepared by passing distilled water through a Sep-Pak and eluting and concentrating using the same procedures as for samples. To eliminate fluorescence contamination from the Sep-Paks and Raman scattering from the solvent (methanol), the blank EEM was subtracted from each sample EEM. Where noted, we corrected the emission spectra for instrumental configuration using correction factors provided by the manufacturer, with some modifications[16].

We present EEMs before (Fig. 1) and after (Fig. 2) correction for instrumental configuration to permit comparison between our results and those of other investigators. Because uncorrected

TABLE 1 Fluorescence maxima for natural water samples

Depth	A	B	Region C	D	E	Reference
Black Sea						
Uncorrected						
1 m	260/450 (1.2)	285/350–360 (1.4)	n.m. (0.9)			This study
28 m	260/460 (1.3)	285/350 (1.2)	n.m. (1.0)			
44 m	260/450 (1.6)	285/350 (1.1)	345/345 (1.2)			
78 m	260/455–460 (2.0)	285/360 (1.0)	345/445 (1.6)			
217 m	260/450 (2.6)	n.m. (1.0)	345/445 (2.4)			
375 m	260/445 (2.7)	n.m. (1.5)	345/445 (2.5)			
Corrected						
1 m	260/435 (0.05)	280/325–345 (0.2)	n.m. (0.03)			This study
28 m	260/435–445 (0.06)	280/345 (0.1)	n.m. (0.05)			
44 m	n.m. (0.08)	285/335 (0.1)	n.m. (0.05)			
78 m	260/445 (0.1)	n.m. (0.07)	345/445 (0.08)			
217 m	260/440 (0.2)	n.m. (0.09)	340/450 (0.18)			
375 m	260/435 (0.2)	280/335 (0.2)	340/445 (0.19)			
Suwannee River fulvic acid						
*	260/460		325/450			S. A. Green (personal communication)
†	230/420		300/415			24
Soil fulvic acid						
‡			350/490	390/509	455/521	25

A through E indicate regions of the EEM. Actual positions of the maxima are indicated by Ex/Em wavelength pairs (in nanometres). Values in parentheses represent relative fluorescence intensities after subtraction of the blank. Fluorescence intensities in regions where no maximum was observed are indicated by 'n.m.'.

* Water, pH 8.5, 5 mg l^{-1}; † pH 4.5; ‡ 40:60 glycerol:water (w:w), pH 6.0, 150 mg l^{-1}.

spectra were collected with the same instrument under identical conditions, they can be directly compared for differences in position and intensity of maxima even below 300 nm, where the correction routine is not valid.

Fluorescence originates from the first excited singlet state of a molecule, regardless of excitation energy. Thus for the EEM of a single simple fluorophore, the position and linewidth of the emission peak do not shift with excitation wavelength. Fluorescence intensity varies along the excitation axis, reflecting the absorption spectrum of the molecule. A cross-section through an EEM parallel to the excitation axis represents a traditional excitation scan, whereas a cross-section parallel to the emission axis is equivalent to an emission scan.

There are three distinct fluorescence maxima in the uncorrected EEMs (Fig. 1). The highest fluorescence intensities occur at excitation 260 nm and emission 440 nm (region A) for all samples except that from the 1 m depth. In the two deep-water samples, there is an emission maximum at 440 nm for excitation at 340 nm (region C). There is fluorescence in this region in the samples from 1 m and 28 m depth as well, but it is not intense enough to create a local maximum. The emission at 440 nm from excitation at two wavelengths could be interpreted as being from a single fluorophore, if the ratio between the two excitation peaks were constant. This clearly is not the case, as the ratio of fluorescence in region A to fluorescence in region C (A : C, Table 1) decreased from 1.33 in the sample from 1 m depth to 1.08 in the sample from 375 m depth. Changes in speciation due to pH variations could cause a similar effect, but the *in situ* pH varied only slightly (8.3-7.7) over the depth interval sampled[17]. Because all samples were acidified and the spectra measured in methanol solution, pH-induced speciation was probably not a factor. Therefore we conclude that at least two separate fluorophores are present, both of which have an emission maximum at 440 nm.

A third fluorophore is responsible for the maximum at Ex/Em = 295/345 (region B). This is the largest peak in the sample from 1 m depth and was present, but less intense, in the samples from 28 m and 375 m depth. Its fluorescence properties are similar to those of the indole ring of tryptophan[18].

The fluorescence in region C in water from all depths sampled is definitely from a mixture of fluorophores. This is indicated by the redshift in the emission maximum at increasingly longer excitation wavelengths (line X-Y; Fig. 3). Fluorescence in regions A and B may be from a single fluorophore in each case, or to the presence of multiple species having similar spectral properties.

The corrected EEMs (Fig. 2) show the same general features, but fluorescence at short-wavelength excitations is enhanced by the correction. Emission maxima in regions A and B are shifted 10-20 nm towards the blue in the corrected spectra (Table 1). Both corrected and uncorrected EEMs indicate that the ultraviolet region is important for distinguishing between samples from different depths.

The ultraviolet absorption spectra of these samples are distinctly different. The shallow samples and the sample from 375 m have a shoulder at 230 nm not seen at 217 m. We cannot relate the absorption at this wavelength to fluorescence, because our shortest excitation wavelength was 260 nm.

The apparent yield of fluorescence at 440 nm with excitation at 260 nm increases with depth. Absorbance values are close to 0.2 in all samples, but the amount of fluorescence per unit absorbance increases twofold from 1.4 in samples from 1 m to 2.7 in samples from 375 m. True quantum yields cannot be obtained because the samples contain a mixture of compounds, some of which may absorb at 260 nm but be non-fluorescent. Previous studies have shown that apparent fluorescence efficiencies are higher in coastal waters than in offshore marine waters[8]. Our observation of lower efficiencies in surface waters than in deep waters may be the result of photodegradation in the upper water column[19-22], which decreases fluorescence intensity but may have a lesser effect on absorbance.

Excitation wavelengths shorter than 300 nm have been used in only a few previous studies, with similar results. A tryptophan-like fluorescence (Ex/Em = 287/348 nm; ref. 18) was observed for waters from a *Trichodesmium* bloom[3], and a tyrosine-like fluorescence (Ex/Em = 275/303 nm; ref. 18) was observed in highly productive Antarctic waters[23]. As the fluorescence signal of proteins arises from these two amino acids, fluorescence of sea water at these wavelengths could be caused by the presence of either dissolved free amino acids or dissolved proteins. The implication here is that DOM fluorescence in surface waters is associated with growth of living organisms.

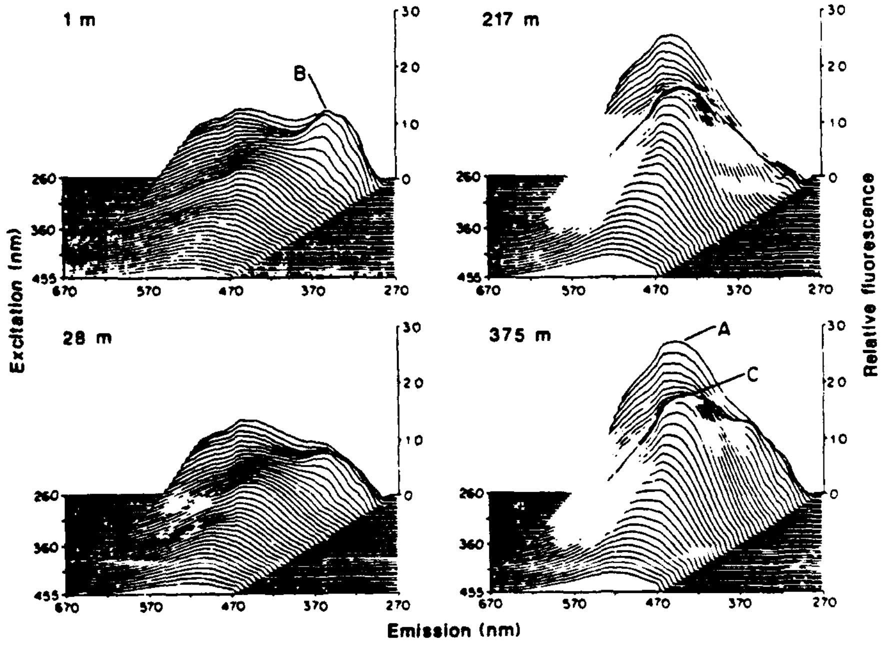

FIG. 1 Uncorrected EEM spectra for concentrated DOM samples from the Black Sea at depths of 1 m, 28 m, 217 m and 375 m. A through C refer to the fluorophore designations presented in Table 1. Instrument settings were the same for each set of spectra. EEMs were generated by concatenating 40 emission spectra collected at excitation wavelengths 5 nm apart between 260 and 455 nm. Excitation and emission bandpasses were 4 nm. The EEM spectrum for a procedural blank has been subtracted from each sample spectrum. All samples were concentrated by a factor of ~67.

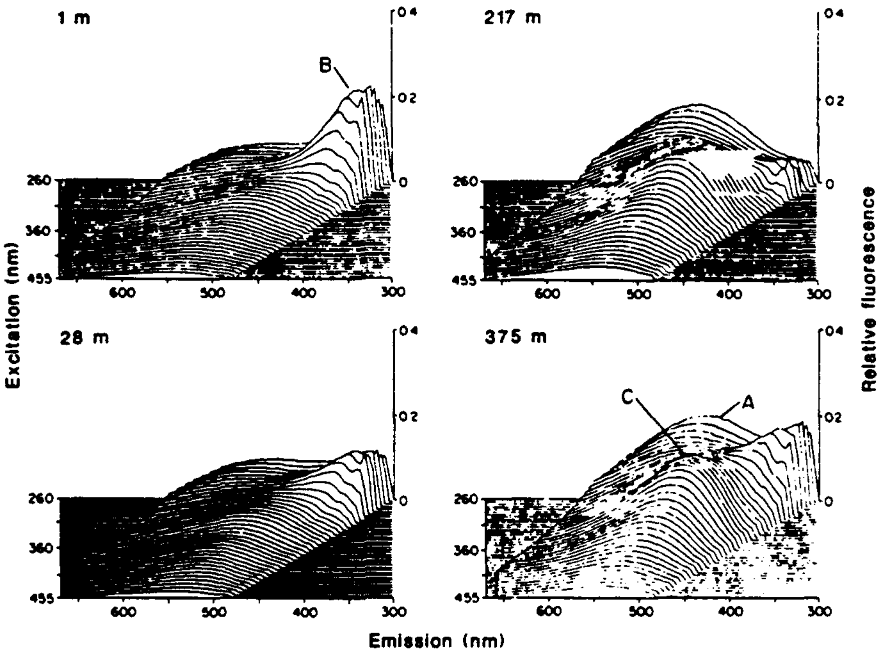

FIG. 2 Corrected EEM spectra for concentrated DOM samples from the Black Sea at depths of 1 m, 28 m, 217 m and 375 m. Spectra are the same as in Fig. 1 after correction for instrumental configuration. The procedural blank was also corrected before subtraction from samples. Data below 300 nm are lost because the correction routine is not valid below that wavelength.

Our EEMs from Black Sea waters are unlike EEMs reported from two other natural sources, both of which contained multiple fluorescing species (Table 1). A Suwannee River fulvic acid had maxima at Ex/Em = 230/420 nm and 300/415 nm (ref. 24). A soil-derived fulvic acid (Contech) had a maximum at Ex/Em = 390/509 nm, with smaller peaks at Ex/Em = 350/490 nm and 455/521 nm (ref. 25). Some of these differences may be because of differences in instrumentation, sample preparation, pH, concentration and solvents. Using our instrumentation, the EEM for Suwannee River fulvic acid (water, pH 8.5, 5 mg l^{-1}) was quite similar to the EEM for Black Sea deep water (Table 1).

These results suggest that EEM evaluation can be used to distinguish between DOM from at least three different sources: soils, rivers and surface sea water. Surface and deep sea water samples are also distinguishable, at least in the Black Sea. Preliminary results (P.G.C., unpublished data) for unconcentrated sea water samples from the Black Sea as well as from other marine and freshwater areas support this conclusion. There are some differences between the concentrated and unconcentrated samples, however, which may be caused by isolation procedures. Fluorescence in region A is less intense in unconcentrated samples, and another maximum (Ex/Em 295-300/405-

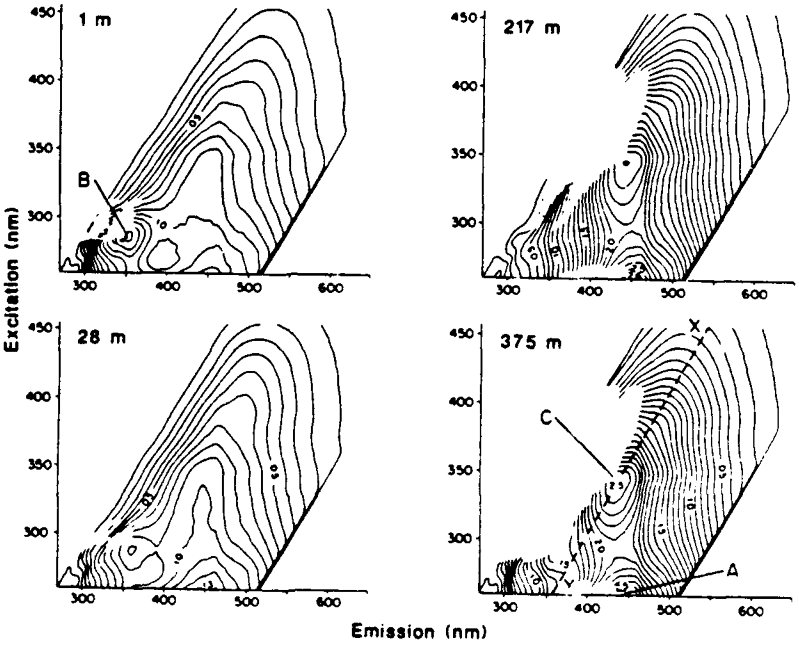

FIG. 3 Contour plots of EEM spectra shown in Fig. 1 for samples from the Black Sea at depths of 1 m, 28 m, 217 m and 375 m. Contour interval is 0.1 relative fluorescence units. Line X-Y in the lower right panel represents the positions of the long-wavelength emission maxima.

410 nm) not observed in the concentrated samples is present. A fluorescence maximum at 310/410 nm has been reported previously in sea water using laser-induced fluorescence[8,21]. The cause of the apparent difference between concentrated and unconcentrated samples needs further investigation. It could have important implications for the study of marine DOM by techniques that require isolation of the material from sea water.

Fluorescent DOM represents part of the gelbstoff signal that must be accounted for in satellite-derived estimates of phytoplankton productivity. The three types of gelbstoff in the ocean (*terrestrial*[1,2], *bloom-related*[3,26-28] and *condensates of non-fluorescent DOM*[2,29]) have distinct chemical compositions. EEM analysis seems to be sufficiently sensitive to distinguish between these and may be used to assess the contribution of each. ☐

Received 29 June; accepted 12 October 1990.

1. Kalle, K. *Dt. hydrogr. Z.* **2**, 117-124 (1949).
2. Kalle, K. *Oceanogr. mar. Biol. A. Rev.* **4**, 91-104 (1966).
3. Traganza, E. D. *Bull. mar. Sci.* **19**, 897-904 (1969).
4. Duursma, E. K. in *Optical Aspects of Oceanography* (eds Jerlov, N. G. & Steemann Nielsen, E.) 237-256 (Academic, New York, 1974).
5. Berger, P., Laane, R. W. P. M., Ilahude, A. G., Ewald, M. & Courtot, P. *Oceanologica Acta* **7**, 309-314 (1984).
6. Cabaniss, S. E. & Shuman, M. S. *Mar. Chem.* **21**, 37-50 (1987).
7. Zepp, R. G. & Schlotzhauer, P. F. *Chemosphere* **10**, 479-486 (1981).
8. Donard, O. F. X., Lamotte, M., Belin, C. & Ewald, M. *Mar. Chem.* **27**, 117-136 (1989).
9. Bricaud, A., Morel, A. & Prieur, L. *Limnol. Oceanogr.* **26**, 43-53 (1981).
10. Carder, K. L., Steward, R. G., Harvey, G. R. & Ortner, P. B. *Limnol. Oceanogr.* **34**, 68-81 (1989).
11. Kalle, K. *Ann. Hydrogr.* **66**, 1-13 (1938).
12. Friederich, G. E., Codispoti, L. A. & Sakamoto, C. M. *Tech. Rept. 90-3* (Monterey Bay Aquarium Research Institute, Monterey, 1990).
13. Coble, P. G. thesis, MIT and Woods Hole Oceanogr. Inst. (1990)
14. Coble, P. G., Gagosian, R. B., Codispoti, L. A., Friederich, G. E. & Christensen, J. P. *Deep Sea Res.* (in the press).
15. Dunlap, W. C. & Susic, M. *Mar. Chem.* **17**, 185-198 (1985).
16. Green, S. G., Simpson, D. J., Zhou, G., Ho, P. S. & Blough, N. V. *J. Am. chem. Soc.* (in the press).
17. Goyet, C., Bradshaw, A. L. & Brewer, P. G. *Deep Sea Res.* (in the press).
18. Wolfbeis, O. S. in *Molecular Luminescence Spectroscopy* Part 1 (ed. Schulman, S. G.) 167-370 (Wiley-Interscience, New York, 1985).
19. Kramer, C. J. M. *Neth. J. Sea Res.* **13**, 325-329 (1979).
20. Hayase, K., Tsubota, J. & Sunada, I. *Mar. Chem.* **25**, 373-381 (1988).
21. Chen, R. F. & Bada, J. L. *Geophys. Res. Lett.* **16**, 687-690 (1989).
22. Kouassi, M. thesis, Univ. Miami (1986).
23. Ewald, M., Stabel, H. & Belin, C. *C. r. hebd. Séanc. Acad. Sci. Paris* **302**, 883-886 (1986).
24. Goldberg, M. C. & Weiner, E. R. in *Humic substances in the Suwannee River, Georgia. US geol. Surv. Open-file Rep.* 87-557, 179-204 (US Dept Interior, Washington, DC, 1989).
25. Lochmuller, C. H. & Saavedra, S. S. *Analyt. Chem.* **58**, 1978-1981 (1986).
26. Yentsch, C. S. & Reichert, C. A. *Bot. Marina* **3**, 65-74 (1961).
27. Sieburth, J. M. & Jensen, A. *J. exp. mar. Biol. Ecol.* **3**, 275-289 (1969).
28. Carlson, D. J. & Mayer, L. M. *Can. J. Fish. aquat. Sci.* **40**, 1258-1263 (1983).
29. Hedges, J. I. *Geochim. cosmochim. Acta* **42**, 69-76 (1978).

ACKNOWLEDGEMENTS. We thank the captain, crew and scientists of RV *Knorr* cruise 134-12 and the organizers of the 1988 Joint US-Turkey Black Sea Expedition. We also thank J. Hedges for a review and L. Sylvester for assistance with preparation of the figures. This work was supported by the NSF, the Environmental Protection Agency and the Office of Naval Research. Woods Hole Oceanographic Institution Contribution 7444.

Appendix C: Computer Programs

"SLM" programs are writen within the software that drives the SLM-Aminco %00C fluorometer. The programs MATBLUE, MATRED and DATBLUE are links routines which collect spectra to be cancatenated into a matrix spectrum.

The routine ADD pastes the 'blue' and 'red' portions (collected with and without filtering the second-order scatter line, respectively) into 43 full range spectra.

The FORTRAN program MATRIX contains subroutines to read and plot the spectra aquired on the SLM instrument. It calls the conertial subroutine PLOT88. Subroutines are used to normalize and intergate the spectra. They can be stored as ascii files.

Bug report

All spectra were collected with the same wavelength limits (ex= 260-470, em= 270-770); I have attempted to make the programs general, but use of other wavelength limits may require soem modifications. The real-time crrection feature does not work during macro data aquisition.

MATRIX program has difficult accessing files in different subdirectories or on floppy disks.

There is very little error trapping in any of these programs. Attempts to read non-existant files, or write over existing files will cause crashes.

SLM Macro: MATBLUE

```
STOP
COROFF
:GET MATBLUE
FR
SELEM
SEON
SIN
WL
:TYPE WLEM
STO3
STAT
:PRINT This program generates an excitation/emission matrix
:PRINT to be read by the MATRIX plotting routine.
:PRINT Status settings must be preset. They should be saved in
:PRINT status file "matrix". Initial wavelengths, increments,
:PRINT filter and gain settings are taken from there.
:PRINT Status is as shown on instrument screen.
:PRINT Input numbers are to coordinate plotting and storage
:PRINT with data.
:PRINT
:PRINT
:PRINT
:PRINT CHECK FOR FILTER
:PRINT
:NAME
:ERASE
:S=260
:PRINT Please enter starting excitation
wavelength:
:INPUT S
:T=S
:ERASE
:S'=270
:PRINT Please enter begining scan
wavelength:
:INPUT S'
:ERASE
:L'=770
:PRINT Enter OVERALL ending scan
wavelength:
:INPUT L'
:ERASE
:I=5
:PRINT Please enter increment value
(inc-ex=inc-em).
:INPUT I
:INC I
:ERASE
:N=43
:PRINT Enter number of scans:
:INPUT N
:REM S&E are ex start &end
:REM S'& E'= em start and end
:X=I*2
:REM end of scan:
:E'=S*2
:E'=E'-X
:REM start of red scan:
:F'=E'
:REM l,k(') are to fill in 0s at ends
:L=X+S
:LL L
:UL L'
:REM Baseline=B=0
:B=0
:REM G=100 at start=y
:Y=530
:GOSUB DATBLUE
:CHAIN MATRED
STOP
```

SLM Macro: MATRED

```
STOP
COROFF
:GET MATRED
FR
SELEM
SEON
SIN
WL
:TYPE WLEM
STO3
STAT
:PRINT This program continues matrix data collection into
:PRINT the red spectral region.
:PRINT Status settings must be preset as MATRED
:PRINT Please put in lp385 filter on emission side.
:PRINT Wavelengths are set by matblue and Stat screen.
:PRINT Status is as shown on instrument screen.
:PRINT
:PRINT
:PRINT
:PRINT
:PRINT
:PRINT !#!#!#!#!#!   INSTALL FILTER   !#!#!#!#!
:PRINT
:S=T
:S'=F'
:N=39
:PRINT Enter number of scans:
:INPUT N
:REM S&E are ex start &end
:REM S'& E'= em start and end
:REM l,k(') are to fill in 0s at ends
:L=I*2
:L=L+S
:E'=L'
:LL L
:UL L'
:REM baseline=B=0
:B=0
:GOSUB DATBLUE
STOP
```

SLM Macro: DATBLUE

```
:REM matrix data collection
STOP
:SETPLOT/C+/S5 0/I
:K=S'-L
:K=K/I
:K'=L'-E'
:K'=K'/I
EMOPEN
:REPEAT N
:IF S'>Y GOTO 65
:REM G=100 for S'>Y
:IF K<0 GOTO 63
:REM left baseline
:REPEAT K
:STORE B 0
:PLOT/L0
:END REPEAT
EXTOLL
EMTOLL
EXOPEN
START
START
:J=E'-S'
:J=J/I
:REM data collection
:REPEAT J
:A=READ
:STORE A 0
:PLOT/L0
:END REPEAT
:STORE B 0
:REM B=0, PLOT TO BASELINE
:IF K'<0 GOTO 61
:REM right baseline
:REPEAT K'
:STORE B 0
:PLOT/L0
:END REPEAT
:SAVE 0 0
EXCLOSE
:IF E'>780 GOTO 48
:REM don't incr UL
EMTOUL
EMUP
EMEXUL
:E'=E'+I
:UL E'
EXTOLL
EXUP
EXEXLL
:S=S+I
EMTOLL
EMUP
EMEXLL
:S'=S'+I
:K=K+1
:K'=K'-1
:SETPLOT/N+
:REM end repeat
:GOTO 67
:K'=0
:GOTO 39
:K=0
:GOTO 18
GA100
:GOTO 12
:END REPEAT
EMCLOSE
:GET MATRED
STOP
```

SLM Macro: ADD

```
:REM fix for gain, filter; add red & blue parts
:I=49
:PRINT Enter first high gain spectrum:
:INPUT I
:N=83-I
:K=44
:PRINT Enter first red (filtered) spectrum:
:INPUT K
:K'=K
:M=83-K
:REM gain cor
:D=10
:CON D
:REPEAT N
:DIV I
:SAVE I 2
:I=I+1
:END REPEAT
:REM filter cor
:LOAD 83 1
:REPEAT M
:DIV K
:SAVE K 2
:K=K+1
:END REPEAT
:REM add red + blue
:I=1
:K=K'
:REPEAT M
:ADD I K
:SAVE I 2
:K=K+1
:I=I+1
:END REPEAT
```

Matrix plotting program

```
c * Includes menu (main program), subroutines maximum, rescale, subtract,
c * block-data sizedat.

c ****************************************************************************
c *********** MENU (MAIN) ********************** MENU (MAIN) *******************
c ****************************************************************************
      program menu
c ** Requires data files from fluorometer in SLM-500C format.
c Calls: getdata, info, maximum, subtract, normabs, rescale, trim, savemat,
c and integrate subroutines.
c Also, Plot88 subroutines: plots, factor, window, zlevel, zcntur, mesh & plot.

c *** various work variables needed by plot88 subroutines:
c [All integers passed to plot88 must be 16 bit (integer*2).]

      implicit integer*2 (i-n)

C COMMON DATA TYPES:
c ** 'datcom' types:
          integer*2 npts,  numrec, ndata
c ** 'size' types:
          integer*2 nxsize, nysize

C DATA TYPES:
      real xdata(35), vertex(16), zlev(51)
      real azimut, elevat, norm, zmax
      integer*2 mask(1360), idig(51), iwgt(51)

c *** file to read, plot labels:
      character*16 zfile

c ***  some control integers:
      integer*2 choice, n0, m0
      integer*2 each, dim, newdim, record
      integer*2 ioport, model, crtport, crtmod
      integer*2 mitport, mitmod, wholport, wholmod, place

c *** and some control characters:
      character ans
c      character*4 place

C COMMON BLOCKS:
c *** work space for large data arrays:
      common /work/ z(200,65)
      common /temp/ ztemp(200,65)
c ** 'datcom' from getdata subroutine:
      common /datcom/ npts, numrec, ndata
      common /size/nxsize, nysize

C DATA BLOCKS:
c *** data to direct mesh subroutine:
      data iedge/0/,idir/1/,iproj/0/,icut/1/, itrim/0/, maxpts/500/,
     1 iframe/1/, zlow/0./, dim/3/, fact/0.8/
```

```
      data azimut/100./, elevat/25./

c *** data to direct contouring routines:
      data ldig/51*-3/, lwgt/51*1/, hgt/0.25/,
     1 narc/5/, cint/0.2/
      data xlabel/'excitation '/, ylabel/'emission '/

c *** spacial control of plotting, upper and lower limits in inches:
      data xlplot/0.0/, xhplot/7.5/, ylplot/0./, yhplot/7.5/
      data mitmod/30/, mitport/9600/
      data whoimod/80/, whoiport/9600/
      data crtmod/99/, crtport/99/

c *** a few random starting values:
      zexists = 0
      zcorn = 0.0
      ioport = crtport
      model = crtmod
      place = 0

C START OF MAIN BLOCK:
c *** Menu to choose file, parameters, games with data
 80   write (*,*) ' Menu '
      write (*,*)
      write (*,*)
      if (model .eq. crtmod) then
            write (*,*) ' 1. Plot to screen '
        elseif (model .ne. crtmod) then
            write (*,*) ' 1. Plot hardcopy '
      endif
      write (*,*)
      write (*,*) ' 2. Integrate'
      write (*,*)
      write (*,*) ' 3. Change dimension/ scaling '
      write (*,*)
      write (*,*) ' 4. Subtract another spectrum '
      write (*,*)
      write (*,*) ' 5. Normalize '
      write (*,*)
      write (*,*) ' 6. Show subsection of spectrum '
      write (*,*)
      if (model .eq. crtmod) then
            write (*,*) ' 7. Set up plotter '
        elseif (model .ne. crtmod) then
            write (*,*) ' 7. Reset to screen plotting '
      endif
      write (*,*)
      write (*,*) ' 8. Save z-matrix '
      write (*,*)
      write (*,*) ' 9. New file '
      write (*,*)
      write (*,*) ' 10. Quit '
      write (*,*)
      write (*,*) ' Please choose a number '
      read (*,*) choice

c*1*1*1*1*1*1*1*1*1*1*1*1*1*1*
```

```
      if (choice .eq. 1) then
        if (zexists .eq. 0) then
          call getdata(z)
         zexists = 1
        endif
c zcorn is to set fixed scaling on several plots, it should be set > zmax.
      z(1,1) = zcorn

c ***  Something to read while waiting for plot set-up.
c *   Maximum gets max & min of z-matrix; info shows parameters.
      call info
      if (dim .eq. 2) then
        write (*,904) cint
 904   format(' Plotting is set to contour mode with contour interval =
    1 ',f5.3,'.')
      elseif (dim .eq. 3) then
        write (*,905)        azimut, elevat
 905   format(' Plotting is set to 3-D mode with azimuth = ',f5.1, ' &
    1 elevation = ',f5.1,'.')
      endif
       write(*,*) 'Constructing plot...please wait. '

c ***  PLOT STARTS
c      * initialize plotter
c
        call plots (0, ioport, model)

c     * reduce size

        call factor(fact)
         call window (xlplot, ylplot, xhplot, yhplot)

c      * type of plot (contour or 3-D))
        if (dim.eq.2) then
c     ** Contour plot
            call zlevel(z, nxsize, nysize, ndata, numrec,
    1 cint, zlev, nlev)
            call zcntur(z, nxsize, nysize, ndata, numrec,
     1 xlplot, ylplot, xhplot, yhplot,zlev,ldig,lwgt,nlev,hgt,narc)

       else
c     ** 3-D plot
      call mesh(z, nxsize, nysize, ndata,numrec, azimut, elevat,
    1 xlplot, ylplot, xhplot, yhplot, iedge, idir, iproj,
    2 iframe, zlow, icut, itrim, mask, vertex)

        endif
c *** end of plot
c
        call plot (0., 0., 999)

c      * reset plotter to screen plot
        model = crtmod
        ioport = crtport
       xhplot = 7.5
       yhplot = 7.5
      endif
```

```
c **  end of menu choice 1.

c*2*2*2*2*2*2*2*2*2*2*2*2*2*2*
     if (choice .eq. 2) then
          call integrate(z)
     endif
c ** end of menu choice 2.

c*3*3*3*3*3*3*3*3*3*3*3*3*3*3*3*
     if (choice .eq. 3) then
     newdim = dim + 1
     if (newdim .eq. 4) newdim =2
     write (*,928) newdim
  928  format( ' Change dimension to ',i1,'-D (y or n) ? ')
     read (*,930) ans
      if (ans.eq.'y') dim = newdim

c *** if in mesh mode:
     if (dim .eq. 3) then
     write (*,*) ' Change line direction (y or no)? '
     read (*,930) ans

       if (ans .eq. 'y') then
            write (*,*) 'For lines along emission spectra enter 1; '
            write (*,*) 'For lines along excitation spectra enter 2; '
            write (*,*) 'For both enter 3. Current setting is ',idir
         read (*,970) idir
       endif

     write (*,*) ' Rotate plot? '
     read (*,930) ans
       if (ans .eq. 'y') then
        write (*,*) 'Azimuth is set at ', azimut,'.'
        write (*,*) 'Elevation is set at ', elevat,'.'
        write (*,*) 'Enter new values (az, el) : '
        read (*, *) azimut, elevat
           endif

     write(*,*)' Reset corner z(1,1) point from ',zcorn,'? (y or n)'
     read(*,930) ans
        if (ans .eq. 'y') then
          write (*,*)' Enter new value: '
          read (*,*) zcorn
       endif
     endif

c *** if in contouring mode:
     if (dim.eq.2) then
       call maximum(zmax)
      cint=  zmax * 0.05
       write (*,*) 'Change contouring interval (y or n) ? '
      write (*,925) cint
  925    format(' (Default interval (5%) is: ',f6.4,')')
      read (*,930) ans

       if (ans.eq.'y') then
         write(*,*) ' Please type new interval: '
         read (*,*) cint
       endif
c        write(*,*) 'Add frame (y or n)?'
c        read(*,930) ans
c        if (ans .eq. 'y') zframe=1
c        do 50 j = 1, nxsize
c  50       z(j,1) = 100.
c        do 51 i = 1, nysize
c        z(1,i) = 100.
c  51     continue
c        endif
      endif

       if (n0 .eq. 1) then
         write(*,*) ' Set negative points to zero?'
        read (*,930) ans
         if (ans.eq.'y') n0=0
           endif

           if (m0 .eq. 1) then
         write(*,*) ' Set points >10^7 to zero?'
        read (*,930) ans
         if (ans.eq.'y') m0=0
           endif

       if (m0 .eq. 0) then
         do 60 j = 1, nxsize
         do 60 i = 1, nysize
           if (z(j,i) .gt. 10e7)  z(j,i)=0
   60    continue
       endif

       if (n0 .eq. 0) then
         do 70 j = 1, nxsize
         do 70 i = 1, nysize
           if (z(j,i) .lt. 0)  z(j,i)=0
   70    continue
        endif

      endif
c ** end of menu choice 3

c*4*4*4*4*4*4*4*4*4*4*4*4*4*4*4*
       if (choice .eq. 4) then
c ** subtract another spectrum, norm = normalization factor

             call subtract(z)

       end if
c ** end of menu choice 4

c*5*5*5*5*5*5*5*5*5*5*5*5*5*5*
       if (choice .eq. 5) then
       write(*,*) ' Normalize to absorbance spectrum (A), or to 1 (1)?'
           read (*,930) ans

             if (ans .eq. 'a') then
         call normabs(z)
        elseif (ans .eq. '1') then
       call rescale(z, 1.0)
     endif
       endif
c ** end of menu choice 5

c*6*6*6*6*6*6*6*6*6*6*6*6*6*6*

    if (choice .eq. 6) then
       call  trim(z)
   endif

c *** Section below allows triming of DIAGONALS, to cut out scatter
c    or Raman emission.
c ** show subsections
c      write (*,*) '  Trim edge (short wavelength emission)'
c      write (*,*) ' (This is not reversible.) How many points to cut?'
c       read (*,*) jcut
c     j1 = 1
c       do 45 i = 1, numrec
c         do 40 j = 1, jcut + j1
c  40        z(j,i) = 0.0
c          j1 = j1 + 1
c  45    continue
c     write (*,*) 'Trim long wavelength points: enter # points to cut:'
c     write (*,*) '(to reverse a previous cut enter a negative number.)'
c       read (*,*) jcut
c       ndata = ndata - jcut
c     endif
c ** end of menu choice 6

c*7*7*7*7*7*7*7*7*7*7*7*7*7*7*7*7*
    if (choice .eq. 7) then
c *** to print picture redefine output parameters and return to
c    plot routines:

c * Set plotter type, com port (first time only):
     if (place .eq. 0) then
         write (*,*)
         write (*,*)
         write (*,*) ' Plotter set-up: '
         write (*,*)
         write (*,*) ' Most HP plotters:  1 (WHOI plotter)'
         write (*,*) ' HP #7475A plotter: 2 '
         write (*,*) ' HP Thinkjet:       3 '
         write (*,*) ' HP Quietjet:       4 '
         write (*,*) ' HP Quietjet plus:  5 '
         write (*,*) ' HP Laserjets:      6 '
         write (*,*)
      write (*,*) ' Please enter appropriate number: '
     read (*,*) place

c * For COM2 add 50 to ioport.
         write(*,*) ' Which COM port leads to plotter (1 or 2)? '
         read (*,*) i
         if (i .eq. 1) com = 0
```

```
          if (i .eq. 2) com = 50
         endif

        if (place .eq. 1) then
         model = whoimod
          ioport = whoiport + com
        elseif (place .eq. 2) then
         model = mitmod
          ioport = mitport + com
        elseif (place .eq. 3) then
         model = 70
          ioport = 0 + com
        elseif (place .eq. 4) then
         model = 72
          ioport = 0 + com
        elseif (place .eq. 5) then
         model = 75
          ioport = 0 + com
        elseif (place .eq. 6) then
         model = 60
          ioport = whoiport + com
       endif

c ** expand plot for paper plotting:
        xhplot = 10.5
        yhplot = 8.5
      endif
c ** end of menu choice 7

c*8*8*8*8*8*8*8*8*8*8*8*8*8*8*8*8*8*8*

      if (choice .eq. 8)  then

        call savemat(z, 0)
c Pass 0 to write z-matrix, 1 to read it.
      endif
c ** end of menu choice 8

c*9*9*9*9*9*9*9*9*9*9*9*9*9*9*9*9*
      if (choice .eq. 9) then
        write(*,*) ' Read raw data file (d) or saved matrix (m)?'
       read (*,930) ans
       if (ans .eq. 'd') then
         call getdata(z)
        zexists = 1
       elseif (ans .eq. 'm') then
         call savemat(z, 1)
        zexists = 1
       endif
      m0=1
      n0=1
      endif
c ** end of menu choice 9

c * 10 * 10 * 10 * 10 * 10 * 10 * 10 * 10 * 10 * 10 * 10 * 10 * 10 * 10 *
c ** quit
      if (choice .eq. 10) goto 110
```

```
c * end of menu choice 10

 930  format(a)
 940  format(f6.3)
 950  format(2f4.1)
 960  format(a4)
 970  format(i1)

c *** return to menu (statment 80):
    goto 80
 100  continue
c *** 100 is the end of do loop, 110 is exit destination from loop

c *** on quit go to line 110:
 110  continue
    stop
    end
c******** END MENU (MAIN) **********************************************

c********* MAXIMUM ************************ MAXIMUM **********************
        subroutine maximum(max)

c ** finds maximum data point in matrix z

C COMMON DATA TYPES:
c ** block 'max' types:
      real*4 exmax, emmax, zmax, exmin,emmin, zmin
c ** block 'datinf' types:
        character*61 rectitle
        character*21 when
      real*4 exll,exul,emll,emul,inc
c ** block 'size' types
        integer*2 nxsize, nysize
c ** block 'datcom' types:
        integer*2 npts, numrec, ndata

C INTERNAL TYPES:
     integer*2 i,j
     real*4 max

C COMMON BLOCKS:
        common /work/ z(200,65)
      common /max/ exmax, emmax, zmax, exmin, emmin, zmin
        common /datinf/ rectitle,when,exll,exul,emll,emul,inc
     common /size/nxsize, nysize
     common /datcom/ npts, numrec, ndata

c *** max:
     zmax = 1e-25
     do 10 j=1,nxsize - 1
     do 10 i=1,nysize - 1
          if (zmax .lt. z(j,i)) then
             zmax = z(j,i)
             exmax = z(nxsize,i)
             emmax = z(j, nysize)
           endif
 10   continue
```

```
      max = zmax
c max is returned value.
c *** min:
      zmin = 1e+25
      do 20  j=1,nxsize - 1
      do 20  i=1,nysize - 1
             if (zmin .gt. z(j,i)) then
                zmin = z(j,i)
                exmin = z(nxsize,i)
                emmin = z(j, nysize)
             endif
 20   continue

c *** excitation/emission limits:
c Assumes last row and column of z contain ex/em wavelengths.
         exll = z(nxsize,1)
         exul = z(nxsize,numrec)
         emll = z(1,nysize)
         emul = z(ndata,nysize)

      return
     end
c******** END MAXIMIUM **************************************************

c******* RESACALE ********************* RESCALE ****************************
      subroutine rescale(z, top)
c ** rescales z-matrix so that maximum value=top. Calls function maximum.

C PASSED TYPES:
       real z(200,65)
           real*4 top

C COMMON DATA TYPES:
c ** block 'size' types:
     *     integer*2 nxsize,nysize
c ** block 'norminf' types:
           real*4 normm, topp

C INTERNAL DATA TYPES:
       real*4 norm, zmax
       integer*2 i,j

C COMMON BLOCKS:
       common /size/nxsize, nysize
           common /norminf/ normm, topp

c topp is the same as top but is allowed into a common block.
       topp = top

           call maximum(zmax)
           norm = top/zmax
           write (*,*) ' Normalization factor is: ',norm, '.'
       if (norm .ne. 1.0) then
        do 10 i = 1, nxsize
        do 10 j = 1, nysize
          z(i,j) = norm * z(i,j)
  10      continue
```

```
      endif
        return
        end
c*******END RESCALE **************************************************

c***** COPY ************** COPY **************** COPY ********
        subroutine copy(z1,z2)
c ***  Copies z1 into z2.

      implicit integer*2 (i-n)

C PASSED DATA TYPES:
        real z1(200,65), z2(200,65)

C BLOCK DATA TYPES:
c ** block 'size' types:
        integer*2 nxsize,nysize

C INTERNAL DATA TYPES:
        integer*2 i,j

C COMMON BLOCK:
      common /size/nxsize, nysize

       do 60 j = 1, nxsize
       do 60 i = 1, nysize
        z2(j,i) = z1(j,i)
  60    continue

        return
        end

c****** END COPY ********************************************************

c****** SUBTRACT ********************** SUBTRACT **************************

        subroutine subtract(z)
c ** subtract another spectrum, norm = normalization factor

C PASSED DATA TYPES:
        real*4 z(200,65)

C BLOCK DATA TYPES:
c ** block 'size' types:
        integer*2 nxsize, nysize
c ** block 'datinf' types:
         character*61 rectitle
         character*21 when
       real*4 exll,exul,emll,emul,inc

C INTERNAL DATA TYPES:
        real*4 ztemp(200,65)
      character*61 title
        character ans
        real*4 norm
        integer*2 i,j
```

```
C COMMON BLOCKS
        common /size/ nxsize,nysize
        common /datinf/ rectitle,when,exll,exul,emll,emul,inc

c ** Preserve title of first record, as 'title'. Recopy to 'rectitle' at end.
      title=rectitle

       write (*,*)' Normalize new spectrum before subtracting? (y,n)'
      read (*,930) ans
         norm = 1.0
         if (ans .eq. 'y') then
            write (*,*) ' Please enter normalization factor: '
            read (*,940) norm
      endif

c **  ztemp is matrix to be subtracted:
        write(*,*) ' Subtract raw data file (d) or saved matrix (m)?'
       read (*,930) ans
        if (ans .eq. 'd') then
          call getdata(ztemp)
         zexists = 1
        elseif (ans .eq. 'm') then
          call savemat(ztemp, 1)
         zexists = 1
      endif

      do 61 j = 1, nxsize - 1
      do 61 i = 1, nysize - 1
            z(j,i) = z(j,i) - (norm * ztemp(j,i))
 61   continue

      rectitle=title

 930  format(a)
 940  format(f6.3)

        return
        end
c******* END SUBTRACT *******************************************************

c****** MATBAT ******************** MATBAT **********************************

        subroutine matbat

c ** To do a bunch of things to a file in batch fashion.

c ** get file name = 'name' *&^%$#@!)(*&%^%$

c ** getdata:
       call getbat(name,z)

c ** subtract background:
         call subtract(z)

c ** save as *.mat

c ** integrate, save as *.int
```

```
c ** normalize to abs

c ** save as *.nor

c ** integrate, save as *.qef

         end

c****** END MATBAT **************************************************


c****** BLOCK DATA *************** BLOCK DATA ***************************
         block data sizedat
      implicit integer*2 (i-n)
c ** size of data arrays
       common /size/nxsize, nysize
      data nxsize /200/, nysize /65/
         end
c***** END BLOCK DATA **************************************************


c * This modual contains subroutines getdata, info, and where

c****** GETDATA ********************************** GETDATA ***************
      subroutine getdata(z)

c ** This subroutine reads binary data from a fluorometer disk into a file
c *  for Plot88. Input data format is "SLM Universal Data Structure".
c ** The maximum number of points allowed in z(x,y) is 16384, so #records
c *  (numrec) x points/rec must not exceed this. No more than 128 records
c ** can be read into one file.

      implicit integer*2 (i-n)

C COMMON data types:
c ** datcom block values (main block & norminf):
         integer*2 npts, numrec, ndata
c ** datinf values, (for info subroutine):
         character*61 rectitle
         character*21 when
         real*4 exll, exul, emll, emul, inc
c ** block fil, file  name info
      character*30 zfile
         character drive
c ** size block (for all subroutines that deal with z matrix):
         integer*2 nxsize, nysize

C INTERNAL DATA TYPES:
      real z(200,65), dump(1024)

c *** junk variables are throw-away parts of the binary data file
      character*64 junk1
      character*95 junk2
      character*100 junk3
      character*52 junk4
      character*86 junk5
      real*4 skip

c *** some control variables:
      integer*2 record, jex, irec, mrec
      character ans

c *** stuff to read from data records
      character*82 words
c  *** extra values to send to info subroutine:
      integer nrec
      character stype, nscan, cor, deriv, smooth, norm
      real*4 exwl, emwl, exbp, embp, offset
       real*8 xaxisll, xaxisul, xmin, xmax
c These numbers are double precision in SLM data files; change to *4 later.
      real*8 emll8, emul8, inc8
       real*4 yaxisll, yaxisul, ymin, ymax

C COMMON BLOCKS:
c *  datcom is stuff needed in the main block, also called by normabs.
       common /datcom/ npts, numrec, ndata
c *  datinf is stuff to go to info subroutine.
       common / datinf/rectitle,when,exll,exul,emll,emul,inc
c *  size is size of z matrix (for all subroutines that deal with z matrix):
       common /size/ nxsize, nysize

c Default file path:
       zfile = 'c:\data\3d\a.dat'

c ** find out which files to read
 3     write (*,*) ' Set to read ', zfile
       write (*,*) ' Which fluorometer files to read? (first, last) '
      write (*,*)' (enter 0 for new name, -1 for new path, -2 to return
     1 to menu)'
      read (*,900) irec, mrec

      if ((irec .eq. 0) .or. (irec .eq. -1)) then
c ** Ask which path to read from:
              call where(zfile, irec)
              goto 3
       elseif (irec .eq. -2) then
        return
          endif
c ** in case of input errors ask again:
      if ((1 .gt. irec) .or. (100 .lt. irec)) goto 3
      if ((1 .gt. mrec) .or. (100 .lt. mrec)) goto 3
      if (mrec .lt. irec) goto 3


c ** Calculate number of files to be read (nrec=numrec, for info sub):
      numrec = mrec - irec + 1

      if (numrec .gt. (nysize-1)) then
        write (*,*)' The maximum number of records is ',(nysize-1),'.'
        write (*,*) ' Records ',irec,' to ',irec+64,' will be read. '
           mrec = irec + 64
       numrec = 65
     end if
```

```
      nrec = numrec

c *** initialize z matrix to 0
      do 10 i = 1, nxsize
        do 10 j = 1, nysize
   10 z(i,j) = 0.0

c  open binary data file

       open(15, file = zfile, access = 'sequential', form = 'binary',
     1  status = 'old', mode = 'read')

c  disk has 128 bytes of junk at start
      read (15) junk1
      read (15) junk1

c  *** find first file to read,
c     each record = 4352 bytes = 43 x junk3(100) + junk4(52)
      record = 1

      do 33, i = 1, irec-1
       do 20 k = 1, 43
  20        read (15) junk3
        record = record + 1
        read (15) junk4
  33   continue

c *** read data
      write(*,*) ' Now reading record: '

      do 30 i = 1, numrec
        write (*,'(i3\)') record

c  nread is the number of numbers (4 bytes) read from each record
c  ndata is the number of data points from each record
c
        read (15) rectitle, when
         read(15) stype, nscan, cor, deriv, smooth, norm
        read(15) npts
         read(15) exwl, emwl, exbp, embp, offset
          read(15) xaxisll, xaxisul, yaxisll, yaxisul, inc8, skip
         read(15) ymin, xmin, ymax, xmax
        read (15) junk5

c *** Save limits on the total scan and min/max data points. ll = lower limit,
c     ul = upper limit. These numbers are to pass to info subroutine.
c     jex is offset to plot excitation wavelength, expressed in steps, i.e.
c     spacing in z-matrix. Wavelength values are placed into the last row
c     (emission) and last colunm (excitation) of the z matrix.

c ** Initial record, set lower wavelength limits & fill in wavelength data:
      if (i .eq. 1) then
        exll = exwl
         emll = xaxisll
         jex = int(emwl-exwl)/(int(inc8))
c   **   inc is real*4, inc8 is real*8; inc is passed to info subroutine
            inc = inc8
      end if
c       (initial record)

       nread = 0
       ndata = 0
      j1=0
c *** Read data file #1:
c *** Here is where data is really read. j1 was offset due to shifting
c starting points for fluorometer scans in old data collection routine.
c Set j1=1, and use old statement 30 if old files are to be read.
        do 40 j =j1, j1+npts
          read (15) z(j,i)
          nread = nread + 1
 40         ndata = ndata + 1
c *** read to end of record:
       k1 = 1024 - nread
        read (15) (dump(k), k = 1, k1)
        record = record + 1
  30    continue
c 30     j1 = j1 + 1  Used for offset data only.
c * end of read loop

c *** ndata is max index of emission data, exul & emul are wavelength limits
         ndata = ndata + j1
c ** if data is manipulated in SLM program exll gets lost:
          if (exll .eq. 0.) then
            exll=emll -10.
        endif

c *** Wavelengths listed in last row (excitation) and column (emission):
              do 50 k=1, nysize-1
          z(nxsize, k) = exll + float(inc*(k-1))
 50           continue

              do 55 j=1, nxsize-1
          z(j, nysize) = emll + float(inc*(j-1))
 55           continue

              exll = z(nxsize, 1)
          exul = z(nxsize,numrec)
              emll = z(1, nysize)
          emul = z(ndata,nysize)

c ** close file
     close (15)
     write (*,*)

 900  format (2I4)
 930  format (a)
 800  return
     end
c********* END GETDATA **************************************************
```

```
c********* WHERE **************** WHERE ********************************
        subroutine where(zfile, i)

C PASSED DATA TYPES
      character*30 zfile
      integer i
        character*15 zpath, zname

      zpath= '   c:\data\3d\'
      zname= 'a.dat        '

c       write(*,*) ' Default path is: ', zpath
c       write(*,*) ' Default file name is: ', zname
      write(*,*)
c 20    write(*,*)' Change path (p), name (n) or both (b)? '
c      read(*,930) ans
c       If ((ans .eq. 'a') .or. (ans .eq. 'A')) then
c          return
      if (i .eq. -1) then
          write(*,*) 'Enter new path name (include drive):'
         read(*,940) zpath
      elseif (i .eq. 0) then
         write(*,*) 'Enter new file name: '
         read(*,940) zname
      endif
      zfile = zpath//zname
      return
 930  format (a)
c ** A cludgy, but essential format statement to avoid blanks in 'zfile':
 940  format (1xtl1a)

        return
        end
c********* END WHERE ***************************************************

c********* INFO ************************ INFO *************************

      subroutine info

c *** This routine displays information about the current data set.

C COMMON DATA TYPES:
c ** datinf types (from getdata):
      character*61 rectitle
      character*21 when
      real*4 exll, exul, emll, emul, inc

c ** datcom block types:
        integer*2 npts, numrec, ndata

c ** norminf types (rescale):
      real*4 normm, topp

c ** max types (from maximum subroutine):
      real*4 exmax, emmax, zmax, exmin, emmin, zmin

C COMMON BLOCKS:
```

```
c ** Common blocks datinf and datcom come from 'getdata'.
      common / datinf/rectitle,when,exll,exul,emll,emul,inc
      common /datcom/ npts, numrec, ndata
c ** norminf is for rescaling routine.
      common /norminf/ normm, topp
c ** max (& min) values are generated in maximum subroutine.
      common /max/ exmax, emmax, zmax, exmin, emmin, zmin

c *** get max and min of z matrix; modifies variables in max_min com block.
         call  maximum(zmax)

      Write(*,900) rectitle
  900  format( ' This data set is titled ', a61)
      Write(*,*) ' Time and date of collection: ',when,'.'
     write (*,*)
      write(*,901) exll,exul
  901  format( ' Excitation wavelengths ',f5.1,' to ', f5.1,'.')
      write(*,902) emll,emul,inc
  902  format( ' Emission wavelengths ',f5.1,' to ',f5.1,' by increments
    1  of ',f3.1,'.')
     write (*,*)
      write(*,904) zmax, exmax, emmax
  904  format(' Intensity maximum is ',f6.1,' at ex = ',f5.1, ' and em =
    1  ',f5.1)
      write(*,905) zmin, exmin, emmin
  905  format(' Intensity minimum = ',f5.1,' at ex = ',f5.1,' and em = '
    1 ,f5.1)
     write (*,*)
      write(*,906) numrec
  906  format(I3,' records have been read from this file.')
c      if (topp .ne. 0.) write (*,910) topp
c  910  format(' Plot has been normalized to ',f3.1)


     return
     end
c************ END INFO ************************************************


c *** This module contains subroutines getabs, normabs, and trim

      subroutine getabs(abs)

c ** This subroutine reads absorbance data from a fluorometer disk into a file
c *  for Plot88. Input data format is "SLM Universal Data Structure".
c *  N.B. There are no global variables in this subroutine.
c *  Absorbance data are put into vector abs(320). Abs values are assumed to
c *  be at wavelengths 190-820 with 2 nm intervals from HP spec, copied into
c *  SLM program.  This was done to allow examination of the spectra, and editing
c *  if needed to remove spikes from the lamp and adjust wavelength discrepency.
c  Calls WHERE

      implicit integer*2 (i-n)

C PASSED DATA TYPES:
      real abs(320)
```

```
C INTERNAL DATA TYPES:
      real dump(1024)

c *** junk variables are throw-away parts of the binary data file
      character*64 junk1
      character*95 junk2
      character*100 junk3
      character*52 junk4
      character*86 junk5
      real*4 skip
      integer lamb

c *** file to read
      character*30 zfile
      character ans
c *** some control integers:
      integer*2  npts

c *** stuff to read from data records
c **  N.B. These are NOT global variables in this subroutine.
      character*61 rectitle
      character*21 when
      character*82 words
      character stype, nscan, cor, deriv, smooth, norm
      real*4 exwl, emwl, exbp, embp, offset
      real*8 xaxisll, xaxisul, xmin, xmax, inc
      real*4 yaxisll, yaxisul, ymin, ymax

C DATA:
c *** data file to read:
      data zfile/'c:\data\3d\abs.dat'/

C START OF GETABS:

c Can't read ASCII files yet, reads from SLM data files only.
c ** find out which files to read
c         write(*,*) ' Read abs data from fluorometer file (f) or HP (h)
c     1 file (must be copied to standard ascii)? '
c         read(*,930) ans

c      if (ans .eq. 'f') then

  3   write (*,*) '  Path is ', zfile
      write (*,*) ' Which record contains absorbance data? '
      write (*,*) ' (file #, or enter 0 for new name, -1 for new path)'
      read (*,900) irec

       if (irec .lt. 1) then
         call where(zfile, irec)
       goto 3
      endif

          write(*,*) ' Looking for file ',irec,', please wait. '
c  open binary data file

       open(15, file = zfile, access = 'sequential', form = 'binary',
     1   status = 'old', mode = 'read')
```

```
c  disk has 128 bytes of junk at start
      read (15) junk1
      read (15) junk1

c  *** find file to read,
c     each record = 4352 bytes = 43 x junk3(100) + junk4(52)

      do 33, i = 1, irec-1
        do 20 k = 1, 43
  20       read (15) junk3
        read (15) junk4
  33  continue

c *** read data

        read (15) rectitle, when
         read(15) stype, nscan, cor, deriv, smooth, norm
        read(15) npts
         read(15) exwl, emwl, exbp, embp, offset
          read(15) xaxisll, xaxisul, yaxisll, yaxisul, inc, skip
         read(15) ymin, xmin, ymax, xmax
        read (15) junk5

c *** Read data file.
c *  Here is where data is really read.
        do 40 k = 1, npts
 40        read (15) abs(k)

c end of read fluor file; if HP file:

c      elseif (ans .eq. 'h') then
c      zfile= 'c:\data\3d\1.hp'
c  5    write (*,*) ' Path is ', zfile
c       write (*,*) ' Enter 1 if OK, 0 for new name, -1 for new path:'
c      read (*,900) irec

c       if (irec .lt. 1) then
c          call where(zfile, irec)
c        goto 5
c      endif

c          write(*,*) ' Looking for file ',irec,', please wait. '
c  open binary data file

c       open(15, file = zfile, access = 'sequential', form = 'binary',
c    1   status = 'old', mode = 'read')

c *** Read data file.
c *  Here is where data is really read.
c        do 50 k = 1, 630
c 50        read (15) lamb, abs(k)
c      endif

c ** close file
      close (15)
      write (*,*)
 900 format (I4)
 930 format (a)
      return
      end
c******* END GETABS **************************************************

c******* NORMABS ***************** NORMABS ***************** NORMABS ***
        subroutine normabs(z)

c *** To normalize fluorescence data to absorbance spectrum.
c **  Calls GETABS to get absorbance data.

      implicit integer*2 (i-n)

C PASSED DATA TYPES:
      real z(200,65)

C BLOCK DATA TYPES:
c ** block 'size' types:
       integer*2 nxsize, nysize
c ** block 'datcom types:
          integer*2 npts, numrec, ndata

C INTERNAL DATA TYPES:
       real abs(320), dump(1024), abk, avk
       character ans

C COMMON BLOCKS:
       common /size/ nxsize, nysize
       common / datcom/ npts, numrec, ndata

C START NORMABS:

c ** Get absorbance data:
        call getabs(abs)

c * Absorbance records are 190-820 nm, with step=2 nm.
c  k is index for abs (1 to 315); for each record (ex wavelength) k is
c  chosen to correspond to either lam-ex (lambda even, abk) or the average of two
c  bracketing values (lambda odd, avk). Every intensity in that scan is then
c   normalized to absorbance at that point.

        do 10 i = 1, numrec
          k = int(z(nxsize, i)/2) - 94
           if (mod(z(nxsize,i), 2.0) .eq. 0) then
                abk=abs(k)
                do 20 j = 1, npts
 20             z(j,i) = z(j,i)/abk
           else
                avk = (abs(k) + abs(k+1))/2.0
                do 30 j = 1, npts
 30             z(j,i) = z(j,i)/avk
           endif
 10       continue

        return
      end
c******** END NORMABS *************************************************

c********* TRIM ******************** TRIM ******************** TRIM *********
      subroutine trim(z)
c *** To show subsets of data matrix. Stores original in z2 matrix;
c trims off data at low index end (if necessary) and re-adjusts numrec &
c ndata to change plotting limits at high index end.
c  Calls COPY

    implicit integer*2 (i-n)

C PASSED DATA TYPES:
    real z(200,65)

C BLOCK DATA TYPES:
c ** block 'work2' types:
     integer*2 numrecO, ndataO
c ** block 'size' types:
       integer*2 nxsize, nysize
c ** block 'datcom' types:
       integer*2 npts, numrec, ndata
c ** block 'datinf types:
     character*61 rectitle
       character*21 when
       real exll, exul, emll, emul, inc

C INTERNAL DATA TYPES:
    real abs(320), dump(1024)
      integer deltai, deltaj
      real  exllN, exulN, emllN, emulN

C COMMON BLOCKS:
      common /work2/ z2(200,65), nrecO, ndataO
    common /size/ nxsize, nysize
      common / datcom/ npts, numrec, ndata
      common / datinf/rectitle,when,exll,exul,emll,emul,inc, cor,nrec

      write (*,*) ' Trim (T) or restore (R) original data? '
      write (*,*) ' (Please restore original if it has already been cut
   1  before cutting again.) '
      read (*,930) ans

      if (ans .eq. 'r') then
c     (restore)
c * old file is in z2 matrix:
        call copy (z2,z)
c ** reset numrec, ndata, wavelength limits:
        ndata=ndataO
        numrec=nrecO
        exll= z(nxsize,1)
        exul= z(nxsize, numrec)
        emll= z(1,nysize)
        emul= z(ndata,nysize)
   write (*,900) exll, exul
   write (*,910) emll, emul
```

```
        else
c       (trim)
c * save original z in z2:
          call copy(z,z2)
          ndataO=ndata
          nrecO=numrec

    write (*,900) exll, exul
  900 format (' Current excitaion limits are: ',f5.1,' to ',f5.1,'.')
    write (*,910) emll, emul
  910 format (' Current emission limits are: ',f5.1,' to ',f5.1,'.')
    write (*,*) 'Please enter new excitation limits: '
        read (*,*) exllN, exulN
    write (*,*) '       and new emission limits: '
        read (*,*) emllN, emulN

        deltai =int((exllN -exll)/inc)
        deltaj =int((emllN - emll)/inc)

        numrec = numrec - deltai - int((exul -exulN)/inc)
        ndata = ndata - deltaj - int((emul -emulN)/inc)

c *** Data shift:
        do 20 j = 1, nxsize - deltaj - 1
        do 20 i = 1, nysize - deltai - 1
  20     z(j, i) = z(j+deltaj, i+deltai)

c *** Wavelength shifts:
        do 30 j =1, nxsize - deltaj - 1
       z(j, nysize) = z(j+deltaj, nysize)
  30  continue

        do 40 i =1, nysize - deltai - 1
       z(nxsize, i) = z(nxsize,i+deltai)
  40  continue

        exll = exllN
        exul = exulN
        emll = emllN
        emul = emulN

        endif

  930 format (a)

        return
        end

c*********************** END TRIM ***************************************

C * This modual contains the subroutines savemat and integrate.

******* SAVEMAT ****************** SAVEMAT ***********************
      subroutine savemat(z, k)
c *** This routine saves a z matrix so it doesn't have to be reread
c     from original files every time.
```

```
c  z is the matrix to be saved (read); k=0 to write, k=1 to read

C PASSED DATA TYPES:
      real z(200,65)
      integer k

C COMMON DATA TYPES:
c ** block 'size' types:
          integer*2 nxsize, nysize

c ** datinf types (from getdata):
       character*61 rectitle
       character*21 when
       real*4 exll, exul, emll, emul, inc

c ** datcom block types:
          integer*2 npts, numrec, ndata

c ** max types (from maximum subroutine):
       real*4 exmax, emmax, zmax, exmin, emmin, zmin

C INTERNAL DATA TYPES:
          integer*2 i,j
          character*30 zfile

C COMMON BLOCKS:
          common / size/ nxsize, nysize
c ** Common blocks datinf and datcom come from 'getdata'.
       common / datinf/rectitle,when,exll,exul,emll,emul,inc
       common /datcom/ npts, numrec, ndata
c ** max (& min) values are generated in maximum subroutine.
       common /max/ exmax, emmax, zmax, exmin, emmin, zmin

       call where(zfile, 0)

       write(*,*) 'Path is: ', zfile

       if (k .eq. 0) then
            open (16, file = zfile, status = 'new')
         Write(16,900) rectitle, when
         write(16,901) exll,exul
         write(16,902) emll,emul,inc
         write(16,904) zmax, exmax, emmax
         write(16,904) zmin, exmin, emmin
         write(16,906) numrec, npts, ndata
         write (16,990) ((z(j,i), j=1,nxsize), i=1,nysize)

       elseif (k .eq. 1) then
         open (16, file = zfile, status = 'old')
         read (16,900) rectitle, when
         read (16,901) exll,exul
         read (16,902) emll,emul,inc
         read (16,904) zmax, exmax, emmax
         read (16,904) zmin, exmin, emmin
         read (16,906) numrec, npts, ndata
         read (16,990) ((z(j,i), j=1,nxsize), i=1,nysize)
       endif
      close (16)
     return

 900  format(a61, a21)
 901  format(2f6.1)
 902  format(3f6.1)
 904  format(f9.4, 2f6.1)
 906  format(3i4)
 990  format (8f10.4:)
 910   format (a)
       end
******* END SAVEMAT *****************************************************

******* INTEGRATE ****************** INTEGRATE ************************
      subroutine integrate(z)
c Trapazoidal integration with step size=inc (wavelength interval).
C PASSED DATA TYPES:
      real z(200,65)

C COMMON DATA TYPES:
c ** block 'size' types:
          integer*2 nxsize, nysize

c ** datinf types (from getdata):
      character*61 rectitle
      character*21 when
      real*4 exll, exul, emll, emul, inc
c ** datcom block types:
          integer*2 npts, numrec, ndata
c ** size block (for all subroutines that deal with z matrix):
          integer*2 nxsize, nysize

C INTERNAL DATA TYPES:
          real*4 intem(2,200), intex(2,200)
          integer*2 i,j,k
          character*30 zfile

C COMMON BLOCKS:
          common / size/ nxsize, nysize
c ** Common blocks datinf and datcom come from 'getdata'.
       common / datinf/rectitle,when,exll,exul,emll,emul,inc
      common /datcom/ npts, numrec, ndata

c  initialize intem/intex:
          do 10 k=1,200
            intem(1,k)=0.0
            intex(1,k)=0.0
            intem(2,k)=0.0
 10         intex(2,k)=0.0

c intem is integration of z along EMISSION scans for each excitation wavelength
          do 20 i=1,numrec
c  excitation wavelength is in last row (nxsize) of z:
            intem(1,i) = z(nxsize,i)
            intem(2,i) = z(1,i)/2.
            do 30 j = 2, (ndata-1)
 30        intem(2,i) = intem(2,i) + z(j,i)
 20      intem(2,i) = (intem(2,i) + z(ndata,i)/2.) * inc

c intex is integration of z along EXCITATION scans for each em wvl
          do 60 i=1,ndata
c  emission wavelength is in last colunm (nysize) of z:
            intex(1,i) = z(i,nysize)
            intex(2,i) = z(i,1)/2.
            do 50 j=2, (numrec-1)
 50         intex(2,i) = intex(2,i) + z(i,j)
 60      intex(2,i) = (intex(2,i) + z(i,numrec)/2.) * inc

c  Write data to file:
      call where(zfile, 0)
      write(*,*) 'Path is: ', zfile
      open (17, file = zfile, status = 'new')

      write (17,901) 260., 0.0, intem(2,1)
      write (17,901) 265., 0.0, intem(2,2)
         do 100 i=3,200
           if (intex(1,i) .ne. 0.0) then
        write (17,901) (intex(k,i-2), k=1,2), intem(2,i)
100        endif

     close (17)
     return

901   format(f6.1, 2f10.2)

         end

******* END INTEGRATE ****************** INTEGRATE ***********************
```

DOCUMENT LIBRARY

March 11, 1991

Distribution List for Technical Report Exchange

Attn: Stella Sanchez-Wade
Documents Section
Scripps Institution of Oceanography
Library, Mail Code C-075C
La Jolla, CA 92093

Hancock Library of Biology &
Oceanography
Alan Hancock Laboratory
University of Southern California
University Park
Los Angeles, CA 90089-0371

Gifts & Exchanges
Library
Bedford Institute of Oceanography
P.O. Box 1006
Dartmouth, NS, B2Y 4A2, CANADA

Office of the International
Ice Patrol
c/o Coast Guard R & D Center
Avery Point
Groton, CT 06340

NOAA/EDIS Miami Library Center
4301 Rickenbacker Causeway
Miami, FL 33149

Library
Skidaway Institute of Oceanography
P.O. Box 13687
Savannah, GA 31416

Institute of Geophysics
University of Hawaii
Library Room 252
2525 Correa Road
Honolulu, HI 96822

Marine Resources Information Center
Building E38-320
MIT
Cambridge, MA 02139

Library
Lamont-Doherty Geological
Observatory
Columbia University
Palisades, NY 10964

Library
Serials Department
Oregon State University
Corvallis, OR 97331

Pell Marine Science Library
University of Rhode Island
Narragansett Bay Campus
Narragansett, RI 02882

Working Collection
Texas A&M University
Dept. of Oceanography
College Station, TX 77843

Library
Virginia Institute of Marine Science
Gloucester Point, VA 23062

Fisheries-Oceanography Library
151 Oceanography Teaching Bldg.
University of Washington
Seattle, WA 98195

Library
R.S.M.A.S.
University of Miami
4600 Rickenbacker Causeway
Miami, FL 33149

Maury Oceanographic Library
Naval Oceanographic Office
Stennis Space Center
NSTL, MS 39522-5001

Marine Sciences Collection
Mayaguez Campus Library
University of Puerto Rico
Mayaguez, Puerto Rico 00708

Library
Institute of Oceanographic Sciences
Deacon Laboratory
Wormley, Godalming
Surrey GU8 5UB
UNITED KINGDOM

The Librarian
CSIRO Marine Laboratories
G.P.O. Box 1538
Hobart, Tasmania
AUSTRALIA 7001

Library
Proudman Oceanographic Laboratory
Bidston Observatory
Birkenhead
Merseyside L43 7 RA
UNITED KINGDOM

50272-101

REPORT DOCUMENTATION PAGE

1. REPORT NO. WHOI-92-24

2.

3. Recipient's Accession No.

4. Title and Subtitle

Applications of Fluorescence Spectroscopy to Environmental Chemistry

5. Report Date June 1992

6.

7. Author(s)

Sarah Anita Green

8. Performing Organization Rept. No. WHOI 92-24

9. Performing Organization Name and Address

The Woods Hole Oceanographic Institution
Woods Hole, Massachusetts 02543

10. Project/Task/Work Unit No.

11. Contract(C) or Grant(G) No.

(C) N00014-89-J-1260

(G)

12. Sponsoring Organization Name and Address

Funding was provided by the Office of Naval Research through Contract No. N00014-89-J-1260.

13. Type of Report & Period Covered

Ph.D. Thesis

14.

15. Supplementary Notes

This report should be cited as: Sarah Anita Green, 1992. Applications of Fluorescence Spectroscopy to Environmental Chemistry. Ph.D. Thesis. MIT/WHOI, WHOI-92-24.

16. Abstract (Limit: 200 words)

This thesis consists of three sections. In chapter two, fluorescence quantum yields and lifetimes were measured for a series of nitroxide-fluorophore adducts, and quenching rates were shown to be high ($k_q \approx 10^8$-$10^{10} s^{-1}$), even at distances of ≈ 12Å. An excellent correlation was observed between k_q and the non-radiative relaxation rate. In the third chapter, diffusional quenching by charged and neutral nitroxides was employed to investigate the electrostatic properties of fulvic and humic acids. Cationic nitroxides were found to be up to 16 times more effective than neutral analogues in quenching the fluorescence of humic materials. This result is attributed to the enhanced coulombic attraction of cations to anionic surfaces. Chapters four, five and six explore the optical properties of colored marine DOM. Absorption spectra were characterized by their log-linearized slopes (S). S is found to be much greater for blue-water samples than for riverine and coastal samples. Fluorescence quantum yields were similar for a wide range of samples. Complete excitation/emission fluorescence spectra were collected and normalized to their respective absorbance spectra. DOM isolated on C-18 columns had somewhat different optical characteristics than whole water samples.

17. Document Analysis a. Descriptors

1. fluorescence
2. marine optics
3. dissolved organic matter

b. Identifiers/Open-Ended Terms

c. COSATI Field/Group

18. Availability Statement

Approved for publication; distribution unlimited.

19. Security Class (This Report) UNCLASSIFIED

20. Security Class (This Page)

21. No. of Pages 234

22. Price

(See ANSI-Z39.18)

See Instructions on Reverse

OPTIONAL FORM 272 (4-77)
(Formerly NTIS-35)
Department of Commerce